DOTTORATO DI RICERCA IN SCIENZE DELLA TERRA

XVIII CICLO DEL CORSO DI DOTTORATO

Using radon as tracer for Non-Aqueous Phase Liquid (NAPL) contamination.

Gabriele De Simone
Dottorando

Prof.ssa Paola Tuccimei
Docente Guida/Tutor: Prof.

Dr. Gianfranco Galli
Cotutor: Prof.

Prof. Claudio Faccenna
Coordinatore: Prof.

firma

firma

firma

firma

Index

Introduction

This study is related to a new analysis technique for hydrocarbons polluted sites through the use of Radon gas.

Radon is a radioactive gas which is naturally present in the earth's crust in variable concentrations. Thirty six radon isotopes have been recognised, but just ^{222}Rn and ^{220}Rn present a significant abundance: ^{222}Rn (^{238}U series) is the most abundant in confined environment because of its larger half-life (3.8 days); ^{220}Rn (^{232}Th series), commonly referred to as Thoron, is characterised by a shorter half-life (55.6 seconds) that makes its indoor concentration much lower.

In industrial areas and in areas where refineries and storage units for hydrocarbons are present, hydrocarbons spills in the subsoil may frequently occur. Hence the need for hydrocarbons remediation actions.

A primary problem concerning the remediation of sites contaminated by NAPL (non-aqueous phase liquids) is to assess the extent of the polluted area. The distribution, extent and amount of pollutants in the subsurface has to be properly assessed in order to arrange appropriate remediation actions.

In order to design appropriate remediation, distribution, extension and amount of pollutants in the subsoil must be well characterized. A possible approach can consist in a survey based on the direct detection of organic carbon in soil gas. This method, however, is only valid in case of soil contamination by volatile hydrocarbons;

Another method applied in the past several years is the use of CO_2 and CH_4 as tracers for NAPL. Variations in percentage of these gases in the soil can be useful for the identification of the polluted area. However, even this method presents difficulties and inaccuracies especially in case of recent pollution.

Because of these difficulties in identification and demarcation of the land polluted by using only surface analysis, activity usually starts with vertical drillings located in the proximity of the source of contamination, or the installation of wells to collect water samples underground, picking carrots etc. within the contaminated area, if known. These methods, however, have a high cost and is almost never possible to define precisely the area of the land involved. This can lead to bad decisions relating to remediation.

In this study the importance of Rn lies in the fact that it has excellent solubility in a wide range of NAPL, so as to form negative anomalies concentration in the soil where the presence of these pollutants is observed. In this way, knowing the soil Radon concentrations in the background area, an area polluted by NAPL could be indirectly localized by making a grid of surface Radon measurements over the area where it is assumed that NAPL pollution occurred.

Radon solubility in NAPLs can be quantified for each NAPL with an individual NAPL/air partitioning coefficient (K NAPL/AIR). The partitioning coefficient K NAPL/AIR is one of the most influential parameters governing the decrease of gas radon concentration in the soil in the presence of NAPLs.

Radon as tracer of NAPL contamination

Radon

Radon is an element of VIIIA Group of the periodic table: it is a noble gas, therefore, does not react with other chemical elements. It is the heaviest of the known gas (density 9.72 g / l at 0 ° C, 8 times more dense than air). it is colorless, odorless, tasteless and is naturally present in soil. It is a radiogenic element (derived from the decay of ^{226}Ra) and radioactive (direct decay into ^{218}Po). Its 26 isotopes, between ^{219}Rn and ^{226}Rn, are part of the uranium and thorium decay chains (Figure 1). Only three of them are found in nature:

The ^{219}Rn (actinion), belonging to ^{235}U decay series, ^{207}Pb final product;

The ^{220}Rn (thoron), belonging to ^{232}Th decay series, ^{208}Pb final product;

The ^{222}Rn (proper radon), belonging to ^{238}U decay series, the final product ^{206}Pb (Bourdon et al., 2003).

The ^{219}Rn comes from the decay of ^{223}Ra and in turn decays to ^{215}Po.

The ^{220}Rn comes from the decay of ^{224}Ra and in turn decays to ^{216}Po.

The ^{222}Rn comes from the decay of ^{226}Ra and in turn decays to ^{218}Po.

The main radon source is soil or surface rocks that contain radium. Radium can reach the surface even in deep gas emissions areas (CO_2, CH_4). In open spaces it is diluted by air currents and reaches low concentrations, while in a closed environment, such as can be an home, radon can accumulate, reaching high concentrations dangerous to human health.

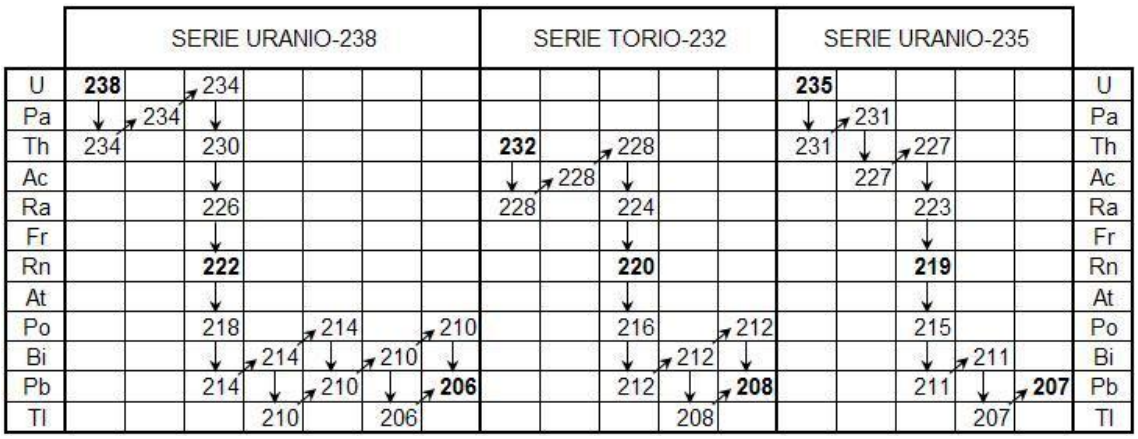

Fig. 1: Uranium and thorium decay series.

Regarding the natural concentrations of the three isotopes of radon, we can refer to the average concentration in the Earth's crust of the parent isotopes.

^{235}U 0.02 ppm (1.5 Bq/kg)

^{232}Th 8.5 ppm (34 Bq/kg)

^{238}U 2.7 ppm (33 Bq/kg)

The ^{238}U is the 99,27% of the isotope uranium complex.

It should also be considered as the average life of the three isotopes of radon, expressed by the half-life parameter:

half-life parameter.

^{219}Rn 3.92 seconds

^{220}Rn 54.5 seconds

^{222}Rn 3.825 days.

As a consequence ^{219}Rn has very low concentrations in nature and is therefore considered of minor importance.

The ^{220}Rn (thoron) is not easily detectable in the environment because of its short half-life, despite the ^{232}Th isotope, that generates it, is relatively abundant in nature. In any case, the distance that the thoron can travel escaping from the source material is minimal.

The ^{222}Rn has the longest half-life and is constantly present in the environment. It is considered the most important of radon isotopes and we usually refer to it with radon-term. Most of the studies on radon and its effects on human health have focused on ^{222}Rn.

Emanation, migration and radon exhalation

These parameters relate to the issue of radon from the ground or from any material. The issue is the release of radon atoms from the mineral grains in the pores and fractures of the material, due mainly to the effect of recoil linked to α decay (Morawska & Phillips, 1993). Migration is the movement of the radon atoms within the material.

The exhalation of radon is the transition from the material to the atmosphere.

Coefficient of emanation

Ratio between the number of radon atoms which leave the solid material and the amount generated from the sample. The number of atoms that leave the solid is always less than the number of generated atoms (De Martino et al., 1998).

In order to be a common mineral can occur radon emanation, it must be formed within the first 0.02 ÷ 0.07 uM from the surface. This is the distance of recoil of a radon atom at the instant of its formation from a radio atom. Radon that is deeper form remains imprisoned and decays in place in its solid products (Sasaki et al., 2004).

The emanation coefficient depends mainly on the natural features of material, such as porosity (Morawska & Phillips, 1993). and water content (Menetrez & Mosley, 1996).

Rate of exhalation

It provides the measurement of the radon released from inside to outside of the sample, that is, into the atmosphere. It is measured in Bq h-1. Its value depends on the enactment and the concentration gradient between inside and outside of the sample (De Martino et al., 1998). Consequently, it is strongly influenced by the environmental conditions (weather conditions, pressure, temperature). The rate of exhalation can be expressed as a *mass exhalation rate*, measured in Bq kg-1 h-1, or still as *surface exhalation rate*, measured in Bq m-2 h-1.

Radon flow from the soil

It defines the amount of radon that is released from the soil into the atmosphere in the unit time (passage at the soil-atmosphere). It is therefore an exhalation rate per unit area and can be expressed in Bq m-2 h-1.

The ubiquitous presence of radon in nature

The Radium (^{226} Ra), parent of the element Radon (^{222}Rn), is present in almost all the minerals of the earth's crust, which is why his daugther nuclide is produced constantly in the environment.

The alpha decay is the most important driver for the release of radon from the mineral matrix. When an atom of radium decays, the newly formed Radon atom is displaced for the recoil effect. The distance that an atom of radon can travel for the recoil can vary from 0.02 to 0.07 microns depending on the structure of the mineral.

Consequently, the possibility that the newborn Radon atom entering or not in the pores space depends on the location of the radium atom with respect to the surface of the grain in which it is contained and from the direction the Recoil. The ratio between the total number of atoms of radon emitted from a mineral matrix and the total number of radon atoms in the pores is expressed by the Emanation Coefficient. This is a nodimensional coefficient and is specific for each mineral matrix. Generally varies between 0.1 and 0.7 and in accordance with an average value is taken as the standard reference: 0.25.

Apart from the presence of Ra and the Emanation Coefficient, the concentration of radon in the interstitial space of the pores precisely depends on the porosity and the density of the mineral matrix. The relationship is t5he following:

$$C_\infty = \frac{\varepsilon A_{Ra} \rho_d}{n} \qquad [\mathrm{Bq/m^3}]$$

where:

C_∞ : radon concentration in the soil pore space (Bq/m^3)

ε : emanation coefficient

A_{Ra} : radium activity concentration of the mineral matrix

ρ_d : bulk density of the mineral matrix n : porosity of the mineral matrix

Generally the concentrations of radon in the soil or in aquifers are comprised between 5 and 50 kBq/m^3, that are mostly, almost always, detectable with modern measuring instruments.

The concentration of radon in the soil or in groundwater remains almost constant, though with a characteristic seasonal variation, in a given place. For these reasons the radon and its lateral and temporal variations, can be used as indicator of anomalies of the subsoil. An important example of this is that the Radon can be indicator of the presence or absence of NAPL in the subsurface.

Assessment of NAPL pollution using radon

The Non-Aqueous Phase Liquids (NAPL) are all the liquids that are immiscible with water as fuels (kerosene, diesel and gasoline), chlorinated solvents or mineral oils. They can be lighter (LNAPL), as fuels, or denser (DNAPL), as chlorinated solvents, than water so they can respectively float on water or sink under water and the interaction between the different phases is really limited because of the immiscibility.

Most of the petroleum products are lighter than water and tend to float on it remaining on the vadose zone, but in sufficient quantity these fluids can reach the saturated zone (groundwater). Near the capillary fringe (immediately above the saturated zone) they expand horizontally and are slowly carried by the aquifer.

In industrial areas and in sites where refineries and storage units for hydrocarbons are present, hydrocarbons spills in the subsoil may frequently occur; hence, the need for hydrocarbons remediation actions. A primary problem concerning the remediation of sites contaminated by NAPL is to assess the extent of the polluted area; the distribution and the degree of contamination in the subsurface has to be properly evaluated in order to arrange appropriate remediation actions. The employment of Rn as tracer of contamination depends on its high solubility in a wide range of NAPL, so as to produce negative anomalies concentration (radon-deficit) in the soil where the presence of these pollutants is observed. Thus, the evaluation of soil Radon concentrations in a background area, compared with data from an area polluted by NAPL, may give an indirect information on the distribution of NAPL in the subsoil, through several measurements over a regular grid covering the study area (Fig.).

Radon solubility in NAPLs can be quantified for each NAPL with an individual NAPL/AIR/WATER partitioning coefficient ($K_{NAPL/AIR/WATER}$). The partitioning coefficient $K_{NAPL/AIR/WATER}$ is one of the most influential parameters governing the decrease of gas radon concentration in the soil in presence of NAPLs.

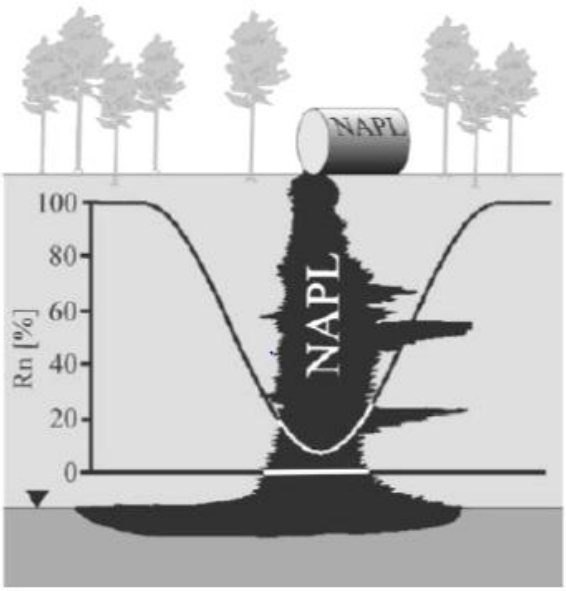

Fig.21. Reduction of soil radon concentration (radon-deficit) in proximity of a contaminated soil volume (from Schubert et al., 2002).

In order to use the radon as a tracer of the presence of NAPL and to obtain a result not only qualitative but also a quantitative estimate of the presence of pollutants, it' s of fundamental importance the understanding of the radon partitioning between gas and water.

If we need a quantitative evaluation of the NAPL volume, occurring in the subsoil, we can precisely measure radon partition coefficients within the specific NAPL mixture and we can use the equation proposed by Schubert (2015) to find saturation volumes of NAPL (S_{NAPL}).

Radon concentration at the equilibrium (C_∞), and the correspondent deficit (ΔC_∞) in non-polluted areas, depends on residual NAPL share (X_{NAPL}), fluid saturation ($S_F = S_{NAPL} + S_W$), that consider both water and NAPL, and radon partition coefficients.

Radon partition coefficients between residual NAPL and soil gas and between soil moisture and soil gas ($K_{NAPL/SG}$ and $K_{W/SG}$) are needed for quantification in the vadose zone (eq. 1) and radon partition coefficients between residual NAPL and water ($K_{NAPL/W}$) for quantification in the aquifer (eq. 2) as shown by following equations from Schubert (2015):

$$C_\infty = \frac{\varepsilon A_{Ra} \rho_d}{n(1 - S_F + K_{W/SG} S_F (1 - X_{NAPL}) + K_{NAPL/SG} X_{NAPL} S_F)}$$

$$C_\infty = \frac{\varepsilon A_{Ra} \rho_d}{n(1 - S_{NAPL} + K_{NAPL/SG} S_{NAPL})}$$

This study moreover focuses on the role of the vaporized fraction of NAPL on changes of radon concentration in the soil gas. The phenomenon is investigated through laboratory experiments regarding either the growth of radon exhalation from material contaminated with increasing volumes of kerosene, or the determination of radon partition between liquid kerosene, water and air, with NAPL vapors enhancing radon transport in the air.

Layout of the thesis

In the first part of the study, soil radon concentrations were monitored at 80 cm depth in a contaminated site of Latium Region.

This area has been chosen because it is affected by NAPL pollution at about 2-3 meters below the ground level, in order to test the "radon-deficit technique" to trace hydrocarbon pollution. These data were compared with those obtained from two different sites located nearby and characterized by similar geo-lithological features, but not contaminated (background areas). Radon measurements have been carried out seasonally, along with measurements of other parameters:

-physical conditions of the soil (water content and temperature at 30 and 80 cm depths);

-soil gas permeability (intrinsic permeability);

-concentrations of other gases in the soil, in particular CO_2 , H_2S and CH_4 .

Maps of soil gases concentrations (radon, CO_2) and intrinsic permeability were produced, using the program Golden Surfer.

This study was conducted with a seasonal monitoring of the polluted area throughout the period of my PhD (2013-2016). In addition, various laboratory experiments were carried out in order to determine Radon partion coefficients ($K_{air/NAPL}$ and $K_{water/ NAPL}$) in a two and three phase system to approach a quantitative determination of the fraction of NAPL in soil pores. Finally, more studies not strictly connected to the main goal of this thesis, but still related to it, have been advanced to refine the measurement techniques of

soil Radon and Radon in water sampes. In this period it was also developed a new instrument for the measurement of the intrinsic permeability of the soil.
All these studies have been published or have been just submitted to international peer review journals. These publications and are listed below:

Chapter 1: **Methods**

Chaper 2: **Results of soil gas and intrinsic permeability seasonal surveys in the study site and in close areas chosen for the determination of the background**

Chapter 3: **Tracing NAPLs contamination in the vadose zone using soil radon (Rend. Online Soc. Geol. It., Vol. 33 (2014), pp. 100-103)**

Chapter 4**: Using natural radon as a tracer of gasoline contamination (Procedia Earth and Planetary Science 13 (2015) 104 – 107)**

Chapter 5: **Laboratory simulation of recent NAPL spills to investigate radon partition among NAPL vapours and soil air (submitted to Applied Radiation and Isotopes)**

Chapter 6: **Correcting for H_2O interference using a RAD7 electrostatic collectionbased silicon detector (Journal of Environmental Radioactivity 162-163, 2016, 146-153)**

Chapter 7: **Soil radon survey to assess NAPL contamination from an ancient spill. Do kerosene vapors affect radon partition? (Submitted to Journal of Environmental Radioactivity)**

Chapter 8: **Using soil radon deficit and geoelectrical data as proxy indicators for residual NAPL contamination**

Chapter 9: **Additional papers on new analytical methods** (This chapter is composed by papers not srictly connected to main goal of the thesis and dealing with the improvement of analytical methods to determine radon concentration in the soil gas, radon dissolved in groundwater and soil intrinsic permeability are reported).

Chapter 9.1: **Calibration of Big Bottle RAD H_2O set-up for radon in water using HDPE bottles (Radiation Measurements 76, 2015, 1-7)**

Chapter 9.2: **Our PET project: an unlimited supply of big and small water sample vials for the assay of radon in water(J Radioanal Nucl Chem, 2015, 307, 2277-2280)**

Chapter 9.3: **Evaluating radon loss from water during storage in standard PET, bio-based PET, and PLA bottles (Radiation Measurements 84, 2016, 1-8)**

Chapter 9.4: **A new technique to measure in situ soil gas permeability (Journal of Geochemical Exploration 148, 2015, 56–59)**

Chapter 10**: Conclusions**

CHAPTER 1

METHODS

1.1 Geochemical methods

For the geochemical analysis were measured concentrations of ^{222}Rn and ^{220}Rn with two radonometers RAD7 from Durridge Company (one preceded by a desiccant unit, one not), the CO_2 concentration with the Dräger X-am 7000 (Dräger) and the VOCs (Volatile Organic Compounds) concentration with a PID (Photoionization Detector) from RAE Systems.

First of all, to verify that was possible to do correctly the measures, it was indirectly estimate the intrinsic permeability of the terrain with a vacuometer and a flowmeter.

All measures were made at a depth of 80 cm from ground level. In each point of measure it was driven an hollow rod in the ground utilizing an hammer and an "hitting" head applied on top of the ground rod (fig.1C). At the end of the rod was applied a mobile driving point (fig.1A) that, once the rod reached the designed depth, was driven 5 cm further down, with a thinner rod, to create a known pressure on the terrain.

At the end of analysis the hollow rods were retrieved with a crick (fig.1E) and the driving points were left in the ground.

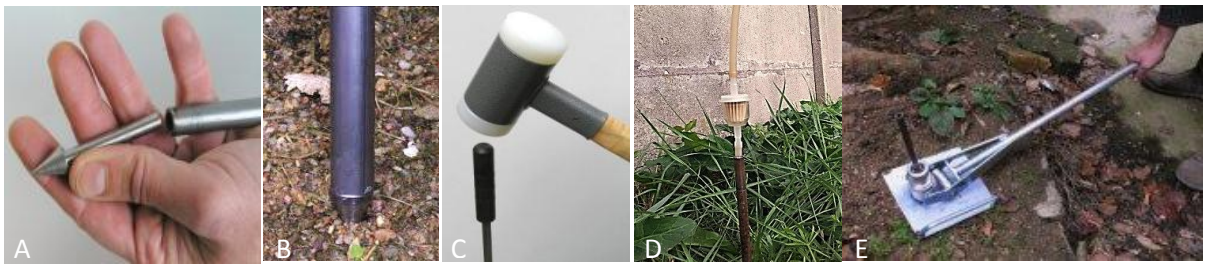

Fig.1 : driving of the hollow rod in the ground (A,B and C), measurements (D) and recuperation of the rod (E)

1.2 Permeameter

The vacuometer is an instrument that makes the vacuum in the soil inspiring the air present in the soil's pores and measuring the decompression induced.

We can indirectly calculate the intrinsic permeability of the soil trough the flow rate Q [$Q = V / t$ ($m^3 \cdot s^{-1}$)] measured by a flowmeter connected at the output of the radonometer and the pressure difference Δp (Pa) measured by the vacuometer, that are respectively directly and inversely proportional to the intrinsic permeability of the soil:

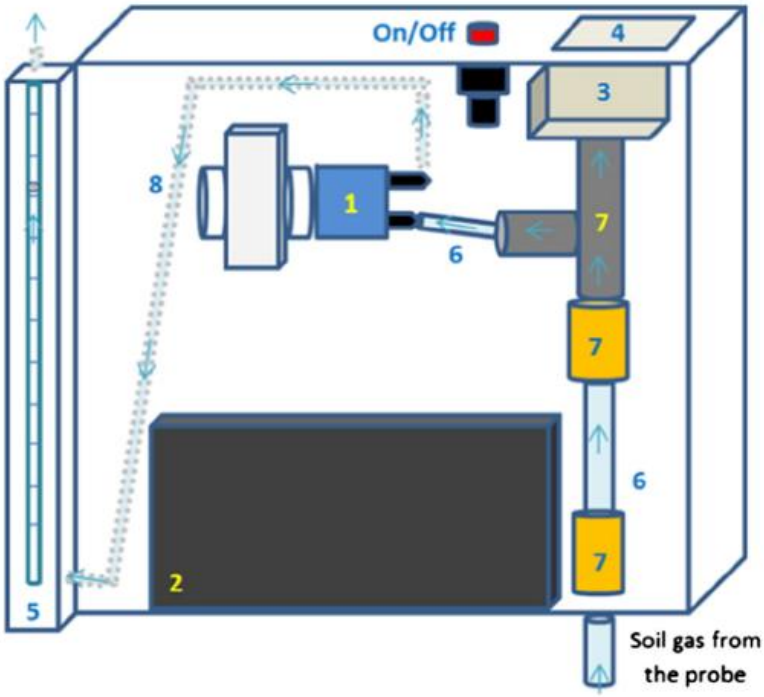

Fig. 2. New permeameter. It consists of a vacuum pump (1), a battery (2), a vacuomete (3), with digital display (4) a fluxmeter (5), vynil tubings (6), metal connectors (7) and electric cables (not shown). Tubings (8) connecting the pump output to the fluxmeter inlet were removed, along with the fluxmeter, at the end of the calibration test (see text for explanation). The arrows indicate air flow within the experimental apparatus.

$$k = \frac{Q \cdot \mu}{F \cdot \Delta p}$$

Where:

Q : flow rate measured by the flowmeter ($m^3 \cdot s^{-1}$)

μ : dynamic viscosity of air at 10° C (1.75 · 10-5 Pa · s^{-1})

F : shape factor of the hollow rod driven into the ground (0,149 m)

Δp : pressure difference between measuring depth and surface (Pa)

1.3 Flowmeter

The flowmeter FR2A13BVBN from Key Instruments (now Brooks Instruments) can measure air flow in a range from 0.1 to 1 liter per minute (LPM) so from 1.6 · 10-6 to 1.6 · 10-5 cubic meter per second. It has an high quality metering valve and an easy reading screen scale that allows to measure the values with an accuracy of ± 5%.

The flowmeter can be directly connected with the output of the radonometer to measure the flow rate of the system.

Fig. 3 : Flowmeter

1.4 Dräger X-am 7000 (CO_2)

The Dräger X-am 7000 is an instrument equipped with infrared sensor that measures CO_2 present in the soil. An infrared (IR) lamp releases IR radiations, through a tube filled with air, toward an IR-rays detector, which measures the amount of IR radiations that hit it. As the light passes through the tube, any gas molecules that are the same size as the wavelength of the IR waves absorb the IR radiations, while letting other wavelengths of light pass through.

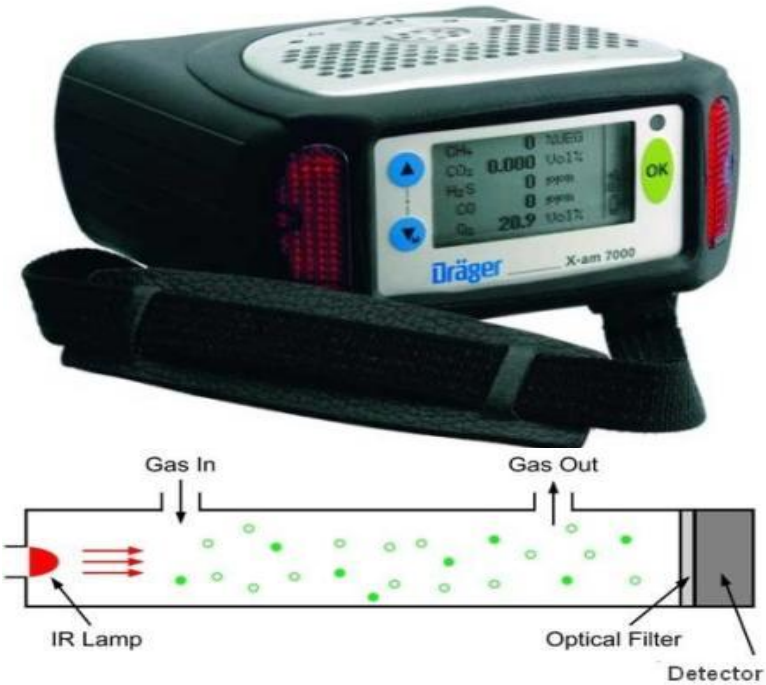

Fig. 4 : CO2 detector

The remaining waves hit an optical filter that absorbs every wavelength of light except the exact wavelength absorbed by CO_2. Finally, an IR detector reads the amount of radiation that was not absorbed by the CO_2 molecules or the optical filter. The difference between the amount of light radiated by the IR lamp and the amount of IR light received by the detector is measured. The difference is proportional to the number of CO_2 molecules in the air inside the tube. The suction of the gases, through a vinyl

hose connected with a small mask, starts when the mask is applied on top of the dispositive because the connection turns on the pump inside it.

1.5 RAD7

The radonometer RAD7 is an instrument that indirectly measures the radon (^{222}Rn and ^{220}Rn), that is an electrically neutral gas, through its decay products (respectively ^{218}Po and ^{216}Po) that, instead, are electrically charged.

The RAD7 is able to distinguish the different isotopic species (^{222}Rn and ^{220}Rn) through the energy associated to the different alpha particles produced by the different isotopes and to measure simultaneously both of them.

Fig. 5: RAD7 (Durridge Co.)

The detector is an electrostatic collection-based silicon detector placed at the center of the instrument's inner cell that is covered by a conductive material.

A power supply provides an electrical current that generates a potential difference of 2000 - 2500 V between the electric conductor and the detector. This creates an electrical field that pushes the positively charged particles on the detector, to which they are fixed.

Radon isotopes' decay radiates an α particle that has a 50% probability to arrive on the detector surface and to generate an electrical signal proportional to its energy. The generated electrical signals are subsequently amplified, measured, counted and converted into digital form. They are collected in a power spectrum represented by a diagram (fig.6) where the abscissa axis shows the energies of α particles (MeV) and the ordinate axis the counts on the detector. Sharing further 200 channels in 8 windows of energy, the RAD7 is able to count separately and simultaneously the decay products of ^{222}Rn and ^{220}Rn, to consider separately the contribution of a single isotope and to exclude from the count the background due to the isotopes of longer average life. We are interested in the analysis of the first four energy windows in the range 6-9 MeV and even more in the energies of 6.00 MeV and 6.78 MeV, respectively connected to ^{218}Po and ^{216}Po.

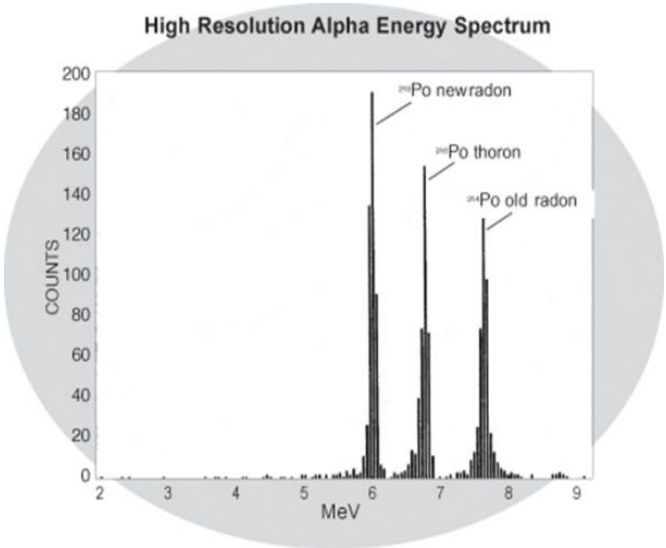

Fig. 6 : Alpha energy spectrum

The radonometer draw off air containing radon or thoron from the soil with a pumping rate of 800 ml/min. There are many different modalities of measuring. We used the "sniff" mode because in this modality the instrument measures the ^{222}Rn and ^{220}Rn only

through the direct decay of, respectively, ^{218}Po and ^{216}Po ignoring the α emissions of successive decays with increased half-life.

The time of response of the instrument is therefore a function of time it takes for the achievement of activity equilibrium between ^{222}Rn and ^{218}Po, which is approximately 15 minutes so almost 4 times radionuclide's father half-life (3,82 minutes). The equilibrium between ^{220}Rn and ^{216}Po is much faster and it's reached in less than a second. The "normal" mode includes the analysis of other isotopes so it has a better accuracy of the measurements but needs more response time. The RAD7 is able to perform a continuous monitoring of activity concentrations, with the possibility of subdividing the measures in smaller intervals. At the end of each cycle it's provided the relative concentration value.

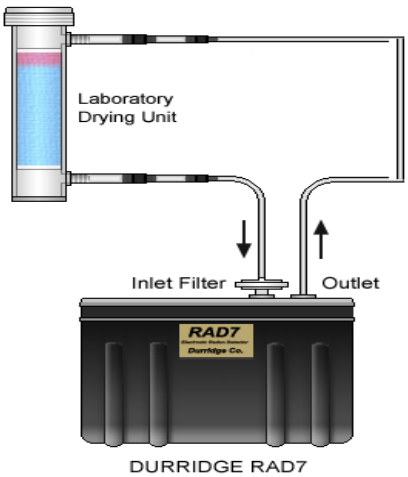

Fig. 7 : RAD7 purging

The instrument is provided with a suction pump that allows to draw the air from pores of the soil, within the measuring system, up to the detector cell. After any measurement, in water, air or soil, the sample cell still contains traces of radon analyzed previously, which could influence the results of subsequent measures so that, at the beginning of any new measure, a "purging" cycle is necessary to clean and dry the sensor with

circulation of dry air in the RAD7. This is obtained by connecting it with a drying unit (drierite) because the ^{218}Po must be absent in the system at starting time. The desiccant unit is composed by a column of calcium sulfates granules ($CaSO_4$) inside a plastic tube of 6 cm diameter and 28 cm height and an air filter placed at the entrance of RAD7 prevents the introduction of dust particles and charged ions in the cell, which could contaminate the detector. The drierite granules, during the flowing of clean air through the entire system, absorb the relative humidity (RH) of the air reducing the humidity in the system until its values become lower than 6-7%. Normally to reach these low RH values the purging should last about 30 minutes. The activity concentration increases until it reaches the equilibrium value with the ^{222}Rn, corresponding to the gas concentration in the soil. In our soil radon measurements have been established to carry out 5 cycles lasting 5 minutes, repeated until equilibration of activity.

1.6 MiniRAE Lite (Photoionization Detector)

The MiniRAE Lite is a photoionization detector (PID) that measures instantaneously the quantitative (ppmv) of the volatile organic compounds (VOCs) present in the sub-soil at a maximum depth or a maximum distance of 30 meters.

This instrument uses a radiation source, an ultraviolet (UV) lamp, to ionize gas molecules and then through an internal pump, that has a sampling flux of 400 cc/min, extracts the gases from the sub-soil by a pipe.The instrument can detect all gases with ionization potentials below 10,6 eV, such as benzene, aromatic compounds, amines, ammonia, ethanol, acetone (Chou, 1999), because the radiation source has a power of 10,6 eV .

Fig. 8 : VOCs detector

1.7 SYSCAL Pro Switch

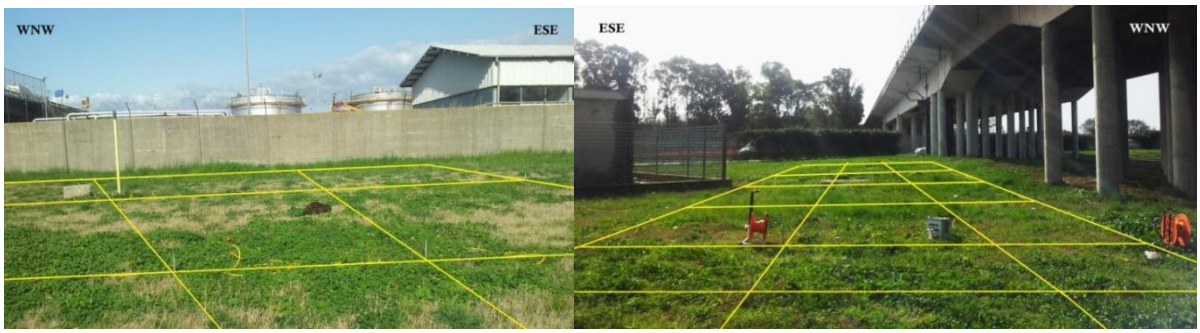

Fig. 9 Geoelectrical arrays: 72 detectors + 48 detectors

Two rectangular grids made, respectively, by 15x5 and 4x12 linear spreads of steel electrodes were utilized to create a 3D image of the resistivity and the chargeability of the subsoil. The first array was oriented with the longest side WNW-ESE with a spacing between the electrodes of 7.5 m in the longest side (x axis) and 2.5 m in the shorter side, with a total size of 35x30 meters; the second one was oriented with the longest side NNE-SSW with a spacing between the electrodes of 2.5 m in both sides with a total length of 27.5 meters and a width of 7.5 meters. It was chosen to overlap the two arrays of 7.5x7.5 meters and to utilize a shorter interdistance in the second array because we

needed a more detailed image of that area particularly in the NNE-SSW direction that was the direction of the spill already detected by previous studies.

The electrodes were connected, by multichannel cables, to a georesistivimeter Syscal PRO (Iris Instrument).IP measurements were collected using a pulse length of 1 s with integral chargeability measurements performed during voltage decay after current shut-off.

The SYSCAL Pro Switch is a ten-channels electrical resistivimeter which includes a transmitter, a receiver and a switching unit, that allows to transform linear surveys in 2D or 3D surveys combining several parallel sequences of same electrodes doing grids of measurements (fig. 12 a).

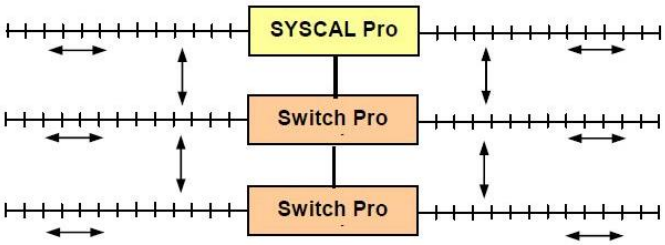

Fig. 10 Switch configuration for 3D imaging

Multi-channel acquisition of resistivity and/or IP data, up to 10 readings at the same time, is obtained using a set of electrodes (normally 24, 48, 72, 96 or 120), connected in a line or in several lines, which number is increased through Switch Pro units that allow to create 3D ground images by overlapping different planar images obtained juxtaposing linear contiguous acquisitions.

Fig. 11 Syscal Pro Switch resistivimeter connected with a screen that shows a single linear bi-dimensional geoelectrical profile

Time domain discharge curves due to Induced Polarisation chargeability (IP) are registered for different depths. Apparent resistivity, ρ, is directly proportional to geometrical coefficient, K [m], and to received potential, V [mV], and is inversely proportional to transmitted current, i [mA]. For the data analysis and the 3D interpretation ERTLab software is used.

CHAPTER 2

Results of soil gas and intrinsic permeability seasonal surveys in the study site and in close areas chosen for the determination of the background

The field part of my PhD study was conduced in a site of Latium Region (Italy) where a hydrocarbons spill occurred and traditional remediation techniques are accomplished. Site location and coordinates are omitted for confidentiality agreement.

The area (Fig. 1) is equipped with wells and piezometers for routine sampling and analysis of pollutants that provide an immediate feedback to this approach. The stratigraphic section from ground level downward consists of about 0.5 m of backfills, 2.5 m of medium sands and 2.5 m of medium-fine sands. The water table fluctuates in the range 0.5 – 2.5 m depth during the year.

A grid of 31 measuring stations was created over a 3000 m^2 large zone, where soil ^{222}Rn, ^{220}Rn, CO_2, CH_4 and intrinsic permeability were determined at 80 cm depth. A survey station was installed in the central part of the study area to evaluate soil gas concentration variability as a function of meteorological parameters.

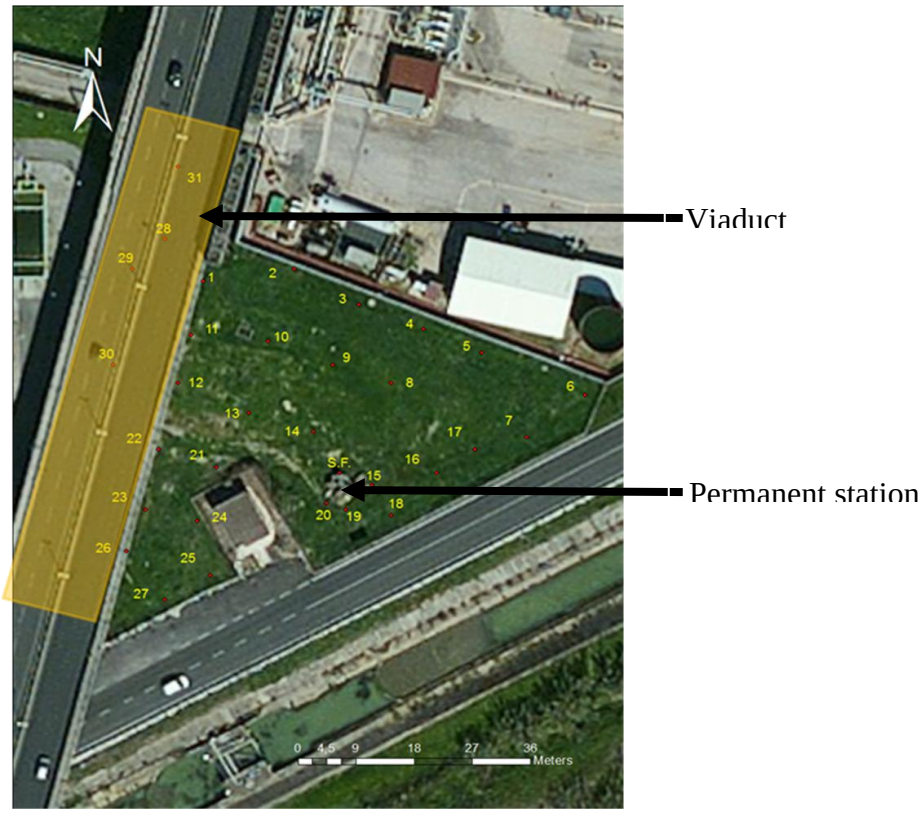

Fig. 1 Study area

The station acquires soil temperature and humidity at 30 and 80 cm depth, in order to assess how relevant rainfalls influence water content in the soil, reducing gas release at soil/atmosphere interface.

This study was conducted with a seasonal monitoring of the polluted area throughout the period of my PhD.

Other three sites (Fig.2), with the same geolithological characteristics, a few hundreds meters far from the polluted site, have been investigated to establish a background referring radon, to identify negative anomalies in the study area. In these areas values of concentration of ^{222}Rn, ^{220}Rn, CO_2 and intrinsic permeability of soil, have been measured seasonally at 80cm depth.

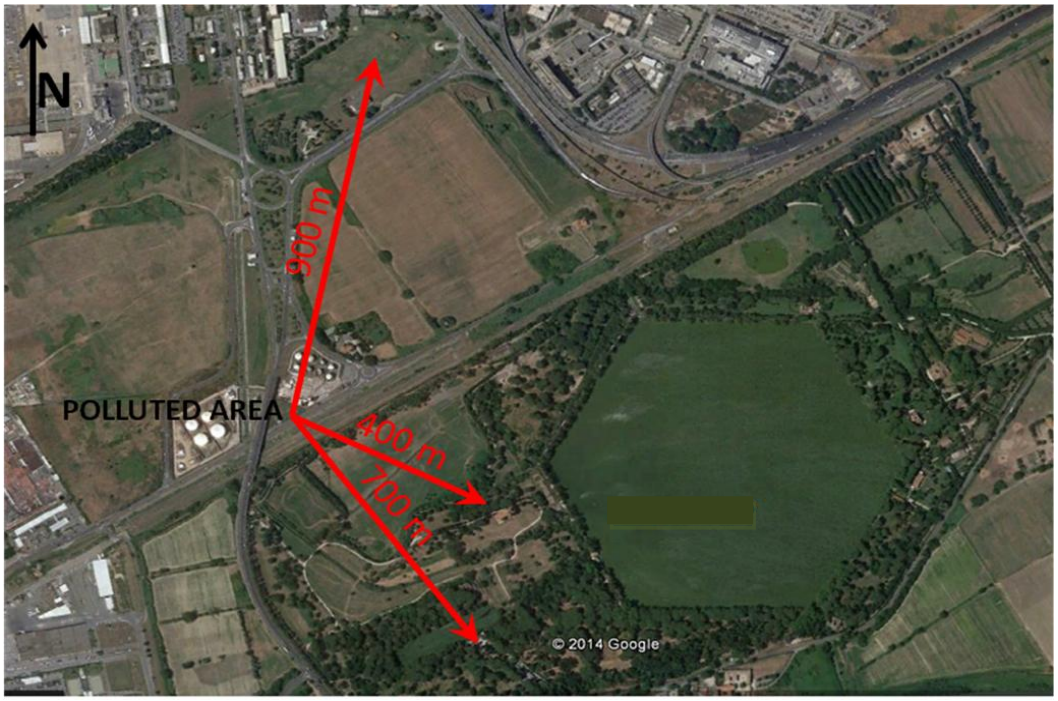

Fig. 2 Background areas

In the study area and in the background sites, data were seasonaly collected from 2013 to 2016. A series of maps was created for each measurement campaign. They are reported in the Appendix.

CHAPTER 3

TRACING NAPLS CONTAMINATION IN THE VADOSE ZONE USING SOIL RADON

Tuccimei P. (a), De Simone G. (a), Curatolo P. (b), Giorgi R. (b), Lucchetti C. (a), Castelluccio M. (a) & Calì A. (b)

(a) Dipartimento di Scienze, Università "Roma Tre", Largo San Leonardo Murialdo 1, 00146 Roma, Italy. E-mail: paola.tuccimei@uniroma3.it

(b) Golder Associates, Roma, Via Sante Bargellini 4, 00157 Roma, Italy

Abstract

Frequent spills of Non-Aqueous Phase Liquids (NAPLs), such as petroleum products or chlorinated solvents, occur all around the world contaminating the soil vadose zone or the aquifer. In order to trace the presence of these substances, radon concentration in soil gas can be employed because of its high solubility in NAPLs. Radon available in the soil pores accumulates in the NAPLs producing a local decrease of its concentration in the vicinity of contaminated area. Thus radon minima in the vadose zone can be used to localize NAPL plumes indirectly.

The suitability of this method is here checked by laboratory simulation of a gasoline spill within a known volume of soil. Radon activity concentration strongly drops down right after the injection of gasoline and progressively increases in the following days. This trend is compared with data from a simultaneous experiment carried out on a volume of the same soil, not contaminated by NAPL.

Finally, an example of field measurements within a site affected by NAPL contamination is documented. Mapping of soil radon concentration at 80 cm depth shows an area where radon deficit is evident. This region is aligned along the directions of groundwater flow induced by pumping for safety operation of the plant. Radon negative anomalies are not due to low gas permeability and are not correlated with soil CO^2. The comparison of soil gas data with those from nearby background areas confirm the soundness of premises.

Introduction

One of the major problems facing prior-remediation risk assessment at abandoned and/or polluted industrial sites, military bases and petrol stations is ground contamination by non-aqueous phase-liquids (NAPLs) such as fuels or mineral oils. Before appropriate clean-up measures can be designed, the distribution of the contaminants in the subsurface has to be explored and its extent traced.

Therefore on-site activities usually begin with drive point profiling, the actual examination points being located either close to the contamination source or, if known, inside the zone that covers the plume of the contamination. However, because of the given local infrastructure or due to low investigation budgets, the number of such soil sampling points is often limited. Consequently it is hardly ever possible to satisfactorily trace the shape of subsurface NAPL contamination, and this may cause wrong decisions concerning the remediation action.

In order to obtain a sufficiently detailed picture of ground contamination, a complementary detection method which allows a denser network of monitoring points should be desirable (Schubert et al., 2002).

The radioactive noble gas radon, a naturally occurring component of soil gas, exhibits very good solubility in a wide range of NAPLs (Barton, 1991; Lewis et al., 1987, Schubert et al., 2002). Consequently, and given the problems outlined above, the idea was put forward that subsurface NAPL contamination partly traps the soil gas radon, resulting in a local reduction of the soil gas radon concentration in the vicinity of the contaminated soil volume (fig. 1).

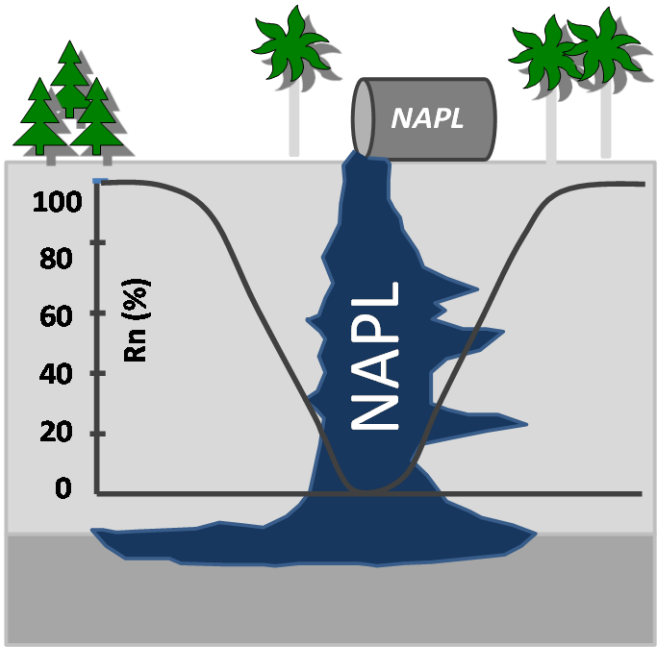

Fig.1 - Local reduction of the soil radon concentration in the area surrounding the contaminated soil volume. Modified after Schubert et al. (2002)

Provided this "NAPL-Effect" is significant, a NAPL contamination could be indirectly localized by carrying out a straightforward radon survey on a sampling grid covering the suspected area.

The aim of this investigation is to verify this principle, reproducing in the laboratory a gasoline spill within a volcanic bedrock and monitor soil radon concentration over a month–period. An example of direct application of this method to a real contaminated site is also presented.

Simulation of a gasoline spill and related radon gas evolution

A large garbage bin was filled with "Tufo di Villa Senni" ignimbrite, a volcanic product available in large quantities in the city of Rome. A PVC tubing (evidenced in blue in fig.2a) allowed us to inject gasoline at the bottom of the container.

An hollow probe was driven into the terrain at a depth of 40 cm, about 10-15 cm above the contaminated soil volume and connected via vynil tubing to a dying unit (identified

as drierite in fig.2a) and to RAD7 radon monitor (Durridge Co.).Soil radon was measured twice before the gasoline injection, immediately after the spill, and five times more in the following weeks. Figure 2b shows clearly the abrupt drop of concentration right after the NAPL input and a gradual increase of soil radon values over time due to progressive volatilization of the gasoline. The recovery of pristine concentration was not obtained indicating the presence of residual NAPL that still accumulates radon, producing a radon deficit.

This demonstrates the potential of radon in soil gas to detect the presence of residual NAPL in the vadose zone of an aquifer.

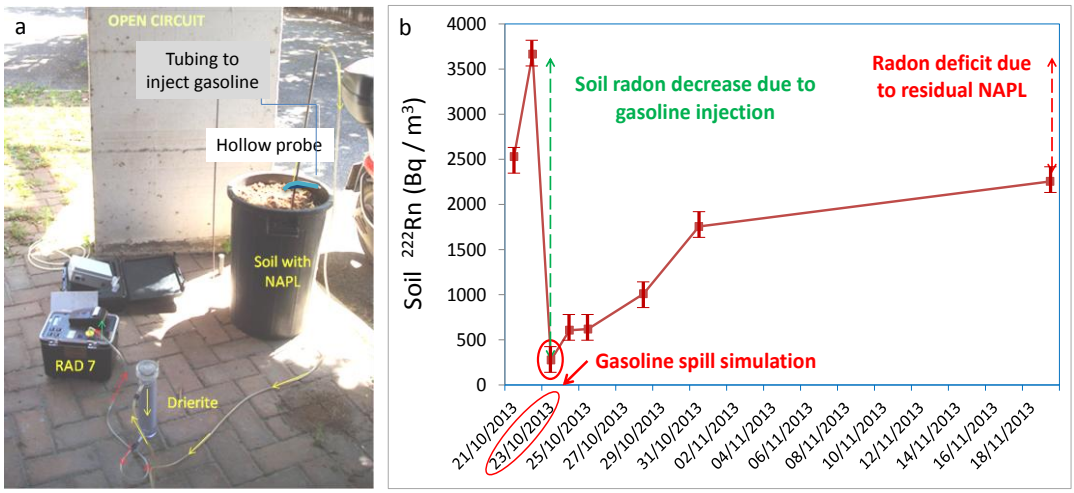

Fig. 2 –Experimental set-up used to simulate a gasoline spill and monitor related soil radon concentration evolution (a). Radon activity concentration in soil gas during the test (b).

Example of radon and CO_2 mapping in a real contaminated site

The "radon-deficit technique", firstly called this way by Semprini et al (1998), was applied to a real contaminated site whose location and coordinates are omitted for confidentiality agreement.

The work was performed in a site of Latium Region (Italy) where a hydrocarbons spill occurred and traditional remediation techniques are accomplished. The area is equipped

with wells and piezometers for routine sampling and analysis of pollutants that provide an immediate feedback to this approach. The stratigraphic section from ground level downward consists of about 0.5 m of backfills, 2.5 m of medium sands and 2.5 m of medium-fine sands. The water table fluctuates in the range 0.5 – 2.5 m depth during the year.

A grid of 31 measuring stations was created over a 3000 m^2 large zone, where soil ^{222}Rn, ^{220}Rn, CO_2, CH_4 and intrinsic permeability were determined at 80 cm depth. A survey station was installed in the central part of the study area to evaluate soil gas concentration variability as a function of meteorological parameters. The station acquires soil temperature and humidity at 30 and 80 cm depth, in order to assess how relevant rainfalls influence water content in the soil, reducing gas release at soil/atmosphere interface.

Soil gas and permeability surveys were performed at the end of the winter in the contaminated site and in a background area, located few hundred meters far away. Similar grids with multiple measuring stations were used here.

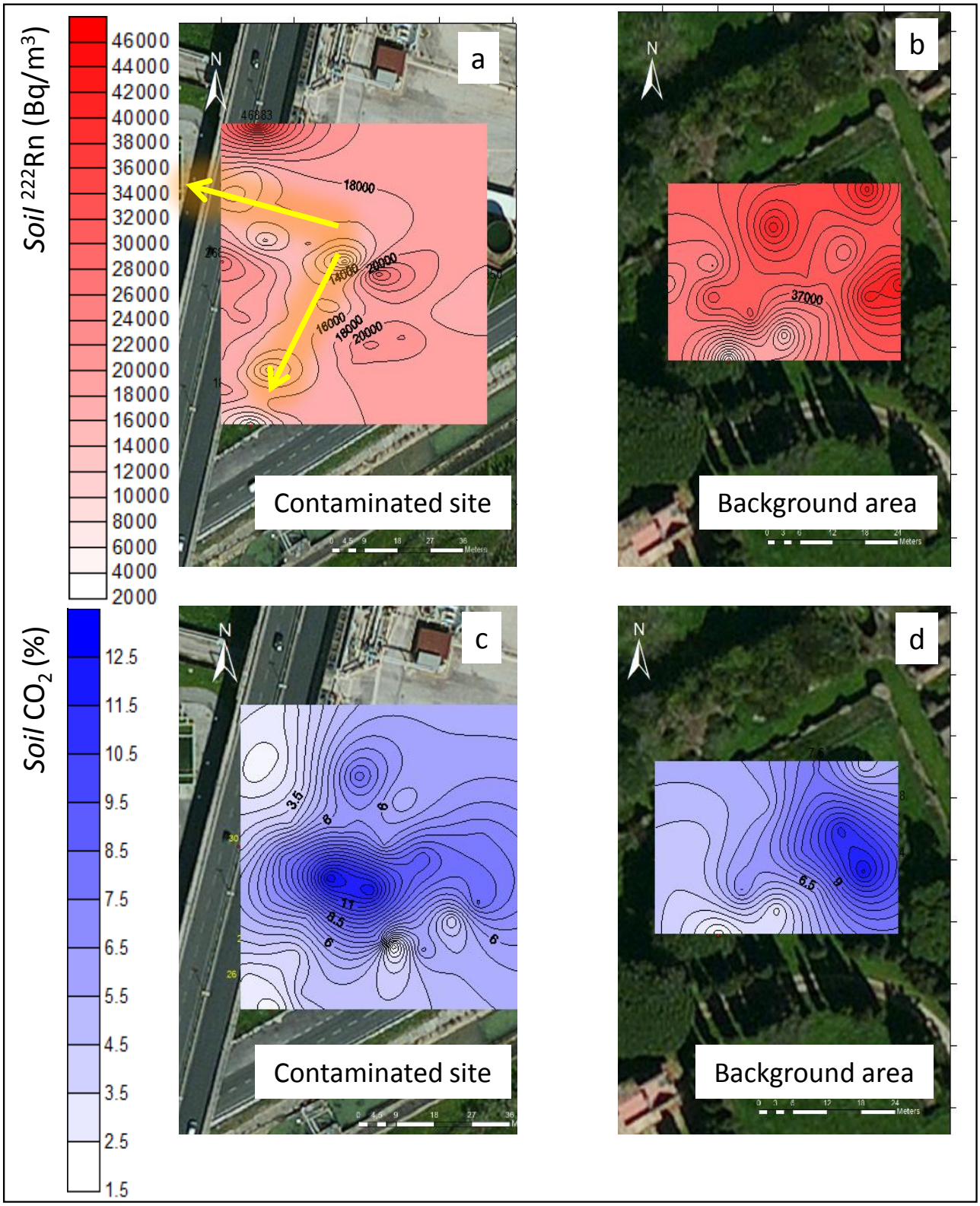

Fig. 3 – Soil ^{222}Rn concentration in the contaminated site (a) and in the background area (b). Soil CO_2 concentration in the contaminated site (c) and in the background area (d).

Winter maps of soil ^{222}Rn concentration in the contaminated area (fig. 3a) and in the background site (fig. 3b) where created using the program Surfer. Figure 2 shows that winter radon concentrations in the study area are, on average, much lower than in the background zone. In particular, radon lower concentrations in the background are around 22,000–23,000 Bq/m^3, while the lowest values in the study area stay around 2,000 – 5000 Bq/m^3, in spite of similar stratigraphy and measuring period. This region is aligned along the directions of groundwater flow induced by pumping for safety operation of the plant (fig. 3a).

Radon negative anomalies in the contaminated site are not due to low soil gas permeability because this parameter is substantially constant everywhere and always reaches high values (> 4.0 · 10-12 m^2).

Another significant result is related to the spatial correlation between soil ^{222}Rn and CO^2. In the background area, the two gases are directly correlated (fig. 3b and 3d) because CO^2 works as carrier for radon. On the other hand, radon minima in fig. 3a are not correlated with CO^2 negative values (fig. 3c), because carbon dioxide is not soluble in NAPL and is not trapped and accumulated by NAPLs. Consequently the highest CO^2 concentrations are located where radon deficits and residual NAPL occur. This finding could be also due to a process of microbial degradation of the NAPL in the subsoil.

Conclusions

The use of the soil radon deficit to delineate the spatial extent of NAPL-bearing zones is demonstrated either by laboratory simulation of a NAPL spill, or through multi-parameter monitoring and mapping in a contaminated site in Latium Region (Italy).

The use of this technique is fruitful to obtain a sufficiently detailed picture of ground contamination for the preliminary evaluation of NAPL contaminated sites to be joined with conventional investigation methods such as drive point profiling or the direct detection of organic carbons and their derivatives in the soil gas.,

In addition, it may be employed to assess the effectiveness of NAPL remediation and to provide an indicator that NAPL has been removed.

Despite the potential suitability of radon surveys as a tool for investigating subsurface NAPL contamination, the detection method presented here also has its limitations. The sensitivity depends on the depth of contamination that is within the range of the diffusion length of radon in soil (plus the depths from which the soil gas samples are taken from). The diffusion length of radon in soil is about 2 meters in dry and sandy soils and even less in more dense/impervious materials.

Finally summer season enhances gas exhalation from soil reducing and partly annealing the radon minima which are much more evident in winter when topsoil behaves as a closed system to radon release to the atmosphere.

References

Barton A. F. M. (1991) - Handbook of solubility parameters and other cohesion parameters 2nd ed., CRC Boca Raton/FL/USA.

Lewis C., Hopke P. K. & Stukel J. (1987) - Solubility of radon in selected perfluorocarbon compounds and water. Industrial Engineering & Chemical Research, 26, 356-359.

Schubert M., Freyer K., Treutler H. C. & Weiss H. (2002) - Using radon-222 in soil gas as an indicator of subsurface contamination by non-aqueous phase-liquids (NAPLs). Geofísica Internacional, 41, 433-437.

Semprini L., Hopkins O.S. & Tasker B.R. (2000) - Laboratory, field, and modeling studies of Radon-222 as a natural tracer for monitoring NAPL contamination." Transport in Porous Media, 38, 223-240.

CHAPTER 4

USING NATURAL RADON AS A TRACER OF GASOLINE CONTAMINATION

*Gabriele De Simone a, Gianfranco Galli b, Carlo Lucchetti a, Paola Tuccimei a**

a: Dipartimento di Scienze, Universit. a "Roma Tre", Roma, Italy

b: Istituto Nazionale di Geofisica e Vulcanologia, Sezione Roma, Roma, Italy

Abstract

Radon concentration in soil gas can be employed to trace the presence of gasoline contamination because it is very soluble in hydrocarbons. Radon available in the soil pores accumulates in the contaminated volume, producing a local deficit at shallow depth that can be easily mapped. The suitability of this method is here checked by field simulation of a gasoline spill and by laboratory experiments where known amounts of a volcanic tuff contaminated with increasing gasoline show proportional drops of radon exhalation rates.

Introduction

Spills of gasoline, or other Non-Aqueous Phase-Liquids (NAPLs) can lead to significant contamination if not handled quickly and properly. Any appropriate actions need a good knowledge of the contaminant extension in the subsoil. Standard practice is to excavate visible contamination or to drill monitoring-wells for the purpose of collecting samples for analysis. However, it is expensive and difficult to satisfactorily trace the shape of subsurface NAPL pollution this way. In order to obtain a sufficiently detailed picture of ground contamination, a complementary detection method which allows a denser network of monitoring points should be desirable [1]. The radioactive noble gas radon, a naturally occurring component of soil gas, exhibits very good solubility in a wide range of NAPLs [1, 2, 3]. Consequently, subsurface NAPL contamination partly traps the soil gas radon,

resulting in a local reduction of the soil gas radon concentration in the vicinity of the contaminated soil volume (Fig.1).

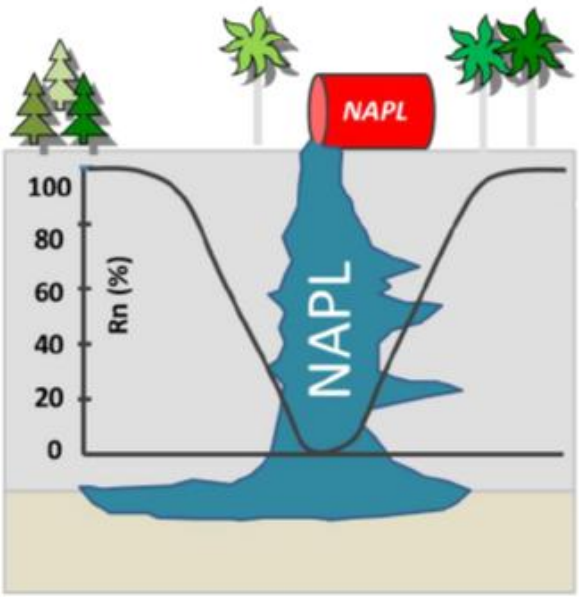

Fig. 1. Local reduction of soil radon concentration in the area surrounding the contaminated soil volume. Modified after Schubert et al. [1]

Provided this “NAPL-Effect” is significant, a NAPL contamination could be indirectly localized by carrying out a straightforward radon survey on a sampling grid covering the suspected area.

The aim of this investigation is to verify the principle, reproducing a gasoline spill within a volcanic bedrock and monitor soil radon concentration over following weeks. Laboratory tests are also presented to quantify radon exhalation decrease as a function of volumes of added gasoline.

Simulation of gasoline spills

In order to verify the principle, gasoline spills were reproduced in the laboratory and in the field, choosing a volcanic bedrock because of its high radon activity concentration (100 – 200 kBq/m^3). Radon in soil gas was then monitored over following weeks to assess its evolution.

Laboratory simulation of a gasoline spill

A large garbage bin was filled with “Tufo di Villa Senni” ignimbrite, a volcanic product available in large quantities in the city of Rome. A PVC tubing (evidenced in blue in Fig. 2a) allowed us to inject gasoline at the bottom of the container. A hollow probe was driven into the terrain at a depth of 40 cm, about 10-15 cm above the contaminated soil volume and connected via vinyl tubing to a drying unit (identified as drierite in Fig. 2a) and to RAD7 radon monitor (Durridge Co.).

Soil radon was measured twice before the gasoline injection, immediately after the spill, and five times more in the following weeks. Fig. 2b shows clearly the abrupt drop of concentration right after the NAPL input and a gradual increase of soil radon values over time due to progressive volatilization of the gasoline. The recovery of pristine

concentration was not obtained, indicating the presence of residual NAPL that still accumulates radon, producing a radon deficit. This demonstrates the potential of radon in soil gas to detect the presence of residual NAPL in the vadose zone of an aquifer.

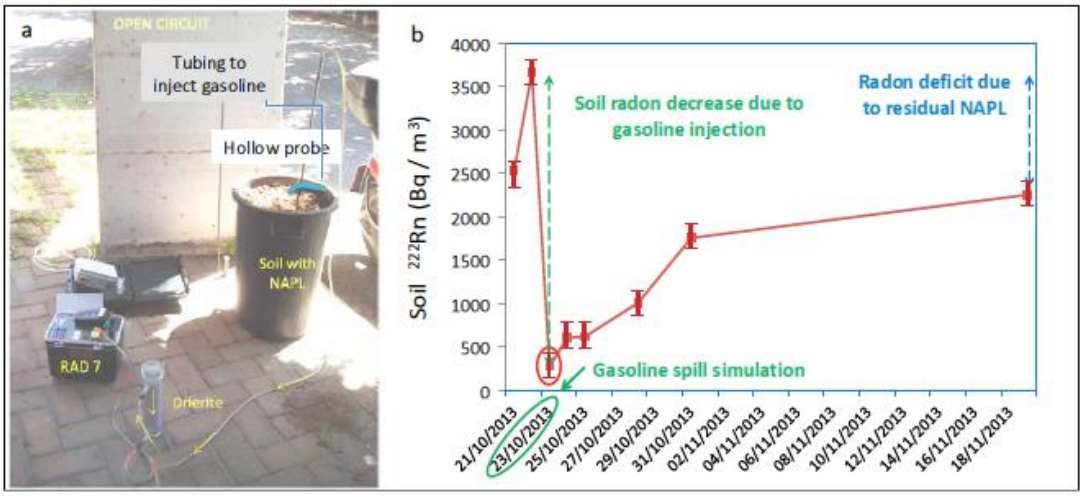

Fig. 2. Experimental set-up used to simulate a gasoline spill and monitor related soil radon concentration evolution (a). Radon activity concentration in soil gas during the test (b).

Field simulation of a gasoline spill

A second spill was reproduced in Vallerano town (Lazio Region, Italy), where pyroclastic flow deposits (Ignimbrite D) from Vico volcano outcrop. Two liters of gasoline were poured in the center of the area at 80 cm depth and soil radon was monitored at 15 sampling stations using a grid of 3x5 m, before, just after the spill and over the following months. Soil radon concentration at the spill point fell from about 700 to 7 kBq/m^3 (few hours after the contamination event). A week later the concentration was still the same, but increased up to about 60 kBq/m3 four months later. It is worth noting that the deficit effect was closely restricted to the contaminated station, because sites located just 3 meters apart just showed slight decreases around half or one third of the starting value. Stations at five meters distance did not display any departure from initial condition (Fig. 3).

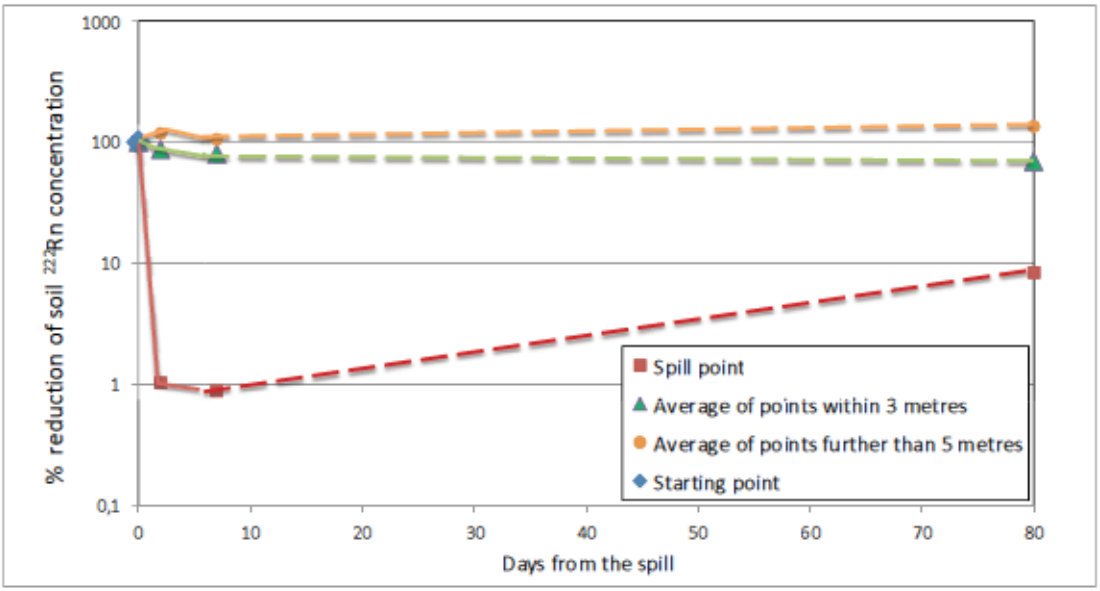

Fig. 3. Percent reduction of soil radon concentration in Vallerano (Lazio Region, Italy), following a simulated gasoline spill at different monitoring stations located over a 3 x 5 m grid of 15 measurements points.

The presence of gasoline is very well indicated by high concentration of H_2S (up to about 370 ppm at the spill point), due to the residual sulphur component in the gasoline after the oil refining process.

Decrease of radon exhalation rate of a volcanic material induced by addition of gasoline

Seven hundreds grams of a volcanic material (Villa Senni tuff from Colli Albani volcano, Roma, Italy) have been grounded, dried at 100°C and placed in a stainless steel accumulation chamber, connected to a drying device (drierite) and to the radon monitor in a closed-loop circuit. The chamber is located in a thermo-refrigerating bath, set at 35°C to keep constant temperature during the measurement and enhance the raon exhalation [4]. The different experiments were carried out adding different amount of gasoline (from 0 to 25 mL) to the tuff, resulting in gasoline/material ratios (mL/kg) from 0 to 50. Each tests had a duration of 24 hours, with 12 two hours long cycles,

keeping relative humidity below 10% inside the radon monitor. As reported in Fig, 4, radon mass exhalation rates exponentially reduce with increasing gasoline volumes, probably because more radon is progressively dissolved in gasoline. These experiments need a further control in order to assess if drierite absorbs vaporized gasoline where radon is partly dissolved.

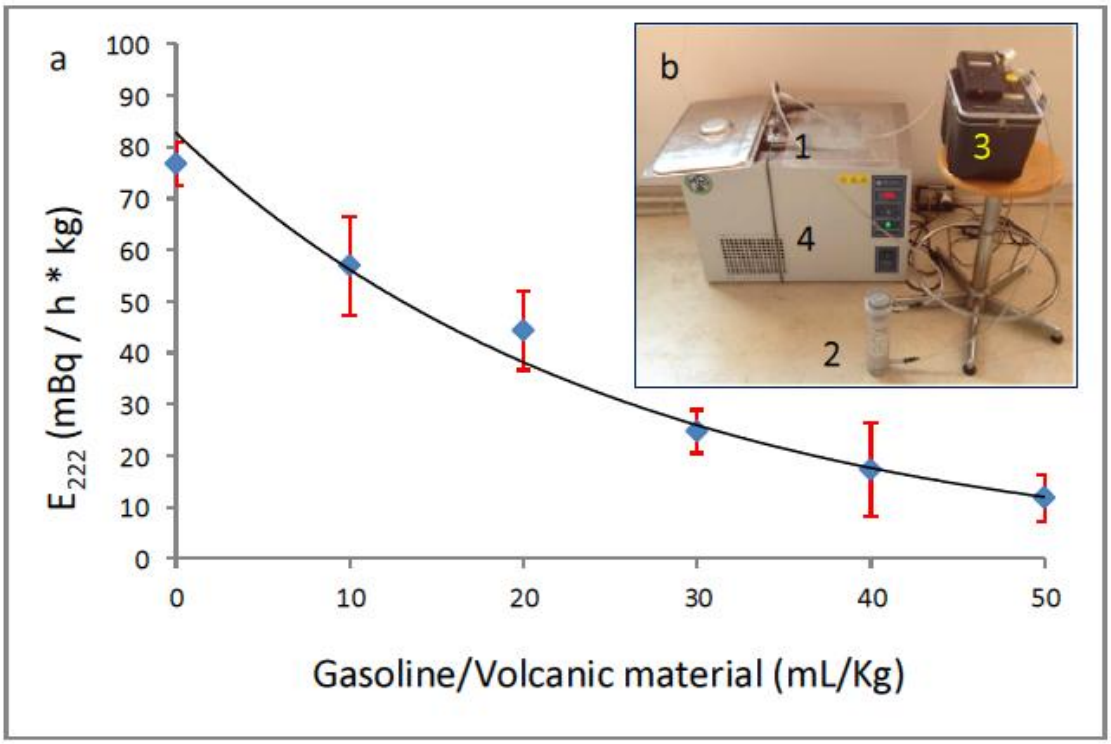

Fig. 4. Decrease of radon exhalation rate of Villa Senni tuff induced by the addition of different volumes of gasoline (a). The experimental set-up consists of: the accumulation chamber containing the contaminated volcanic material (1), the drierite (2), the radon monitor (3), the thermorefrigerating bath (4), connected by vinyl tubing in a closed-loop circuit (b).

References

1. Schubert M, Freyer K, Treutler HC, Weiss H. Using radon-222 in soil gas as an indicator of subsurface contamination by non-aqueous phaseliquids (NAPLs). Geofísica Internacional 2002; 41: 433-437.

2. Barton AFM. Handbook of solubility parameters and other cohesion parameters. 2nd ed. Boca Raton/FL/USA: CRC; 1991.

3. Lewis C, Hopke PK, Stukel J. Solubility of radon in selected perfluorocarbon compounds and water. Industrial Engineering & Chemical Research 1987; 26: 356-359.

4. Tuccimei P, Castelluccio M, Moretti S, Mollo S, Vinciguerra S, Scarlato P. Thermal enhancement of radon emission From geological materials. Implications For laboratory experiments on rocks under increasing deformation. In: Benjamin V, Szigethy J, editors. Horizons in Earth Science Research, Volume 4, New York: Nova Science Publishers; 2011. p. 247-256.

CHAPTER 5

LABORATORY SIMULATION OF RECENT NAPL SPILLS TO INVESTIGATE RADON PARTITION AMONG NAPL VAPOURS AND SOIL AIR.

Gabriele De Simone a, Carlo Lucchetti a,Francesca Pompilj a, Gianfranco Galli b, Paola Tuccimei a.

a: Dipartimento di Scienze, Universit. a “Roma Tre”, Roma, Italy

b: Istituto Nazionale di Geofisica e Vulcanologia, Sezione Roma, Roma, Italy

Abstract

Soil radon is employed to trace residual NAPL (Non-Aqueous Phase Liquid) contamination because it is very soluble in these substances and is strongly depleted over polluted volumes of the subsoil. The solubility of radon into NAPL vapors, generally poorly considered, is investigated here, either as growth of radon exhalation from a material contaminated with increasing volumes of kerosene, or as radon partition between liquid kerosene, water and total air, considered ad the sum of kerosene vapors plus air.

Radon concentration in soil gas can be employed to trace the presence of gasoline contamination because it is very soluble in hydrocarbons. Radon available in the soil pores accumulates in the contaminated volume, producing a local deficit at shallow

depth that can be easily mapped. The suitability of this method is here checked by field simulation of a gasoline spill and by laboratory experiments where known amounts of a volcanic tuff contaminated with increasing gasoline show proportional drops of radon exhalation rates.

1. Introduction

In the last two decades radon has been used as environmental tracer for the localization and assessment of residual Non-Aqueous Phase Liquid (NAPL) contamination in soil (Semprini et al., 2000; Hohener and Surbeck, 2004; Schubert et al, 2001; 2005; 2015). It was shown that a local radon deficit (compared to site specific radon background concentration) corresponds to portions of the subsoil that are contaminated with NAPL, because of preferential partitioning of radon into the residual organic phase. Hence, carrying out a straightforward survey of the local radon distribution pattern in the soil gas allows to localize the contaminated zone (Schubert et al., 2015).

Nevertheless, quantitative estimation of the NAPL saturation of the soil pore space requires the knowledge of the radon partition coefficient specific for the NAPL present. This study focuses on the role of the vaporized fraction of NAPL on changes of radon concentration in the soil gas in case of recent spill, when a significant amount of vapors can be still found in the soil gas. The phenomenon is investigated through laboratory experiments regarding either the growth of radon exhalation from material contaminated with increasing volumes of kerosene, or the determination of radon partition between liquid kerosene, water and air, with NAPL vapors enhancing radon transport in the air. Many instruments employed to measure radon (such as RAD7 produced by Durridge Company Inc. or Trace Environmental Level detector by Pylon Electronics Inc.) make use of a desiccant, such as drierite (WA Hammond Drierite Co., Ltd) to avoid the interference of water molecules on the electrostatic collection of radon daughters (De Simone et al., 2016), but drierite is suspected to absorb NAPL vapors, capturing the radon dissolved in it, as well (De Simone et al., 2016), so the desiccant is not introduced in the experimental set-up. However, it is still possible to use electrostatic collection-

based radon monitors, provided that proper corrections for absolute humidity are applied, as in the case of RAD7 (De Simone et al., 2016).

2. Material and Methods

The soil used for the experiments is of volcanic origin and has been collected from Valle della Caffarella area (Roma, Italy) where ignimbrites from Colli Albani Volcano largely outcrop. This kind of material (known as Pozzolanelle ignimbrite) is a member of Villa Senni Unit and has been chosen for the experiments because it is enriched in ^{226}Ra (150 ± 5 Bq/kg) and ^{232}Th (221 ± 5 Bq/kg), precursors of ^{222}Rn and ^{220}Rn, respectively (Castelluccio, 2010).

Groundwater employed for the determination of radon partition coefficient between kerosene, water and air is very rich in ^{222}Rn (238 ± 2 Bq/L, Lucchetti et al., 2016) because it circulates within a volcanic aquifer related to Colli Albani volcano ("Complesso delle Vulcaniti Indifferenziate" hydrogeological unit, Capelli et al., 2012).

Kerosene used for the experiments is distributed by PIC S.r.l., as "Petrolio Bianco", white petroleum. It is a clear liquid formed from hydrocarbons obtained from the fractional distillation of petroleum between 150 °C and 275 °C, resulting in a mixture with a density of 0.78–0.81 g/cm^3 composed of carbon chains that typically contain between 6 and 16 carbon atoms per molecule.

The accumulation chamber is a modified pressure cooker, connected to a RAD7 radon monitor (Durridge Co.) in a closed-loop circuit. The description of the experimental set-up can be found in Tuccimei et al. (2009; 2011).

Radon contained in water solution was captured onto charcoal canister and counted using a NaI(Tl) scintillator (3 × 3 in.), optically coupled to a photomultiplier, at INGV laboratories, Roma (see Lucchetti et al., 2016).

Volatile Organic Compounds (VOCs) concentration was determined using a MiniRaeLite (Extratech) photoionization detector, equipped with a built-in pump to sample the air in the closed-loop circuit.

3. Experimental

3.1 Measurements of radon exhalation at increasing kerosene content

Experiment 1

The experimental setup used for experiment 1 is reported in Fig. 1. The experiment configuration, consists of: i) an accumulation chamber where 650 g of a dried ignimbrite are placed; ii) vinyl tubing to connect the chamber to a radon monitor in a closed-loop array; iii) a RAD7 radon monitor (Durridge Co.) kept in a laboratory oven set at 43; °C and iv) a thermo-refrigerating bath hosting the accumulation chamber, set at 35°C to keep the exhalation temperature at constant condition. This procedure was planned to guarantee a nominal temperature difference of 8°C between the radon monitor and the accumulation chamber to avoid condensation effects of NAPL on the surface of the silicon detector, considering that no drierite or other traps are included in the circuit.

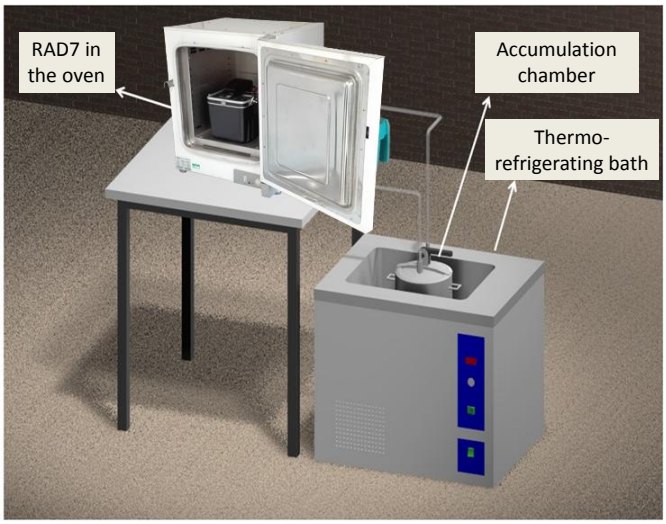

Fig.1. Set-up used for experiment 1. See text for explanation.

Several tests were carried out to quantify the effect of increasing kerosene content (0, 5 10, 15, 20, 25 mL) on radon exhalation. At the end of each test (24-hour long), the amount of kerosene vapors was measured by introducing a MiniRae Lite photo-ionization detector (Extratech) for total Volatile Organic Carbon (VOC) in the circuit. Proper clamps were employed to avoid the loss of air during the insertion of the Minirae Lite. Radon exhalation rate (E_{220}, Bq h^{-1} kg^{-1}) was calculated from each test using the ^{220}Rn (thoron) signal which was stronger than that of ^{222}Rn and reached the equilibrium already in the first 2-hour cycle. Exhalation rates (E_{220}) were obtained according the following equation:

$$E_{220} = {}^{220}Rn_C * V_b * \lambda_{220} / M \qquad \textit{(equation 1)}$$

where:

$^{220}Rn_C$ (Bq/m^3) = average thoron activity concentration (^{220}Rn), corrected for decay occurred during transport from the accumulation chamber to RAD7 and for the water interference

V_b (m^3) = total free volume of the circuit (0.0053 m^3)

λ_{220} (h^{-1}) = ^{220}Rn decay constant

M (kg) = mass of dried material (about 0.650 kg)

The average thoron activity concentration is calculated as follows:

$^{220}Rn_C$ *(Bq/m^3)* = ^{220}Rn / *(W * D)*
(equation 2)

with

W = correction, if necessary, for the water content in RAD7 that reduces the efficiency of the silicon detector (see De Simone et al., 2016)

D = correction for decay.

3.2 Determination of radon partition coefficients between kerosene, water and air

Experiment 2 (I-type)

A large volume of spring water was sampled and transferred into a water enricher, to keep it well-mixed by continuous circulation. About 0.58 L were spilled into a bottle, where dissolved radon was stripped by air bubbling, absorbed onto a charcoal canister and gamma-counted (Galli et al., 1999); 0.37 L were introduced into the stopper of a 0.73 L separatory funnel placed upside down, where 0.37 L of kerosene had been previously added (Fig. 2a). Consequently, a ratio of 1 : 1 between kerosene and water was obtained, as in Schubert et al. (2005).

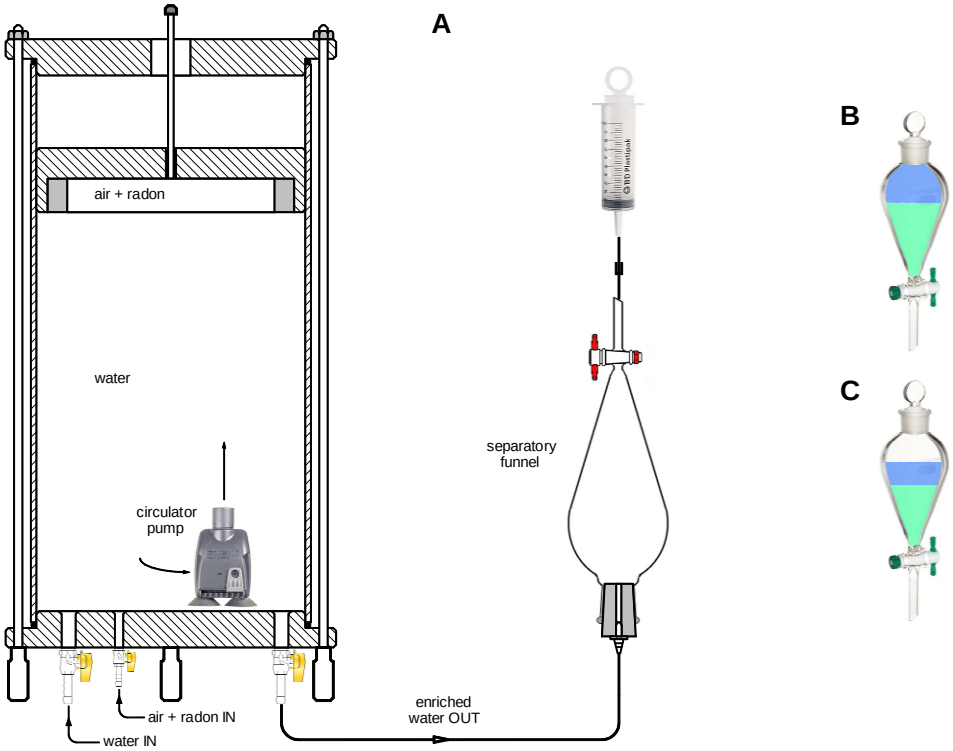

Fig. 2. Set-up used for experiment 2 (Fig. 2a). Separatory funnel for determination of radon partition coefficients between kerosene and water (I-type, Fig. 2b) and between kerosene-water-air (II- and III-type Fig. 2c).

The separatory funnel was then vigorously shaked for 3 minutes and after a time of 5 minutes, necessary for the complete separation of the phases, water was collected from the funnel (now in normal position, Fig. 2b) into another 0.58 L bottle. Radon was then stripped from the bottle, absorbed onto a charcoal canister and counted. This procedure was repeated four times for calculating radon partition coefficient between kerosene and water.

Radon partition coefficient between kerosene and water ($K_{ker\text{-}wat}$) was calculated according to the following equation:

$$K_{ker\text{-}wat} = (C_1 - C_2) / C_2 \qquad \textit{(equation 3)}$$

where:

C_1 (Bq/L) = ^{222}Rn activity concentration in the spring water before the separation C_2 (Bq/L) = ^{222}Rn activity concentration in the water after the separation

This type of experiment was performed at 22°C.

Experiment 2 (II-type and III-type)

The same procedure, conveniently modified, was replicated 13 times for determining radon partition coefficients among kerosene, water and air. In this group of tests, we changed the volumes of reacting phases to 0.05 : 1 : 1 (kerosene : water : air) and experimental temperature was increased at 32°C (the same conditions of experiment 1). This set of trials was organized in two parts where partition between kerosene-water (II-type) and water-air (III-type) was investigated separately, since only one phase (water or air) can be analyzed at a time, otherwise radon partition may be altered.

The procedure for the II-type tests has been already described, with the only difference regarding volumes of employed phases (0.36 L of water and air and 0.018 L of kerosene, Fig. 2c). As in this case the volume of water is not enough to fill the 0.58 L bottle, a complementary volume of water without radon (0.22 L) had been previously added. III-type tests were repeated with a separatory funnel according to the above procedure, but aspiring air from the top of the funnel turned upside down, using a syringe and enhancing this extraction by adding a correspondent volume of water from the stopper. Extracted air was then injected into a 2.7 L radon free chamber (previously evacuated of a correspondent air volume), connected to a pumping system and to a charcoal canister where the aliquot of radon previously delivered to the air phase is captured and then counted by gamma spectrometry. The background radon

concentration into radon chamber was measured and subtracted to the radon partitioned in the air phase.

Radon partition coefficient between kerosene and water from II-type tests was calculated according to a modified version of equation 3:

$$K_{ker\text{-}wat} = (C_1 - C_2 - C_{3m}) / C_2 \qquad \textit{(equation 4)}$$

where C_{3m} (Bq/L) = average of ^{222}Rn activity concentration in the air from III-type test carried out in similar experimental conditions.

Radon partition coefficient between kerosene and air ($K_{ker\text{-}air}$) was calculated according to the following equation:

$$K_{ker\text{-}tot\ air} = (C_1 - C_3 - C_{2m}) / C_3 \qquad \textit{(equation 5)}$$

where:

C_3 (Bq/L) = ^{222}Rn activity concentration in the air after the separation

C_{2m} (Bq/L) = average of ^{222}Rn activity concentration in the water from II-type test carried out in similar experimental conditions.

Duration of mixing and waiting times for phases separation was increased once (tests 15 and 16 in Table 2) at 15 an 90 minutes, respectively as in Schubert (2005), to verify the efficiency of radon extraction and separation.

4. Results and discussion

4.1 Change of radon exhalation at increasing gasoline content without desiccant (experiment 1)

This experiment simulates a recent spill of kerosene with a significant aliquot of vapors still present in the soil. The effect of increasing kerosene content on ^{220}Rn exhalation

from Pozzolanelle ignimbrite is displayed in Fig. 3a. Each data point was obtained from the ratio between the exhalation rate of an aliquot of material not contaminated with kerosene (defined as blank) and the same portion of ignimbrite doped with kerosene, in order to take into account the natural variability of this kind of volcanic product. Obtained data are reported in Table 1.

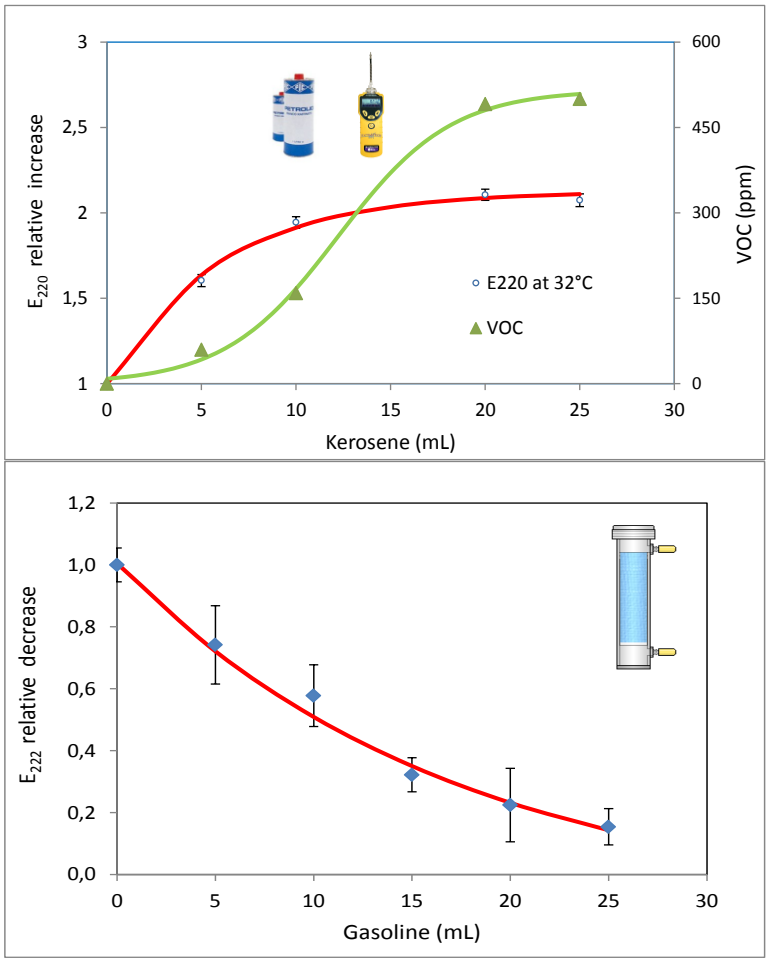

Fig. 3. Increase of relative radon (^{220}Rn) exhalation rate of Pozzolanelle ignimbrite at growing kerosene content from experiment 1. Drierite was not used to dry air in the circuit; VOC concentration was measured using a MiniRaeLite (Extratech) photoionization detector (Fig. 3a). Relative decrease of radon (^{222}Rn) exhalation rate from Pozzolanelle *ignimbrite at growing NAPL content (gasoline), with desiccant included in the circuit (Fig. 3b), modified from De Simone et al. (2015).*

Although temperature of the thermo-refrigerating bath was set at 35°C, the effective exhalation temperature inside the accumulation chamber was 32°C, as recorded by a relative humidity / thermocouple data logger placed inside.

Table 1
Data set from experiment 1.

Kerosene (mL)	$E_{220\ at\ 32°C}$ (kBq / h * Kg)	$E_{220\ at\ 32°C}$ BLANK (kBq / h * Kg)	E_{220} relative increase at 32°C	VOC (ppm) *
0	15.2 ± 0.1	15.2 ± 0.1	1.00 ± 0.01	0
5	24.3 ± 0.5	15.2 ± 0.1	1.60 ± 0.04	59
10	31.7 ± 0.3	16.3 ± 0.2	1.94 ± 0.03	159
20	32.2 ± 0.3	15.3 ± 0.2	2.09 ± 0.03	491
25	27.6 ± 0.3	13.3 ± 0.2	2.11 ± 0.04	500

*uncertaintines are about 5%

Figure 3a shows that ^{220}Rn exhalation rate progressively rises at increasing kerosene contents up to a plateau value. The VOC trend demonstrates that also NAPL vapors rise up to a constant concentration (500 ppm) when the volume of the added kerosene is greater than 20 mL. This could be due to the transport of NAPL vapors through the experimental circuit, which enhance radon concentration in the air because of its preferential partitioning in the kerosene vapors (detected as VOC). Both VOC and radon concentration in the air phase reach equilibrium conditions when stable NAPL and radon partition between phases are reached.

This trend is opposite to what observed by De Simone et al. (2015) who performed similar experiments using drierite in the circuit (Fig. 3b) which absorbed NAPL vapors (gasoline in that case) along with its dissolved radon content, reducing the relative radon exhalation rate. Experiment 1 demonstrated that radon is preferentially dissolved in NAPL, compared to air. The effect of radon partitioning by NAPL vapors prevails

over that of radon dissolution in the liquid NAPL absorbed by the ignimbrite (comparable to the residual component in case of ancient spills).

4.2 Radon partition coefficients among kerosene, water and air (experiment 2)

In order to quantify the partition of radon among kerosene, water and air (comprising the NAPL vapors component), experiment 2 was carried out using kerosene. Experimental results are reported in Table 2.

Average partition coefficient between kerosene and water at 22°C is equal to 19.8 ± 3.4 (I-type test), which is much lower than values reported by Schubert et al. (2005) at 20°C (55.6 ± 6.3), for a mixture of hexadecane, 1,2-dimethylcyclohexane and 1-hexadecene in equal proportions, named as "petroleum", but referred to as "kerosene" in Schubert et al. (2007). Probably, the efficiency of radon stripping from the spring water was not complete during the mixing because of the large volume of kerosene which did not produce an effective radon exchange between water and kerosene bubbles. This is why experiment 2 (II- and III-types) was carried out, reducing the volume of kerosene, compared to that of water and air to 0.05 : 1 : 1.

Average partition coefficient between kerosene and water at 32°C (II-type test), is equal to 35.8 ± 3.4 (II-type test). Results are still lower than those reported by Schubert et al. (2005) at 20°C (55.6 ± 6.3), but our experiments were performed at higher temperature and using a different NAPL.

As far as III-type tests are concerned, partition coefficients between kerosene and total air ($k_{\text{ker-tot air}}$) equal to 6.2 ± 0.6. It is worth stressing that the air phase contains also kerosene vapors where radon gas is partly dissolved. Consequently, we report a tentative approach to estimate separately radon partition between kerosene and air and

kerosene and kerosene vapors, using results from experiment 1, where radon released by a solid source (ignimbrite) not-uniformly contaminated with kerosene is doubled (2.1 times) at nearly equilibrium conditions, admitting that kerosene vapors concentration in the air phase reached stable conditions as well. If we assume that equilibrium kerosene vapors at the same temperature (32°C) is likely attained during experiment 2, where the liquid radon source (spring water) gave off radon, reaching a stable partition between phases, then we can propose the following calculation. If the radon partition in the total air is multiplied by 2.1, it is possible to approximate the partition between kerosene and air ($K_{ker\text{-}air}$), without the contribution of vapors. Furthermore, if radon concentration in the pure air component is divided by 1.1, the partition of radon between kerosene and kerosene vapors ($K_{ker\text{-}ker\ vap}$) can be estimated. $K_{ker\text{-}air}$ and $K_{ker\text{-}ker\ vap}$ result to be 12.9 ± 1.2 and 11.8 ± 1.1, respectively.

The value of the former parameter at 32°C is slightly lower than that reported by Schubert et al., (2005) at 20 °C, who obtained it multiplying the experimentally obtained $K_{ker\text{-}wat}$ by the wellknown Ostwald coefficient, expressing air/water partitioning at different temperature.

Finally, in presence of kerosene vapors the partition coefficients of radon between phases ($K_{ker\text{-}air\ tot}$) is lower because more radon is dissolved into gaseous phases (air + kerosene vapors) and thus removed from the liquid. This is important for the quantification of soil NAPL pollution in the vadose zone and the application of remediation actions.

Table 2
Data set from experiment 2. Typical volume ratios between kerosne, water and air are 0.0 5: 1 : 1, except for tests 1 to 4

Test	T (°C)	2-phases	3-phases			
		$K_{ker\text{-}wat}$ I-type	$K_{ker\text{-}wat}$ II-type	$K_{ker\text{ - }tot\ air}$ III-type	$K_{ker\text{-}air}$ §	$K_{ker\text{-}ker\ vap}$ §
1 *	22	19.9 ± 3.1	-	-	-	-
2 *	22	16.1 ± 2.2	-	-	-	-
3*	22	24.2 ± 4.5	-	-	-	-
4*	22	19.0 ± 3.0	-	-	-	-
5	32	-	32.5 ± 3.0	5.5 ± 0.6	11.6 ± 1.3	10.5 ± 1.1
6	32	-	32.6 ± 3.3	5.6 ± 0.6	11.8 ±1.3	10.7 ± 1.1
7	32	-	38.3 ± 5	6.5 ± 0.7	13.7 ± 1.5	12.4 ± 1,3
8	32	-	38.5 ± 3.4	6.7 ± 0.7	14.1 ± 1.5	12.8 ± 1.3
9	32	-	40.2 ± 5.7	7.1 ± 0.8	14.9 ± 1.7	13.6 ± 1.5
10	32	-	36.0 ± 3.1	6.1 ± 0.7	12.8 ± 1.5	11.6 ± 1.3
11	32	-	34.4± 4.0	5.7 ± 0.6	12.0 ± 1.3	10.9 ± 1.1
12	32	-	32.3 ± 4.2	5.8 ± 0.6	12.2 ± 1.3	11.1 ± 1.1
13	32	-	37.6 ± 3.8	6.1 ± 0.7	12.8 ± 1.5	11.6 ± 1.3
14	32	-	33.6 ± 3.0	5.8 ± 0.6	12.2 ± 1.3	11.1 ± 1.1
15 **	32	-	40.2 ± 5.0	6.9 ± 0.8	14.5 ± 1.7	13.2 ± 1.5
16 **	32	-	33.6 ± 3.4	6.0 ± 0.6	12.6 ± 1.3	11.5 ± 1.1
17	32	-	35.8 ± 3.4	6.2 ± 0.6	12.9 ± 1.2	11.8 ± .1.1

*Volume ratio of kerosene and water is 1:1
**Mixing time:15 min; separation time: 90 min
§ Calculated (see text for explanation)

5. Conclusions

Small-scale laboratory experiments were carried out to monitor the dissolution and preferential partition of radon in the vapor plume, occurring in case of recent NAPL spills. Experiment 1 demonstrated that NAPL vapors may enhance soil radon exhalation and concentration when a large amount of vapors occurs, modifying soil radon distribution patterns. The introduction of a desiccant to dry soil gas emphasizes that radon is preferentially dissolved into NAPL vapors and is transported through the soil, before being absorbed by drierite. This also puts forward the interference that a desiccant may have on soil radon measurements.

Experiment 2 provided radon partition coefficients between kerosene, water and air, considered as the sum of air and kerosene vapors. This is crucial to correctly interpret

radon data in a real open-system setting in presence of NAPL vapors, as during the employment of remediation based on soil venting or dual-phase extraction.

Acknowledgements

Authors gratefully acknowledge Golder Associates, Roma, Italy for providing us with a MiniRaeLite (Extratech) photoionization detector to measure VOC contents in the closed set-up of experiment 3.

We are also grateful to Stefania Moretti for preparation of Figure 1.

References

Capelli, G., Mastrorillo L., Mazza R., Petitta M, 2012. Carta delle Unità Idrogeologiche della Regione Lazio. Scala 1.250 000. Regione Lazio.

Castelluccio, M., 2010. Soil radon concentration survey in Caffarella Valley test site (Rome) Ph.D. Thesis in Geodynamics at the "Roma Tre" University.

De Simone, G., Galli, G., Lucchetti, C., Tuccimei, P., 2015. Using natural radon as a tracer of gasoline contamination. 11th Applied Isotope Geochemistry Conference, AIG-11 BRGM, September 2015, Orleans (France). Procedia Earth and Planetary Science 13, 104-107. 10.1016/j.proeps.2015.07.025

De Simone, G., Lucchetti, C. Galli, G., Tuccimei, P., 2016. Correcting for H_2O interference using electrostatic collection-based silicon detectors. Journal of Environmental Radioactivity, 162-163, 146-153. DOI: 10.1016/j.jenvrad.2016.05.021.

Hohener, P., Surbeck H., 2004. Radon-222 as a Tracer for Nonaqueous Phase Liquid in the Vadose Zone: Experiments and Analytical Model. Vadose Zone J. 3(4), 1276-1285.

Lucchetti. C., De Simone. G., Galli G., Tuccimei. P., 2016. Evaluating radon loss from water during storage in standard PET, bio-based PET and PLA bottles. Radiat. Meas. 84, 1-8. DOI: 10.1016/j.radmeas.2015.11.001.

M. Schubert, K. Freyer, H.C. Treutler, H. Weiß, J., 2001. Using the Soil Gas Radon as an Indicator for Ground Contamination by Non-Aqueous Phase-Liquids. Soils Sediments 1(4), 217-222.

Schubert, M., Peña, P., Balcázar, M., Meissner, R., Lopez, A. Flores, J.H., 2005. Determination of radon distribution patterns in the upper soil as atool for the localization of subsurface NAPL contamination. Radiat. Meas. 40, 633 – 637.

Schubert, M., Lehmann, K., Paschke, A., 2007. Determination of radon partition coefficients between water and organic liquids and their utilization for the assessment of subsurface NAPL contamination. Sci Total Environ 376 , 306–316.

Schubert, M., 2015. Using radon as environmental tracer for the assessment of subsurface Non-Aqueous Phase Liquid (NAPL) contamination – A review. Eur. Phys. J. Special Topics 224, 717–730. 240.

Semprini, L., Hopkins, O.S., Tasker, B.R., 2000. Laboratory, field, and modeling studies of Radon-222 as a natural tracer for monitoring NAPL contamination. Transp. Porous Med. 38, 223.

Tajika, Y., Yasuoka, Y., Omori, Y., Sorimachi, A., Ishikawa, T., Mori, Y., Mukai, T., 2014 Effect of a Desiccant on the Measurement of Radon Concentration in Air. Jpn. J. Health Phys. 49 (4) 190- 193.

Tuccimei, P., Castelluccio, M., Soligo, M., Moroni, M., 2009. Radon exhalation rates of building materials: experimental, analytical protocol and classification criteria. In: "Building materials: Properties, Performance and Applications", Donald N. Cornejo e Jason L. Haro Editori, Nova Science Publishers, Hauppauge, NY, ISBN: 978-1-60741-082-9, 259-273.

Tuccimei, P., Castelluccio, M., Moretti, S., Mollo, S., Vinciguerra, S., Scarlato, P., 2011. Thermal enhancement of radon emission from rocks. Implications for laboratory experiments under increasing deformation. In: Horizons in Earth Science Research, Volume 4, ISBN 978-1-61122-763-5, Editor: Benjamin Veress and Jozsi Szigethy. Nova Science Publishers, chapter 9, 247-256.

CHAPTER 6

CORRECTING FOR H_2O INTERFERENCE USING A RAD7 ELECTROSTATIC COLLECTION-BASED SILICON DETECTOR

G. De Simone a, C. Lucchetti a, G. Galli b, P. Tuccimei a

a: Universit. a "Roma Tre", Dipartimento di Scienze, Largo San Leonardo Murialdo 1, 00146 Roma, Italy

b: Istituto Nazionale di Geofisica e Vulcanologia, Sezione Roma 1, Via di Vigna Murata 605, 00143, Roma, Italy

Abstract

The effect of water molecules on the electrostatic collection of ^{218}Po ions onto the surface of silicon detectors (neutralization) is evaluated through the comparison with a scintillation cell (ZnS), not affected by air humidity. A radon monitor (RAD7, Durridge Company) was connected to a stainless steel radon chamber, equipped with the scintillation cell. Radon gas, extracted from an acidified $RaCl_2$ source, was injected into the chamber and the amount of water molecules in the system was alternatively lowered or increased (from 0.00075 to 0.014 g of water in RAD7) by connecting the chamber to a desiccant or to a bubbling water bottle. The relative efficiency of the silicon detector with respect to the scintillation cell decreases with the growth of water molecules inside RAD7. This dependence, with a fixed i) electrostatic chamber geometry and ii) nominal high voltage, diverges during the humidification or the drying phase because it is in turn influenced by the length of interaction of polonium atoms with water molecules, which

impacts on the size of ^{218}Po clusters and thus on the neutralization process. For water contents higher that 0.01 g in RAD7, this effect is greatly enhanced. Temperature in the investigated range (18.5 e 35.6 °C) does not affect the efficiency of electrostatic collection-based silicon detectors.

Based on these experiments, admitting a certain error on the efficiency (from 1.8 to 7.5%, depending on the water content), proper corrections were developed to adjust soil radon readings, when a desiccant is removed. This operation is necessary if recent Non-Aqueous Phase Liquids (NAPLs) leakage has occurred in the subsoil to avoid the sorption and possible later release of radon by Drierite, with related partition between the solid and liquid phases (water and NAPL).

Introduction

Radon is a radioactive gas naturally present in the environment at different levels. It reaches highest activity concentration in the subsoil and in groundwater, whereas it is less abundant at the surface. Radon may accumulate inside edifices built on radon precursors-enriched geological bedrocks, especially during cold and rainy periods, when the climate favours radon accumulation in the soil and its migration to indoor environments. Long exposure to indoor radon increases the risk of lung cancer, especially forsmokers and people exposed to second hand smoke (EPA, 2003). Consequently, assessment of health risks and mitigation actions of edifices are required, either from indoor radon or in-soil radon data. Among methods routinely employed to detect radon in the environment, those based on solid state silicon detectors and radon (^{222}Rn and ^{220}Rn) daughters electrostatic collection (Chao et al., 1997; De Martino et al., 1998; Roca et al., 2004; Tuccimei et al., 2006; Lucchetti et al., 2016) are very frequently used. It is well known that their counting efficiency is influenced by environmentalparameters such as humidity, temperature and pressure (Chu and Hopke, 1988; Hopke, 1989; Roca et al., 2004; Tuccimeiet al., 2006). Temperature and water content in soil gas affectthese measurements because water molecules in the counting chambers of radon monitors cause the neutralization of radon progenies, reducing the electrostatic efficiency of silicon detector. Desiccants such as calcium sulphate (Drierite) are employed to reduce this effect, but during humid summer time it is difficult todry efficiently soil gas and the interference from water molecules needs to be corrected for. Radon is also used as tracer for environmental processes (Quindos et al., 2013), such as: indicator of atmospheric dynamics (Cuculeanu and Lupu, 2001); precursor of rock deformation and degassing phenomena in volcanic settings (Tuccimei et al., 2010; Scarlato et al., 2013); tracer of groundwater discharge into rivers (Cook et

al., 2003), coastal ocean (Cable et al., 1996) or surface reservoirs (Corbett et al., 1997); for the assessment of residual NAPLs (Non-Aqueous Phase Liquids) contamination of soils and aquifers (Semprini et al., 2000; Schubert et al., 2002; Schubert, 2015).

In order to use radon as NAPL tracer, we investigated if Drierite interferes with NAPLs in contaminated soil. Proper experiments were carried out in laboratory repeatedly connecting in a closed loop a RAD7 instrument, a Drierite column previously polluted with NAPL vapors and a small radon chamber (2.83 L) with a fixed activity of radon (see Fig. 1): at the end of each test, after measuring the equilibrium radon concentration, a partial purging of the RAD7 and the Drierite column was performed for a time of 5 min, not long enough to remove completely the absorbed NAPL. Since radon concentration is expected to decrease in successive experiments for decay and dilution, this process has been accounted for; nonetheless we observed firstly a decrease (28%) with respect to the expected value, then successive experiments showed progressive increases of radon concentrations (16 and 23%). As a matter of fact, firstly, NAPL vapor absorbed in the Drierite captures radon (test 2), reducing its concentration in the circuit; successive experiments (test 3 and 4) showed that NAPL still absorbed in the Drierite column is partially released to the closed loop, leading to a consequent rise of radon in the circuit. Accordingly, when soil radon measurements are carried out in presence of recent NAPLs contamination (De Simone et al., 2015a), these substances are extracted during soil gas sampling and then absorbed by desiccant material, partitioning radon gas between the air and the absorbed liquid phases (the NAPL and the water). This leads to an interference difficult to deal with and thus desiccants should be removed. This is why we developed proper experiments to correct radon concentration detected by RAD7 electrostatic collection-based silicon detectors for the weight of water molecules in the system.

Material and methods

Radon activity concentration was measured using a RAD7 monitor (Durridge Co.), an electrostatic chamber operated at a nominal voltage of 2000 e 2500 V, equipped with a solid state silicon detector which collects radon daughters onto its surface and detects and separates alpha particles emitted by them, on the basis of their energies. This allows to select only the short-lived ^{218}Po (with a half-life of about 3 min) to measure ^{222}Rn, reaching the radioactive equilibrium between them in just 15 min.

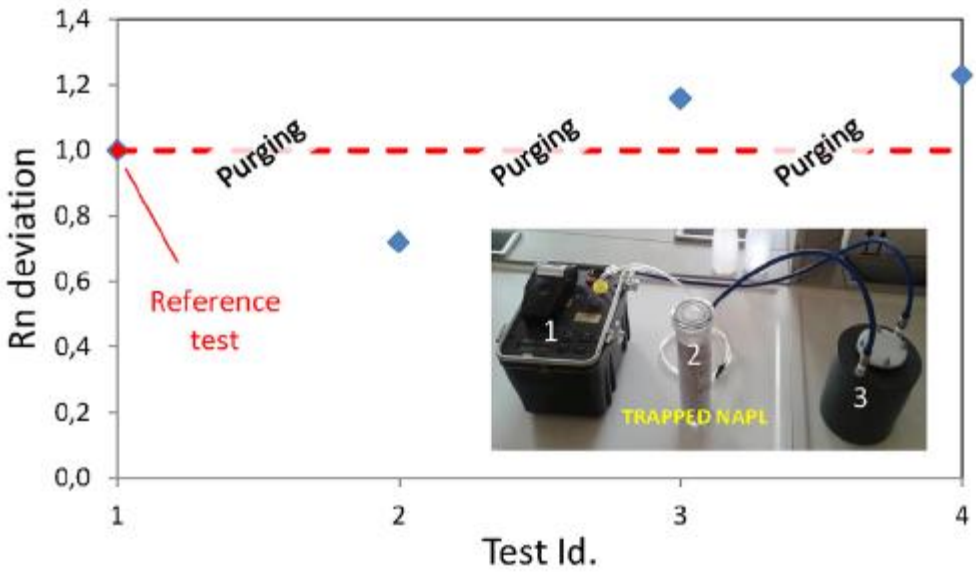

Fig. 1. Radon deviation from expected values when NAPL vapors are trapped into the Drierite column (2) in successive tests. 1) RAD7; 3) Small radon chamber. See text for explanation.

This option (the Sniff mode, according to RAD7 protocols) allows to change experimental conditions fast and perform the test relatively rapidly. In order to reduce the water content in the counting chamber of the instrument, a cylinder of calcium sulphate (Drierite) is generally employed. Temperature and relative humidity are recorded inside the instrument. A pump guarantees the circulation of the air in the set-up. Radon concentration in the radon chamber was determined with a scintillation cell

(ZnS) coupled to a photomultiplier (De Simone et al., 2015b) to have radon reference values not affected by changing water conditions, as described in the following sections.

Experimental

In order to obtain the dependence of decreased detection effi-ciency of the RAD7 ilicon detector on absolute humidity, ad-hoc experiments were designed using a 56 L stainless steel radon chamber equipped with a scintillation cell (ZnS) coupled to a photomultiplier, which is not sensitive to humidity. Radon gas was extracted from an acidified (pH < 2) $RaCl_2$ source added with Ba (2500 Bq), and injected in the chamber. Relative humidity and thus weight of water molecules in the system, at constant temperature, were progressively changed by connecting the chamber to Drierite (opening stopcocks O and Q and closing stopcocks P and R) or to a bubbling water bottle (opening stopcocks O and R and closing stopcocks P and Q) for drying or humidifying the closed circuit. When reached desired condition, RAD7 was connected in a closed loop to the chamber (opening stopcock P and closing stopcocks O, Q and R) and RAD7 readings were compared with activity concentrations given by the scintillator at each step (with an average duration of 30 e 45 min per step) (Fig. 2). It is worth noting that the scintillator data used for efficiency calculation were always obtained from an exponential interpolation of counts recorded after at least 5h from the RAD7 connection to the radon chamber, to account for the establishment of new equilibrium conditions (secular equilibrium and radon diffusion within the new system configuration) and to reduce the error.

A number of experiments were carried out according to a planned sequence of drying or humidification phases in order to study the repeatability and the dependence of results on the sequence path. As a result, correction factors of activity concentration values

obtained using RAD7 (defined as efficiency of the electrostatic collection-based silicon detector) were calculated as the ratio:

$Efficiency_i = A_{Rn\ RAD7\ i} / A_{Rn\ CR\ i}$

and plotted versus the amount of water in the RAD7, being $A_{Rn\ RAD7\ i}$ the i-th average radon activity concentration measured by the RAD7 (printed raw readings) in each step and $A_{Rn\ CR\ i}$ the corresponding i-th radon activity concentration in the radon chamber. Each A Rn CR was calculated by exponential interpolation ($A_{Rn\ CR\ i} = k*Y_0 *e^{B*t}$) obtained as described above, of data registered by a multichannel analyzer set in multiscaler mode, during each experiment configuration, where:

k: calibration factor (Bq m^{-3} cpm^{-1})

Y_0 : counts (cpm) at t=0

B: exponential time constant (min^{-1})

t: time (min)

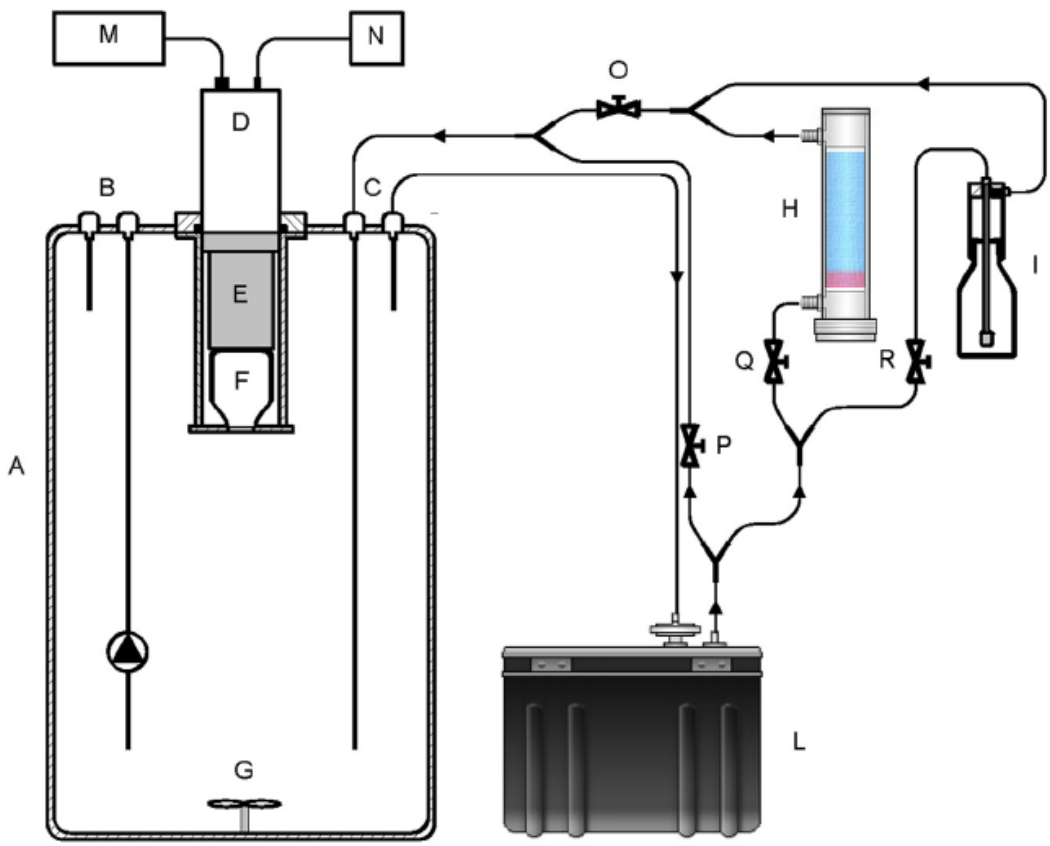

Fig. 2. Experimental set-up. A) radon chamber; B) air tight connectors (CPC) to be used when air circulation needs a pump; C) air tight connectors (CPC) when air circulation is guaranteed by an outer device; D) signal processing module; E) photomultiplier; F) scintillating flask; G) fan; H) desiccant column (Drierite); I) humidifying device; L) Durridge RAD7; M) multiscaler, N) low voltage supply; O), P), Q) and R) stopcocks.

Absolute humidity values in the detection volume, expressed as grams of water inside RAD7 (gH2ORAD7), are inferred from the psychrometric diagram as a function of the atmospheric pressure, temperature and relative humidity and calculated using equation:

$$gH_2O_{RAD7} = kgH_2O/\ Kg\ dry\ air*1000*\rho\ air\ T\ *V_{RAD7}$$

$kgH_2O/\ Kg\ dry\ air$: kilograms of water contained in a kilogram of dry air

$\rho\ air\ T$: air density at a given temperature (kg/m^3)

V_{RAD7} : inner volume of RAD7 monitor (0.000768 m^3) with

$kgH_2O/ Kg\ dry\ air = (0.622*RH/100*Psat)/P- (RH/100*P\ sat)$

(Gatley, 2013)where:

RH: relative humidity

P sat : water saturation pressure at a given temperature (Pa)

P: atmospheric pressure (Pa)

The water saturation pressure is calculated as follows:

P sat = exp [65.81 - 7066.27/(T + 273.17) - 5.976 ln (T + 273.159)]

(Gatley, 2013) with:

T = temperature in °C

The atmospheric pressure effect can be considered negligible, since a 10 mBar difference affects the water content for just 1%, being the 1 sigma uncertainties on water content greater.

Results and discussion

It is known that water molecules dispersed in air reduce the collection of positively charged radon daughters on the silicon detector surface placed in an electrostatic chamber operated at constant nominal high voltage (HV). Electric field lines, oriented as shown in Fig. 3, influence not only the collection of the radon daughters, but also the trajectory of water-polonium clusters, which may hit the detector even though partly neutralized (Chu and Hopke, 1988; Hopke, 1989; Mesbah et al., 1997; De Martino et al., 1998; Roca et al., 2004; Tuccimei et al., 2006).

Proper experiments were carried out to assess the correction factor (efficiency) trend as a function of the water content inside a RAD7 (Serial Number, S.N. 2408) by using the experimental apparatus reported in Fig. 2. The water content was changed from 0.00075 to 0.014 g (approximately from 5 to 69% relative humidity at about 26 ± 1 _ C).

All the obtained efficiency values are plotted in Fig. 4 versus the water content inside RAD7 along with a linear interpolation for water contents <0.010 g H_2O. The correction provided by Capture, the software developed by Durridge Co. for data acquisition and analysis, is also reported; the fit has been obtained from the ratios between raw and Capture corrected data. Capture correction agrees with the experimental data obtained from RAD7 (S.N. 2408) up to about 0.003 g H_2O in RAD7 volume; for higher water contents it underestimates the correction. With reference to our experimental data, we note a decrease of the efficiency at increasing water contents due to neutralization processes; it is also evident that the higher the water content, the higher the scatter of efficiency data, especially observed during drying phases; furthermore, efficiency values obtained during drying starting from wet conditions generally lay below those obtained during humidification starting from dry conditions, this being very evident over 0.010 g H_2O in RAD7. In order to highlight this, plots of efficiency data for water contents less than 0.010 g H_2O are shown in Fig. 5, (selecting data obtained during humidification) and in Fig. 6 (choosing data from drying), along with the linear interpolation equations.

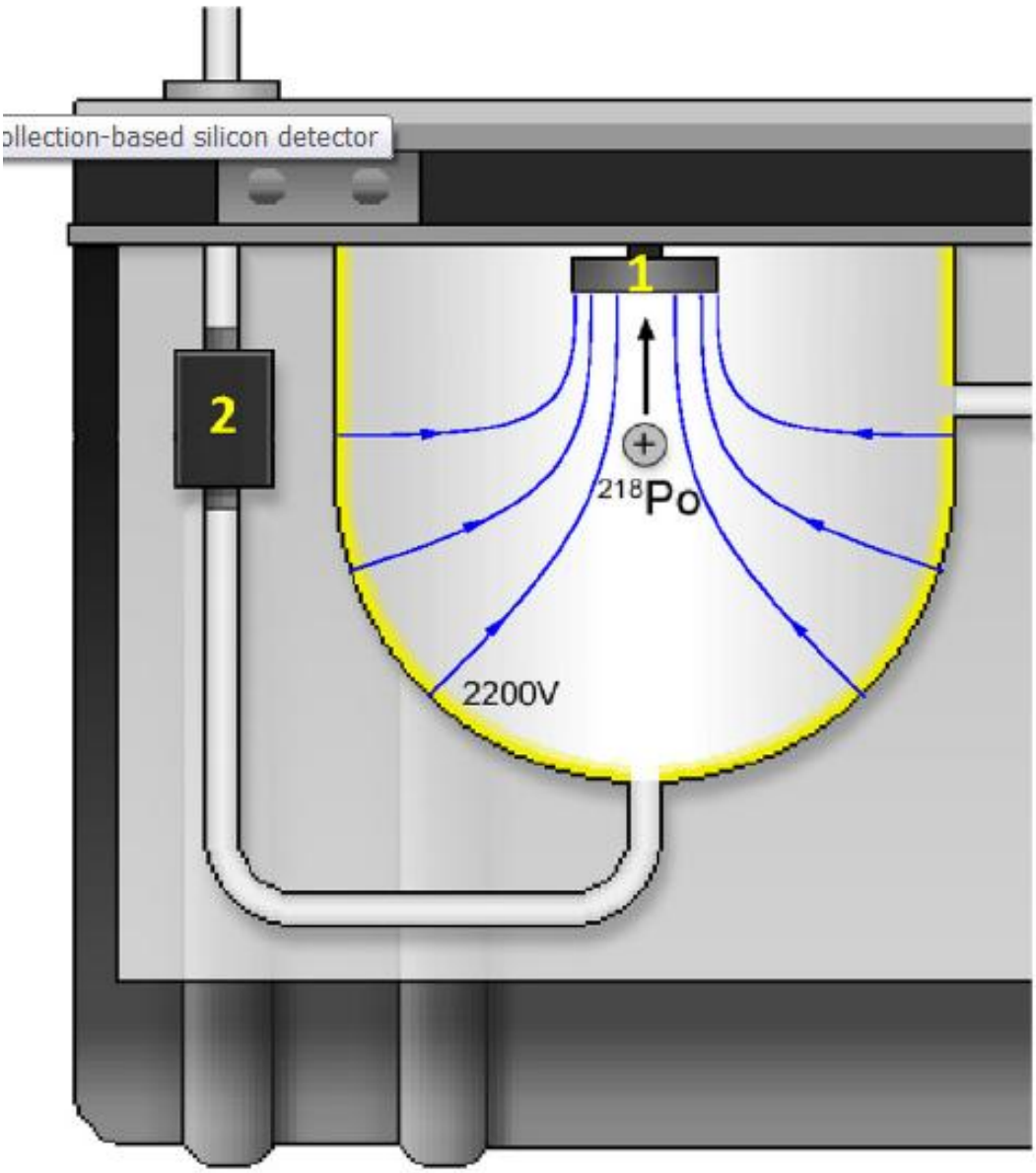

Fig. 3. Electric field lines in the counting chamber of RAD7. 1) solid-state, ionimplanted, planar, silicon alpha detector, 2) Temperature/Relative Humidity sensors. The scheme was kindly provided by Durridge Co.

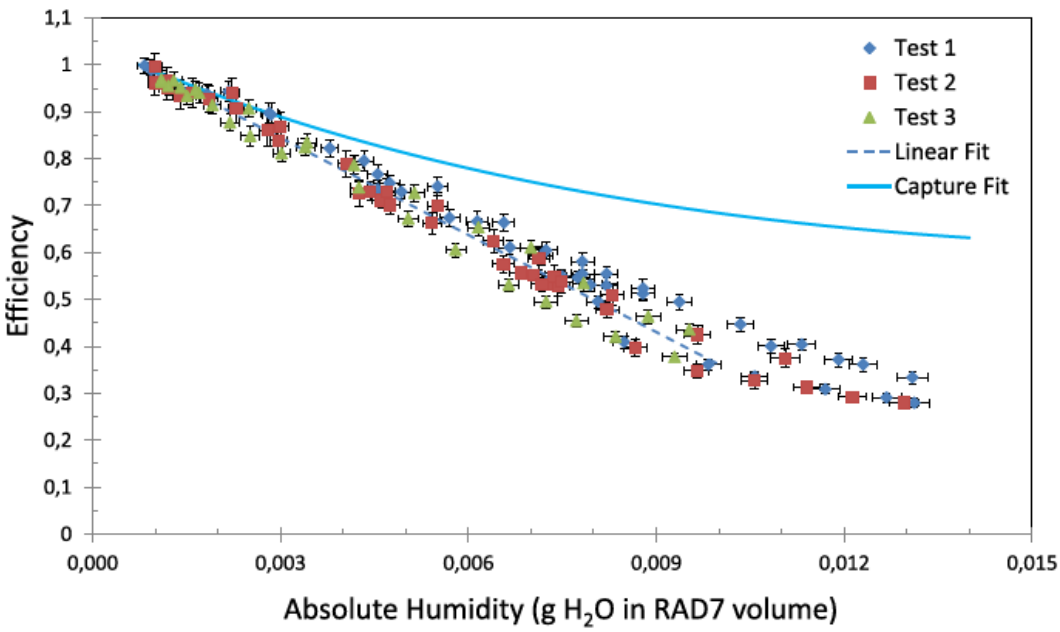

Fig. 4. Efficiency of the electrostatic collection-based silicon detectors against the water content inside RAD7 from three different experiments. The linear fit of all data up to 0.01 g of water in RAD7 volume is reported for comparison with Figs. 5e7 where data are selected based on the degree and the changing trend of absolute humidity (humidification or drying). The solid line represents the correction given by Capture (see text for explanation)

The trend in Fig. 5 is more regular since the test starts from dryer conditions, definitely more suitable for the use of RAD7, as recommended by Durridge (Durridge, 2009). Fig. 6, reporting experimental data starting from wet conditions, shows a slightly different trend with a higher scatter at higher values of water. Finally, Fig. 7 refers to linear fits of data acquired during drying and humidifying for water contents greater than 0.010 g H_2O; in this case the trends are clearly different and the experiment history must be accounted for, since water molecules deposited over the silicon detector surface cause an even stronger degradation in the detected alpha particles energy and consequently their removal from the ^{218}Po peak.

This is also evident in the case of Fig. 8 in which, during drying, theoretical efficiency data from interpolation in Fig. 6 are compared with experimental efficiency data: the latter at the beginning lay below the former and progressively approach them since the

water molecules attached to the system walls (including the detector surface) are being removed along with the water-polonium clusters.

Finally, the temperature effect on the RAD7 response has been investigated. Consequently a specific experiment has been carried out at a water content nearly constant, varying greatly the temperature from 18.5 °C to 35.6 °C (see Fig. 9). The plot in Fig. 9a shows experimental efficiency data superimposed on the available data set (Fig. 4) from 0.005 to 0.008 g H_2O in RAD7 and the related interpolation fit. Data from this experiment, plotted versus the water content, follow reasonably the available data set, apart from an initial 10% deviation (average value of 6%) for low absolute humidity. According to what evidenced before, efficiency data from this experiment have been plotted (Fig. 9b) along with temperature and water content versus the chronological measure identification: again interpolated data are approached only after a time needed for the system equilibrium to be reached, i.e. water removal from the detector. As a matter of fact, initial efficiency values are about 11% lower than corrected efficiency (average value of 7%) in agreement with Fig. 9a. Therefore the temperature dependence must be evaluated only after correcting the data set for a factor depending from the initial disequilibrium (ratio between experimental and interpolated efficiency). Adjusted data follow the trend obtained varying the absolute humidity while keeping almost constant the temperature (Fig. 5); therefore the dependence of the RAD7 response from temperature is negligible. Results obtained performing various experiments showed that the corrective factor depends on i) the amount of water in the detection volume, ii) the history of the measurements done, i.e. increasing water content starting from dry conditions or vice versa.

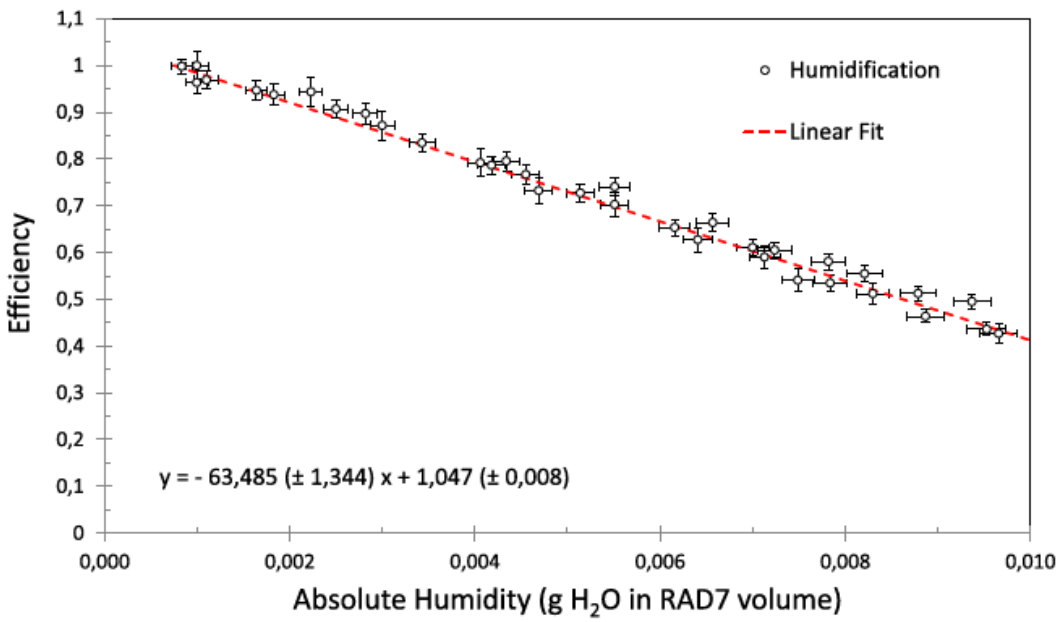

Fig. 5. Efficiency of the electrostatic collection-based silicon detectors against the water content inside RAD7. Data from the humidification phases of the three different experiments up to 0.01g of water in RAD7 volume are selected. The linear fit is reported for comparison with Figs. 4, 6 and 7.

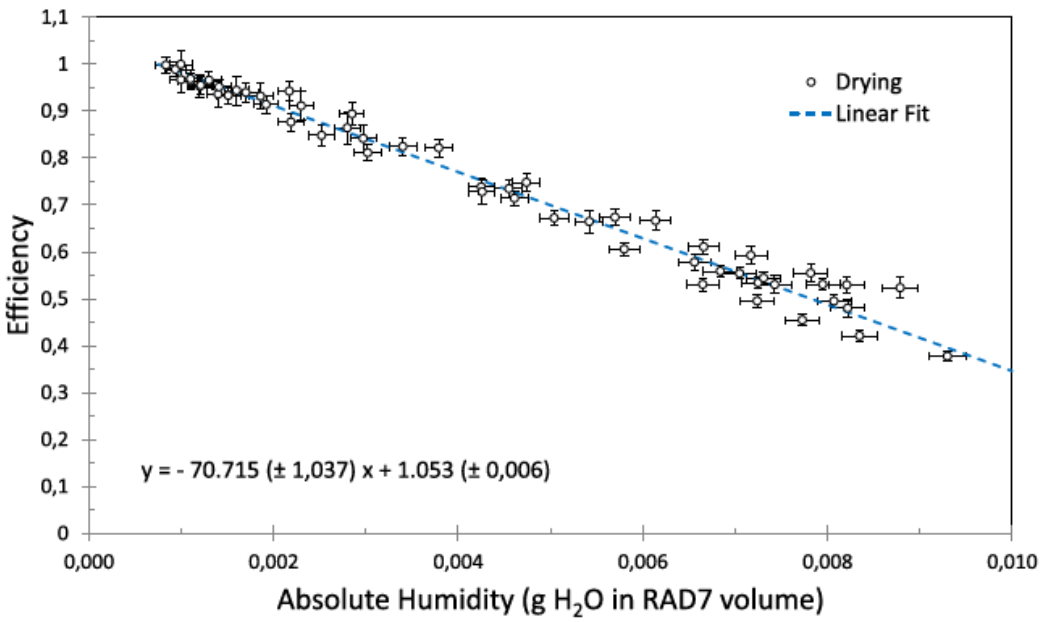

Fig. 6. Efficiency of the electrostatic collection-based silicon detectors against the water content inside RAD7. Data from the drying phases of the three different experiments up to 0.01 g of ater in RAD7 volume are selected. The linear fit is reported for comparison with Figs. 4, 5 and 7.

The following linear interpolation equations have been found:

$Y = 1$ for X (g H_2O) < 0.00075

(Guantario, 1997; Durridge, 2009).

$Y = (- 68.999 \pm 0.771) X + (1.052 \pm 0.005)$
for $0:00075 < X$ (gH_2O)$< 0:010$; all data

$Y = (- 63.485 \pm 1.344) X + (1.047 \pm 0.008)$
for $0.00075 < X$(gH_2O) < 0.010; humidifying only

$Y = (- 70.715 \pm 1.037) X + (1.053 \pm 0.006)$
for $0.00075 < X$ (gH_2O) < 0.010; drying only

$Y = (- 38.903 \pm 7.474) X + (0.840 \pm 0.087)$
for $0:010 < X$ (gH_2O) < 0.014; humidifying only

$Y = (- 21.323 \pm 4.573) X + (0.558 \pm 0.055)$
for $0:010 < X$ (gH_2O) < 0.014; drying only

In any case, even i) ignoring the history effect and consequently the time required for the recovery of the full efficiency of electrostatic collection and ii) using the linear interpolation of all available data (Fig. 5), radon concentration values can be still inferred also in very critical conditions (water contents up to 0.010g H_2O in the RAD7). For example, the following average deviations from the corrected efficiency values have been calculated:

- gH_2O < 0.004: 1.8%
- $0.004 <$ gH_2O < 0.007: 4.1%
- $0.007 <$ gH_2O < 0.010: 7.5%.

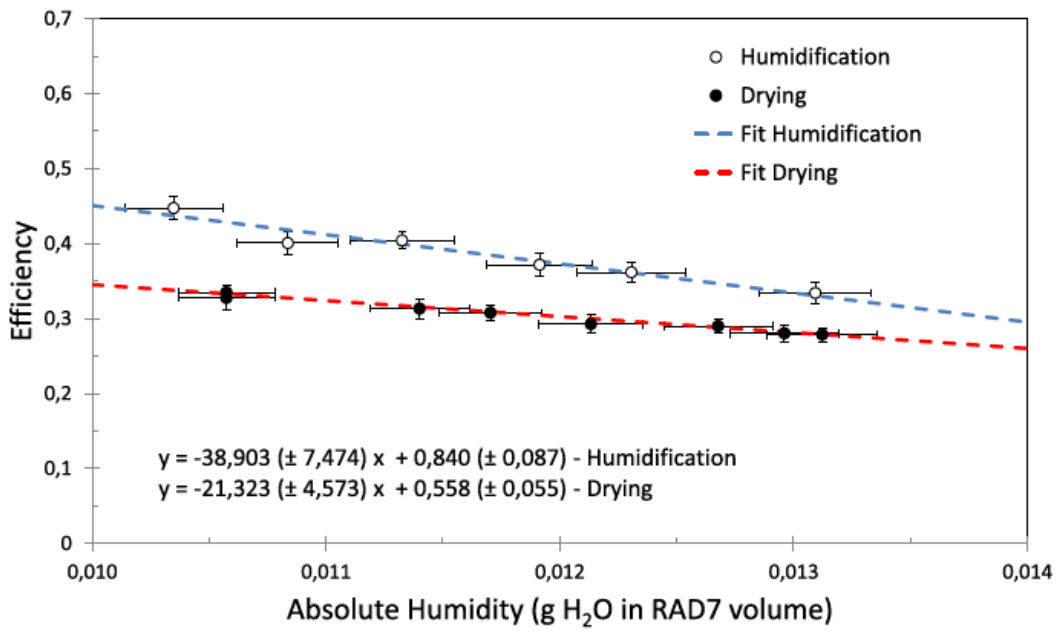

Fig. 7. Efficiency of the electrostatic collection-based silicon detectors against the water content inside RAD7. Data from the humidification and the drying phases of different experiments with more than 0.01 g of water in RAD7 volume are selected. The linear fits are reported for comparison with Figs. 4e6.

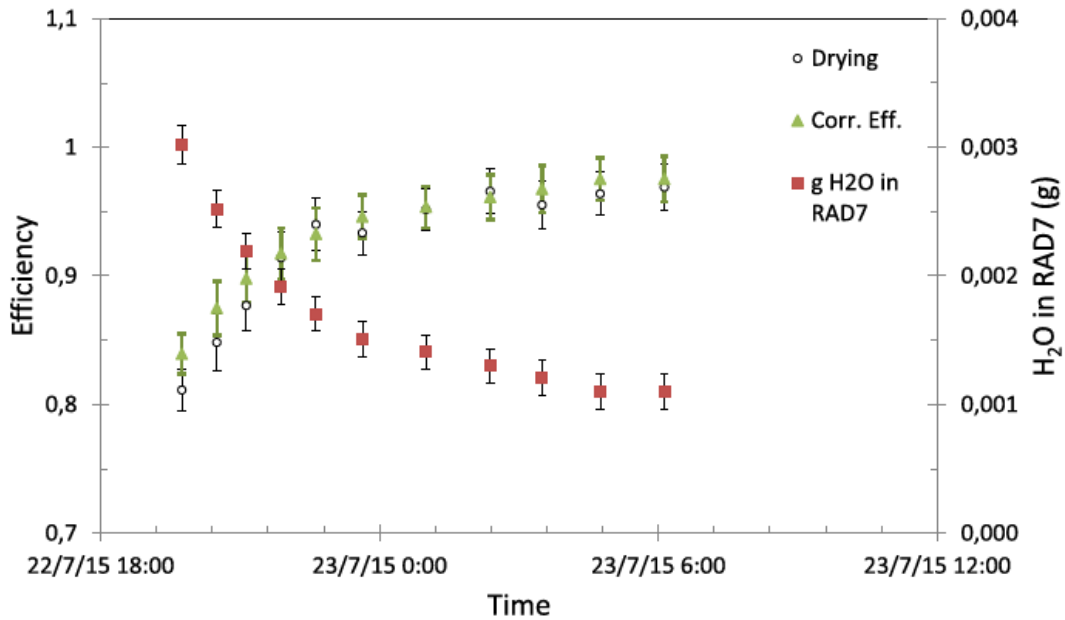

Fig. 8. Efficiency of the electrostatic collection-based silicon detectors and water content inside RAD7 overnight. Data are shown for low absolute humidity, during the drying phase. Corrected efficiency values based on linear fits in Fig. 6 (drying trend) are reported to show the effect of water-polonium clusters on the timing of efficiency recovery.

Finally, we tested with the same experimental setup also the other RAD7s (S.N. 0608 and 2504) we generally employ in field surveys, to verify whether their responses were similar to that obtained for RAD7 S.N. 2408. Results are summarized in Table 1. Efficiency data are very different; efficiency relative deviations have been calculated with respect to RAD7 S.N. 2408. Deviation of RAD7 S.N. 0608 is about 14% higher, irrespective of the water content (0.004e0.014 g H_2O); deviation of RAD7 S.N. 2504 is again higher and ranges from 23% to 57% at increasing water contents.

Results demonstrate that corrections are different for each RAD7 since they depend even on small differences among instruments regarding i) detection chamber, ii) silicon detector, iii) temperature and RH sensors, iv) applied high voltage, v) pump volume rate, vi) electronics and vii) assembly.

A comparison with Capture correction shows that deviations from all investigated RAD7s are very different and generally increase with water contents; therefore each RAD7 must be characterized when not used according to the manufacturer recommendation, i.e. without Drierite. Capture correction works very well for every instrument up to 0.003 g H_2O in RAD7, corresponding for example to RH = 15% at 25 °C, even beyond the recommended limit (RH < 10% at ambient temperature).

Conclusions

Soil radon is actually used as tracer of NAPLs contamination in the vadose zone of aquifers because it is more soluble in NAPLs than in water or in air and a deficit of it in soil gas (known as soil radon deficit technique, Semprini et al., 2000) pinpoints the volume of polluted subsoil. The use of desiccants to dry soil air interferes with the residual NAPL vapor, absorbing it and partition radon between the solid and the liquids. In further measurements carried out with the same Drierite column, without changing or purging it completely, NAPL vapors still absorbed onto the column may be released to the system, heavily affecting results (De Simone et al., 2015a).

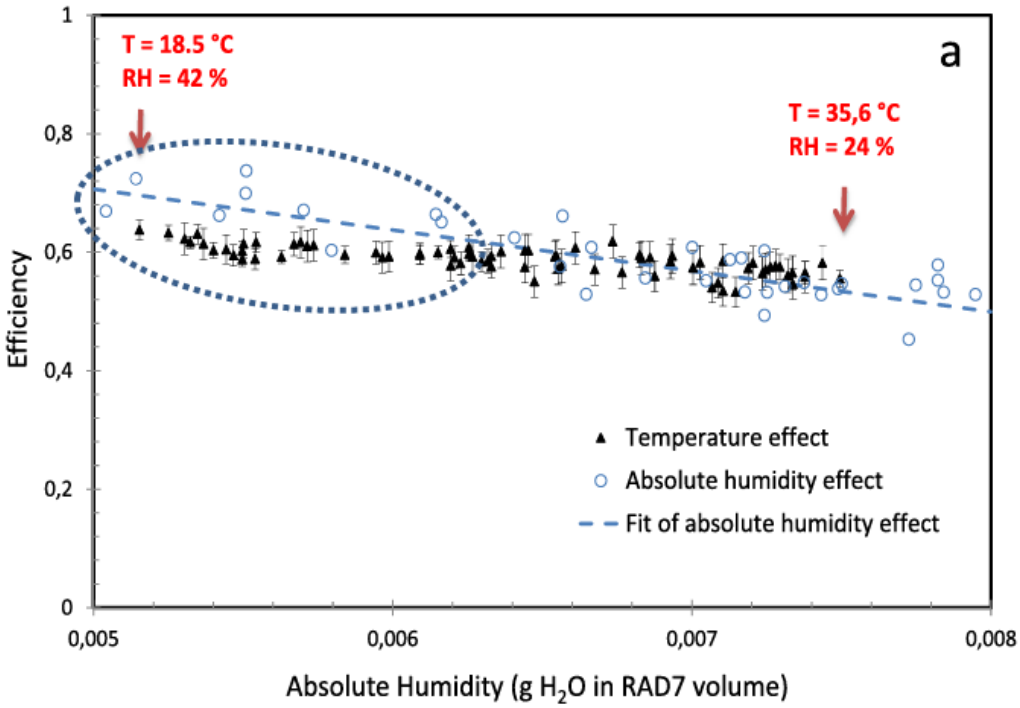

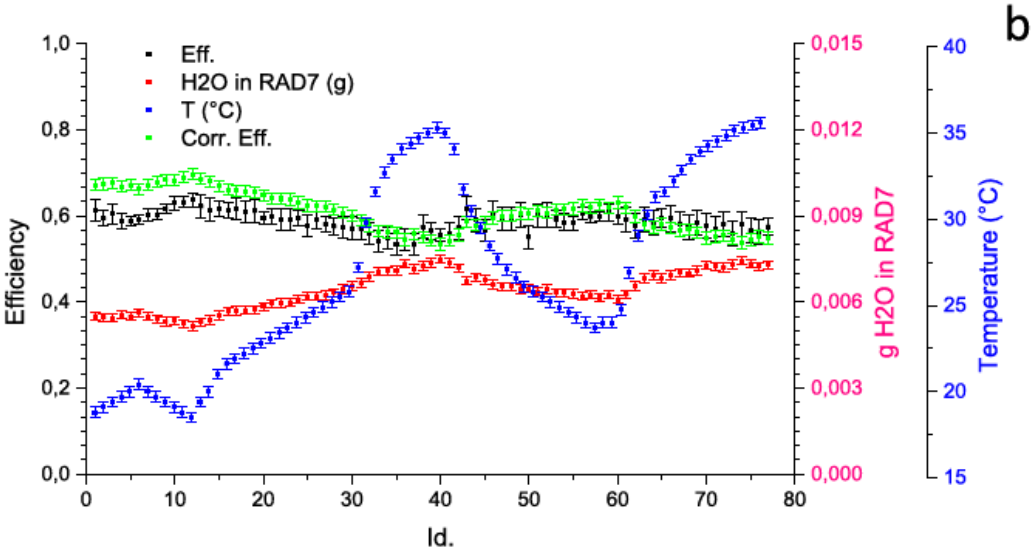

Fig. 9. Effect of changing temperature (from 18.5 to 35.6 _ C) on the efficiency of the electrostatic collection-based silicon detectors. This influence is shown against the grams of water inside RAD7 (Fig. 9a). Errors are quoted as 1 sigma. A comparison with data from Fig. 4, representing the effect of absolute humidity at nearly constant temperature (26.1 ± 0.3), is shown along with relative linear fit. In Fig. 9b, the experimental efficiency is compared with the efficiency corrected for the effect of water inside RAD7 (see fit in Fig. 4) and is shown during the test (as progressive identification data) along with water and temperature changes. See text for explanation.

Table 1

Efficiency deviation of RAD7 S.N. 0608 and S.N. 2504 and Capture correction compared to RAD7 S.N. 2408 efficiency as a function of RAD7 water content.

Water (g)	Efficiency Relative Deviation			
	S.N. 2408	S.N. 0608	S.N. 2504	Capture
0.004	1.00	0.14	0.23	0.07
0.006	1.00	0.14	0.29	0.17
0.008	1.00	0.16	0.38	0.35
0.01	1.00	0.18	0.52	0.66
0.012	1.00	0.10	0.45	0.75
0.014	1.00	0.15	0.57	1.14

As a consequence the use of Drierite should be avoided, irrespective of manufacturer recommendation, and proper correction for the efficiency of RAD7 electrostatic-based silicon detectors have to be applied to account for the effect of water molecules on the electrostatic collection of ^{218}Po ions. Ad-hoc corrections have been obtained for a specific RAD7 at different water contents. The temperature influence has been ruled out.

Various RAD7s have been tested showing different behavior at similar water content, making the characterization of every single instrument necessary. Capture correction agrees with our experimental data up to 0.003 g H_2O in RAD7 volume, diverging progressively at increasing water contents.

References

Cable, J.E., Burnett, W.C., Chanton, J.P., Weatherly, G.L., 1996. Estimating groundwater discharge into the northeastern Gulf of Mexico using radon-222. Earth Planet. Sci. Lett. 144, 591e604.

Chao, C.Y.H., Tung, T.C.W., Chan, D.W.T., Burnett, J., 1997. Determination of radon emanation and back diffusion characteristics of building materials in small chamber tests. Build. Environ. 32, 355e362.

Chu, K.-D., Hopke, P.K., 1988. Neutralization kinetics for polonium-218. Envir. Sci. Tech. 22, 711e717.

Cook, P.J., Favreau, G., Dighton, J.C., Tickell, S., 2003. Determining natural groundwater influx to a tropical river using radon, chlorofluorocarbons and ionic environmental tracers. J. Hydrol. 277, 74e88.

Corbett, D.R., Burnett, W.C., Cable, P.H., Clark, S.B., 1997. Radon tracing of groundwater input into par pond, Savannah river site. J. Hydrol. 203, 209e227.

Cuculeanu, V., Lupu, A., 2001. Deterministic chaos in atmospheric radon dynamics. Deterministic chaos in atmospheric radon dynamics. J. Geophys. Res. Atmos. 106, 961e968.

De Martino, S., Sabbarese, C., Monetti, G., 1998. Radon emanation and exhalation rates form soils measured with an electrostatic collector. Appl. Radiat. Isot. 49, 407e413.

De Simone, G., Galli, G., Lucchetti, C., Tuccimei, P., 2015a. Using natural radon as a tracer of gasoline contamination. P. Earth Planet. Sci. 13, 104e107, 11 the Applied Isotope Geochemistry Conference, AIG-11 BRGM.

De Simone, G., Galli, G., Lucchetti, C., Tuccimei, P., 2015b. Calibration of BIG Bottle RAD H2O set-up for radon in water using HDPE bottles. Radiat. Meas. 76, 1e7.

Durridge, 2009. RAD7 Radon Detector User Manual.

(EPA) Environmental Protection Agency, 2003. EPA Assessment of Risks from Radon in Homes. 402-R-03e003. U.S. Environmental Protection Agency, Washington, DC.

Gatley, D.P., 2013. Understanding Psychrometrics, third ed. ASHRAE, Atlanta (GA), USA. ISBN 978-1-936504-31-2.

Guantario, C., 1997. Influenza dell'umidit. a sulla efficienza di rivelazione di radon mediante rivelatore allo stato solido. Tesi di Laurea in Ingegneria Nucleare. Universit. a "La Sapienza", Roma, Italy.

Hopke, P.K., 1989. Use of electrostatic collection of ^{218}Po for measuring Rn. Health Phys. 57, 39e42.

Lucchetti, C., De Simone, G., Galli, G., Tuccimei, P., 2016. Evaluating radon loss from water during storage in standard PET, bio-based PET and PLA bottles. Radiat. Meas. 84, 1e8.

Mesbah, B., Fitzgerald, B., Hopke, P.K., Pourprix, M., 1997. New technique to measure the mobility size of ultrafine radioactive particles. Aerosol Sci. Tech. 27, 381e393.

Quindos, L.S., Sainz, C., Fuente, I., Gutierrez, J.L., Gonzalez, A., 2013. The use of radon as tracer in environmental sciences. Acta Geophys. 61, 848e858.

Roca, V., De Felice, P., Esposito, A.M., Pugliese, M., Sabbarese, C., Vaupotich, J., 2004. The influence of environmental parameters in electrostatic cell radon monitor response. Appl. Radiat. Isot. 61, 243e247.

Scarlato, P., Tuccimei, P., Mollo, S., Soligo, M., Castelluccio, M., 2013. Contrasting radon background levels in volcanic settings: clues from ^{220}Rn activity concentrations measured during long-term deformation experiments. B. Volcanol. 75, 751. http://dx.doi.org/10.1007/s00445-013-0751-0.

Schubert, M., Freyer, K., Treutler, H.C., Weiss, H., 2002. Using radon-222 in soil gas as an indicator of subsurface contamination by non-aqueous phase liquids (NAPLs). Geofis. Int. 41, 433e437.

Schubert, M., 2015. Using radon as environmental tracer for the assessment of subsurface non-aqueous phase liquid (NAPL) contamination e a review. Eur. Phys. J. Spec. Top. 224, 717e730.

Semprini, L., Hopkins, O.S., Tasker, B.R., 2000. Laboratory, field, and modeling studies of Radon-222 as a natural tracer for monitoring NAPL contamination. Transp. Porous Med. 38, 223e240.

Tuccimei, P., Moroni, M., Norcia, D., 2006. Simultaneous determination of ^{222}Rn and ^{220}Rn exhalation rates from building materials used in central Italy with accumulation chambers and a continuous solid state alpha detector: influence of particle size, humidity and precursors concentration. Appl. Radiat. Isot. 64, 254e263.

Tuccimei, P., Mollo, S., Vinciguerra, S., Castelluccio, M., Soligo, M., 2010. Radon and thoron emission from lithophysae-rich tuff under increasing deformation: an experimental study. Geophys. Res. Lett. 37, L05406. http://dx.doi.org/10.1029/2009GL041652, 12 March 2010.

CHAPTER 7

SOIL RADON SURVEY TO ASSESS NAPL CONTAMINATION FROM AN ANCIENT SPILL. DO KEROSENE VAPORS AFFECT RADON PARTITION ?

*Gabriele De Simone a, Carlo Lucchetti a, Francesca Pompilj a, Gianfranco Galli b, Paola Tuccimei a, * Curatolo P. c, Giorgi R. c*

a: Universit. a "Roma Tre", Dipartimento di Scienze, Largo San Leonardo Murialdo 1, 00146 Roma, Italy

b: Istituto Nazionale di Geofisica e Vulcanologia, Sezione Roma 1, Via di Vigna Murata 605, 00143, Roma, Italy

c: Golder Associates, Via Sante Bargellini 4, 00157 Roma, Italy, Pierpaolo_Curatolo@golder.it; RGiorgi@golder.it

Abstract

A soil radon-deficit survey was carried out in a site polluted with kerosene (Rome, Italy) in winter 2016 to assess the contamination due to the NAPL residual component in the vadose zone and to investigate the role of the vapor plume. Radon is indeed more soluble in the residual NAPL than in air or water, but laboratory experiments demonstrated that it is also preferentially partitioned in the vapors that transport it and may influence soil radon distribution patterns. Specific experimental configurations were designed and applied to a 31-station grid to test this hypothesis; two RAD7 radon monitors were placed in-series and connected to the top of a hollow probe driven up to

80-cm depth; the first instrument was directly attached to the probe and received humid soil gas, which was counted and then conveyed to the second monitor through a drierite cylinder capturing moisture and eventually the NAPL volatile component plus the radon dissolved in vapors. Readings from the two instruments were cross-calibrated through specifically designed laboratory experiments and compared. They correspond within the error range, so the presence of significant NAPL vapors, eventually absorbed by drierite, was ruled out. This is in agreement with low concentrations of soil VOCs. Accordingly, the radon-deficit is ascribed to the residual NAPL in the soil pores, as shown very well also by the obtained maps. Preferential areas of radon-deficit were recognised, as in previous surveys. An average estimate of 58 L (47 Kg) of residual NAPL per cubic meter of terrain is provided on the basis of original calculations, developed from published equations.

1. Introduction

In the last two decades soil radon has been used as tracer of residual Non-Aqueous Phase Liquid (NAPL) contamination since it is extremely more soluble in these substances than in water or air, resulting in a concentration-deficit compared to background values in close unpolluted areas. The mapping of this process, known as "radon-deficit technique" (Semprini, 2000) allows to identify the contamination affecting the vadose zone of an aquifer.

A recent and complete review on that was provided by Schubert (2015), which emphasizes the radon preferential solubility in the residual component of NAPL (mainly liquid blobs or films attached to soil particles), without specific mention to NAPL vapors. Certainly a NAPL contamination plume may have a multiphase flow and the partition of radon into the vapor plume, generally not considered, should be investigated more deeply.

Recent laboratory studies (De Simone et al., 2016a; b) suggested that the volatile component of NAPL dissolve radon gas and is responsible for radon transport through the subsoil. De Simone et al. (2016b) demonstrated that radon exhalation is enhanced in a closed experimental set-up at increasing soil saturation with kerosene, but showed that the employ of a desiccant reduces the radon concentration in the closed-loop circuit because drierite absorbs NAPL vapors and the radon dissolved in them.

In order to investigate how soil radon activity concentration at 80-cm depth is affected either by the residual or the vapor phase of kerosene, with the further goal of examining the interaction of vapors with the desiccant, proper field measurements were carried out in a site, which was already introduced in a previous work (Tuccimei et al., 2014). Two RAD7 (Durridge Co.) radon monitors were placed in-series and connected to the top a hollow probe; the first instrument was directly coupled to the probe and received humid

soil gas, which was counted and then delivered to the second monitor through a drierite cylinder capturing moisture and eventually NAPL vapors with dissolved radon. Readings from the two instruments were cross-calibrated through specifically designed laboratory experiments and compared to test the hypothesis that the first RAD7 records higher radon, if a significant component of vapors (detected as VOCs) still present in the soil, enhances radon transport through it and is then absorbed by the desiccant placed between the two monitors.

2. Geological setting and previous mapping

The "radon-deficit technique", was applied to a NAPL contaminated site whose specific location and coordinates are omitted for confidentiality agreement. The area is located in Latium Region (Italy) where a kerosene spill occurred and site characterization and monitoring actions are in progress. Wells and piezometers for sampling and analysis of pollutants provide an immediate feedback to soil gas surveys. The litho-stratigraphic sequence from top to bottom consists of about 0.5 m of backfills, 2.5 m of medium sands and 3 m of medium-fine sands. The water table fluctuates in the range 0.5 – 2.5 m depth during the year (Tuccimei et al., 2014).

A grid of 31 measuring stations was created over a 3,000 m^2 large zone, where soil ^{222}Rn, ^{220}Rn, CO_2, CH_4 and intrinsic permeability are seasonally monitored at 80 cm depth. A survey station was installed in the central part of the study area to evaluate soil gas concentration variability as a function of meteorological parameters.

Soil gas and permeability surveys performed at the end of the winter in the contaminated site and in a background area (located few hundred meters far away) provided the most significant and clear maps because the closed-system conditions,

typical of this season, kept better the differences between soil gas in the contaminated areas and in the background. Winter maps (February 2013) of soil ^{222}Rn concentration in the contaminated area (Fig. 1a) and in the background site (Fig. 1b) from Tuccimei et al. (2014) are reported here for the assessment of the pollutant distribution. Figure 1 shows that winter radon concentrations in the study area are, on average, much lower than in the background zone. In particular, radon lower concentrations in the background are around 22,000–23,000 Bq/m^3, while the lowest values in the study area stay around 2,000 – 5,000 Bq/m^3, in spite of similar stratigraphy and measuring period. This region is aligned along the directions of groundwater flow induced by pumping for safety operation of the plant (Fig. 1a). Radon negative anomalies in the contaminated site are not due to soil gas permeability because this parameter is substantially constant everywhere and always reaches high values (> 4.0 · 10-12 m^2).

Another significant result is related to the spatial correlation between soil ^{222}Rn and CO_2. In the background area, the two gases are directly correlated (Fig. 1b and 1d) because CO_2 works as carrier for radon (Giordano et al., 2016). The area is actually located at the periphery of a large volcanic-geothermal province with high regional heat flow (Cataldi et al., 1995). The entire region is characterized by extensive CO_2 release both from localized manifestations and diffuse degassing (Rogie et al., 2000; Chiodini and Valenza, 2007; Carapezza et al., 2012). The CO_2 has a deep origin (Chiodini et al., 2004; Barberi et al., 2007; Carapezza and Tarchini, 2007; Ciotoli et al., 2013; Carapezza et al., 2015) and it is also associated with deep geothermal reservoirs, known from deep boreholes and geophysics (seismic and gravimetric surveys) hosted in the Meso-Cenozoic carbonatic rock successions that outcrop in the Apennines, sealed atop by allochtonous argillitic flysch and by the post-orogeny Neogene marine clayey succession (Giordano et al., 2014 and references therein).

On the other hand, radon minima in the contaminated site (Fig. 1a) are not correlated with CO_2 negative values (Fig. 1c), because carbon dioxide is not soluble in NAPL and is not trapped by and accumulated in these substances. Consequently the highest CO_2 concentrations are roughly located where radon deficits and residual NAPL occur. This finding could be also due to a process of microbial degradation of the NAPL in the subsoil.

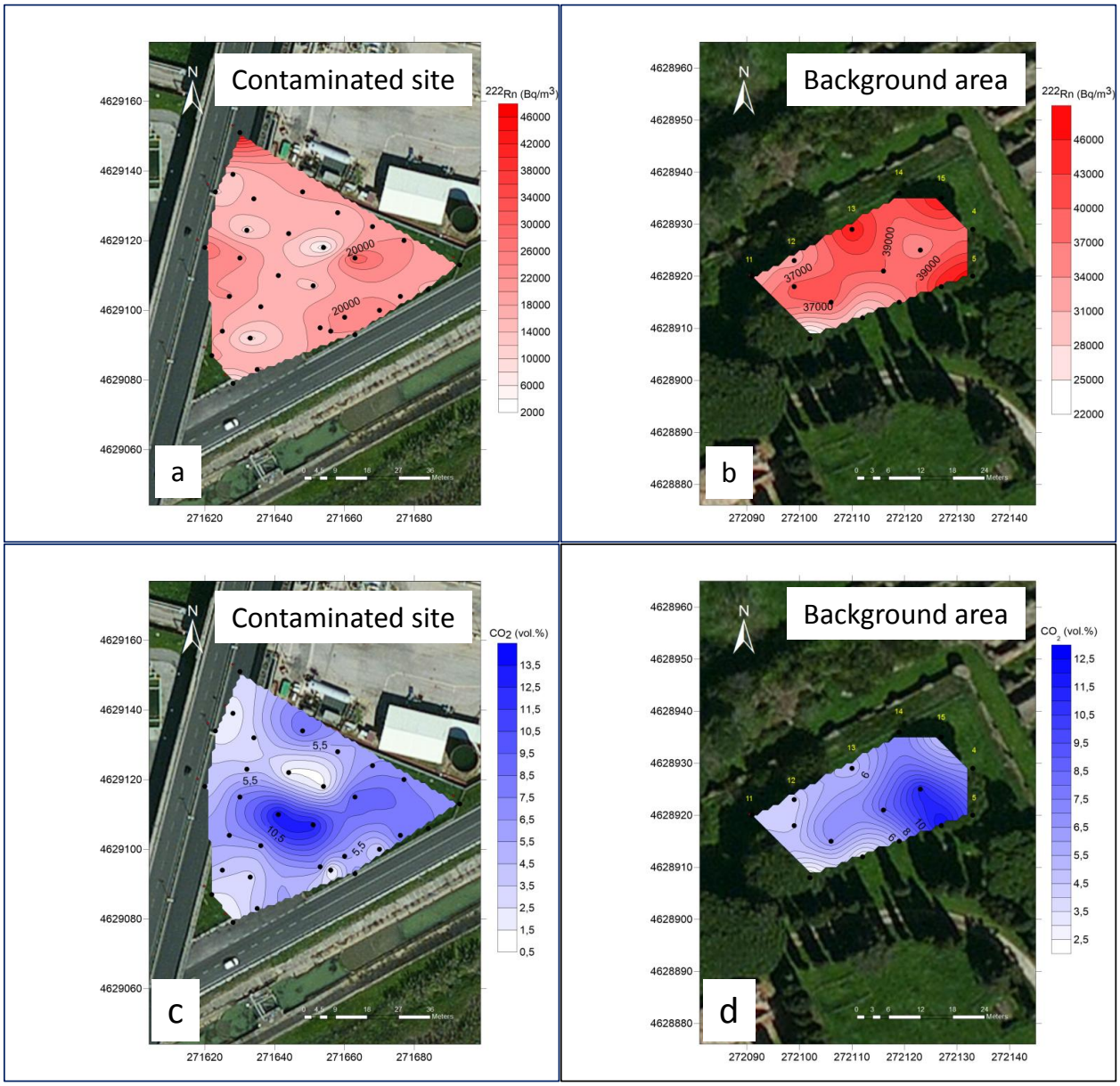

Fig. 1. Mapping of soil radon (Fig. 1a and Fig. 1b) and soil CO_2 (Fig. 1c and Fig. 1d) carried out in the contaminated area (Fig. 1a and Fig. 1c) and in a close background site (Fig. 1b and Fig. 1d) during late winter 2013 (modified from Tuccimei et al., 2014).

3. Material and Methods

3.1 Field survey

In order to investigate how soil radon activity concentration at 80-cm depth is affected either by the residual or the vapor phase of kerosene, using or not a desiccant cylinder, proper field measurements were carried out in the study area during the winter 2016. The soil radon survey was repeated over the 31-measuring stations grid (Tuccimei et al., 2014) and in the permanent station. Two RAD7 (Durridge Co.) radon monitors were placed in-series and connected to the top of a hollow probe placed in correspondence of each measuring station (Fig. 2); the first instrument was directly coupled to the probe and received humid soil gas, which was counted and then conveyed to the second device through a drierite cylinder which absorbed soil moisture and eventually NAPL vapors with the radon dissolved in them. The top of the hollow probe was then connected to a MiniRaeLite (Extratech) photoionization detector, equipped with a built-in pump to sample the air and measure Volatile Organic Compounds (VOCs) concentration.

Three RAD7s were used for the survey. RAD7-A (upstream of the drierite) and RAD7-C (downstream of the drierite) for a first experimental array (configuration 1); then RAD7-A (whose water content had increased a lot during the 25-minute long measurement) was replaced by a purged and dried new RAD7 (RAD7-B), while RAD7-C was not, because was kept dried by the desiccant (configuration 2). At the end of the second measurement, RAD7-A, meanwhile separately purged using another drierite cylinder, replaced RAD7-B, returning to the first array. The two configurations were employed alternately to optimise working time.

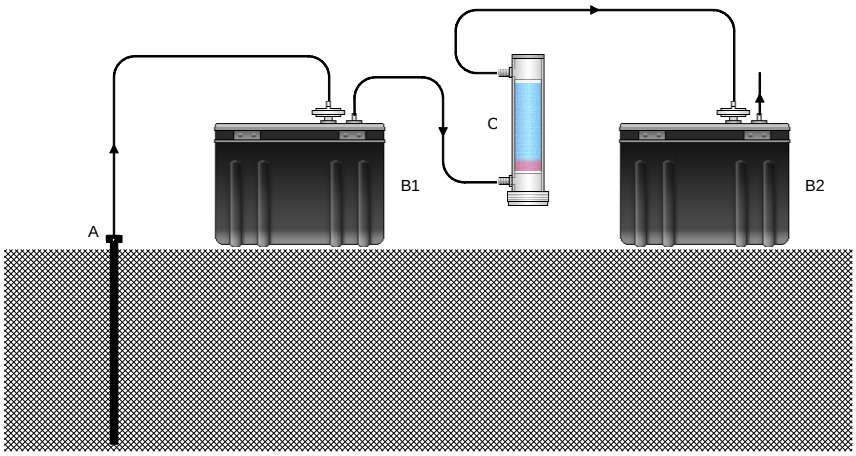

Fig. 2. Field-survey experimental configuration consisting of: a hollow probe driven up to 80-cm depth (A), in series connected to a first RAD7 (RAD7-A or RAD7-B, B1), a cilynder of drierite (C) and a second RAD7 (RAD7-C, B2).

3.2 Laboratory inter-calibration between the two RAD7s connected in series

In order to compare results obtained by the first (with high internal humidity) and second (low humidity) RAD7s, proper cross-calibration tests were performed in the laboratory (Fig. 3), keeping the same experimental configurations used in the field and changing the water content in the RAD7s inner volumes in a range (6 - 13 g H_2O) correspondent to field conditions. The laboratory set-up is reported in Fig. 3.

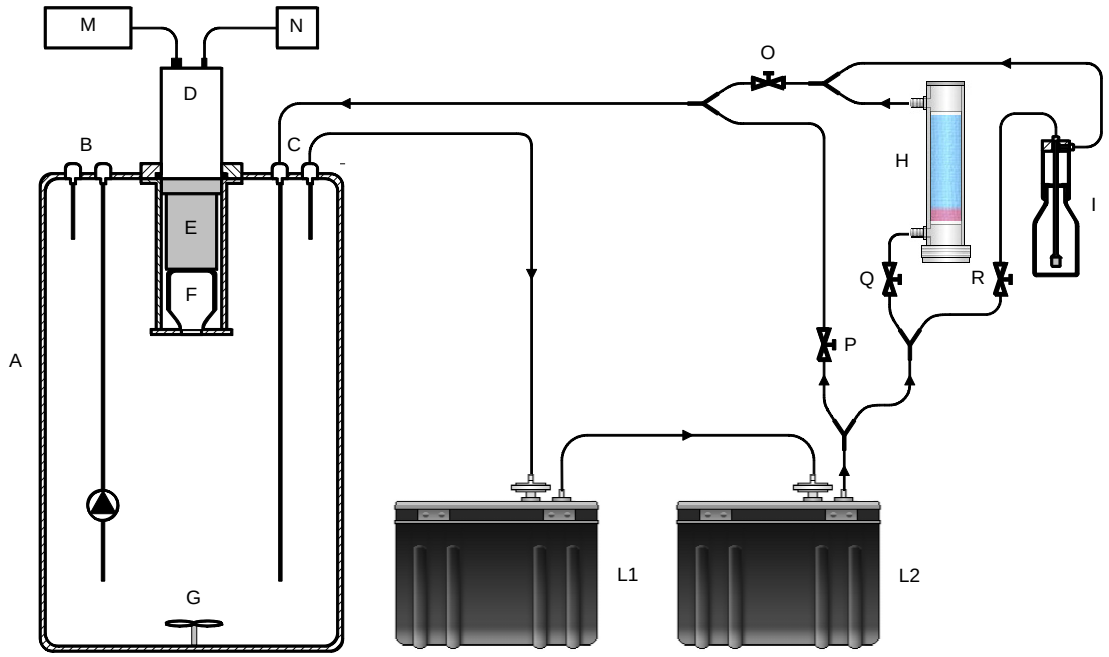

Fig. 3. Laboratory experimental set-up. A) radon chamber; B) air tight connectors (CPC) to be used when air circulation needs a pump; C) air tight connectors (CPC) when air circulation is guaranteed by an outer device; D) signal processing module; E) photomultiplier; F) scintillating flask; G) fan; H) desiccant column (drierite); I) humidifying device; L1 and L2) Durridge RAD7s (L1: RAD7-A or RAD7-B; L2: RAD7-C); M) multiscaler, N) low voltage supply; O), P), Q) and R) stopcocks.

Soil radon source was represented by a 56 L stainless steel radon chamber equipped with a scintillation cell (ZnS) coupled to a photomultiplier, which is not sensitive to humidity. Radon gas was extracted from an acidified (pH < 2) $RaCl_2$ source added with Ba (2500 Bq), and injected in the chamber. Relative humidity and thus weight of water molecules in the system, at constant temperature, were progressively changed by connecting the chamber to drierite (opening stopcocks O and Q and closing stopcocks P and R) or to a bubbling water bottle (opening stopcocks O and R and closing stopcocks P and Q) for drying or humidifying the closed circuit. When reached desired condition, the two RAD7s (RAD7-A and RAD7-C for configuration 1 and RAD7-B and RAD7-C for configuration 2) were connected to the chamber (opening stopcock P and closing stopcocks O, Q and R) and radon activity concentrations from the two instruments were measured at each humidity step (with an average duration of 90 min per step) (Fig. 3).

This calibration takes into consideration the effect of various factors on radon activity concentrations recorded by the first and the second instrument (different calibration coefficients; different response to the absolute humidity, specific for any single RAD7; different values of relative humidity provided by probes of radon meters placed upstream and downstream, with the readings from RAD7-A and B affected by an underpressure produced by the pump of the RAD-C placed downstream).

4. Results

4.1 Field survey

Soil radon data from the 31 measuring stations are plotted in Fig. 4. The ratio between soil radon activity concentration detected by the RAD7s located upstream of the drierite and correspondent values from the instrument placed downstream are shown for both experimental configurations (Fig. 4).

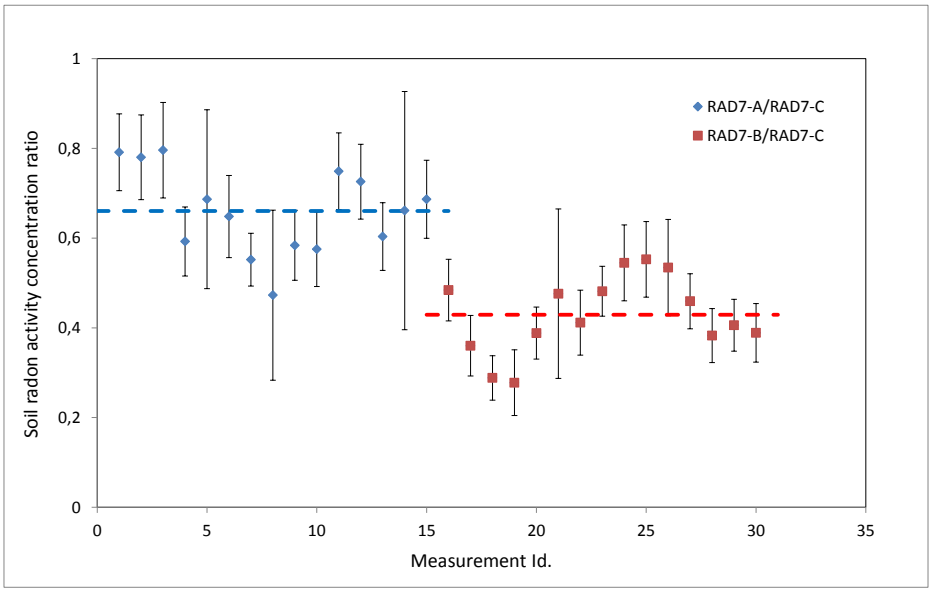

Fig. 4 – Soil radon activity concentrations measured using radon monitors (either RAD7-A or RAD7-B) located upstream and without drierite divided by correspondent values detected by RAD7-C placed behind a drierite column and connected in series with the first instrument (Fig. 2). See text for explanation. RAD7-A/RAD7-C is configuration 1, RAD7-B/RAD7-C corresponds to configuration 2.

Admitting that instruments are well calibrated and no significant kerosene vapors are present in the soil, we could expect ratios lower than 1 for both configurations because the RAD7 located upstream of the drierite is interfered by the water molecules that lower the efficiency of electrostatic collection of the silicon detector compared to the second monitor which is not (effect 1). On the other hand, the presence of NAPL vapors could enhance radon signal recorded from the first RAD-7s, because radon dissolved into vapors would not reach entirely the second instrument because of the absorption of vapors and of radon dissolved in the volatile component of kerosene by the drierite (effect 2, De Simone et al., 2016a). This effect could be masked and counterbalanced by effect 1, resulting in unpredictable soil radon activity concentration ratios between the two devices; since the intensity of the two phenomena is not known, it is necessary to approach them separately and then verify any dependence from the kerosene vapors (VOCs).

Figure 4 shows that both configurations are characterized by ratios lower than 1, but configurations 2 provides lower values compared with configuration 1, suggesting that RAD7-A and RAD7-B are differently affected by the water molecules interference on silicon detector electrostatic collection, as reported in De Simone et al. (2016a). This is why specific cross-calibration of the two instruments in both configurations has been performed in the laboratory.

4.2 Laboratory inter-calibration between the two RAD7s connected in series

According to the experimental set-up described in section 3.2, radon activity concentrations recorded by RAD7-C were compared with data from RAD7-A (Fig. 5a) or RAD7-B (Fig. 5b) as a function of the absolute humidity from RAD7-C. Two different fits were obtained for absolute humidity ranging from 6 to 9.5 and from 9.5 to

13 mg H_2O in RAD7 volume, for the correction of field survey data collected according to configuration 1 (Fig.5a). Just one fit was used from 6 to 12 mg H_2O in RAD7 volume for the cross-calibration of instruments in configuration 2 (Fig. 5b).

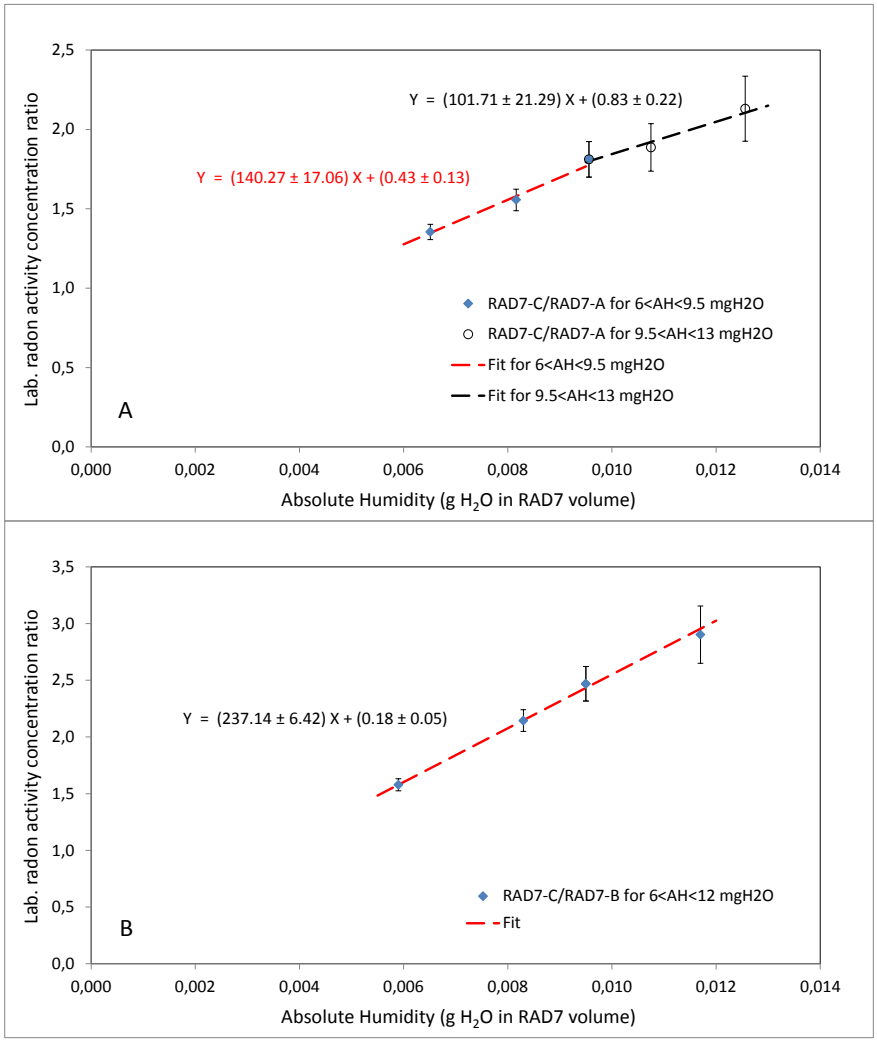

Fig 5. Effect of absolute humidity on the ratio between radon activity concentrations detected by RAD7-C (placed downstream) and the correspondent value measured by a first radon monitor (RAD7-A in Fig. 5a and RAD7-B in Fig. 5b) directly connected in series with an upflow radon chamber (Fig. 3). See text for explanation.

The obtained equations of cross-calibration as a function of absolute humidity were applied to soil radon activity ratios measured in the field (see Fig. 4) according to the following calculations:

Configuration 1:

$$R\ C = Rn\ F\_RAD7\text{-}C\ /\ (Rn\ F\_RAD7\text{-}A * Fc) \quad (1)$$

where:

R C is the corrected ratio between the reading of the radon measured in the field by RAD7-C (Rn F_RAD7-C) and the value which the first instrument would have provided if located in place of RAD7-C (configuration 1)

Rn F_RAD7-A is the radon measured in the field by RAD7-A

Fc are the cross-calibration factors between radon measured in the laboratory by RAD7-C and radon measured in the laboratory by RAD7-A and are equal to:

$$FC = m\ AH + c \quad (2)$$

with

m = slope of the linear fits in Fig. 5a

AH = absolute humidity or gram of H_2O in RAD7 volume

c = intercept of the linear fits in Fig. 5a

For configuration 2, the equations are similar, but radon data from RAD7-A have to be replaced with radon data by RAD7-B.

Corrected ratios for both configurations are plotted in Fig. 6 and approach the unity, demonstrating that, once corrected for AH, either the RAD7 placed upstream of the drierite or the second instrument located downstream give exactly the same results. It is worth stressing that the response of the three instruments to AH is different, as shown in De Simone et al. (2016a). In addition, it seems that there is not an effect due to kerosene vapors, because in that case soil radon activity ratios in Fig. 6 would have been higher than one, accounting for an aliquot of radon dissolved in the vapors and captured by the drierite.

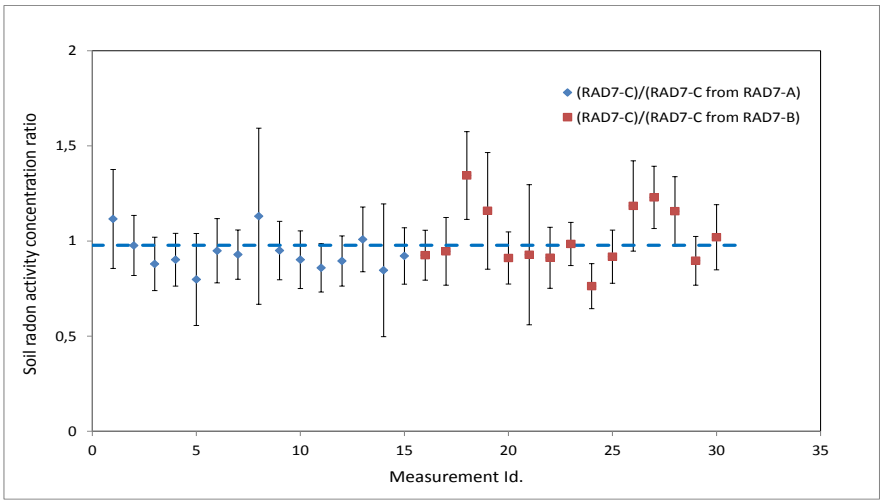

Fig. 6 – Soil radon activity concentrations measured using RAD7-C monitor placed behind a drierite column compared with values from the upstream monitor if placed downstream (RAD7-C position) after correction with laboratory cross-calibration. See text for explanation.

4.3 Maps of soil radon from the two RAD7s

Using the corrected values, two soil radon maps were obtained using radon data from the first and second instrument (Fig. 7). The two maps are very similar and basically correspond to the survey maps carried out in Winter 2013 and reported in Fig. 1a.

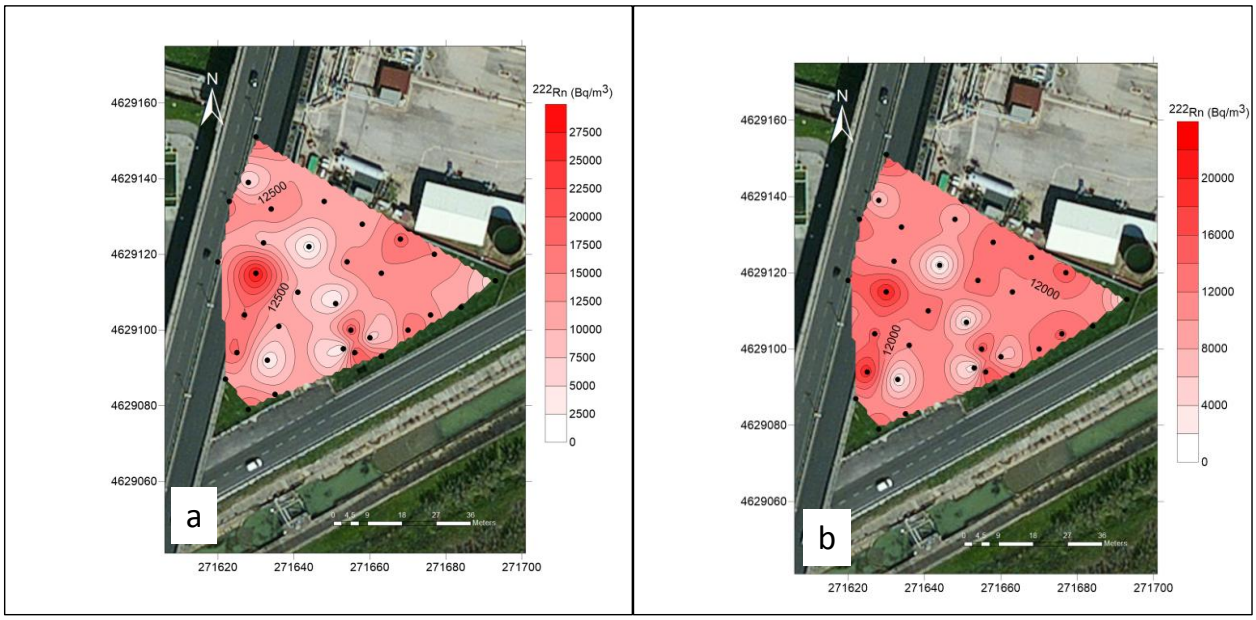

Fig. 7. Maps of soil radon obtained during winter 2016 for radon monitors located upflow (either RAD7-A or RAD7-B, Fig.7a) and downflow (RAD7-C, Fig. 7b) of a drierite column, corrected for the experimental configuration and absolute humidity on the basis of the laboratory cross-calibration. See text for explanation.

4.4 Map of soil VOCs

Figure 8a reports the distribution of VOCs measured from the 31 stations using the MiniRaeLite (Extratech) photoionization detector. Concentration are very low (up to 7.2 ppm, Table 1) and no correlation with radon-deficit is displayed (Fig. 8c). The scarce presence of vapors is in agreement with the information provided by radon data which did not show any preferential transport by the NAPL volatile phase with associated capture on the drierite.

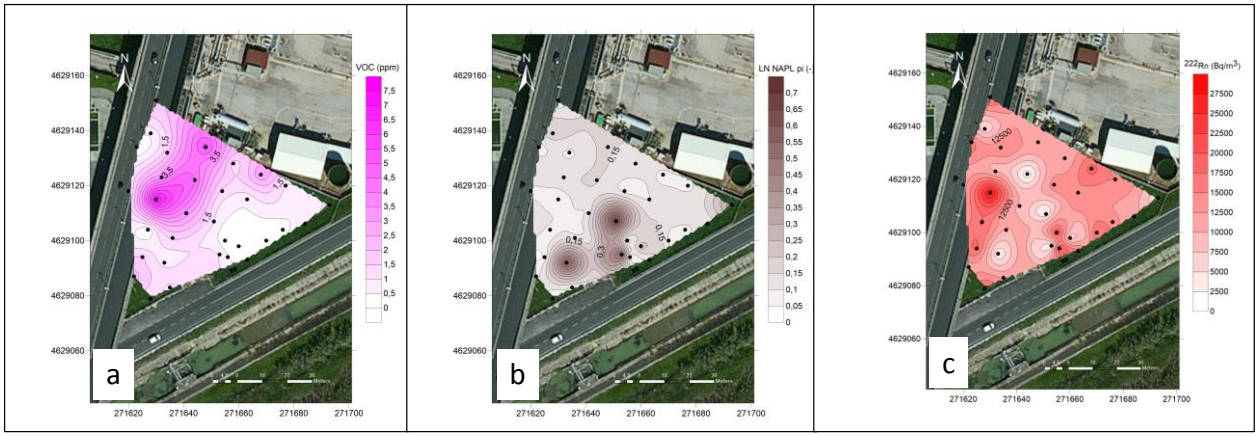

Fig. 8. Maps of soil VOCs (Fig. 8a), calculated fraction of residual kerosene (NAPLPi, Fig 8b, see section 4.5) and soil radon (Fig. 8c) obtained during the winter 2016.

4.5 Evaluation of radon deficit and fraction of NAPL in the subsoil

Provided that NAPL vapors are very low, we have tried to estimate the fraction of residual kerosene (NAPLPi) in the portion of subsoil partially saturated with fluids. Starting from the equation (equation 3) provided by Schubert (2015), we have obtained a new calculation (equation 4):

$$C_\infty = \varepsilon A_{Ra} \rho_d / n \, (1 - S_F + K_{W/SG} S_F (1 - X_{NAPL}) + K_{NAPL/SG} X_{NAPL} S_F \qquad (3)$$

where:

C_∞ : radon concentration in the soil pore space (Bq/m^3)

ε : emanation coefficient = 0.2

A_{Ra} : radium activity concentration of the mineral matrix (226Ra = 31.4 ± 0.6 Bq/kg)

ρ_d : bulk density of the mineral matrix (2.65 g/cm^3)

n : porosity of the mineral matrix = 0.37

S_F : total fluid saturation of the pore space

X_{NAPL} : NAPL fraction of S_F

$K_{W/SG}$: radon partition coefficient between water and soil gas, quantified by Weigel (1978)

$K_{NAPL/SG}$: radon partition coefficient between NAPL and soil gas

Equation 4 is resolved with respect to fraction of NAPL in the pore space (NAPLPi) as follows:

$$NAPL_{Pi} = \frac{-J \pm \sqrt{J^2 - 4\,C\,H}}{2\,H} \qquad (4)$$

where:

J, C, H: site-specific polynomials whose explanation is provided in the Appendix

NAPL Pi is related to XNAPL from the following equation:

$$X_{NAPL\,i} = (NAPL_{Pi} / A) / ((NAPL_{Pi} / A) + W_{Pi} / B) \qquad (5)$$

with

A, *B*: site-specific polynomials whose explanation is provided in the Appendix

WPi : fraction (mass) of water in the pore space

Values ascribed to all parameters in the equation are reported in Tables 1 and 2. Fractions of residual NAPLs (NAPLPi) range from 0.056 to 0.663 with an average value of 0.156. The map of NAPLPi (Fig. 8b) is very different from that of VOCs (Fig. 8a), but is inversely correlated with that of soil radon (fig. 8c), with higher fractions of residual NAPL in the pore space corresponding to radon-deficits. This is a further evidence that kerosene vapors do not play a significant role in soil radon distribution patterns which are influenced only by the residual NAPL (NAPLPi).

Finally, we can use the average fraction of residual NAPL in the pore space to evaluate the average volume of NAPLs in a cubic meter of polluted terrain. Given a porosity of 0.37 for medium sands, we have that 370 L are occupied by pores which still retain an average NAPL fraction (NAPL Pi) of 0.156 (Table 1) which corresponds roughly to 58 L of NAPL per cubic meter. Since the density of NAPLs is 0.81, we can estimate about 47 Kg of residual NAPLs in a cubic meter of terrain.

5. Conclusions

Radon-deficit technique shows the location of residual NAPLs in the soil. The presence of significant NAPL vapors is ruled out by the comparison of radon data obtained by two RAD-7s connected in series and separated by a column of drierite. After a rigorous cross-calibration of the two instruments, soil radon data corresponds within the error range and VOCs concentrations are accordingly very low, as expected for an ancient spill. An evaluation of the fraction of residual NAPL in the soil is provided. Its distribution matches very well the radon deficit. In conclusion, we could assess the contamination by residual kerosene, but could not recognize the effect of kerosene vapors on radon transport through the soil and the interference with the drierite. This approach works very well and has the potential to be applied successfully to recent

spills where the vapor plume is supposed to be more extended. A new version of the equation proposed by Schubert (2015) is here developed and applied. An estimate of 58 L (47 Kg) of residual NAPL per cubic meter of terrain is provided.

Very high radon-deficits are found, obviously, when radon concentrations are extremely low: in those cases estimations of NAPLPi can be affected by very large uncertainties unless errors associated with radon measurements are kept low.

References

Barberi, F., Carapezza, M.L., Ranaldi, M., Tarchini, L., 2007. Gas blowout from shallow boreholes at Fiumicino (Rome): Induced hazard and evidence of deep CO2 degassing on the Tyrrhenian margin of Central Italy. J Volcanol Geotherm Res, 165, 17–31.

Carapezza, M.L., Tarchini, L., 2007. Geochemical evidence of huge magmatic degassing from the quiescent Alban Hills volcano (Rome, Italy). J Volcanol Geotherm Res, 165, 5-16.

Carapezza, M. L., Tarchini, L., Granieri, D., Martelli, M., Gattuso, A., Pagliuca, N., Gattuso , A., Ranaldi, M., Ricci, T., Grassa, F., Rizzo, A., Pizzino, L., Sciarra, A., 2015. Gas blowout from shallow boreholes near Fiumicino International Airport (Rome): Gas origin and hazard assessment. Chem Geol, 407, 54-65.

Chiodini, G., Cardellini, C., Amato, A., Boschi, E., Caliro, S., Frondini, F., Ventura, G., 2004. Carbon dioxide Earth degassing and seismogenesis in central and southern Italy. Geophys Res Lett, 31(7), L07615 1-4.

Chiodini, G., Valenza, M., 2007 (Eds). Results of INGV-DPC-V5 Project: the catalogue of italian gas emissions. Open website : googas.ov.ingv.it (last access 13 March 2015)

Ciotoli, G., Etiope, G., Florindo, F., Marra, F., Ruggiero, L., Sauer, P.E., 2013. Sudden deep gas eruption nearby Rome's airport of Fiumicino. Geophys Res Lett, 40(21), 5632-5636.

De Simone, G., Lucchetti. C. Galli. G., Tuccimei. P., 2016a. Correcting for H2O interference using electrostatic collection-based silicon detectors. J Environ Radioactiv, 162-163, 146-153.

De Simone, G., Lucchetti, C., Pompilj, F. , Galli, G., Tuccimei, P., 2016b. Laboratory simulation of recent NAPL spills to investigate radon partition among NAPL vapours and soil air (2016b). Accepted by Appl Radiat Isotopes.

Rogie, J. D., Kerrick, D. M., Chiodini, G., Frondini, F., 2000. Flux measurements of nonvolcanic CO2 emission from some vents in central Italy, J Geophys Res, 105, 8435–8445.

Schubert, M., 2015. Using radon as environmental tracer for the assessment of subsurface Non-Aqueous Phase Liquid (NAPL) contamination – A review. Eur. Phys. J. Special Topics 224, 717–730.

Semprini, L., Hopkins, O.S., Tasker, B.R., 2000. Laboratory, field, and modeling studies of Radon-222 as a natural tracer for monitoring NAPL contamination. Transp. Porous Med. 38, 223.

Tuccimei, P., De Simone, G., Curatolo, P., Giorgi, R., Lucchetti, C., Castelluccio, M. Calì, A., 2014. Tracing NAPLs contamination in the vadose zone using soil radon. Rend online Soc Geol It, 33, 100-103, DOI:10.3301/ROL.2015.24.

Weigel, F., 1978. Radon. Chem. Ztg. 102, 287-299.

Appendix

Starting from equation 3, proposed by Schubert (2015) to calculate soil radon concentration in the pore space (C∞), we have developed a new calculation (equation 4) where radon concentration in the polluted sites are firstly compared to soil radon values in close unpolluted areas to calculate the radon deficit (Di, see Table 1). Equilibrium radon concentration in the background are determined using a simplified version of equation 3:

$$C_{\infty} = \varepsilon A_{Ra} \rho_d / n$$

Eq. (A.1)

From the comparison of equations A.1 and 3, it turns out that:

$$D_i = 1 / n (1 - S_F + K_{W/SG} S_F (1 - X_{NAPL}) + K_{NAPL/SG} X_{NAPL} S_F)$$

Eq. (A.2)

Now, since the total fluid saturation of the pore space (SF) is the sum of SNAPL and SW, that are the pores fractions occupied by NAPL (SNAPL) and water (SW), respectively, and these two terms (Tables 1 and 2) can be expressed as:

$$S_{NAPL\,i} = NAPL_{Pi} / ((\gamma_{NAPL} / \gamma_{di}) - (\gamma_{NAPL} / \gamma_s))$$

Eq. (A.3)

$$S_{W\,i} = W_{Pi} / ((\gamma_{Wi} / \gamma_{di}) - (\gamma_{Wi} / \gamma_s))$$

Eq. (A.4)

or simplifying, $S_{NAPL\,i} = NAPL_{Pi} / A$ and $S_{W\,i} = W_{Pi} / B$

where:

$$A = ((\gamma_{NAPL} / \gamma_{di}) - (\gamma_{NAPL} / \gamma_s))$$

Eq. (A.5)

$$B = ((\gamma_{Wi} / \gamma_{di}) - (\gamma_{Wi} / \gamma_s))$$

Eq. (A.6)

then,

$S_{F\,i} = (NAPL_{Pi} / A) + (W_{Pi} / B)$
Eq. (A.7)

If parameters defined in equations from A.3 to A.7 are inserted in equation A.2 and then the latter is developed and solved with respect to NAPLPi, we obtain equation 4, where the following polynomials are defined:

$C = (W_{Pi} / B) – (n\, D_i\, W_{Pi}/B) + (n\, K_1\, D_i\, W_{Pi}/B) + (n\, D_i\, W_{Pi}^2 / B^2) – (n\, D_i\, K_1\, W_{Pi}^2 / B^2)$
Eq. (A.8)

$D = (2\, n\, D_i\, W_{Pi} / A\, B) – (2\, n\, D_i\, K_1\, W_{Pi} / A\, B) + (1/A) – (n\, D_i / A) + (n\, K_1\, D_i / A)$
Eq. (A.9)

$E = (n\, D_i / A^2) – (n\, D_i\, K_1 / A^2)$
Eq. (A.10)

$F = (n\, D_i\, K_2\, W_{Pi} / A\, B) – (n\, D_i\, K_1\, W_{Pi} / A\, B)$
Eq. (A.11)

$G = (n\, D_i\, K_2 / A^2) – (n\, D_i\, K_1 / A^2)$
Eq. (A.12)

$H = E – G$
Eq. (A.13)

$J = D – F$
Eq. (A.14)

Note that $K_{W/SG}$ and $K_{NAPL/SG}$ are labelled as K_1 and K_2, respectively.

The solution to the following calculation:

$H\, NAPL_{Pi}^2 + J\, NAPL_{Pi} + C = 0$
Eq. (A.15)

is the above mentioned equation 4:

$$NAPL_{Pi} = \frac{-J \pm \sqrt{J^2 - 4\,C\,H}}{2\,H}$$

where actually two **solutions**, one **positive** and one **negative** are provided, but only the positive one (deriving from the negative sign in front of the square root) is meaningful. Fractions of NAPL in the pore space (NAPLPi) are reported in Table 1 for all the stations of the grid.

CHAPTER 8

GEOPHYSICAL INVESTIGATION IN THE STUDY AREA

Methods

Two rectangular grids made, respectively, by 15x5 and 4x12 linear spreads of steel electrodes were utilized to create a 3D image of the resistivity and the chargeability of the subsoil. The first array was oriented with the longest side WNW-ESE with a spacing between the electrodes of 7.5 m in the longest side (x axis) and 2.5 m in the shorter side, with a total size of 35x30 meters; the second one was oriented with the longest side NNE-SSW with a spacing between the electrodes of 2.5 m in both sides with a total length of 27.5 meters and a width of 7.5 meters. It was chosen to overlap the two arrays of 7.5x7.5 meters and to utilize a shorter interdistance in the second array because we needed a more detailed image of that area particularly in the NNE-SSW direction that was the direction of the spill already detected by previous studies.

The electrodes were connected, by multichannel cables, to a georesistivimeter Syscal PRO (Iris Instrument).

IP measurements were collected using a pulse length of 1 s with integral chargeability measurements performed during voltage decay after current shut-off.

Instruments

The SYSCAL Pro Switch is a ten-channels electrical resistivimeter which includes a transmitter, a receiver and a switching unit, that allows to transform linear surveys in 2D or 3D surveys combining several parallel sequences of same electrodes doing grids of measurements (fig. 12 a).

Fig. 12 : a) switch configuration for 3D imaging; b) Syscal Pro Switch resistivimeter connected with a screen that shows a single linear bi-dimensional geoelectrical profile

Multi-channel acquisition of resistivity and/or IP data, up to 10 readings at the same time, is obtained using a set of electrodes (normally 24, 48, 72, 96 or 120), connected in a line or in several lines, which number is increased through Switch Pro units that allow to create 3D ground images by overlapping different planar images obtained juxtaposing linear contiguous acquisitions.

Time domain discharge curves due to Induced Polarisation chargeability (IP) are registered for different depths.

Apparent resistivity, ρ, is directly proportional to geometrical coefficient, K [m], and to received potential, V [mV], and is inversely proportional to transmitted current, i [mA].

For the data analysis and the 3D interpretation ERTLab software is used.

Geophysical investigation in the study area

A resistivimeter Syscal PRO switch (Iris Instrument) was employed according to a pole-dipole configuration array, with a maximum penetration of 3 meters, corresponding to about the groundwater table depth. Two rectangular grids, partially overlapping, made, respectively, by 15x5 and 4x12 linear spread of steel electrodes were utilized to create a 3D image of the resistivity and the chargeability of the subsoil.

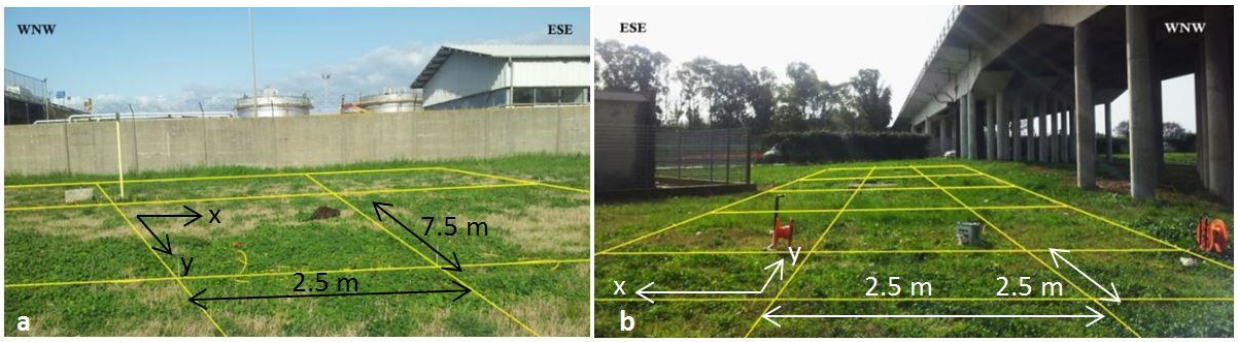

Fig. 1 : grids for 3D geoelectrical image of the subsoil

The first array was oriented with the longest side WNW-ESE with a spacing between the electrodes of 7.5 m in the longest side (x axis) and 2.5 m in the shorter side, with a total size of 35x30 meters; the second one was oriented with the longest side NNE-SSW with a spacing between the electrodes of 2.5 m in both sides with a total length of 27.5 meters and a width of 7.5 meters. It was chosen to overlap the two arrays of 7.5x7.5 meters and to utilize a shorter interdistance in the second array (fig. 2, yellow rectangle) because we needed a more detailed image of that area particularly in the NNE-SSW direction that was the direction of the spill already detected by previous studies. The electrodes were connected, by multichannel cables, to the resistivimeter so resistivity and chargeability were simultaneously measured in time domain.

Resistivity was measured during the injection of the direct current pulse, with a pulse length of 1 s, while chargeability was measured during voltage decay as the remaining

potential after the current has been switched off, so corresponding to the integral of the decay curve during the defined time window of 280 ms (fig. 3).

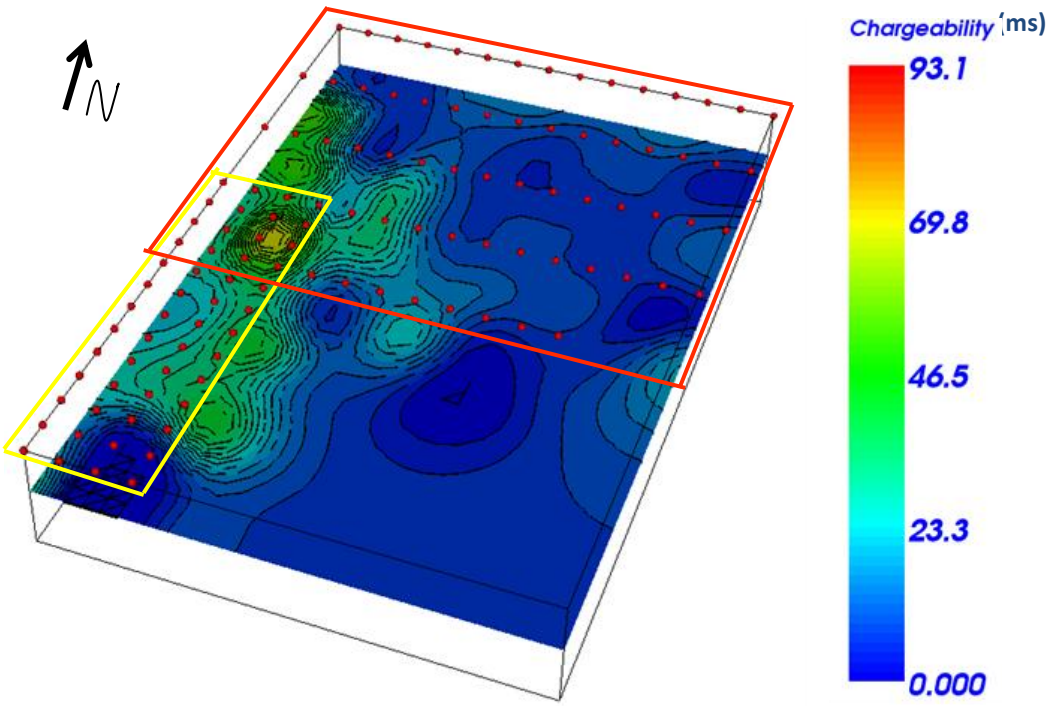

Fig. 2 : chargeability map at 2,75 m depth made overlapping the two grids.

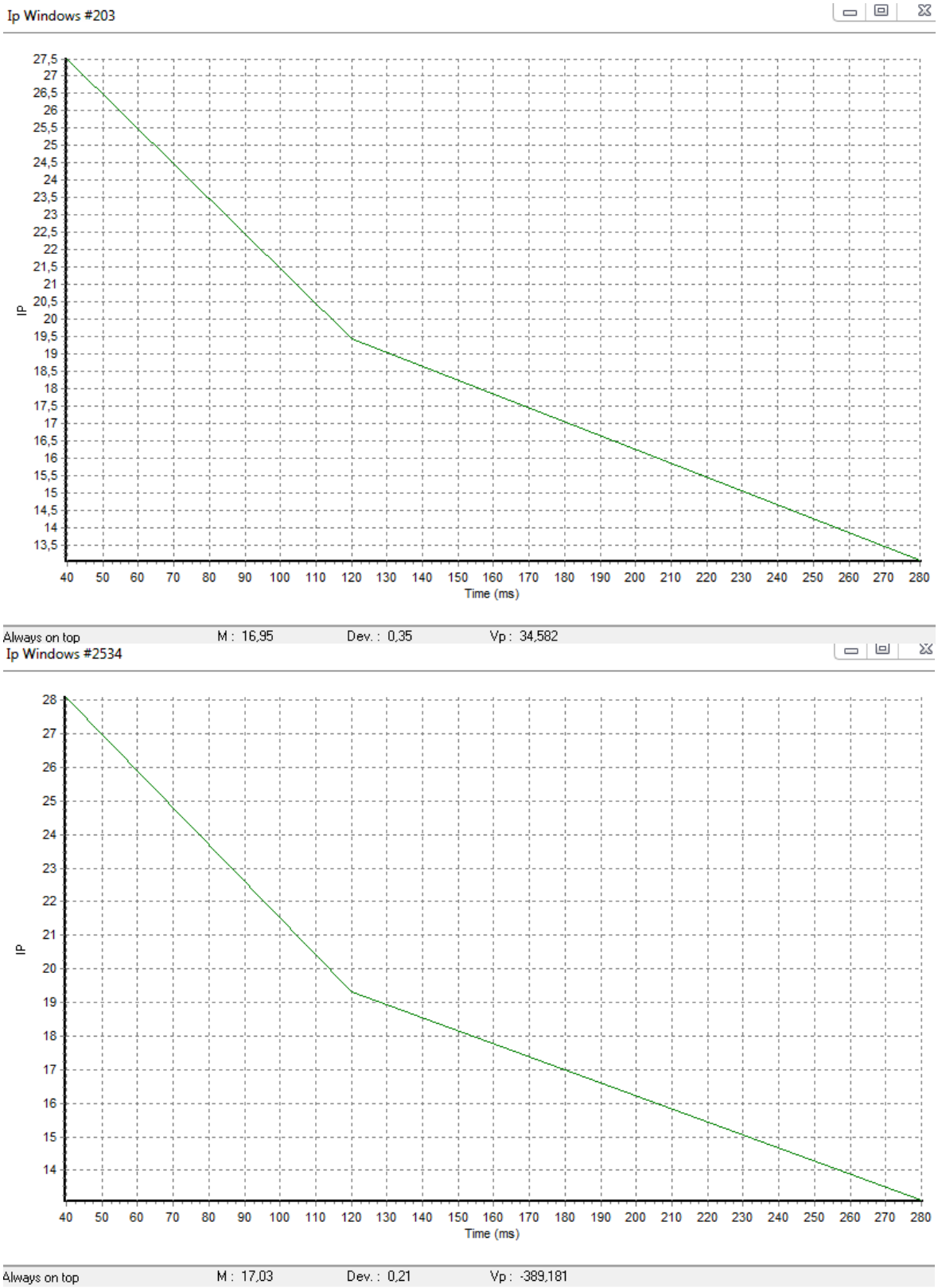

Fig. 3 : Induced Polarization (IP) windows; voltage decay curves in interval time of 280 ms (almost all measures has a double discharge trend that changes after about 120 ms)

Switch units allow to transform linear surveys, that have bi-dimensional vertical response (x;z), in grids surveys, that have tri-dimensional response (x;y;z), measuring, contemporaneously, in both x-z and y-z perpendicular directions, using the same electrodes combining several parallel sequences to obtain 2D (x;y) and 3D (x;y;z) images of the subsoil.

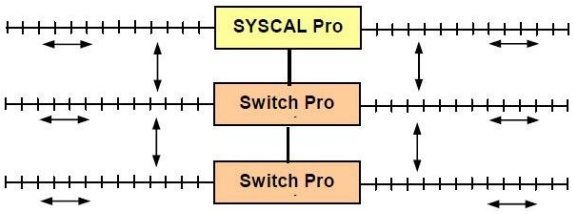

Fig. 4 : Switch configuration for grids surveys

The narrow zone characterized by positive anomaly of resistivity (fig. 5b, blue ellipse) well reflects negative anomaly of radon NNW-SSE trend, and therefore the presence of the pollutant residue.

We can say that that high values reflect the presence of NAPL, that is electrical insulator, and can cause a rise in resistivity because his free-phase products displace water in saturated soil (Johansson et al., 2015). The chargeability positive values, instead, coincide with the direction of groundwater flow, due to induced pumping, and may be due to water leaching the soil, cleaning it from the residual kerosene allowing, therefore, soil's grains polarization. Where the chargeability values are lower, corresponding with radon deficit, this could probably be due to the pollutant residue, in the form of kerosene film, that, by coating soil particles, electrically isolates soil grains not allowing grain polarization (Johansson et al. 2015). The positive chargeability anomaly, therefore, could be used to monitor the remediation of the contaminated site

verifying that, with the passage of time, the narrow zone with highest chargeability values extends its area covering the entire range.

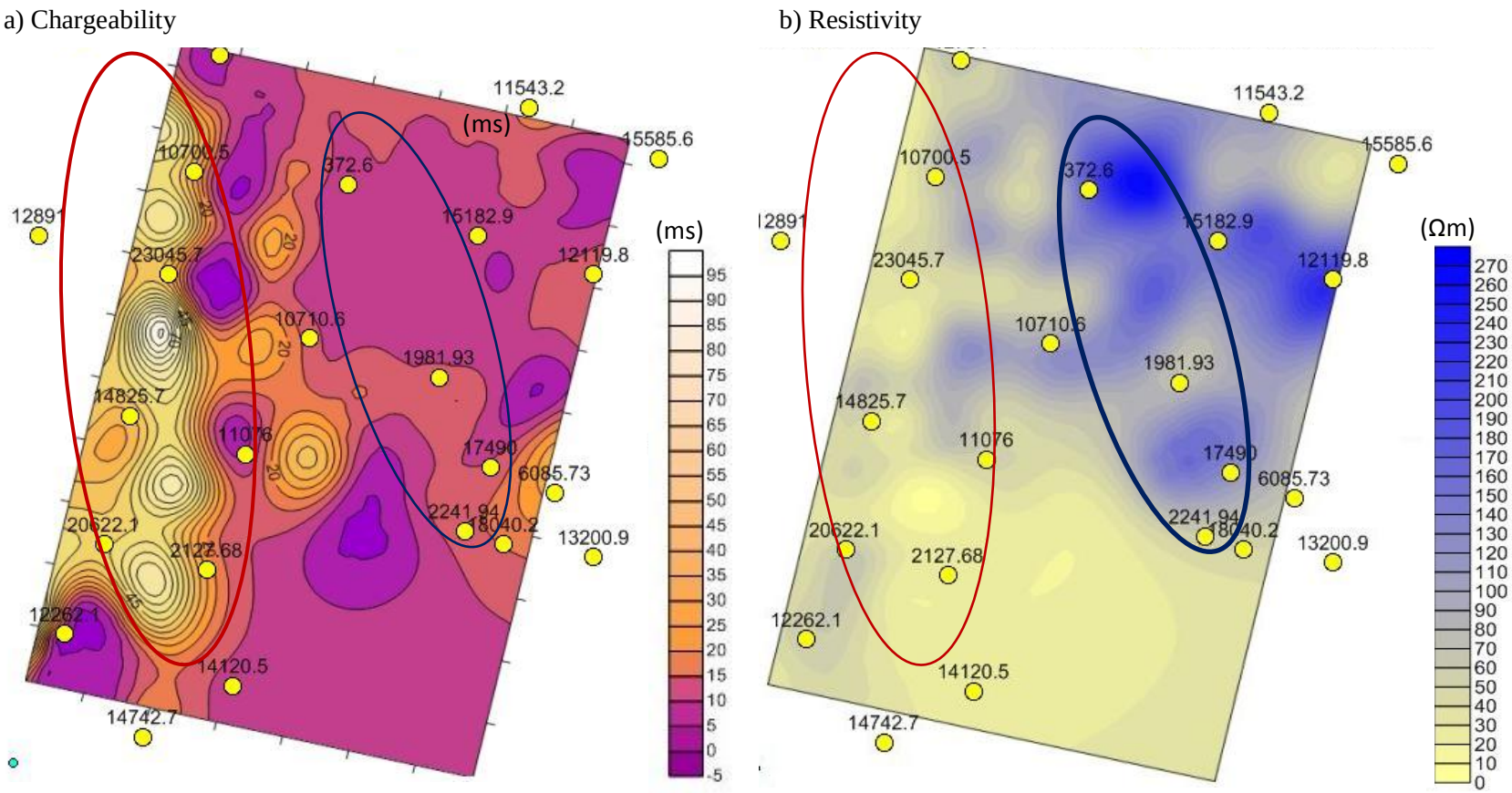

Fig. 5 : chargeability (a) and resistivity (b) maps vs radon values (yellow points); red ellipse: leached soil, blue ellipse: residual kerosene, yellow ellipse: other residual kerosene

3D images of the subsoil (fig. 6a) allow to better study the subsoil showing that about between 50 cm and 80 cm, upper than geochemical analysis, there are some about N-S aligned spots of high resistivity that could be interpreted as residual kerosene spots in the vadose zone that are not visible in geochemical outcomes because we measured gas from deeper areas.

3D Induced Polarization image shows the continuity of the anomaly alignment and it confirms that that continuity could be due to pumping flow.

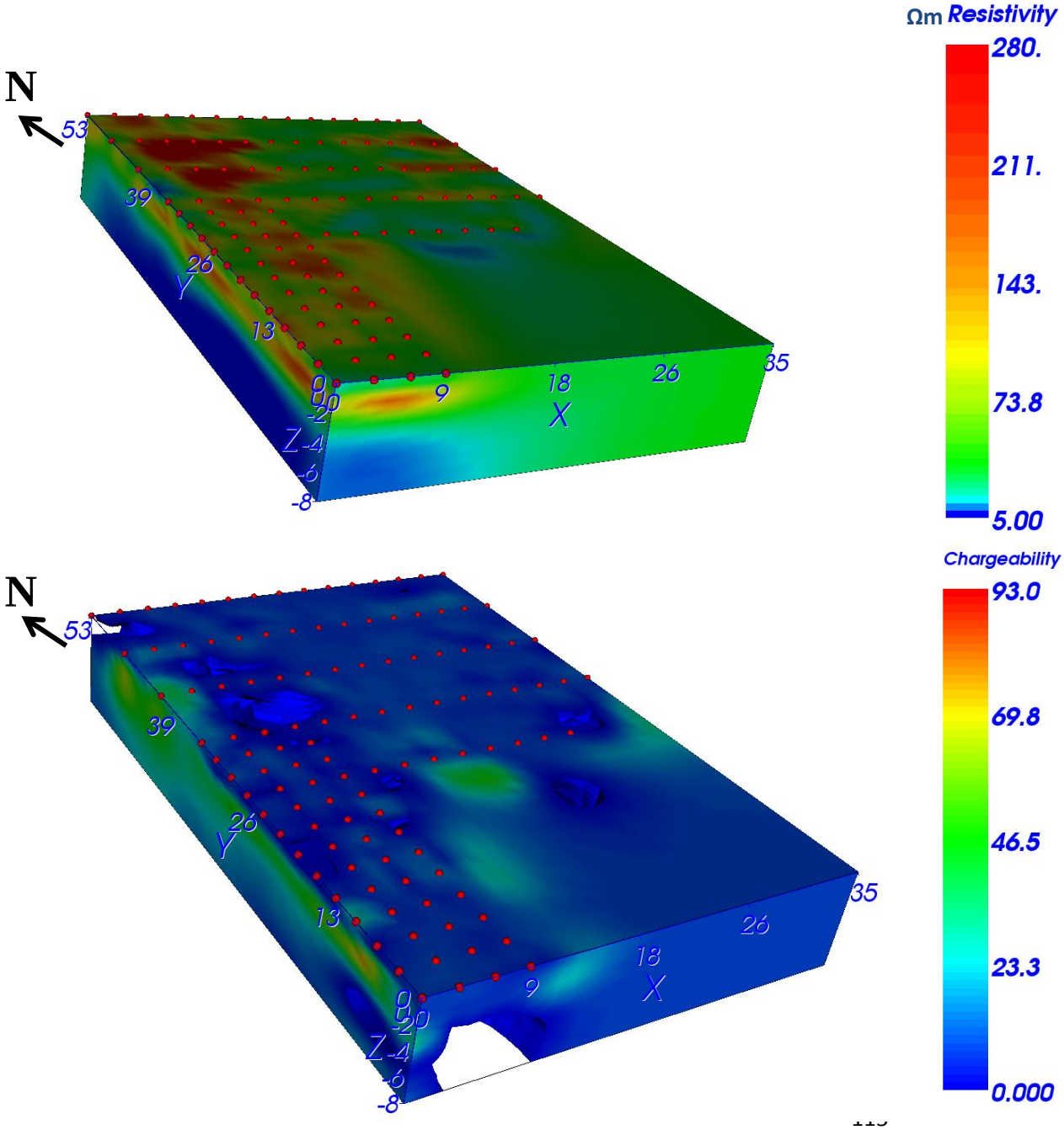

Fig. 6 : 3D imaging of the subsoil

Discussion

Assessment of subsurface NAPL contamination by comparison of soil radon deficit and resistivity positive anomalies was verified in a polluted area near Rome.

The research area has a known stratigraphy that is constituted by about 0.5 m of backfills, 2.5 m of medium sands and 2.5 m of medium-fine sands and the water table fluctuates in the range of 0.5-2.5 m below ground level during the year. (Tuccimei et al., 2014) Radon outcomes in the study area, with respect to background, show that average radon deficit is about 66% and significantly lower values (lower than 6500 Bq/m^3 , fig. 2) reach deficit higher than 72% pinpointing the main still polluted area.

Residual kerosene, in dry and sandy soils, can influence radon occurring in the soil with a radon diffusion length of about 2 meters. (Tuccimei et al., 2014) The surveys were carried out in winter when topsoil behaves as a closed system to soil gases release to the atmosphere so radon values aren't lowered by seasonal influence.

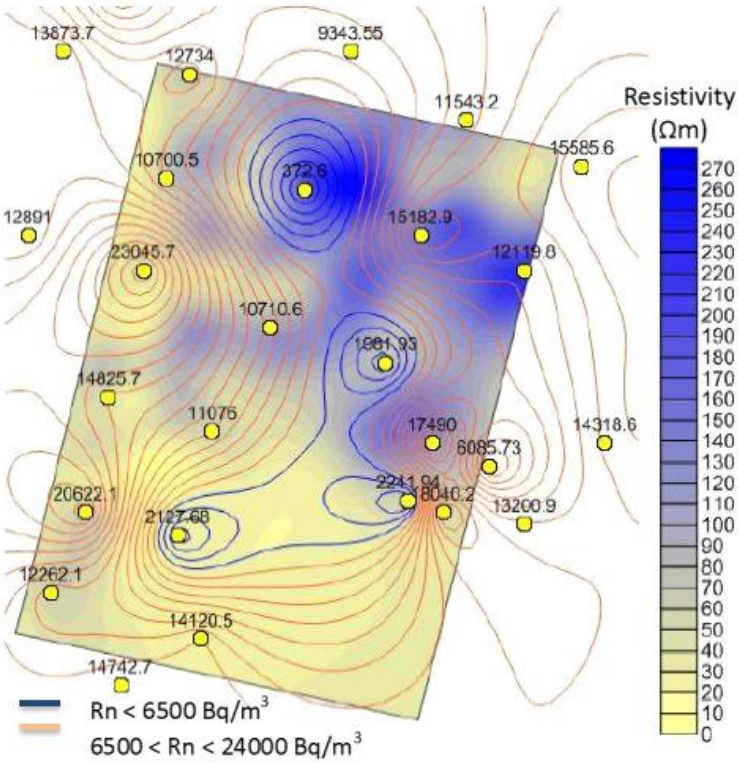

Fig. 7 : 222Rn- Resistivity

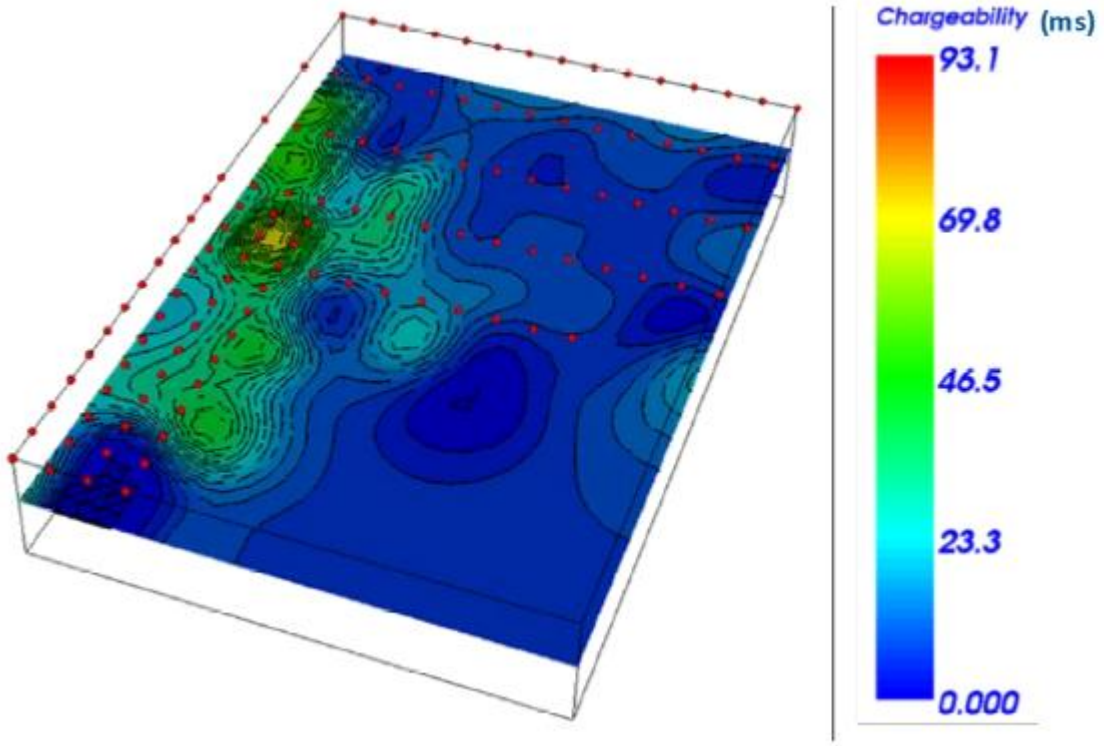

Fig. 8 Soil Chargeability. Highest values pinpoint the remediation working

To better delineate residual kerosene extension some geoelectrical surveys were carried out in addiction to soil radon survey.

Resistivity variation can be due to many reasons so it isn't useful make resistivity surveys alone but it may be interesting in addiction to other survey's techniques.

The narrow zone characterized by positive anomaly of resistivity, in fact, well reflects negative anomaly of radon NNW-SSE trend, and therefore the presence of the pollutant residue. It can be said that, here, high values are due to NAPL occurrence in the soil because kerosene is an electrical insulator and it can cause a rise in resistivity (Johansson et al., 2015).

The chargeability positive values, instead, coincide with the direction of groundwater flow, due to induced pumping, and may be due to water leaching the soil, cleaning it

from the residual kerosene allowing, therefore, soil's grains polarization. Where the chargeability values are lower, corresponding with radon deficit, this could probably be due to the pollutant residue, in the form of kerosene film, that, by coating soil particles, electrically isolates soil grains not allowing grain polarization (Johansson et al. 2015). The positive chargeability anomaly, therefore, could be used to monitor the remediation of the contaminated site verifying that, with the passage of time, the narrow zone with highest chargeability values extends its area covering the entire range.

We, also, compared soil radon of last measurement campaign (February 2016) with radon values from previous measurement campaign made in the same season three years before. Radon values from last survey are lower than the antecedents and it can be due to NAPL saturation because radon concentration is more sensitive to changes in NAPL saturation of the soil pores (S NAPL) at low values (S NAPL < 5%) and not very sensitive above NAPL saturations higher than 10% (Schubert, 2015).

The combination of these techniques is useful to obtain a sufficiently detailed picture of ground contamination so the simultaneous use of geochemical and geophysical techniques can be employed to assess the effectiveness of NAPL remediation and to provide an indicator that NAPL has been removed.

Conclusions

In conclusion we can affirm that soil radon deficit technique, already corroborated as NAPL tracer, can be implemented by resistivity surveys that in addition to soil radon investigation can better define the residual polluted area through overlaying resistivity excess and radon deficit comparing them to nearby areas that have same lithology with same characteristics. In all polluted area radon values are lower than background values (<23000 Bq/m^3) but the lowest values (independent from permeability and CO_2

variations) are aligned about NNW- SSE with a NE-SW deviation in the southern part of the area. Chargeability surveys are useful to understand how remediation is working and how residual kerosene films or blobs are distributed

CHAPTER 9

ADDITIONAL PAPERS ON NEW ANALYTICAL METHODS

9.1 CALIBRATION OF BIG BOTTLE RAD H_2O SET-UP FOR RADON IN WATER USING HDPE BOTTLES

Gabriele De Simone a,Gianfranco Galli b, Carlo Lucchetti a, Paola Tuccimei a,

a: Dipartimento di Scienze, Universit. a "Roma Tre", Roma, Italy

b: Istituto Nazionale di Geofisica e Vulcanologia, Sezione Roma, Roma, Italy

Abstract

Glass bottles are generally employed for water sampling because glass is impervious to radon and is not lost during sample storage. On the other hand, glass is fragile and may break, so 1 L High Density PolyEthylene (HDPE) bottles (Thermo Scientific Nalgene) are tested in place of glass vessels employing Big Bottle RAD H_2O device (Durridge Company) coupled with RAD7 monitor. The purpose of this calibration is to quantify radon loss during storage in HDPE bottles, evaluate possible radon uptake by known volume of desiccant (Drierite, granular $CaSO_4$) and quantify radon interaction with the rubber and plastic parts of the experimental circuit. These processes have been eparately investigated, performing proper experiments for the assessment of their influence on esulting radon data using seven series of solutions at known activity concentrations in

the range from 27 to 194 Bq/L. Percent radon loss during storage in 1 L HDPE bottles has been estimated at 0.0045 min_1. Radon absorption by desiccant, expressed as equivalent' volume of Drierite is 0.673 ± 0.092 L and is somehow independent, within errors, from i) the amount of water already absorbed in Drierite, ii) a recirculation time greater than 30 min and iii) radon concentrations. Radon absorption/desorption from rubber and plastic parts of the experimental device has been assessed as a function of concentration gradient between the inner volume of the circuit and the pores of polymer's. A final algorithm accounting for the above described physical processes has been developed for long runs (2 e 3 h). A simplified calculation method for short easurements (30 min) is also provided.

Introduction

Activity concentration of radon in groundwater is routinely measured using a variety of methods: Lucas cell, liquid scintillation, ionization chambers, gamma and alpha spectrometry of radon gas extracted by aerating the water sample.

Glass bottles are generally employed for sampling the water, especially when the measurement is not performed rapidly, but a delay may follow, because glass is impervious to radon and is not lost during sample storage. On the other hand, glass is fragile and the transport of glass bottles may induce the rupture, especially when springs or wells to sample are located along bumpy country or mountain roads. The need for shatterproof bottles led us to replace the 2.5 L glass bottles provided by Durridge Company Inc. with 1 L HDPE (High Density PolyEthylene) narrow-mouth bottles (Thermo Scientific Nalgene). They are 19.7 - 7.3 cm (height_outer diameter) with a cap size 2.7 - 4.3 cm (height outer diameter). Themouth size and the screw closure are compatible with the holed cap and aerator used by Durridge in the standard Big Bottle RAD H_2O configuration. The choice of this kind of plastic is also due to its low gas permeability; actually HDPE barrier membranes are employed to prevent radon and vapor intrusion into residential andcommercial buildings (Jir. anek et al., 2008).

A calibration of Big Bottle RAD H_2O equipment coupled with HDPE bottles was then performed against an activated charcoal collector counted by gamma spectrometry and the radon chamberof INGV (Istituto Nazionale di Geofisica e Vulcanologia)-Roma

using standard solutions at different radon activity concentration in order to: 1) account for radon loss during sample storage in HDPE containers; 2) evaluate the radon uptake by known volume of desiccant (granular $CaSO_4$); 3) quantify radon absorption/desorption by the rubber and plastic parts of the experimental system

depending on the concentration gradient between air radon concentration in the closed-loop setup and radon concentration in the polymer's pores; 4) find an algorithm for the assessment of radon concentration based on the measurement provided by RAD7 in 30 min.

Materils and methods

Seven series of radon-containing solutions were produced and measured using the Big Bottle RAD H_2O device coupled with RAD7 radon detector (Durridge Company). Radon was collected from a radon source, injected in a water enricher and sampled. One or two water samples per series were also extracted for cross-calibration purposes using an activated charcoal collector counted by gamma spectrometry at INGV e Rome Radionuclides Laboratory.

Big Bottle RAD H_2O equipmen

The Big Bottle RAD H_2O is an accessory designed for RAD7 radon detector (Durridge Company) that enables users to measure radon in 2.5 L water samples with high sensitivity. It consists of several components, a 2.5 L glass bottle (standard configuration), an aeration system, a bubble trap, a temperature data logger, vinyl tubings, a Laboratory Dryer and RAD7 (Fig. 1). RAD7 is a monitor that uses ^{218}Po, the short-lived daughter of radon (with a 3-min half-life), without interference from other radiations. The detector is a solid-state, ion-implanted, planar, silicon electrostatic collector that measures the energy of alpha particles converting them directly to an electric signal. During the measurements the built-in pump runs continuously, aerating the sample and delivering radon to RAD7. The clip stays open during the whole run and the radon rich air flows through the closed-loop circuit, reaching an equilibrium with the

radon remaining in the water. Eight to twelve 15-min cycles are set. During the first 15 min RAD7 responds to the growth of radon in the measurement chamber, so the first cycle is ignored in the calculation. The radon

extraction efficiency is calibrated against the average temperature of the airewater interface monitored about halfway up the bottle using the temperature data logger. Relative humidity detected by a probe placed inside the instrument is kept at about 5%, because water molecules in the inner chamber influence the electrostaticcollection efficiency of the detector.

Radon chamber

Radon chamber available at INGV e Rome (Fig. 2, component A) is a 56 L stainless steel container with an alpha sensitive detector fitted across its cap. The detector is made of a scintillating flask

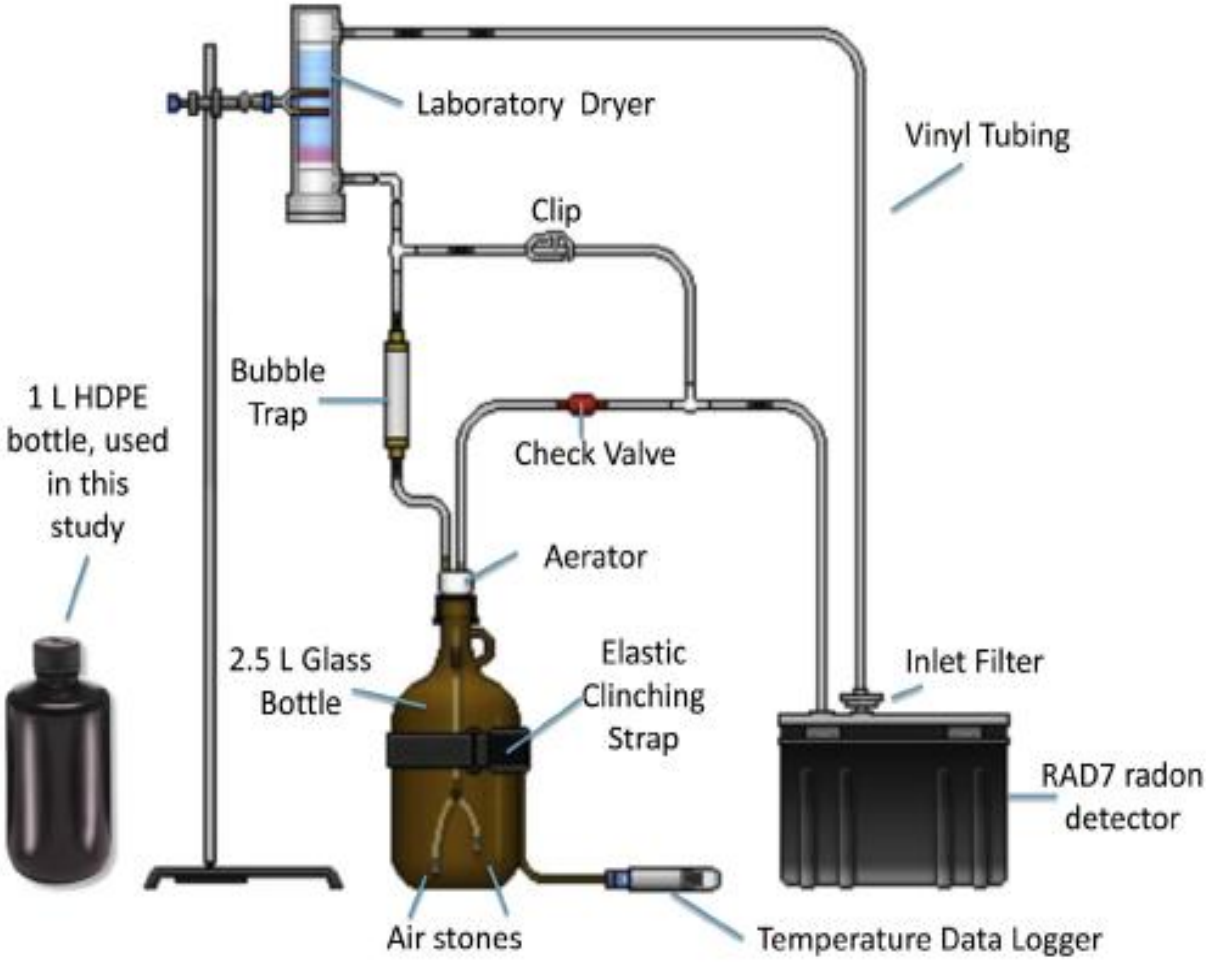

Fig. 1. Configuration of Big Bottle RAD H2O (modified from Big Bottle RAD H_2O manual, Durridge Company Inc., available at www.durridge.com). The standard 2.5L glass bottle is here replaced with 1 L HDPE bottle. Durridge Co. is recently commercializing 'soda'bottles made from polyethylene terephthalate (PET, with a suitable adaptor) in place of glass bottles. PET bottles are appropriate to store radon-containing water because gas loss turned out to be even lower than that observed for HDPE and LDPE (Leaney and Herczeg, 2006). G. De Simone et al. / Radiation Measurements 76 (2015) 1e7 2

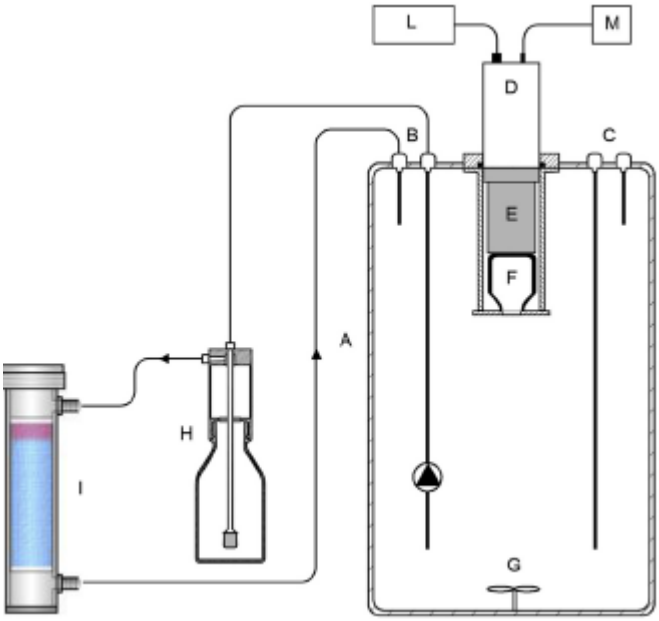

Fig. 2. Experimental setup circuit for Drierite characterization. A) radon chamber; B) air tight connectors (CPC) to be used when air circulation needs a pump; C) air tight connectors (CPC) when air circulation is guaranteed by an outer device; D) signal processing module; E) photomultiplier; F) scintillating flask; G) fan; H) humidifying device; I) desiccant column (Drierite); L) multiscaler; M) low voltage supply.

(Fig. 2, component F), an Algade™ 120 cm^3 pyrex glass bottle coated by polyethylene, optically coupled to a photomultiplier (Fig. 2, component E); electrical pulses are formed by a Tesys™ signal processing module (Mod. SPM 02) (Fig. 2, component D) and sent to a counter: a multichannel analyzer (either a Silena™ Mod.

Cato or an Ortec™ Multichannel PCI card) sets as multiscaler (Fig. 2, component L). Four air tight connectors (CPC, Colder Products Company) (Fig. 2, components B, C) are available to connect radon sensors in a closed loop; two of them (Fig. 2, component B) are connected to an internal pump to let air circulate through sensors

working only for diffusion. In the chamber there is a fan (Fig. 2, component G) to ensure a uniform radon concentration in the inner volume. The sensitivity of the detector for radon in the radon chamber is 0.0174 cpm/Bq m^{-3}

Preparation of radon-containing solution

Seven series of radon-containing solutions were produced. Radon was collected from a radon source, a 300 cm^3 glass bottle containing 100 cm^3 of an acidified (pH < 2) liquid solution of $RaCl_2$, activity 3.5 kBq, added with Ba, thus preventing significant radium precipitation. The bottle cap is properly modified to allow the

extraction of radon gas by connecting a syringe to a CPC connector and unscrewing a little plastic cap to restore the needed amount of air in the source volume.

Then radon rich air was injected into a water enricher. This device (Fig. 3) is made of a plexiglass cylinder, two PVC caps, the lowest being equipped with waterproof connectors to i) supply or withdraw water, ii) supply radon gas and iii) supply electricity to a submerged pump. A floating PVC structure, allowing to choose the

amount of water to be enriched in the range 1 e 8 L, has a cavity in which radon gas is trapped when injected from the lower PVC cap. Water is enriched by its continuous circulation upward where the radon gas is trapped. Radon activity concentrations were: 27 ± 1, 47 ± 2, 78 ± 2, 80 ± 3, 126 ± 4, 186 ± 5 and 194 ± 5 Bq/L. Three 1 L samples of each

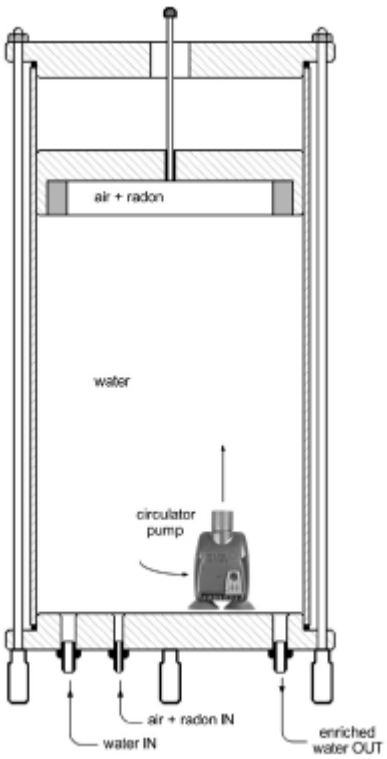

Water enricher, used for preparing radon-containing solution.

solution were sampled and measured using the Durridge experimental apparatus described above, at increasing time from the sampling (1, 24, 48, 72 and 96 h) to estimate radon loss during storage in HDPE bottles. One or two water samples per series were extracted for cross-calibration purposes using an activated charcoal c collector counted by gamma spectrometry at INGV e Rome Radionuclides Laboratory (Galli et al., 1999).

Description of physical processes

From the analysis of plots showing radon concentration vs time, various physical processes affecting data, other than decay, obviously, have been identified: - radon loss during storage in HDPE bottle; - radon absorption by desiccant; - radon absorption/desorption from rubber and plastic parts of the measuring system These

processes have been separately investigated, performing proper experiments for the assessment of their influence on the resulting radon concentration value, leading also to corrected 'equivalent' volumes to be used in calculations.

Radon loss during storage in HDPE bottle

High Density PolyEthylene is a thermoplastic material made from petroleum. Known for its large strength to density ratio, HDPE is commonly used in the production of plastic bottles, corrosionresistant piping and geomembranes. Its density can range from 0.93 to 0.97 g/cm^3 Percent radon loss during sample storage in 1L HDPE NALGENE bottles (Fig. 4) has been estimated at (6.5 ± 0.3) % d^{-1} (linear fit), but Fig. 3 also provides an exponential fit of radon data closely

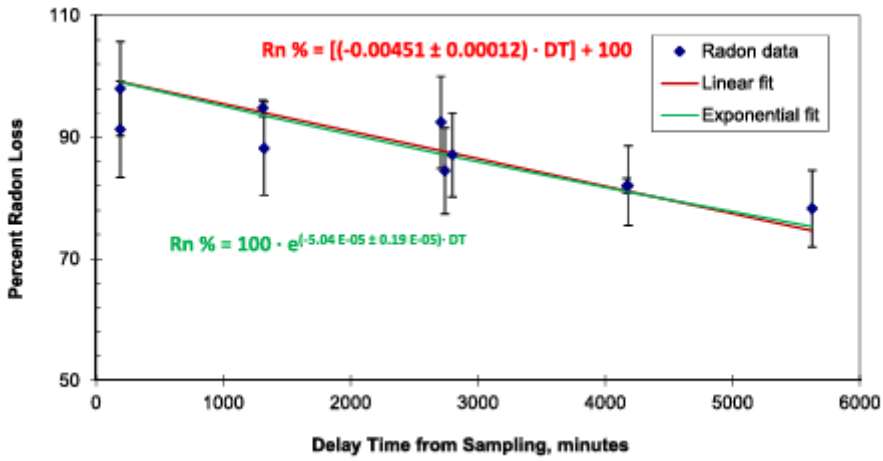

Percent radon loss during storage in 1 L HDPE bottles manufactured by NALGENE versus delay time from the sampling.

corresponding to the linear interpolation. This loss is nearly comparable to that obtained by Leaney and Herczeg (2006) that stored water samples in 2.5 L HDPE Winchesters bottle, even if their data indicate for the same storage time a slightly lower radon decrease, probably due to a lower surface/volume ratio. The observed radon loss is

probably due to the combined effect of diffusion through HDPE and of adsorption onto its surface during sample storage (Fern. andez et al., 2004). The last process has beenconsidered the basis for radon loss in water samples stored in polyethylene bottles by Saito (1983), whereas others (Arafa, 2002; Jir. anek et al., 2008; Ashry et al., 2011) working on waterproof radon membrane mainly refer to diffusion. Following this view the estimated radon loss would correspond to a radon diffusion coefficient of $1.85 \cdot 10^{-12}$ m^2/s, considering that outer surface area of the

bottle is about $5.04 \cdot 10^{-12}$ m^2 and its thickness about 2 mm. This result is in the order of the values reported in the literature for polyethylene membrane: $4.6 \cdot 10^{-12}$ m^2/s (Arafa, 2002; Ashry et al., 2011) and $5.8 \cdot 10^{-12}$ m^2/s (Jir.anek et al., 2008). However the issue of radon adsorption and diffusion is very complex to address and quantify and is beyond the scope of this paper, so we will refer more generally to radon loss during sample storage, as reported also in Leaney and Herczeg (2006).

Radon absorption by desiccant

The sensitivity of an electrostatic chamber used for radon measurements is inversely proportional to the absolute humidity and depends on the electrostatic field which drives charged radon daughters toward the solid state detector. The chamber geometry and the applied voltage define the electrostatic field; in order to strongly reduce variations in the collection of radon daughters on the detector surface, a desiccant (Drierite) is employed in the Big Bottle RAD H_2O instrument. The behavior of the desiccant column Fig. 2, component I), a cylinder 29 cm high, with an outer diameter of 6.5 cm containing a Drierite volume approximately of 435 cm^3, has been investigated by connection in a close loop with a humidifying device (Fig. 2, component H) and a radon chamber (Fig. 2, component A). As a result the ‘equivalent’ desiccant volume has been obtained, i.e. a

volume which accounts for radon absorption in Drierite. Experiments have been carried out at various high radon concentrations, flux times and quantities of water already absorbed by Drierite, to assess the ‘equivalent’ Drierite volume as a function of the above mentioned parameters. Also the behavior of connection tubes in the circuit has been investigated and their volume per linear meter per minute determined to account for the other path through which radon is lost.

A description of a typical experiment follows. After injection of radon in the chamber, its internal fan was switched on to ensure a uniform radon distribution and in a 5 h time radon also diffused to the scintillation cell and the secular equilibrium between radon and its daughters was reached. Then the fan was switched off and the experimental apparatus was connected to the radon chamber; the internal pump was switched on and the radon enriched air started fluxing through the humidifying device (a glass bottle employed in a radon degassing unit), then entered the desiccant column and went back to the radon chamber. Each experiment lasted for a time ranging from 30 min to 2 h, then the apparatus was disconnected and the fan switched on again; finally at least 12 h were waited for establishing a new equilibrium in the radon chamber and for the acquisition of data needed for calculation of the radon concentration in the chamber at the time when the humidifying device and the desiccant column were disconnected.

Concentrations in the chamber before and after each experiment were calculated through exponential fit of available data or by average of concentration values corrected by proper decaying factors (Fig. 5).

Given the volume of the radon chamber and that of the humidifying device (a(T)V w þV a), where a(T) is the solubility of radon in water, V w is the water volume and V a is the air volume in the device, on the basis of the free volume in the desiccant column and of the ‘equivalent’ volume of the connection tubing, the ‘equivalent’ Drierite

volume was calculated. Data, reported in Table 1, are grouped and eventually repeated to focus on the equivalent volume values as a function of the different investigated parameters. Average equivalent volumes are also reported, showing a limited variability within the errors. The average Drierite equivalent volume obtained without data replication is 0.673 ± 0.092 L.

Radon absorption/desorption from rubber and plastic parts of the measuring system

Radon absorption/desorption from rubber and plastic parts of the Durridge measuring system is assessed by analyzing plots of concentration values vs time, as shown in Fig. 6a-c.

Fig. 6a shows radon data of a water sample measured after a long purging of the experimental apparatus with radon free air. The decrease of detected activity concentration during the 3h run, not justified by the concurring radioactive decay, radon loss during storage in HDPE bottles and continued drierite absorption, is largely

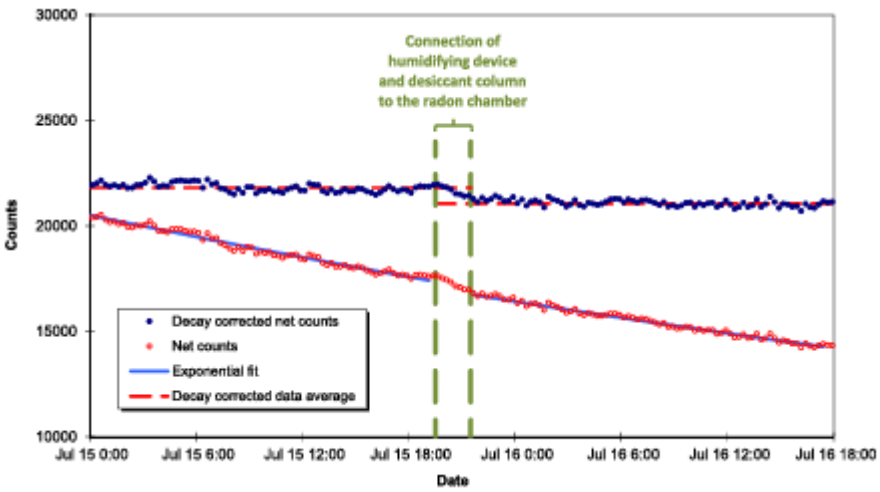

Example of data acquired by the multichannel analyzer during the experiment for the determination of the drierite 'equivalent' volume.

due to radon absorption from the plastic and rubber elements within the circuit when the concentration gradients are large. If a second sample of the same solution is measured, after a 30 min purging (Fig. 6b), the air radon concentration gradients between the closed-loop setup and the polymer's pores is much lower because the pores already contain the gas, resulting in data point aligned along a gently sloping line. This indicates that radon gas is slightly absorbed from plastic or rubber elements. Fig. 6c reports another scenario when a low radon solution is degassed and

measured using the same experimental set-up, previously employed for other experiments. In this case the gradient is reversed and the circuit releases the radon amount trapped in the polymer's pores, displaying a radon rising trend during the 2h run. By exponential fit of experimental data acquired from 30 to 120 e 180 min, we obtain a time constant (t) which accounts for the radon decay (t Rn), loss during storage in HDPE bottle (t HDPE) and for the absorption/desorption from rubber and plastic parts of the measuring system (t DS). Being known the constants of radon decay and radon loss during sample storage in HDPE bottles, the absorption/desorption time constant can be calculated, thus a correction to the radon concentration provided by RAD7 instrument for the first 30 min can be carried out:

$$\frac{1}{\tau} = \frac{1}{\tau_{Rn}} + \frac{1}{\tau_{HDPE}} + \frac{1}{\tau_{DS}}$$

$$\tau_{DS} = \frac{\tau \cdot \tau_{Rn} \cdot \tau_{HDPE}}{\tau_{Rn} \cdot \tau_{HDPE} - \tau \cdot \tau_{HDPE} - \tau \cdot \tau_{Rn}}$$

Calculation model

An equation accounting for the above described physical processes has been developed for the calculation of the dissolved radon concentration using the Durridge Big Bottle RAD H 2 O instrument and 1 L HDPE bottles. A comparison with an already characterized method has been performed: for each radon enriched solution to analyze with the Durridge Big Bottle RAD H 2 O instrument one or two water samples were extracted at the same time for cross-calibration purposes by using a radon degassing unit in which radon dissolved in water is transferred to an activated charcoal collector, then counted by gamma spectrometry at INGV e Rome Radionuclides Laboratory (Galli et al., 1999). Finally a simplified calculation method is provided for 30 min measurements.

Detailed model

Radon concentrations in water were obtained with the Durridge Big Bottle RAD H 2 O instrument by applying the following equation, where background concentration in recirculating air is negligible:

$$C_w = C_{a\ FIT30}\ \mathrm{AF} \cdot (V_a + \alpha(\mathrm{T})V_w)/(\mathrm{LB\ DS\ DF}\ V_W)$$

With

$$V_a = V_{R7} + V_d + V_t + V_b$$

Where

Cw : original radon concentration in the water (Bq/m^3).
Ca $_{FIT30}$: radon concentration value at t=30 min of an exponential fit of RAD7 data recorded during each 15 min run (from 30 to 120/180 min) (Bq/m^3).
AF: adjustment of instrument calibration factor (1.038 in this case).
T: temperature of water in bottle (°C) (see Fig. 1)
$\alpha(T) = 0.105 + 0{:}405\ e^{-0.0502T}$: equilibrium coefficient from Fritz von Weigel equation (Weigel, 1978)

V_w : volume of water in bottle (1.02E-03 m^3).
V_{R7} : internal volume of the RAD7 (0.768E-03 m^3)
V_d : equivalent desiccant column volume (0.673E-03 m^3)
V_t : volume of tubing & aerator (0.054E-03 m^3)
V_b : volume of bubble trap (0.051E-03 m^3)
V_a : total volume of air in the system (1.546E-03 m^3)
LB: loss factor during sample storage in HDPE bottle as a function of storage time (= 1 - 0.0045 t/100 or = $e^{-5.04\,E-05\,t}$, being t (min) the time elapsed between water ampling and the beginning of the run).
DS: absorption/desorption factor from rubber and plastic parts of the measuring system (= $e^{-t/t\,DS}$, being t = 30 min e see Section 3.3).

Table 1. Effect of fluxing time, water gain and radon concentration on Drierite equivalent volumes. Letters identify different experiments.

		Equivalent volume (1E-03 m^3)								
		A	B	C	D	E	F	G	H	I	Average
Time (min)	30	0.728	0.649	0.848	0.701	0.665	–	–	–	–	0.718 ± 0.079
	60	0.556	0.760	0.623	0.638	0.676	0.825	0.545	0.661	0.552	0.648 ± 0.096
	120	0.634	0.642	0.695	0.566	0.656	0.848	–	–	–	0.674 ± 0.095
Water gain (%)	0–4	0.556	0.760	0.623	0.638	0.676	0.825	–	–	–	0.680 ± 0.098
	5–35	0.545	0.728	0.649	0.848	0.701	0.634	0.642	0.695	–	0.680 ± 0.088
	36–50	0.661	0.665	0.566	0.656	–	–	–	–	–	0.637 ± 0.047
	51–65	0.552	0.848	–	–	–	–	–	–	–	0.700
Rn (kBq/m^3)	0–20	0.638	–	–	–	–	–	–	–	–	0.638
	20–40	0.556	0.760	0.623	0.661	0.552	0.656	–	–	–	0.635 ± 0.077
	40–60	0.825	0.545	0.649	0.848	0.701	0.696	0.566	0.848	–	0.710 ± 0.121
	60–80	0.676	0.728	0.665	0.634	0.642	–	–	–	–	0.669 ± 0.037

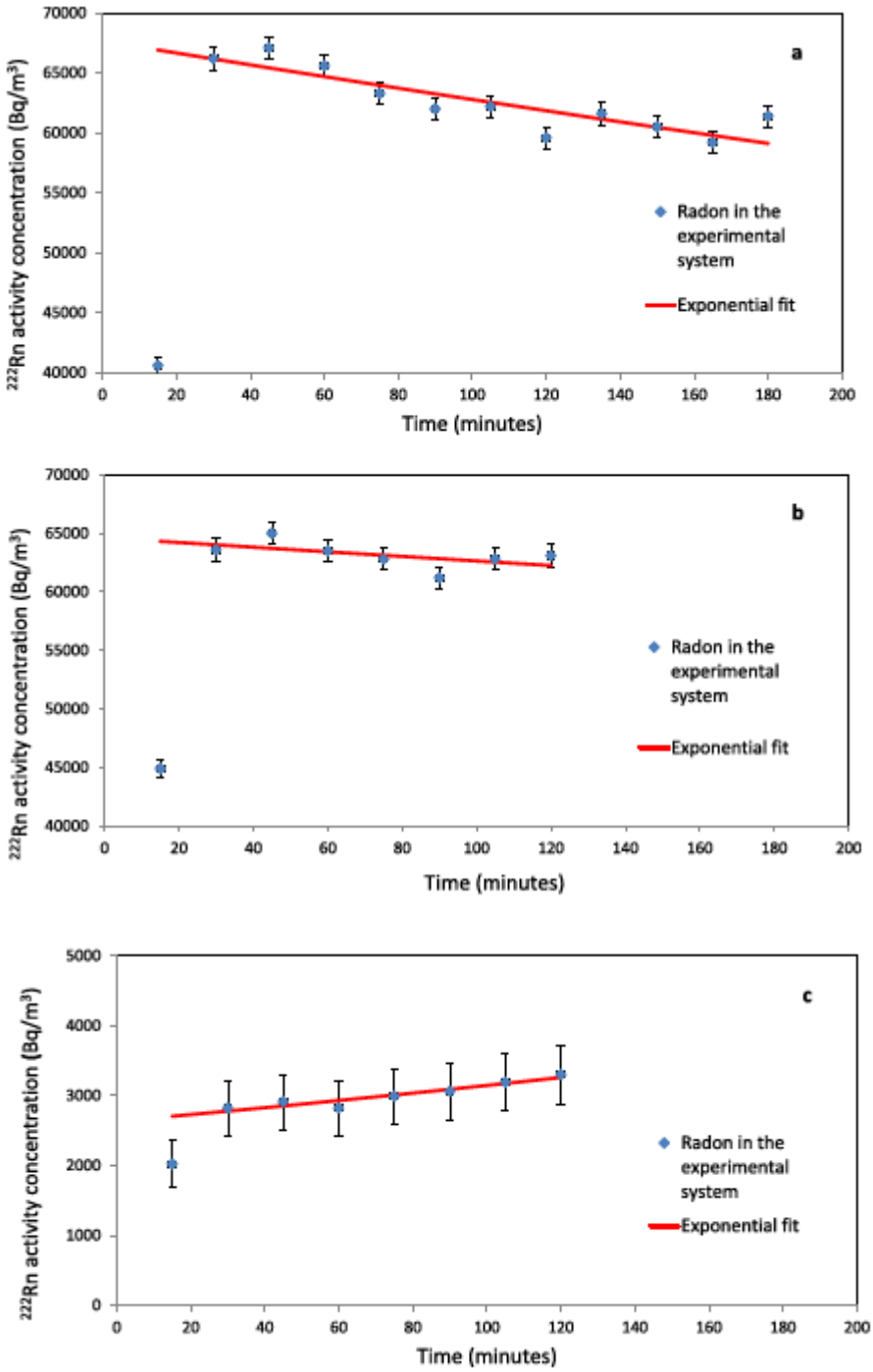

Radon activity concentration detected during 2 or 3 h long measurements using the Big Bottle RAD H 2 O device. Radon data decrease (a), stay almost constant (b) or increase (c) during the run as a function of concentration gradients between radon in the closed-loop set-up and in the polymer's pores. G. De Simone et al. / Radiation Measurements 76 (2015) 1e7 6

Table 2. Comparison of radon activity concentration determined using INGV method, Big Bottle detailed method and Big Bottle simplified 30 min method.

Rn (Bq/L) INGV method	Rn (Bq/L) Big Bottle detailed method	Rn (Bq/L) Big Bottle simplified 30 min method
194 ± 5	193 ± 10	193 ± 11
186 ± 5	180 ± 10	176 ± 10
	180 ± 9	179 ± 10
	180 ± 10	183 ± 11
126 ± 4	126 ± 7	125 ± 7
	123 ± 7	124 ± 7
	126 ± 7	125 ± 7
80 ± 3	79 ± 4	79 ± 4
	81 ± 4	79 ± 5
	79 ± 4	79 ± 5
78 ± 2	75 ± 4	74 ± 4
	71 ± 4	72 ± 4
	70 ± 4	72 ± 4
	77 ± 4	78 ± 5
47 ± 2	50 ± 3	50 ± 3
	46 ± 2	–
	48 ± 3	48 ± 3
27 ± 1	29 ± 2	30 ± 2
	29 ± 2	28 ± 2
	28 ± 2	28 ± 2

DF: Decay Factor (= $e^{-t/t_{Rn}}$, where t (min) is the time elapsed between water sampling and 30 min after the beginning of the run and t Rn (min) the radon average life).

Radon concentration data from each experiment are reported in Table 2, showing a good match with values obtained with a reference calibrated method. Only in the experiment at 78 Bq/L, with four bottles used instead of three, two values differ more than one standard deviation from the reference value, maybe due to the insufficient water recirculation res

ponsible for radon dilution by air during the sample collection.

Simplified model

A simplified calculation method was developed to shorten the time required for the measurement, useful during geochemical surveys and/or for Drierite consumption. A minimum time of 30 min is needed, considering the RAD7 pump flow (~0.8 L/min), the volume of the water sample (~1 L), the ^{218}Po average life and an acquisition time of 15 min, referred to a single cycle. A correction coefficient (S) was introduced, the average of (Ca FIT30/DS)/C_{a30} ratio obtained from each experiment, being C_{a30} the radon concentration provided by RAD7 at 30 min. Again, stated the background concentration in recirculating air is negligible:

$$C_w = C_{a\,30}\ \mathrm{AF}\ \mathrm{S}(V_a + \alpha(\mathrm{T})V_w)/(\mathrm{LB}\ \mathrm{DF}\ V_w)$$

C_{a30} : equilibrium radon concentration in air provided by RAD7 at 30 min, acquisition time set to 15 min (Bq/m^3)
S: correction coefficient for simplified method (1.0176 ± 0.0170).

Conclusions

A simplified method based on the measurement at 30 min to calculate dissolved radon concentration has been developed, based on the RAD7 Big Bottle setup replacing glass with HDPE bottles and considering various physical processes: radon loss during storage in HDPE bottles, absorption/desorption caused by diffusion through Drierite and circuit components. In particular, the 'equivalent' Drierite volume is somehow independent, within errors, from i) the amount of water already absorbed in Drierite, ii) a recirculation time greater than 30 min minimum time to have a response from the Durridge Big Bottle RAD H_2O instrument) and iii) radon concentrations. The main advantages of this method employed during geochemical surveys are i) fragile glass bottles have been replaced by HDPE bottles, ii) the time required for each measurement has been shortened and iii) the Drierite consumption has been reduced.

References

Arafa, W., 2002. Permeability of radon222 through some materials. Radiat. Meas. 35, 207e211.

Ashry, A.H., Abou-Leila, M., Abdalla, A.M., 2011. Measurement of radon permeability through polyethylene membrane using scintillation detector. Radiat. Meas. 46, 149e152.

Fern. andez, P.L., Quind. os, L.S., Sainz, C., Gom. ez, J., 2004. A theoretical approach to the measurement of radon diffusion and adsorption coefficients in radonproof membranes. Nucl. Instrum. Methods Phys. Res. B 217, 167e176.

Galli, G., Guadoni, C., Mancini, C., 1999. Radon grab sampling in water by means of radon transfer in activated charcoal collectors. In: Proceedings of the Fourth International Conference on Rare Gases Geochemistry. 8e10 October, 1997, vol. 22C. University of ROMA TRE e Italy. Il Nuovo Cimento, pp. 583e587, 3e4.

Jir.anek, M., Rovensk.a, K., Fro. nka, A., 2008. Radon diffusion coefficient e a material property determining the applicability of waterproof membranes as radon barriers. In: Proceedings of the American Association of Radon Scientists and Technologists 2008 International Symposium, Las Vegas NV, September 14e17,
2008.

Leaney, F.W., Herczeg, A., 2006. A rapid field extraction method for determination of radon-222 in natural waters by liquid scintillation counting. Limnol. Oceanogr. Methods 4, 254e259.

Saito, M., 1983. Correction for loss of radon-222 in water sample caused by the use of a polyethylene bottle. Radioisotopes 32, 109e112.

Weigel, F., 1978. Radon. Chem. Ztg. 102, 287e299.

9.2 OUR PET PROJECT: AN UNLIMITED SUPPLY OF BIG AND SMALL WATER SAMPLE VIALS FOR THE ASSAY OF RADON IN WATER

Paola Tuccimei a, Derek Lane-Smith b, Gianfranco Galli c, Carlo Lucchetti a, Gabriele De Simone a, Jesse Simko b, Ian Cook b, Charlotte E. Bond c.

a: Dipartimento di Scienze, Universit. a "Roma Tre", Roma, Italy

b: DURRIDGE Company, Billerica, MA, USA

c: Istituto Nazionale di Geofisica e Vulcanologia, Sezione Roma, Roma, Italy

Abstract

Abstract RAD7 and BigBottle system has been developed, using large glass bottles, but these are fragile andawkward to carry around. In searching for a better solution, we tested polyethylene terephthalate (PET) bottles for water samples storage to estimate radon loss over time. Two sets of experiments with 0.355 and 1.75 L bottles demonstrated that PET is a suitable material for storage. If correction for ^{226}Ra content in water is applied, we can also calculate the rate of radon loss (0.03 ± 0.08 % day^{-1}).

Introduction

Big bottle systems have been developed for the determination of dissolved radon, using large glass bottles, or jugs. But these are fragile and awkward to carry around. In searching for a better solution, it was noted that Coke and similar bottles, made of polyethylene terephthalate (PET), are engineered to contain CO_2 at high pressures even if heated by the sun; furthermore the availability of a wide range of sizes would be an added benefit. So a special Teflon aerator for soda drinks has been developed and the Capture software has been upgraded, with graphics and analysis, for every size of PET bottle. Experiments, consisting of taking multiple samples of a water and analyzing them on different days, have been carried out to characterize the PET material with respect to glass.

Theory

Soda drinks plastic bottles are available worldwide and represent a virtually unlimited supply of water samplers for the assay of radon in water. Glass is technically the best candidate for that, even though it is fragile and its transport may induce the rupture. The need for inexpensive and robust containers led us to test the performances of plastic bottles when water is stored for a period of 2 weeks before radon determination.

Some investigations are reported in literature for different plastics: 1.3 L PET, 2.5 L HDPE (High Density Polyethylene) and 2 L LDPE (Low Density Polyethilene) bottles [1]. In similar studies, other authors [2, 3] tested 1.1 and 1 L HDPE bottles respectively, demonstrating a radon loss of about 20 % for a 4-day storage. PET seems to be the best solution for storing.

Experimental

A commercial instrument from Durridge Co., RAD7 radon monitor (www.durridge.com), was used for the measurement of dissolved radon with addition of the BigBottle RADH2O accessory (Fig. 1). RAD7 performs alpha spectrometric analyses in order to identify the a particles emitted by ^{218}Po (SNIFF mode), in equilibrium with ^{222}Rn after at least 15 min, or ^{214}Po and ^{218}Po in equilibrium after 3 h (NORMAL mode), when the maximum sensitivity is

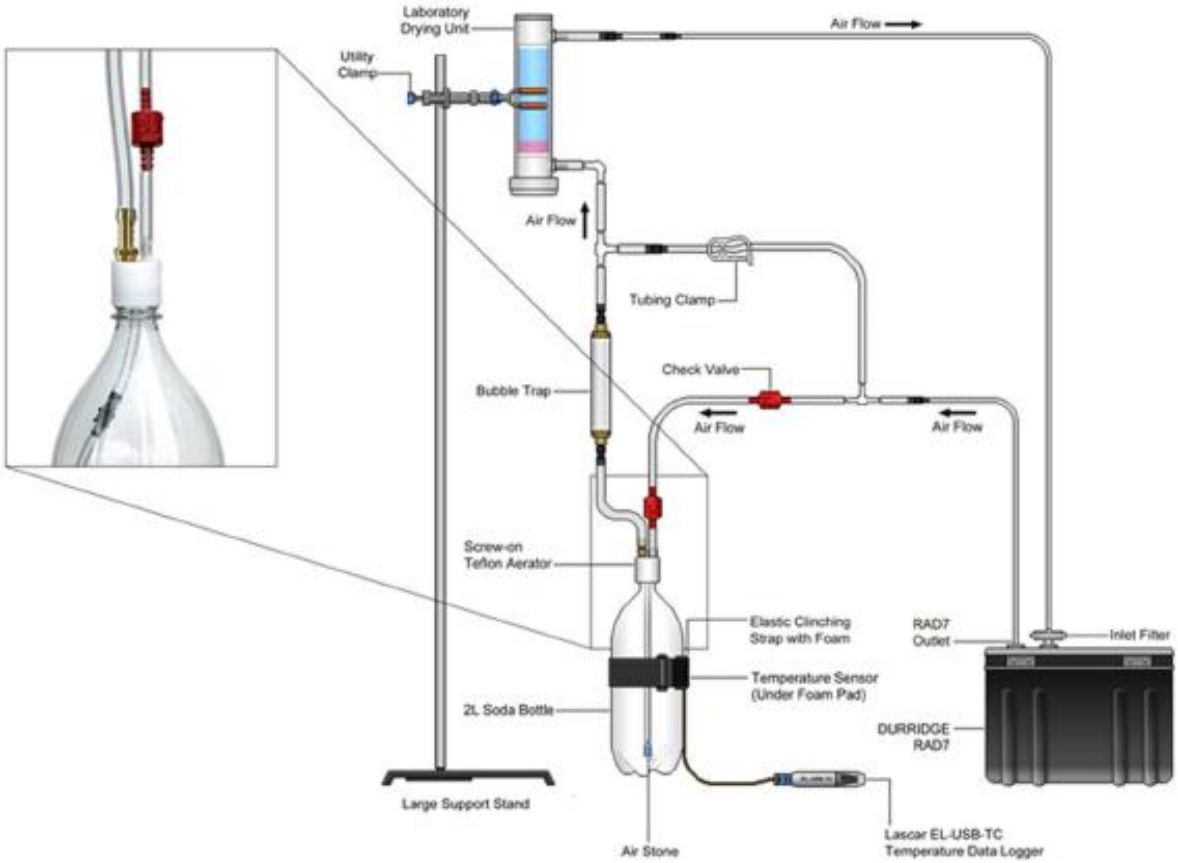

Fig. 1. Experimental set-up

required and there is not a necessity for a fast response and detailed time resolution. Extraction of dissolved radon is performed by pumping air into the bottle delivered through the bubble trap and the desiccant (drierite) to RAD7 in a closed loop.

Temperature is recorded by a data logger in order to assess the effective radon activity transferred to the circulating air measured by RAD7. Two groups of experiments have been carried out in order to verify the seal of PET bottles to radon loss during storage. Set A measurements employed a mix of groundwater and town water (reservoir) to obtain different concentrations of ^{222}Rn from 0.3 to 62.5 Bq/L, stored in 0.355 PET bottles. Set B tests were performed with spring water from Roma (Italy) characterized by a high radon concentration and stored in 1.75 L PET bottles.

Both series of experiments used the special Teflon aerator for soda bottles, changing a little bit the protocol of measurements. They both selected the ‘‘sniff mode’’ and no less than eight 15-min cycles were always chosen. Set A experiments made use of the pump on for the first three cycles (when the complete equilibrium between radon in water and radon extracted from air was reached) and working in automatic (switching on and off, periodically)

in the following, also opening the tubing clamp between the T-connectors to allow the air flow to bypass the bottle (see Fig. 1). The final radon value was then calculated as the average of data from all cycles, except for the first two.

Set B measurements kept the pump on for the entire run and the dissolved ^{222}Rn activity concentration was obtained from an exponential fit at 30 min of data from all cycles (without the first 2 or 3). This choice derives from the absorption/leakage of radon from the drierite and the rubber/plastic part of the experimental apparatus [3].

Results and discussion

This section reports the results of the two set of experiments carried out with Durridge Co. RAD7 and BigBottle RADH_2O device.

Set A experiments

Various mix of waters were prepared at different radon concentration (0.3, 8.0, 29.2, 1.1 and 62.5 Bq/L). The first sample of each series was immediately measured to obtain the initial radon concentration value to be used for reference with respect to other samples measured at later times of storage; normalized radon activity concentration values (A i /A 0), corrected for decay, were plotted versus time (Fig. 2) and 1 r error evaluated. 0.355 L PET bottles have a negligible radon loss during storage and the A i /A 0 ratio increases over time. This is due to the presence of dissolved ^{226}Ra and possibly to radium sorbed during storage, but the lack of a separate radium measurement prevents the application of a specific correction for the radium contribution. Furthermore, it is worth noting that, PET material does not contain any trace of uranium or radium [4, 5].

Set B experiments

Various water samples at high radon concentration (236 ± 8 Bq/L) have been collected with brand new 1.75 L PET bottles from a spring in Roma municipality (Italy) and stored from 1 to 15 days before measurement. A first bottle has been analyzed the day of sampling as a reference (A 0), the others in the following days (A i); consequently a set of A i /A 0 values have been obtained and showed in Fig. 3 along with 1 r errors. No correction for ^{226}Ra has been made at this stage. As in experiment A an increasing trend of A i /A 0 ratios is observed. This confirms that PET is a good material for water storage and ^{226}Ra is certainly present in water. Furthermore, a certain amount of radium is possibly sorbed onto the material during storage [6].

Total radon activity concentration has been measured as the sum of radon in equilibrium with dissolved ^{226}Ra and excess radon from water–rock interaction.

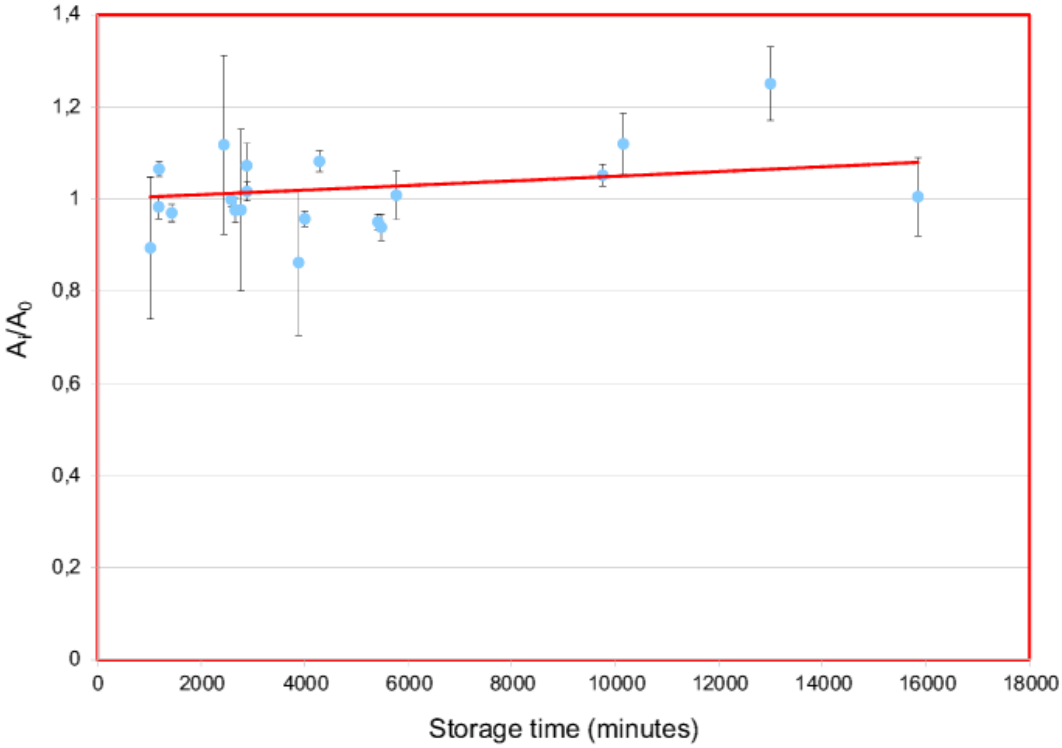

Fig. 2 Plot of A i /A 0 ratios versus storage time from set A experiments

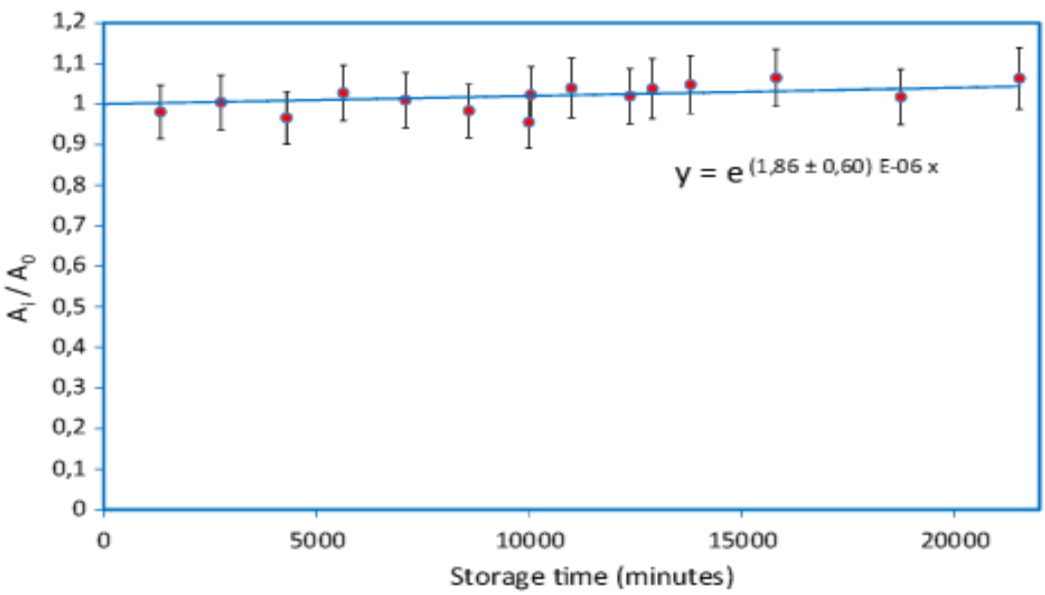

Fig. 3 Plot of A i /A 0 ratios versus storage time from set B experiments

The first contribution becomes relevant for samples analyzed after a time equal to four ^{222}Rn half-life since large errors are introduced by applying correction for decay factor.

In Fig. 4 a simulation of radon activity concentration corrected with different hypothetical ^{226}Ra content (1.25, 2.5,5 and 10 Bq/L) has been carried out showing how big theerror can be, especially at higher radium concentration. In this case the sealing property guaranteed by PET material is underestimated.

The ^{226}Ra content in Roma spring water has been estimated at 1.00 ± 0.09 Bq/L, repeatedly measuring by gamma spectrometry a sealed water sample at increasing times from sampling for at least 22 days. This test takes into account the combination of dissolved radium and a possible fraction of it sorbed by the bottle during storage.

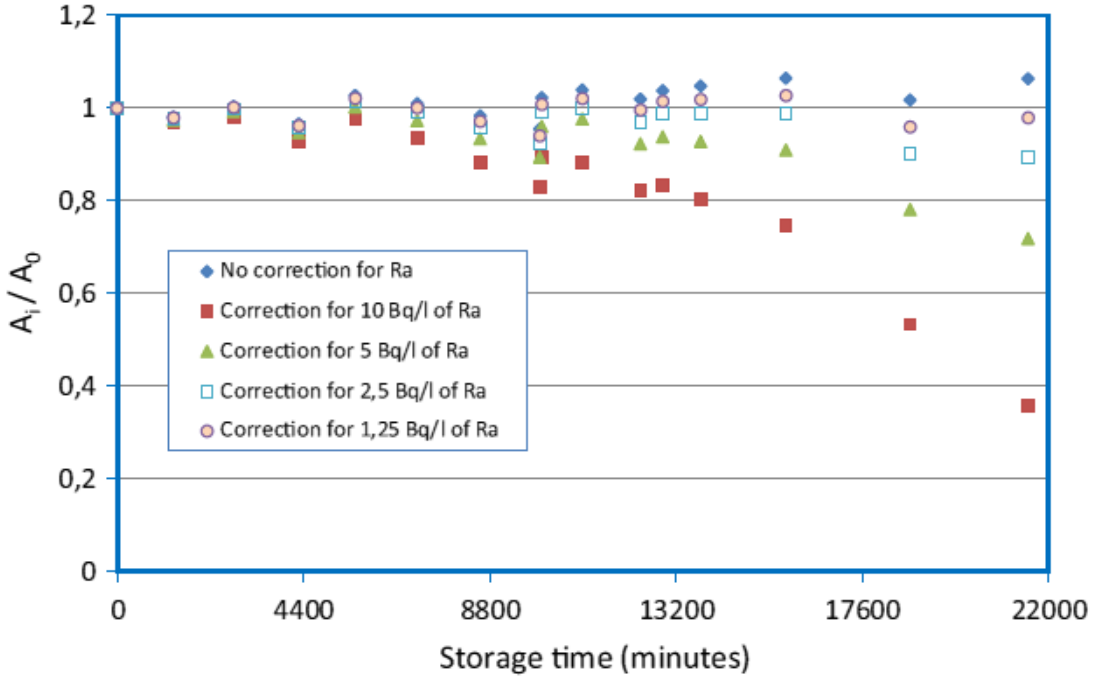

Fig. 4 Plot of A i /A 0 ratios versus storage time from set B experiments corrected with four hypothetical estimations of ^{226}Ra content in water. 1 r errors are 5–7 %, depending on activity concentrations

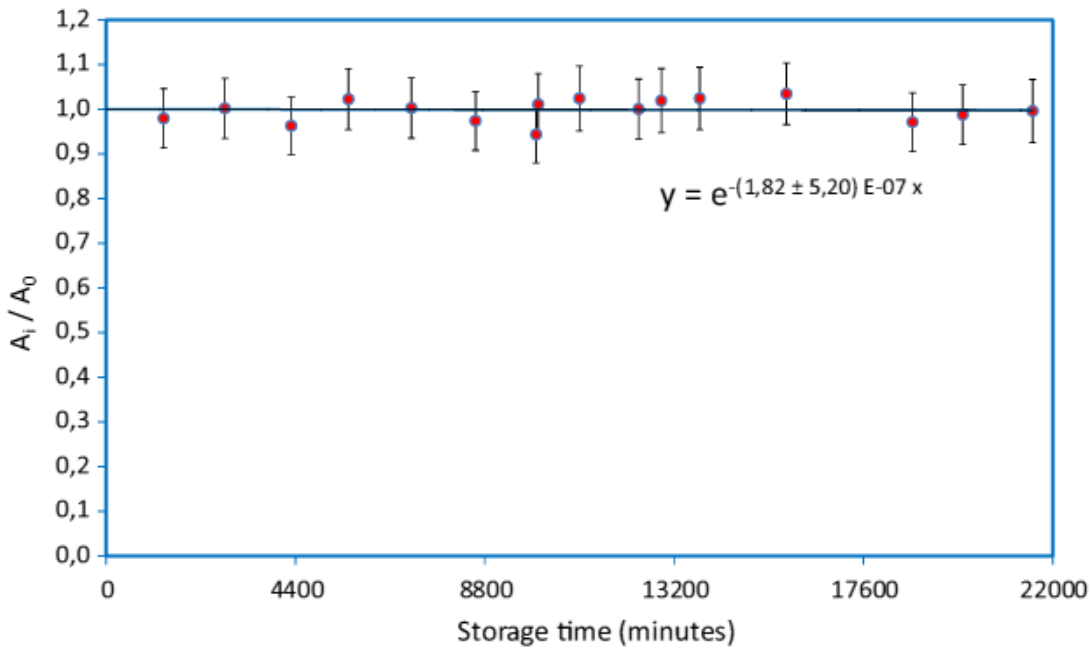

Fig. 5 Plot of A i /A 0 ratios versus storage time from set B experiments corrected with the real ^{226}Ra content in water (1.00 ± 0.09 Bq/L)

Details on the procedure for Ra determination is beyond the scope of this work.

The plot in Fig. 5 has been obtained introducing the correction for ^{226}Ra. An exponential interpolation taking into account the joined effect of ^{222}Rn ingrowth from ^{226}Ra dissolved in the water and sorbed by the bottle, has been applied, leading to the correct estimation of radon loss. This way, 1.75 L PET bottles loose around 0.4 % of initial radon after 15 days of storage, with a rate of (0.03 ± 0.08) % day^{-1}.

Conclusions

Various experiments demonstrated that soda drinks PET bottles, available in a wide range of size, are suitable for storing water samples and better than other plastic materials (HDPE and LDPE) for the assay of dissolved radon.

Due to the determination of dissolved ^{226}Ra, a proper correction has been applied to radon activity concentration leading to the correct estimation of the rate of radon loss from 1.75 PET bottles (0.03 ± 0.08) % day^{-1}

.

References

1. Leaney FW, Herczeg A (2006) A rapid field extraction method for determination of radon-222 in natural waters by liquid scintillation counting. Limnol Oceanogr 4:254–259

2. Saito M (1983) Correction for loss of radon-222 in water sample caused by the use of a polyethylene bottle. Radioisotopes 32:109–112

3. De Simone G, Galli G, Lucchetti C, Tuccimei P (2015) Calibration of BIG Bottle RAD H 2 O set-up for radon in water using HDPE bottles. Radiat Meas 76:1–7

4. Bach C, Dauchya X, Chagnonc MC, Etienne S (2012) Chemical migration in drinking water stored in polyethylene terephthalate (PET) bottles: a source of controversy. Water Res 46:571–583

5. Whitt M, Vorst K, Brown W, Baker S, Gorman L (2012) Survey of heavy metal contamination in recycled polyethylene terephthalate used for food packaging. J Plast Film Sheeting 29:163–173

6. Stringer CE, Burnett WC (2004) Sample bottle design improvements for radon emanation analysis of natural waters. Health Phys 87:642–646

9.3 EVALUATING RADON LOSS FROM WATER DURING STORAGE IN STANDARD PET, BIO-BASED PET, AND PLA BOTTLES

Carlo Lucchetti a, Gabriele De Simone a, Gianfranco Galli b, Paola Tuccimei a,

a: Dipartimento di Scienze, Universit. a “Roma Tre”, Roma, Italy

b: Istituto Nazionale di Geofisica e Vulcanologia, Sezione Roma, Roma, Italy

Abstract

Polyethylene terephthalate (PET) and polylactic acid (PLA) bottles were tested to evaluate radon loss from water during 15 days of storage. PET bottles (lower surface/volume-ratio vials) lost 0.4e7.1% of initial radon, whereas PLA bottles lost 3.7% of it. PET bottles with volume of 0.5 L, lower surface/weight ratio, and hence higher thickness display proportionally reduced radon loss. Corrections for dissolved radium are needed during analyses. Formulas for calculating degassing efficiency and water interference on electrostatic collections are developed.

1 Introduction

At present, polyethylene terephthalate (PET) is widely used in the large-scale production of bottles to store soda drinks and other beverages, because it is light, hygienic, and maintain the fizzy taste of carbonated drinks for adequate periods. Although it is one of the safer plastics, PET is not intended for repeated use. Bottles made from this porous plastic are difficult to clean, and can harbor bacteria, particularly when used many times. In addition, studies suggest that repeated use of PET containers might release bis(2-ethylhexyl) phthalate (DEHP), an endocrine-disrupting compound and probable human carcinogen, as well as antimony, an eye, skin, and lung irritant at high doses (Shotyk et al., 2006; Sax, 2010). This plastic material (classified as 1, according to the Society of the Plastic Industry (SPI) resin identification coding system) is recyclable, but the quality degrades with each cycle. Therefore, PET is typically "downcycled" into products such as fleece apparel, carpet fibers, and plastic straps.

Although petroleum is the major source of PET, bio-based plastic products are also increasingly used currently for packaging, thereby reducing CO_2 emissions. Coca-Cola plantbottle™, a PET plastic partly made from plants, commercialized since 2009 in 28 countries all over the world, and Acqua Lilia plantbottle™ in Italy are some of the examples. Another example is the Bio Bottle made from Ingeo™ PLA, a polylactic biopolymer, used by Acqua S. Anna in Italy for Rebruant and Vinadio springs.

Soda drinks and mineral water plastic bottles provide a global and virtually unlimited supply of water sample vials for the assay of radon in water, although glass is technically the best choice for that. However, glass is fragile and its transport often leads to breakage. Thus, the need for shatterproof bottles led us to test the performances of plastic bottles of different types, thicknesses, and surface/volume ratios to store samples of water for a period of 2 weeks, before radon measurement.

Some investigations are reported in the literature for 1.3-L PET, 2.5-L HDPE (high-density polyethylene), and 2-L LDPE (low-density polyethylene) bottles (Leaney and Herczeg, 2006). Radon losses during a 12-day storage are lower in PET (about 7% after 4 days), and higher in HDPE (about 15% after 4 days) and LDPE (27% after 4 days) bottles. In this study, radon losses are reported after 4 days, for comparison with other shorter records. Saito (1983) showed that 1.1-L HDPE bottles lose about 20% of initial radon after 4 days. The value is lower than that measured by Leaney and Herczeg (2006), probably because of lower surface/volume ratio. De Simone et al. (2015) tested 1-L HDPE bottles and found a radon loss of about 22% for a 4-day storage. This is the highest loss among those quoted for HDPE, which could be attributed to a corresponding higher surface/volume ratio. Finally, Tuccimei et al. (2015) tested 0.355- and 1.75-L PET bottles and demonstrated a negligible decrease of radon concentration after 15 days of storage.

These studies demonstrate that PET bottles show better performance than those of HDPE and LDPE in storing water for the assay of radon, with the lowest loss. It is also evident that the lower the surface/volume ratio of the bottle is, the better the performance, with other parameters being unchanged. In this study, Coca-Cola PET bottles (1.75, 1.25, and 0.5 L) and two bio-based plastic vials (1.5-L Acqua Lilia plantbottle™ and 1-L Acqua S. Anna Bio Bottle) were tested to evaluate radon loss during storage. In order to investigate the way in which this parameter influences gas loss, 0.5-L PET bottles (Acqua di Nepi mineral water) were also included in the second step of this test, with approximately the same surface/volume ratios as 0.5-L CocaeCoca vials, but different thicknesses of PET.

2. Materials and methods

2.1. PET and PLA bottles

PET and PLA bottles are manufactured in two steps: (i) preforms, including the thread or the mouthpiece for the cap of the finished bottle are produced by plastic injection into molds and (ii) the preforms are cast to their final shapes in a stretch blow molder. The weight of each bottle, regardless of its volume, depends on the preform characteristics; weights ranging from 15 to 40 g are commonly used. Hence, thickness will be affected, which needs to be investigated.

2.2. Natural groundwater enriched with ^{222}Rn

Groundwater from a 5-L/min discharge spring in Valle della Caffarella area (Roma, Italy, Fig. 1) was chosen for the experiments, because of its high radon content (236 ± 8 Bq/L, Pizzino, 2015) and the location of the area being only few kilometers from Roma Tre University and Istituto Nazionale di Geofisica e Vulcanologia (INGV) laboratories, where measurements were performed. Groundwater belongs to "Complesso delle Vulcaniti Indifferenziate" hydrogeological unit (Capelli et al., 2012), consisting of products from Colli Albani volcano (3 and 4 in Fig. 1b). Its composition is Ca e HCO_3, with abundant potassium and sodium (Pizzino, 2015), typical of groundwater in high-potassium volcanic areas of the Roman Comagmatic province (Conticelli and Peccerillo, 1992). The salinity of the source is about 740 mg/L (electrical conductivity at 25 °C is865 mS/cm) and very constant. The effect of salinity on radon solubility can be considered negligible in our experiments, as reported in Leaney and Herczeg (2006), where much higher salinity solutions (NaCl = 80, 16,500, 35,000, and 53,000 mg L - 1) were tested.

Groundwater was sampled nine times from January to June 2015, and radon activity concentration was always measured using a RAD7 monitor with Big Bottle RAD H_2O accessory and crosschecked using activated charcoal collectors counted by gamma spectrometry (Galli et al., 1999). This independent method shows radon activity concentration ranging from 236 to 240 Bq/L from January to June 2015, also in agreement with data reported in Pizzino (2015).

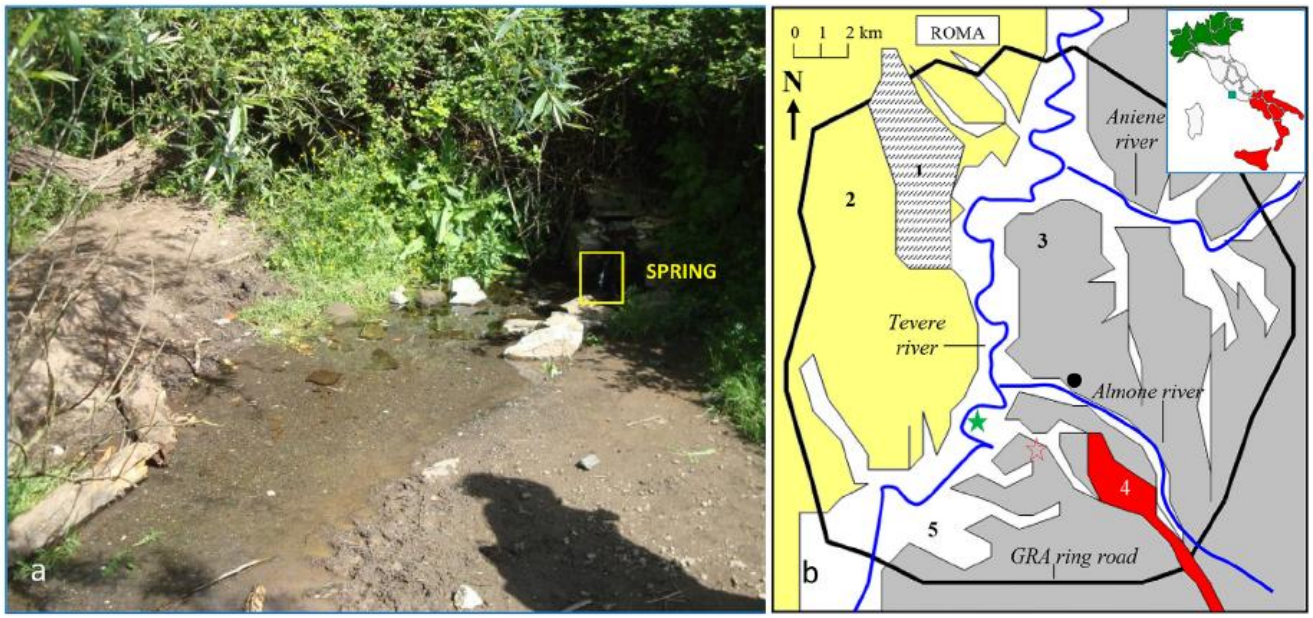

Fig. 1. Valle della Caffarella spring (a) is placed in Roma (Italy). Its location is shown by the closed circle in (b), where a simplified geological map of the city is reported. 1) Plio-pleistocene marine to transitional deposits; 2) Sabatini district volcanoes; 3) Colli Albani district ignimbrites; 4) Colli Albani district lavas; 5) Alluvial sediments of River and its tributaries. Stars indicate Roma Tre University (closed green) and INGV (open red) laboratories. (For interpretation of the references to colour in this figure legend, the reader is referred to the web version of this article.)

The variability of ^{222}Rn concentration (238 ± 2 Bq/L) is lower than the average analytical uncertainty of gamma spectrometry (238 ± 4 Bq/L). At least three different bottles of any investigated series were sampled every time: 1.75-L PET (Coca-Cola), 1.25-L PET (Coca-Cola), 0.5-L PET Coca-Cola, 0.5-L PET Acqua di Nepi, 1.5-L plantbottle™ (Acqua Lilia), and 1-L BioBottle™ (Acqua S. Anna), making water

overflow the bottle to replenish the volume at least thrice. The first bottle of all the six types was measured in the following hours to have a zero time value (A 0), which could be used as a reference for no radon loss during storage. The other bottles were measured in the following days, following a scheduled program to complete the monitoring over 15 days of storage.

2.3. RAD7 monitor with Big Bottle RAD H_2O accessory

The RAD7 monitor (Durridge Co., Inc.) is equipped with an electrostatic PIPS collector (passivated ion-implanted planar silicon detector) of alpha emitters and a spectrum analyzer, to select countings of different radon daughters. Mode "Sniff" allows us to use only the short-lived ^{218}Po to detect ^{222}Rn, which has the advantage of attaining equilibrium with the parent in just 15 min. Therefore, it is possible to set the cycle time at 15 min and repeat it for a minimum of seven times (and often up to 12 times). During the tests, the pump was on for the entire run to ensure equilibrium between dissolved and extracted radon. Air was extracted using a Teflon aerator, which consists of a single 23-cm-long vinyl tubing with an air stone fixed at its lower end, and a cap at the upper end, delivering incoming air from RAD7 via a check valve to the bottle and retransmitting it through the bubble trap to the desiccant drierite). Dried air is then conveyed to RAD7 in a closed-loop circuit. A data logger records the temperature at the bottleeelastic clinching strap interface during the measurement for calculating the radon solubility coefficient. The experimental apparatus is shown in Fig. 2. Typical analytical uncertainties for radon concentration values of 200 Bq/L are about 5% (i.e., 200 ± 10 Bq/L).

2.4. Gamma-ray spectrometer

Radon measurements can be made by g rays emitted by ^{214}Pb and ^{214}Bi, radon short-lived daughters, using a g spectrometer when the secular equilibrium is reached. The low-background spectrometer available at INGV laboratories, Rome, consists of a shield made of lead, either casting or pellets, surrounding a NaI(Tl) scintillator (3x3 in.), optically coupled to a photomultiplier. The pulse shaping is performed by a preamplifier and an amplifier, and the counting of peaks at 295, 352, and 609 keV is done by a 4-k multichannel analyzer. The spectrometer response is verified daily by counting an activated charcoal canister containing a standard source of ^{226}Ra (376 ± 10 Bq).

2.5. Radium calculation

A Marinelli beaker (1.035 L) was filled with water from Valle della Caffarella spring, and analyzed 33 times with a g spectrometer over 2 months to evaluate the radium content. The radon concentration plot (Fig. 3) results from the decay of the initial excess radon summed to the radon in equilibrium with radium; hence, the plot was interpolated with the following exponential function:

$$y = y_0 + Ae^{R0\,x} \qquad (1)$$

y = radon concentration (Bq/L) at time t (min),
y_0 = radon concentration (Bq/L) in equilibrium with ^{226}Ra (C Ra in Eq. (2)),
A = initial excess radon concentration (Bq/L),
R_0 = time constant (min^{-1}), and

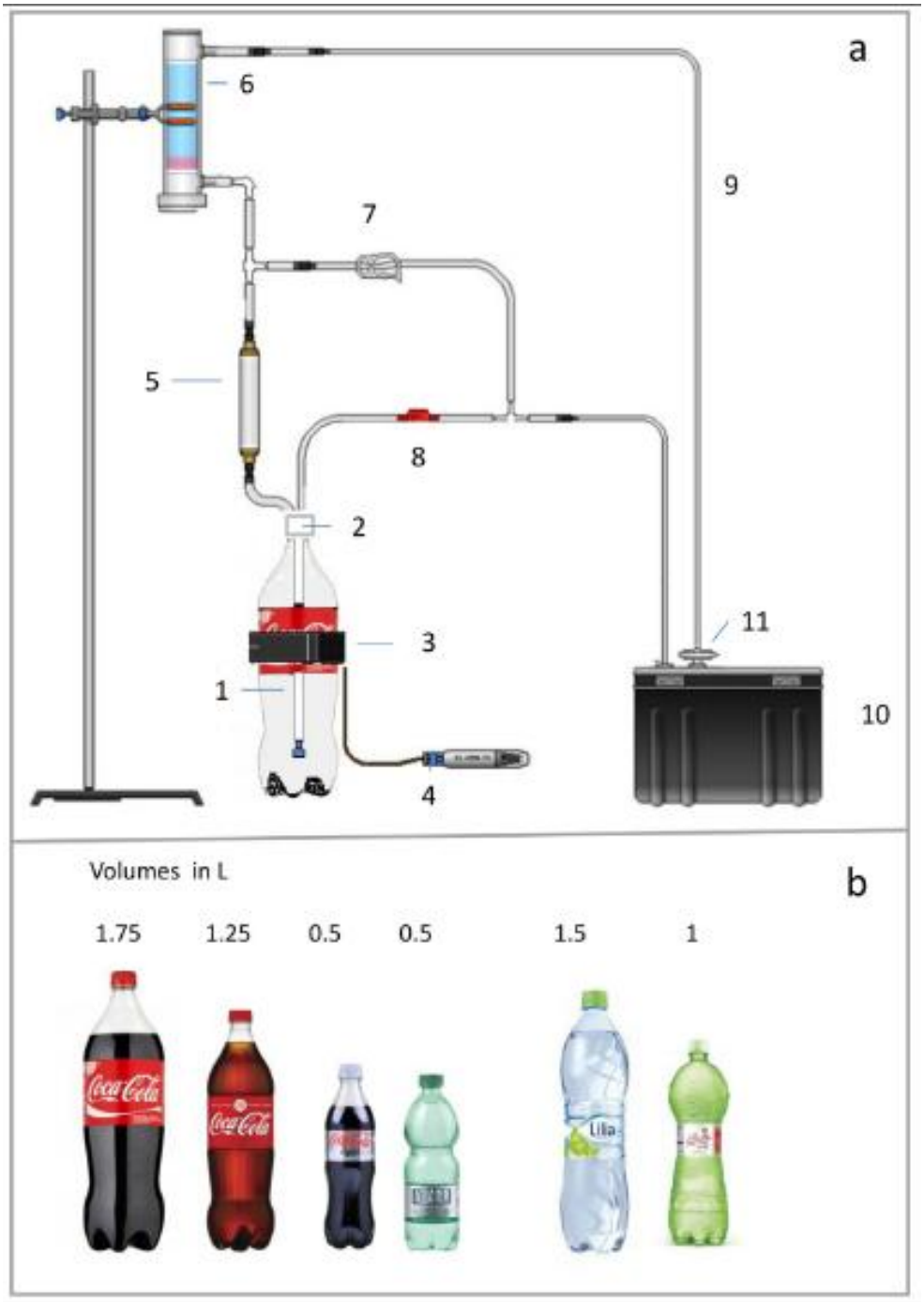

Fig. 2. Big Bottle RAD H_2O configuration (a, modified from Big Bottle RAD H_2O manual, Durridge Co., Inc., available at www.durridge.com). 1) Plastic soda bottle; 2) Screw-on Teflon aerator, with a single air stone; 3) Elastic clinching strap; 4) Temperature data logger; 5) Bubble trap; 6) Laboratory dryer; 7) Clip; 8) Check valve; 9) Vinyl tubing; 10) RAD7 radon detector; 11) Inlet filter. Plastic bottles used for the experiments (b). From left to right: 1.75-L PET Coca-Cola bottle, 1.25-L PET Coca-Cola bottle, 0.5-L PET Coca-Cola Light bottle, 0.5-L PET Acqua di Nepi mineral water bottle, 1.5-L Coca-Cola plantbottle™, commercialized in Italy by Acqua Lilia, 1-L "BioBottle" made from Ingeo™ PLA, used by Acqua S. Anna.

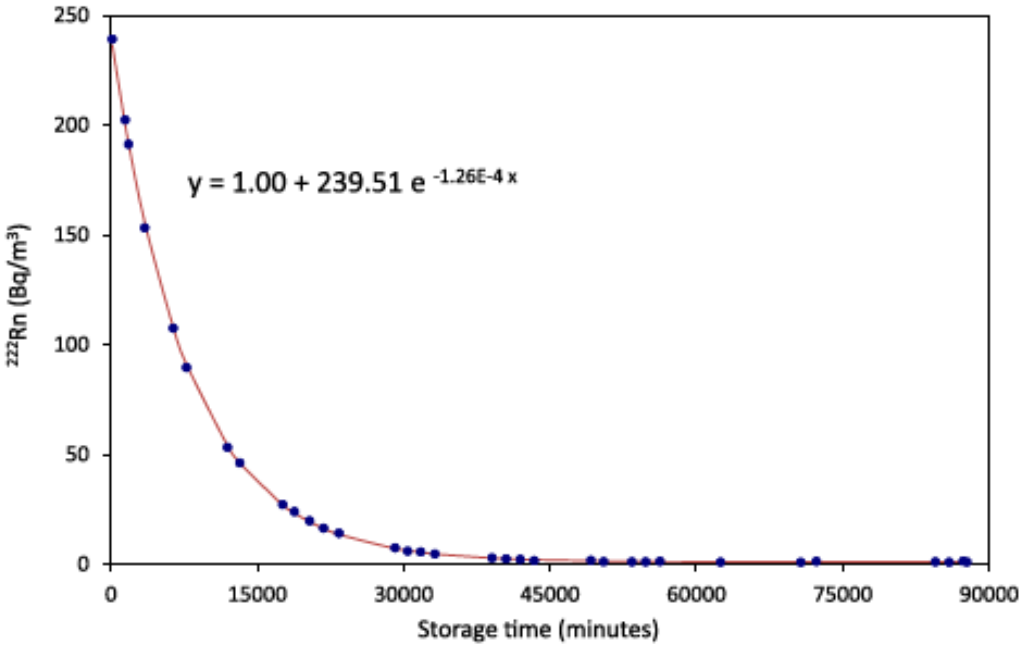

Fig. 3. Plot of radon measurements over 2 months for determination of dissolved ^{226}Ra. Errors (1 s) are enclosed in the symbols.

Table 1. *Volumes of bottles used for the experiments.*

Bottle	Coca175 (mL)	Coca125 (mL)	Coca50 (mL)
A	1809	1282	524
B	1808	1284	524
C	1820	1286	524
D	1789	–	526
E	1809	–	–
F	1790	–	–

Bottle	Lilia150 (mL)	Nepi50 (mL)	Ingeo100 (mL)
A	1514	517	1111
B	1530	513	1117
C	1523	520	1113
D	–	517	–
E	–	515	–
F	–	514	–

x = time elapsed from sampling (min).

2.6. Radon-in-water calculation

Radon activity concentration in water samples was calculated using the following equation (modified from De Simone et al., 2015), where background concentration in recirculating air is negligible:

$$C\ w = (Ca_{FIT30}\ (\ (V_a + \alpha\ (T)Vw) - V_h/\alpha(T)) - C_{Ra}\ )/DF \times AF \qquad (2)$$

where:

$V_a = V_{R7} + V_d + V_t + V_b$

C_w = original radon concentration in the water, corrected for ^{226}Ra (Bq/m^3),
Ca_{FIT30} = radon concentration value at t = 30 min of an exponentialfit of RAD7 data recorded during each 15-min run (30e120/180 min) (Bq/m^3),
T = temperature of water in the bottle (°C) (Fig. 2),
$\alpha(T) = 0.105 + 0.405\ e^{-0.0502\ T}$ = equilibrium coefficient from Fritz von Weigel equation (Weigel, 1978)
V_w = volume of water in bottle (see Table 1),
V_{R7} = internal volume of the RAD7 (0.768E-03 m^3),
V_d = equivalent desiccant column volume (0.673E-03 m^3),
V_t = volume of tubing and aerator (0.053 E-03 m^3),
V_b = volume of bubble trap (0.051E-03 m^3),
V_a = total volume of air in the system (1.545E-03 m^3),
$V_h/\alpha(T)$ = radon loss in the head space of air above the water in the plastic bottle, where V_h is the head space volume,
C_{Ra} = ^{226}Ra concentration in the water (1.00 ± 0.09 Bq/L),
DF = Decay Factor ($=e^{-t/t_{Rn}}$, where t (min) is the time elapsed between water sampling and 30 min after the beginning of the run and t Rn (min) is the radon average life, 7938), and
AF = adjustment of instrument calibration factor (0.9966, in this case)

Table 2

Classification of experiments on the basis of bottle characteristics (plastic type and size), air stone type, radon concentration classes, and departure of the 30-min datum from the exponential fit (within 1 s, within 2 s, or beyond 2 s). N denotes the number of measurements in the highest activity class for each bottle type.

Bottle	N	>50 Bq/L			<50 Bq/L		
		<1 σ	1–2 σ	>2 σ	<1 σ	1–2 σ	>2 σ
Air stone included in the Durridge soda bottle aerator kit							
1.25 – PET	6	5	1	–	–	–	–
1.75 – PET	5	2	3	–	–	–	–
1.5 – BIO PET	5	4	1	–	–	–	–
1 – PLA	2	2	–	–	–	–	–
Air stone borrowed from the standard Durridge big bottle aerator kit							
0.5 – PET	8	5	3	–	6	4	–
1.25 – PET	6	6	–	–	4	2	1
1.75 – PET	8	6	1	1	7	2	–
1.5 – BIO PET	8	5	3	–	3	4	1
1 – PLA	10	10	–	–	6	–	1
0.5 – PET (Nepi)	4	3	1	–	6	1	–

Radon concentration fit (Ca FIT30) was obtained by interpolating a data set ranging from 30-45 to 135-180 min (depending on the available cycles). The choice of the first datum used for the interpolation, 30 or 45 min, derives from statistical test, as illustrated in the following. The 30-min datum is critical, because its value is influenced by factors such as (i) degassing efficiency related to the bottle size and the type of air stone, (ii) time required to attain equilibrium between radon concentration in the two phases (waterand air), and (iii) radon activity in the closed loop. All the experiments were classified based on bottle characteristics (plastic type and size), air stone type (the original was replaced because of its rupture), radon concentration classes, and departure of the 30-min datum from the exponential fit (within 1 σ, between 1 and 2 σ, or beyond 2 σ, see Table 2).

The class with higher activity for each experimental setup (given by the Big Bottle configuration reported in Fig. 2 and a single bottle type) was used to evaluate its efficiency by checking the plot of 30-min datum of each run, i.e. within 1 σ, between 1

and 2 σ, or beyond 2 σ from the relative fit curve. If deviations from the fit are included in the normal distribution (<32% beyond 1 σ and <5% beyond 2 σ), the test configuration is evaluated as efficient and the first datum for the interpolation is at 30 min.

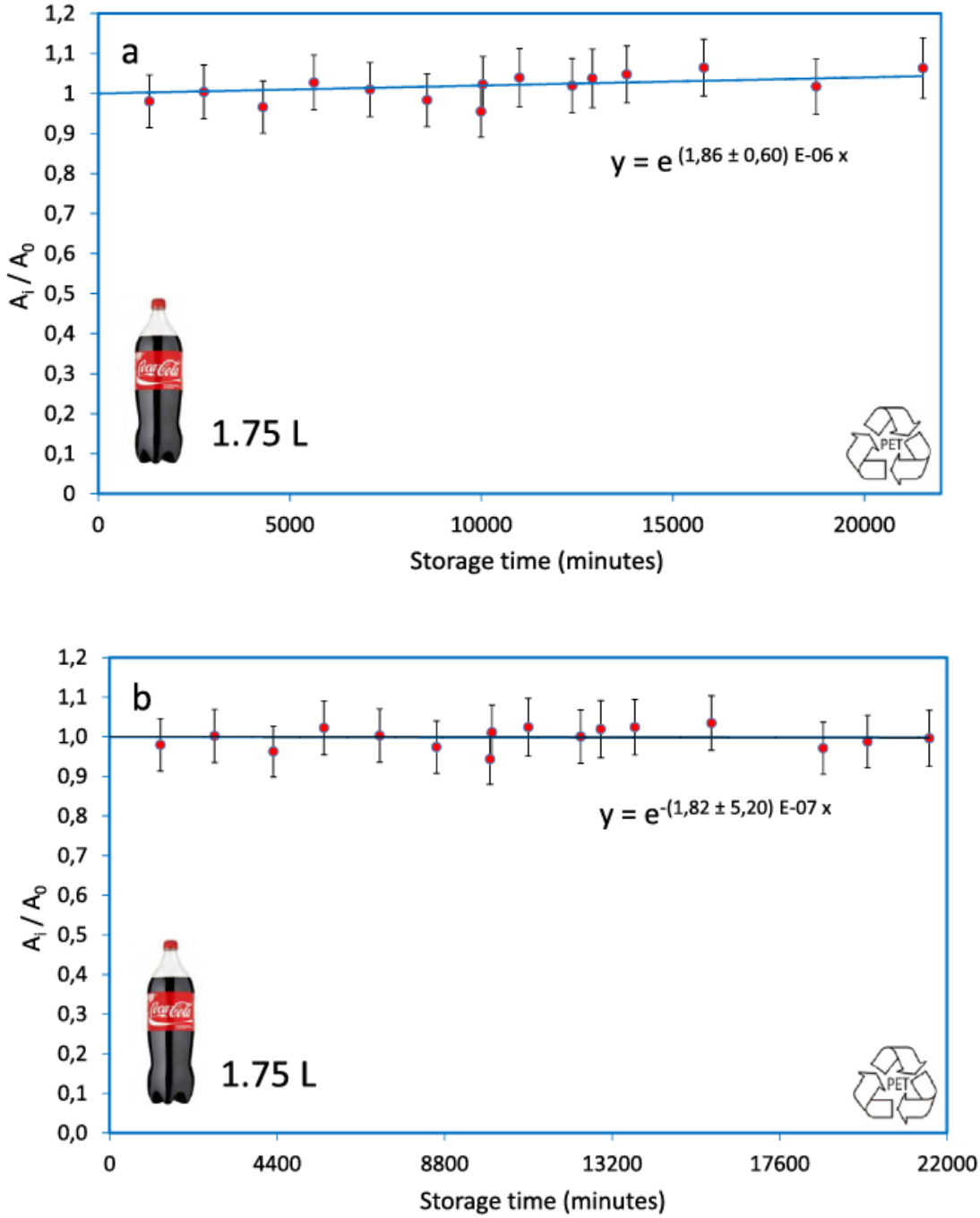

Fig. 4. Plot of A i /A 0 versus storage time in 1.75-L PET bottles. Data are corrected for (a) decay and (b) decay and ^{226}Ra content in water (1.00 ± 0.09 Bq/L). Modified from Tuccimei et al. (2015).

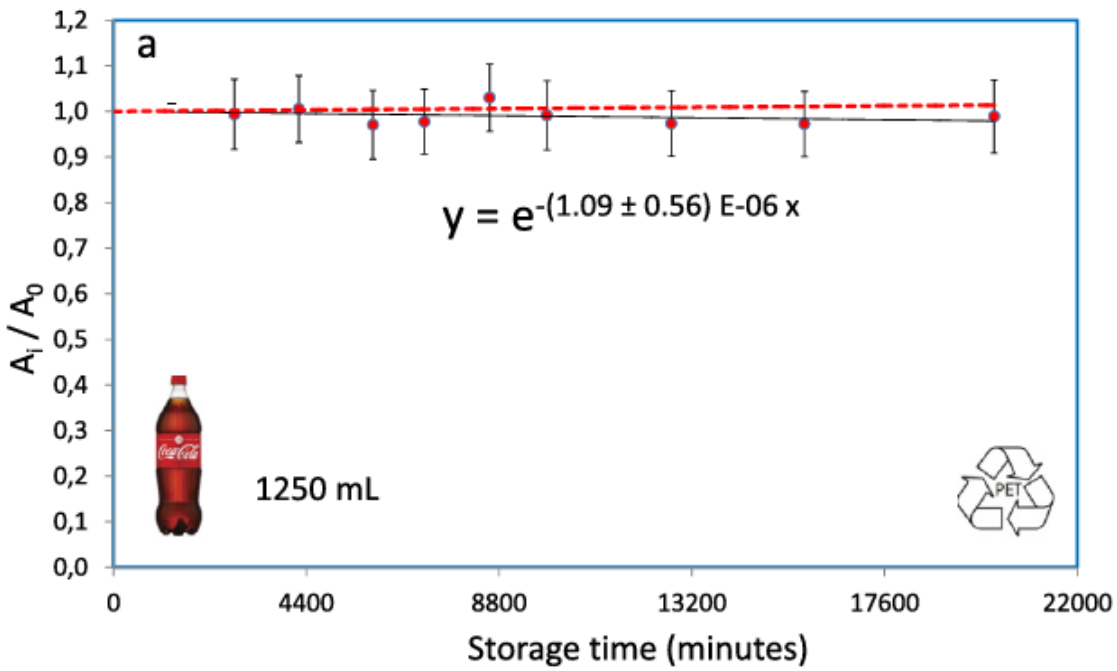
a
y = e-(1.09 ± 0.56) E-06 x
1250 mL
PET
Ai / A0
Storage time (minutes)
0
4400
8800
13200
17600
22000
0,0
0,1
0,2
0,3
0,4
0,5
0,6
0,7
0,8
0,9
1,0
1,1
1,2

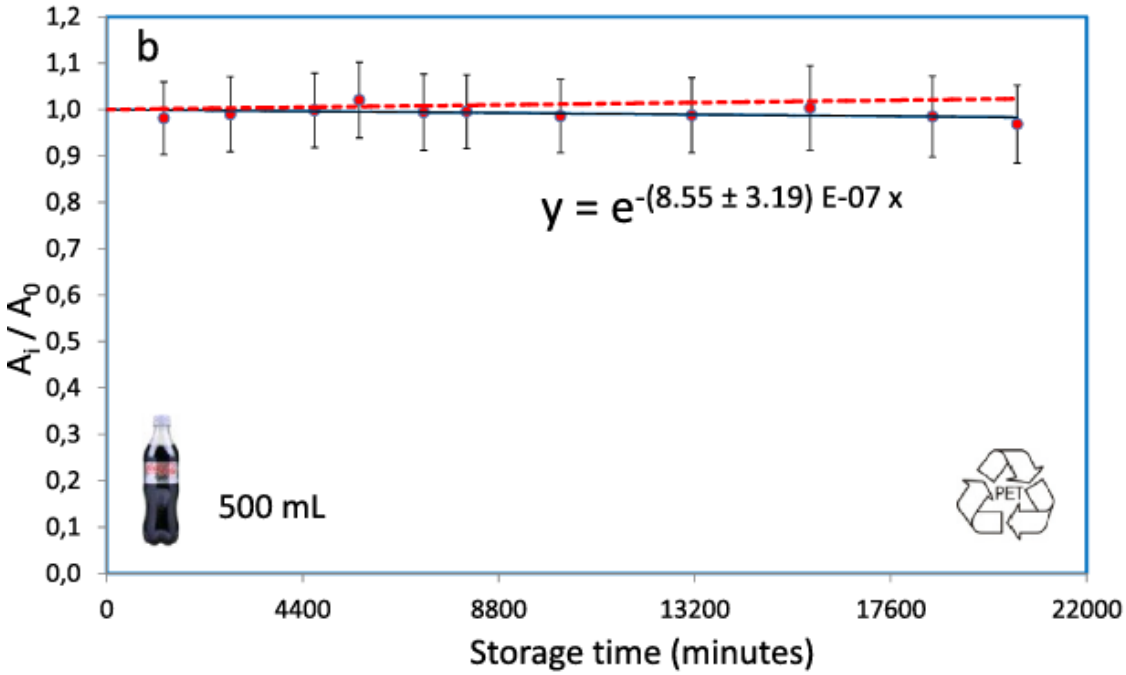
b
y = e-(8.55 ± 3.19) E-07 x
500 mL
PET
Ai / A0
Storage time (minutes)
0
4400
8800
13200
17600
22000
0,0
0,1
0,2
0,3
0,4
0,5
0,6
0,7
0,8
0,9
1,0
1,1
1,2

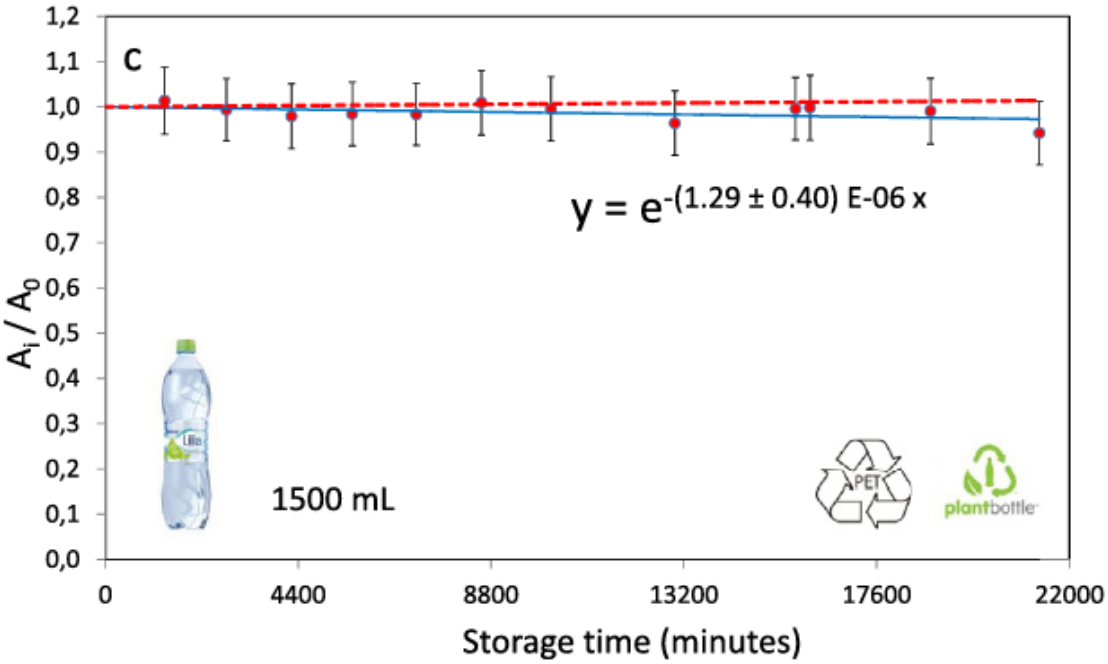

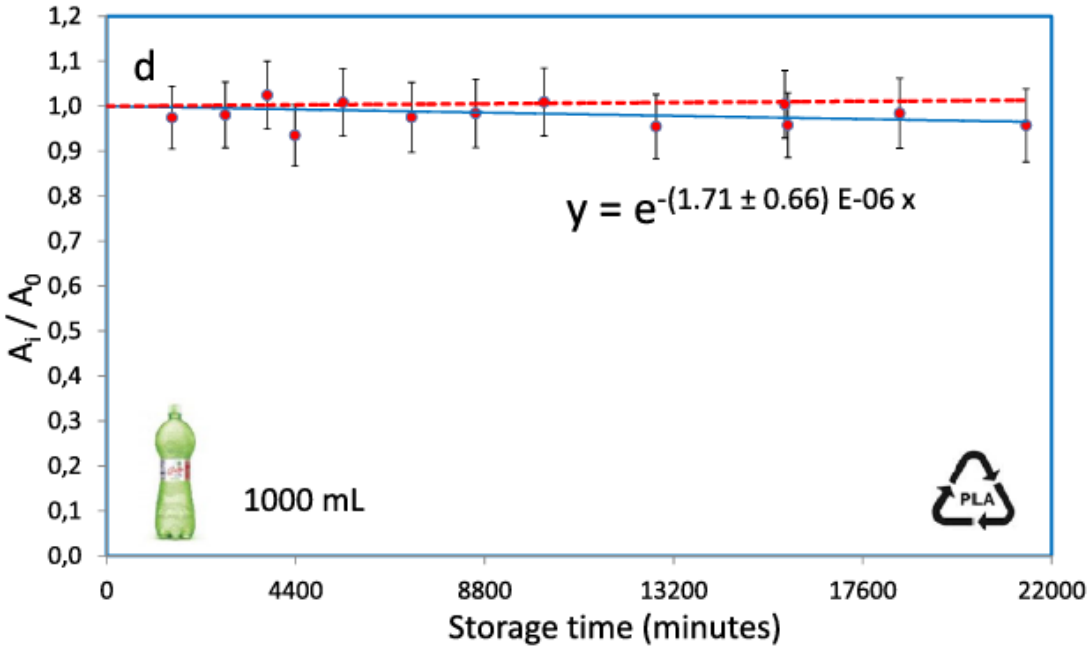

Fig. 5. Plot of A i /A 0 versus storage time in different volumes of PET and PLA bottles. Data are corrected for decay and ^{226}Ra content in water (1.00 ± 0.09 Bq/L). Red dashed lines indicate the radon loss without correction for radium. (For interpretation of the references to colour in this figure legend, the reader is referred to the web version of this article.)

included in the normal distribution (<32% beyond 1 σ and <5% beyond 2 σ), the test configuration is evaluated as efficient and the first datum for the interpolation is at 30 min. On the contrary, if deviations from the fit exceed normal distributions, the setup is not considered as completely efficient and the first datum for the interpolation is at 45 min. This may depend on the degassing efficiency if the aerator does not approach the bottom of the bottle and the equilibrium condition is reached later.

In the second step of evaluating radon data from classes with lower activities, if deviations of the 30 min datum for the class with the highest activity were included in the normal distribution, the data are checked singularly and the datum at 30 min is eliminatedonly in cases of large deviations. On the contrary, if deviations from

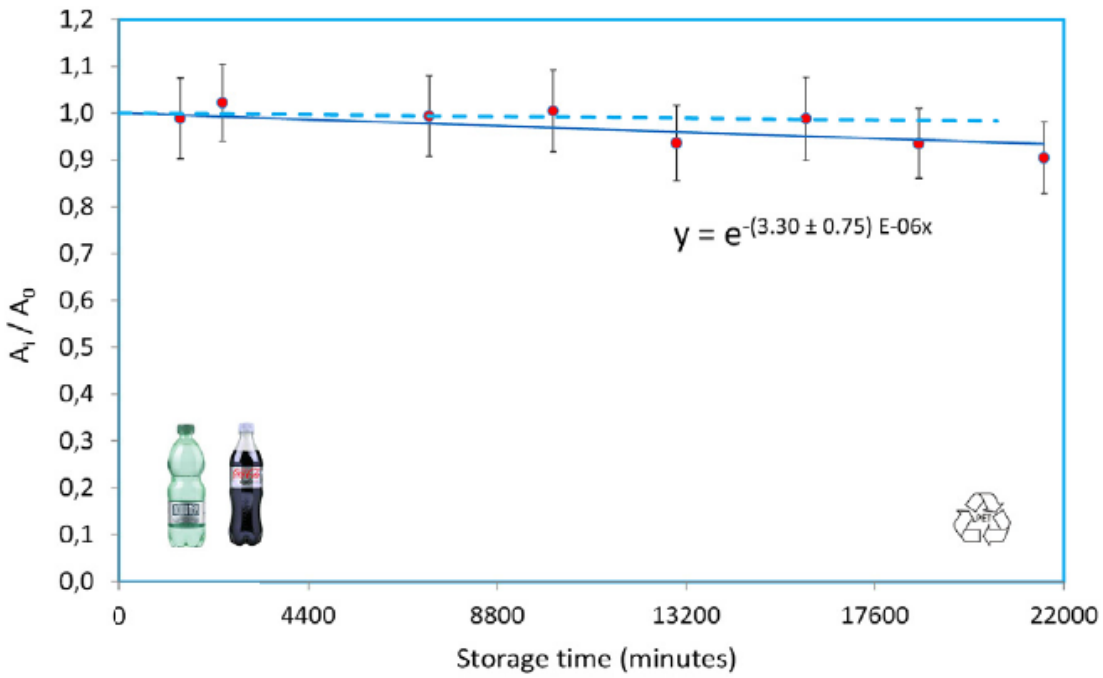

Fig. 6. Plot of A i /A 0 versus storage time in 500-mL PET bottles with different thicknesses, but similar surface/volume ratios. Data are corrected for decay and ^{226}Ra content in water (1.00 ± 0.09 Bq/L). Data refer to 0.5-L Acqua di Nepi mineral water bottle, and blue dashed line indicates the radon loss in 0.5-L Coca-Cola bottles (Fig. 5). (For interpretation of the references to colour in this figure legend, the reader is referred to the web version of this article.)

the fit for the higher activity class were not included in the normal distribution, the 30-min datum is not considered and the interpolation started from the 45-min data point.

At ambient temperatures >23 °C, the correction due to radon loss in the head space was applied to consider the radon loss due to the thermal dilatancy of Ingeo™ PLA. When the cap is opened at the beginning of the measurement, the radon concentration in this volume (V h) attains equilibrium with water and escapes from the system. This loss is expressed by V h /a in Eq. (2). There was no evidence of this ratio becoming zero for petroleum- and bio-based PET. This may be due to the coefficient of thermal expansion of PET, which ranges from 20 to 80 x 10^{-6} °K^{-1} (Saleh and Lubineau,2014), and is lower than that of PLA (80 - 90 x 10^{-6} °K^{-1} Gao, 2012).

In addition, PET becomes unstable at 72 °C, whereas PLA has a glass transition temperature of 55 °C.

No correction was applied for absolute humidity in the system for the temperature range of 15e23 _ C, with a relative humidity inside the instrument of about 4e5%, because of no interference from the water molecules on the electrostatic collection of ^{218}Po.

When the temperature inside RAD7 exceeds 23 °C and the relative humidity exceeds 5%, that is, 0.75 x 10^{-3} g of water in the RAD7 inner volume, a correction is applied to the radon concentration value at t = 30 min. This value is substituted in Eq. (1) for Ca_{FIT30} :

$$Ca_{FIT30\_corr} = Ca_{FIT30}\ (1{:}05\ (59 \times gH_2O_{RAD7})) \qquad (3)$$

Table 3
Radon loss during 15-day storage in PET and PLA bottles.

Bottle	Time (min)	A_1/A_0	$\sigma A_1/A_0$
1.75-L PET (Coca-Cola)	0	1.000	0.000
	1334	0.980	0.066
	2757	1.002	0.067
	4300	0.963	0.065
	5631	1.023	0.068
	7095	1.003	0.067
	8585	0.974	0.066
	9992	0.943	0.064
	10042	1.011	0.069
	10999	1.024	0.073
	12374	1.000	0.067
	12902	1.019	0.072
	13797	1.024	0.070
	15810	1.034	0.069
	18744	0.971	0.066
	19911	0.988	0.067
	21532	0.996	0.071
1.25-L PET (Coca-Cola)	0	1.000	0.000
	1335	1.017	0.077
	2758	0.993	0.073
	4231	1.005	0.076
	5921	0.971	0.071
	7096	0.977	0.074
	8583	1.030	0.076
	9890	0.991	0.072
	12732	0.973	0.072
	15769	0.972	0.071
	20102	0.989	0.075
0.5-L PET (Coca-Cola)	0	1.000	0.000
	1280	0.981	0.078
	2775	0.990	0.081
	4663	0.998	0.080
	5668	1.020	0.082
	7115	0.994	0.082
	8081	0.995	0.079
	10187	0.986	0.079
	13133	0.987	0.081
	15791	1.003	0.091
	18537	0.985	0.087
	20442	0.968	0.084
1.5-L PET (plantbottle™)	0	1.000	0.000
	1354	1.013	0.074
	2761	0.993	0.069
	4248	0.979	0.072
	5633	0.984	0.070
	7095	0.983	0.068
	8582	1.009	0.071

Bottle	Time (min)	A_1/A_0	$\sigma A_1/A_0$
	10172	0.995	0.071
	12997	0.964	0.071
	15752	0.996	0.069
	16079	0.998	0.072
	18831	0.990	0.072
	21316	0.942	0.070
1.0-L PLA (Acqua S. Anna)	0	1.000	0.000
	1521	0.975	0.070
	2760	0.980	0.073
	3739	1.024	0.075
	4382	0.935	0.068
	5499	1.008	0.075
	7098	0.975	0.078
	8588	0.984	0.076
	10185	1.009	0.075
	12791	0.954	0.072
	15788	1.004	0.075
	15858	0.958	0.072
	18462	0.984	0.078
	21408	0.957	0.081
0.5-L PET (Acqua di Nepi)	0	1.000	0.000
	1426	0.989	0.086
	2406	1.022	0.083
	7215	0.994	0.086
	10104	1.005	0.088
	12979	0.936	0.081
	15994	0.988	0.088
	18621	0.935	0.075
	21541	0.904	0.076

3. Results and discussion

Total radon concentration in groundwater is the sum of ^{222}Rn in equilibrium with dissolved ^{226}Ra and excess radon from watererock interaction.

watererock interaction. This component may be interpreted as recoil flux from mineral surfaces (Krishnaswami et al., 1982) or as a combination of recoil and diffusion of radon from microfractures or aquifer solids surfaces (Rama and Moore, 1984; Davidson and Dickson, 1986; Andrews et al., 1989; Vinson et al., 2009). As described by Tuccimei et al. (2015), the effect of radium has to be considered when correcting radon

data for radioactive decay, particularly for longer storage times. Moreover, if no correction is applied, radon concentration may apparently increase over time, in case of significant radium activity (Tuccimei et al., 2015). The amount of dissolved radium in Valle della Caffarella spring was obtained by the interpolation of 33 radon data obtained by gamma spectrometry during a period of 2 months (Fig. 3), using an exponential function (Eq. (1)). The result of the interpolation is

$$y = 1.00 + 239:51\ e^{-1:26E-4x}$$

Consequently, 1.00 ± 0.09 Bq/L (y 0 in Eq. (1) and C Ra in Eq. (2)) of radon has been subtracted in all radon measurements before applying the correction for radioactive decay (DF in Eq. (2)). The fitting also provides the initial excess radon (239.51 ± 0.84 Bq/L), which when summed to ^{222}Rn in equilibrium with dissolved radium agrees with the value of 236 ± 8 Bq/L, reported by Pizzino (2015). It is worth noting that the time constant (R 0 in Eq. (1)) corresponds to ^{222}Rn decay constant (expressed in minutes).

3.2. Radon loss during 15-day storage from PET and PLA plastics

A statistical test was conducted on the data reported in Table 2. As a result, the datum at 30 min was excluded from the data set used for the interpolation, only for 1.75-L PET bottles, when the air stone included in the standard soda bottle aerator kit was used.

A plot of radon loss (A i /A 0) versus storage time in 1.75-L PET bottles (Fig. 4) was presented in Tuccimei et al. (2015). Data are corrected for decay (Fig. 4a) and decay and ^{226}Ra content in water (1.00 ± 0.09 Bq/L, Fig. 4b).

These data are compared and discussed against radon loss of groundwater from Valle della Caffarella spring stored in PET and PLA bottles for 15 days (Fig. 5). In all cases,

^{222}Rn activity concentration is corrected for radioactive decay and ^{226}Ra content (1.00 ± 0.09 Bq/L). Each graph also reports the exponential fitting of row data, not corrected for dissolved radium. If no correction for radium is applied, the exponential fitting of red dashed lines in Fig. 5 simulates a slight increase of radon concentration during storage in PET (petrol- and plant-based types) and PLA bottles, which is impossible. This confirms that a correction is needed, particularly for increasing storage time.

Corrected data demonstrate minor losses from all bottles, ranging from about 0.03% (1.75-L PET) to 0.25% (1-L PLA) per day, resulting in about 0.4 and 3.7% in 15 days. However, the relative differences are significant and depend on the surface/volume ratios of the bottles and the thickness of the plastic material. The discussion is reported in the following section. Fig. 6 reports the radon loss from 0.5-L PET bottles used by Acqua di Nepi mineral water, with the volume and surface/volume ratio same as Coca-Cola, but different surface/weight ratio and hence plastic thickness. Radon loss is the highest among the measured values and approaches 0.35% per day, that is, 5.20% in 15 days. All radon data used in Figs. 4e6 are reported in Table 3.

The gas loss rates of bio-based PET and PLA bottles were about 0.19 and 0.25% per day, respectively, resulting in 2.8 and 3.7% after 15 days.

Table 4
Averages of volumes, surface/volume ratios, weights, surface/weight ratios, and radon loss rates of plastic bottles used for the experiments.

Bottle (L)	Water volume (L)	Surface (cm^2)	Surface/Volume (cm^{-1})	Weight (g)
1.75 – PET	1.804	913	0.506	36.1
1.5 – BIO PET	1.519	845	0.556	23.2
1.25 – PET	1.284	714	0.556	36.1
1 – PLA	1.114	663	0.596	24.6
0.5 – PET	0.524	412	0.786	17.4
0.5 – PET (Nepi)	0.516	402	0.779	12.4

Bottle (L)	Weight (g)	Surface/Weight ($cm^2\,g^{-1}$)	Radon loss rate ($10^{-6}\,min^{-1}$)
1.75 – PET	36.1	25.3	−0.18 ± 0.52
1.5 – BIO PET	23.2	36.5	−1.29 ± 0.40
1.25 – PET	36.1	19.8	−1.09 ± 0.56
1 – PLA	24.6	27.0	−1.71 ± 0.66
0.5 – PET	17.4	23.7	−0.86 ± 0.32
0.5 – PET (Nepi)	12.4	32.3	−3.30 ± 0.75

3.3. Radon loss dependence on surface/volume ratios and thickness of plastic bottles

Table 4 presents the surface/volume and surface/weight ratios (roughly related to the plastic thickness) of PET (petrol- and biobased types) and PLA bottles. Surface integral revolution (Eq. (4)) can be applied to the bottle profile, f(x), to calculate the surface area (S) of the bottles:

$$S = 2\pi \int_{x_1}^{x_2} f(x)\sqrt{1 + [f'(x)]^2}\, dx \qquad (4)$$

Eq. (4) can be approximated using the geometry of the truncated cones (5) as

$$S = \pi \sum_i a_i (R_{2\,i} + R_{1\,i}) \qquad (5)$$

where a is the apothem and R 2 and R 1 are the truncated cone radii. The plot of radon loss rates versus surface/volume ratios (Fig. 7) shows the direct correlation between the two parameters, regardless of the plastic types, except for the 0.5-L PET (Coca-Cola)

characterized by a surface/weight ratio significantly lower (i.e., larger thickness) than that of 0.5-L PET (Acqua di Nepi), having a similar surface/volume ratio. Consequently, with regard to radon loss rates, bottle thickness can partly balance higher surface/volume ratios.

4. Conclusions

The results suggest that PET, either petrol- or bio-based types, and PLA are much suitable for storing natural water for the assay of radon. Their performances are much better than those of other plastics investigated in the literature (LDPE and HDPE). If radon loss rates after 4 days of storing are compared with available data from literature, PET bottles loose from about 0.1 to 1.4% and PLA 1% against the rates of HDPE, from 15 to 22% (Saito, 1983; Leaney and Herczeg, 2006; De Simone et al., 2015) and LDPE 27% (Leaney and Herczeg, 2006).

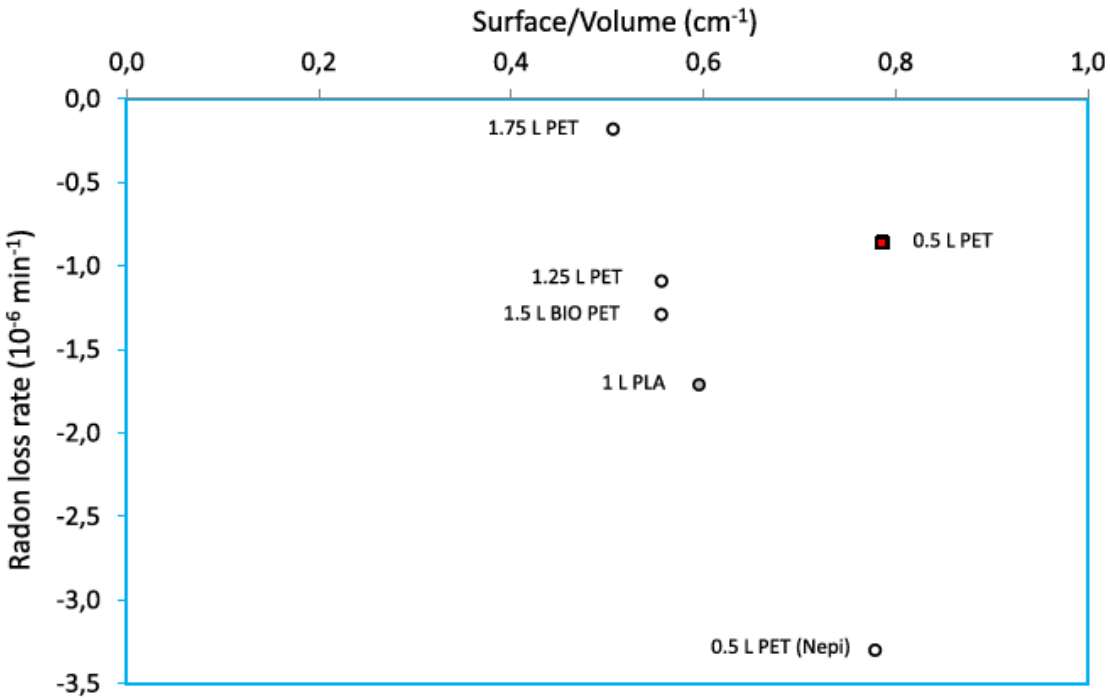

Fig. 7. Plot of radon loss rate versus surface/volume ratio of plastic bottles. 1-s errors range from 0.3 x 10^{-6} to 0.7 x 10^{-6} min^{-1}

literature, PET bottles loose from about 0.1 to 1.4% and PLA 1% against the rates of HDPE, from 15 to 22% (Saito, 1983; Leaney and Herczeg, 2006; De Simone et al., 015) and LDPE 27% (Leaney and Herczeg, 2006).

Surface/volume ratios and thickness of different PET bottles were examined to verify their role on radon loss rates over a period of 15 days. The main factor affecting radon loss rate of a given material is its surface/volume ratio, because either diffusion or adsorption, indicated as possible involved processes in the literature (Saito, 1983; Arafa, 2002; Fern. andez et al., 2004; Ashry et al., 2011; De Simone et al., 2015), is surface dependent. A higher bottle thickness reduces radon loss rates when considering bottles having similar surface/volume ratios as in the case of 0.5-L Coca-Cola and Acqua di Nepi mineral water PET bottles.

An accurate and precise determination of dissolved ^{226}Ra in water samples is necessary, particularly for measurements after at least a week from sampling.

Performances of Big Bottle RAD H_2O device with the soda bottle aerator kit coupled to RAD7 radon monitor (Durridge Co., Inc.) were evaluated in terms of degassing efficiency, and the effects of temperature and grams of water in the RAD7 inner volume on the radon daughter electrostatic collection were investigated. Proper corrections were developed and applied.

References

Andrews, J.N., Ford, D.J., Hussain, N., Trivedi, D., Youngman, M.J., 1989. Natural radioelement solution by circulating groundwaters in the Stripa granite. Geochim. Cosmochim. Acta 53, 1791e1802.

Arafa, W., 2002. Permeability of radon222 through some materials. Radiat. Meas. 35, 207e211.

Ashry, A.H., Abou-Leila, M., Abdalla, A.M., 2011. Measurement of radon permeability through polyethylene membrane using scintillation detector. Radiat. Meas. 46, 149e152.

Capelli, G., Mastrorillo, L., Mazza, R., Petitta, M., 2012. Carta delle Unit. a Idrogeologiche della Regione Lazio. Scala 1.250 000. Regione Lazio.

Conticelli, S., Peccerillo, A., 1992. Petrology and geochemistry of potassic and ultrapotassic volcanism in central Italy: petrogenesis and inferences on the evolution of the mantle sources. Lithos 28, 221e240.

Davidson, M.R., Dickson, B.L., 1986. A porous flow model for steady state transport of radium in groundwater. Water Resour. Res. 22, 34e44.

De Simone, G., Galli, G., Lucchetti, C., Tuccimei, P., 2015. Calibration of Big Bottle RAD H2O set-up for radon in water using HDPE bottles. Radiat. Meas. 76, 1e7. Fern. andez, P.L., Quind. os, L.S., Sainz, C., Gom. ez, J., 2004. A theoretical approach to the measurement of radon diffusion and adsorption coefficients in radonproof membranes. Nucl. Instrum. Methods Phys. Res. B 217, 167e176.

Galli, G., Guadoni, C., Mancini, C., 1999. Radon grab sampling in water by means of radon transfer in activated charcoal collectors. In: Proceedings of the Fourth International Conference on Rare Gases Geochemistry. 8e10 October, 1997. Il Nuovo Cimento, vol. 22. University of ROMA TRE, Italy, 3e4, 583-587.

Gao, F., 2012. Advances in Biopolymer Nanocomposites. Woodhead Publishing Series in Composites Science and Engineering, Oxford.

Krishnaswami, S., Graustein, W.C., Turekian, K.K., Dowd, J.F., 1982. Radium, thorium,and radioactive lead isotopes in groundwaters: application to the in situ determination of adsorption-desorption rate constants and retardation factors. Water Resour. Res. 18, 1663e1675.

Leaney, F.W., Herczeg, A., 2006. A rapid field extraction method for determination of radon-222 in natural waters by liquid scintillation counting. Limnol. Oceanogr. Methods 4, 254e259.

Pizzino, L., 2015. Idrochimica delle acque sotterranee e Natural Gas Hazard nell'area urbana di Roma. Tesi di Dottorato in Scienze della Terra. Universit. a “Roma Tre”. Rama, Moore, W.S., 1984. Mechanism of transport of UeTh series radioisotopes from solids into ground water. Geochim. Cosmochim. Acta 48, 395e399.

Saito, M., 1983. Correction for loss of radon-222 in water sample caused by the use of a polyethylene bottle. Radioisotopes 32, 109e112.

Saleh, M.N., Lubineau, G., 2014. Understanding the mechanisms that change the conductivity of damaged ITO-coated polymeric films: a micromechanical investigations. Sol. Energy Mater. Sol. Cells 130, 199e207.

Sax, L., 2010. PET containers may release di (2-ethylhexyl) phthalate (DEHP). Environ. Health Perspect. 118, 445e448.

Shotyk, W., Krachler, M., Chen, B., 2006. Contamination of Canadian and European bottled waters with antimony from PET containers. J. Environ. Monit. 8, 288e292.

Tuccimei, P., Lane-Smith, D., Galli, G., Simko, J., Cook, I., Bond, C.E., Lucchetti, C., De Simone, G., 2015. Our PET project: an unlimited supply of big and small water sample vials for the assay of radon in water. J. Radioanal. Nucl. Chem. http://dx.doi.org/10.1007/s10967-015-4532-4.

Vinson, D.S., Vengosh, A., Hirschfeld, D., Dwyer, G.S., 2009. Relationships between radium and radon occurrence and hydrochemistry in fresh groundwater from fractured crystalline rocks, North Carolina (USA). Chem. Geol. 260, 159e171.

Weigel, F., 1978. Radon. Chem. Ztg. 102, 287e299.

9.4 A NEW TECHNIQUE TO MEASURE IN SITU SOIL GAS PERMEABILITY

Mauro Castelluccio a, Gabriele De Simone a, Carlo Lucchetti a, Massimo Moroni b, Paola Tuccimei a,

a: Dipartimento di Scienze, Universit. a "Roma Tre", Roma, Italy

b: GEOEX s.a.s., C.so Matteotti 44, 00041 Albano Laziale, Roma, Italy

Abstract

Intrinsic permeability is crucial to assess gases and volatile compounds transport through soil. In situ measurements of this parameter are based on Darcy equation, an empirical relation that describes the flow of a fluid through a porous medium. A new technique for in situ measurement of soil gas permeability was developed and deeply tested in several terrains. The new instrument was successfully calibrated against RADON JOK, a permeameter which is widely employed all over the world. The new device provides rapid responses and is easy to carry in the field. It can be employed in the range of $3 \times 10^{-13} – 8.0 \times 10^{-11}$ m^2 , extending the upper detection limit of RADON JOK (1.8×10^{-11}). Its use is recommended to investigate radon and other gas transfer through the soil and to map radon or CO_2 potentials of a given site. It could be also employed in environmental studies where the transfer of volatile pollutants is of primary concern.

1. Introduction

Measurements of soil permeability to gases have taken on added significance in recent years as a result of increased efforts to determine entry rates of radon into buildings and to develop methods of mapping the radon potential of soils (Mosley et al., 1996).

Pollutants in groundwater can be a source of exposure to residents of houses overlying contaminated aquifers. Volatile compounds may migrate through soil gas and enter below-grade basements under negative pressure. Soil permeability was found to be the overriding factor controlling advective TCE intrusion into basements (Fischer and Uchrin, 1996). Evaluation of gas movement is also important for estimating transport of volatile and semivolatile organic compounds from contaminated sites through the unsaturated zone to the groundwater. The use of soil venting, or soil vapor extraction, as a technique for remediating contaminated sites has resulted in increased interest in gas transport in the unsaturated zone (Rathfelder et al., 1995). Migration of gases from landfills, such as methane formed by decomposition of organic material, is important in many areas (Moore et al.,1982; Thibodeaux et al., 1982). Soil gas composition has also been used as a tool for mapping organic contaminant plumes and for mineral and petroleum exploration. In addition to that, pesticide volatilization contributes to air pollution, especially in areas of intensive agriculture. Of all the pesticides, soil fumigants are potentially the most volatile because of their high vapor pressures. Soil fumigation is used for controlling soilborne pathogens and parasitic nematodes, and the practice is essential for the production of high value crops such as strawberry and tomato, among many others (Gan et al., 1982).

Since the measurement of soil gas permeability is crucial in all these cases concerning environmental hazard and remediation, we developed and tested a new apparatus to

determine the in situ intrinsic permeability of subsoil, which has the advantage to take into consideration the influence of natural moisture, density, and effective porosity of soil, compared with indirect estimation such as particle size analysis.

2. Theory

Theoretical framework for gas permeability measurement is based on Darcy's equation. The soil is assumed to be homogeneous and isotropic and a standard state is considered. Furthermore the air is assumed to be incompressible (pressure differences are very much smaller than the atmospheric pressure). The gas permeability of soil, k (m^2), is calculated from the equation below (Damkjaer and Korsbech, 1992; Neznal et al., 2004):

$$k = \frac{\mu \cdot Q}{F \cdot \Delta P} \tag{1}$$

where μ (Pa s) is the dynamic viscosity of air (at 10 °C, μ = 1.75 × 10–5 Pa s), Q (m^3 s^{-1}) is the air flow through the probe, F (m) is the shape factor of the probe and ΔP (Pa) is the pressure difference between surface and the active area of the probe.

Critical point is the determination of the shape factor F. A solution was found in Damkjaer and Korsbech (1992). Resultant formula is as follows:

$$F = \frac{2\pi L}{\ln\left(\frac{2L\sqrt{\frac{(4D-L)}{(4D+L)}}}{d}\right)} \tag{2}$$

where L (m) is the length of the active area of the probe head, D (m) is the depth below the surface and d (m) is the diameter of the active area. It is worth stressing that that active area is the internal surface area of the measuring cavity which is created at the lower end of the sampling probe to enable the air collection. Further details on air withdrawal from the soil are provided in the next section.

3. Field techniques

The principle of this equipment consists of air withdrawal by means of negative pressure. Air is pumped out from the soil through a specially designed probe (manufactured by Radon v.o.s.) with a constant surface of contact between the probe head and the soil. The constant active area is created in the head of the probe (driven into the soil to about 80 cm depth) by the extrusion of a lost tip by means of the punch wire inside the probe by an exact distance (Fig. 1). The internal volume of the cavity, which is created at the lower end of the sampling probe, is large enough to enable the sample collection. The probes use the approximation L N d, with a shape factor F = 0.149 m (L = 50 mm, d = 12 mm and D = 825 mm).

The experimental setup consists of a miniature vacuum pump produced by Fürgut GmbH, connected to a vacuum gauge, manufactured by SMC, with a rated pressure range between 0 and -101 kPa. A flux meter from 0 to 5 L min-1 (produced by Key Instruments) was originally included in the experimental arrangement. A battery is used to provide energy to instruments (Fig. 2). The pressure gauge is connected via vynil tubing to the head of the probe on one side and to the pump on the other. Air from the pump was then made to flow through the flux meter and finally escape to the outer

environment. The vynil tubings and metal connectors (components 6 and 7 in Fig. 1) have been kept to a minimum to reduce gas leakage.

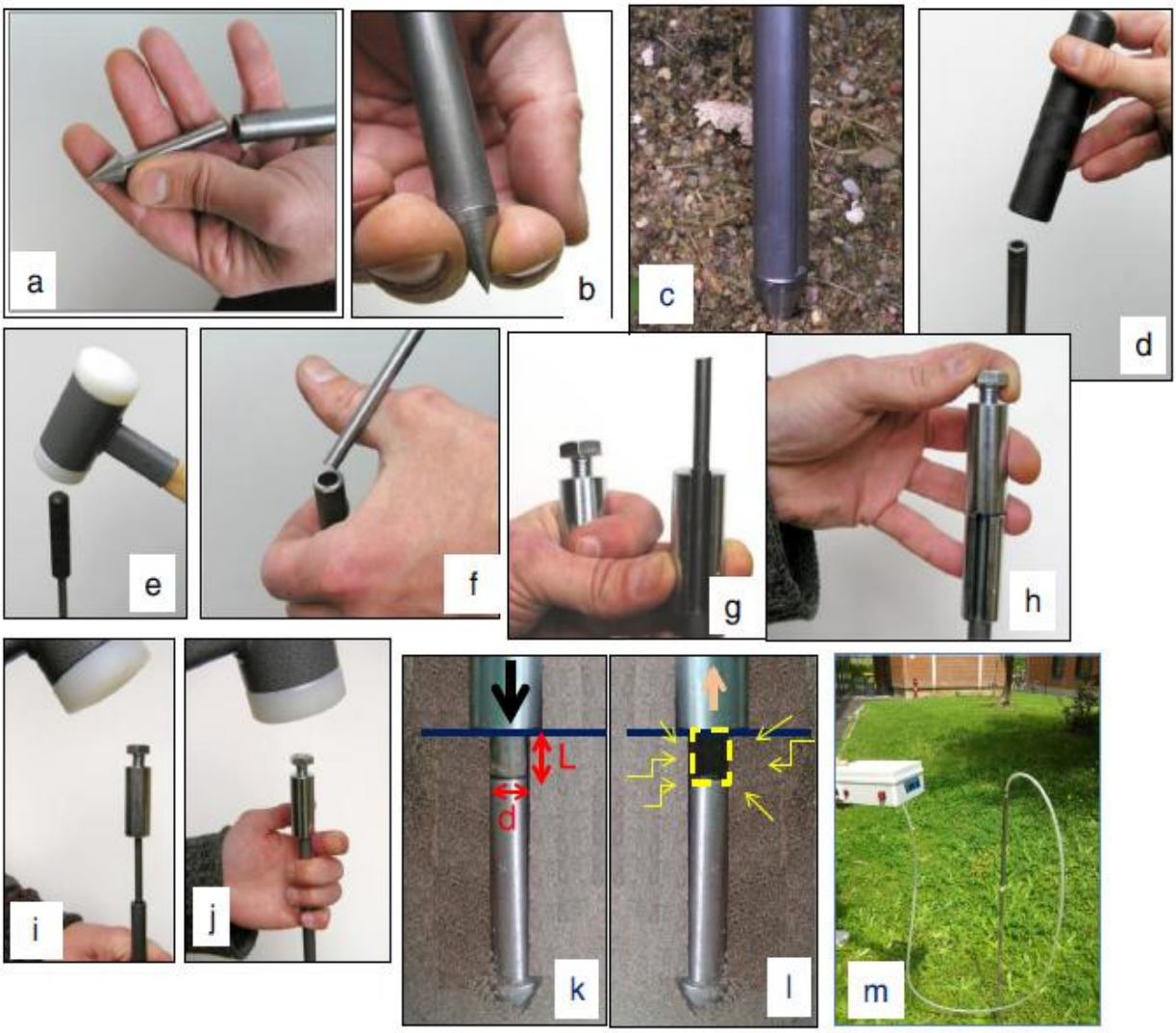

Fig. 1. Setting up the experimental system for permeability measurement—Photo sequence. Inserting the sharp tip into the lower end of the sampling probe (a and b); the probe with the tip is prepared at the sampling place (c); preparing the drive in head (d); the probe is pounded to the desired depth using a hammer (e); inserting of the punch wire into the probe (f); inserting of the distance ring (g); fixing the distance screw till it touches the distance ring (h); the sharp tip is moved to the exact distance using the punch wire and the adjusted distance screw (i and j); when done, the sharp tip is extruded and, after removal of the punch wire, a cylindrical cavity of known volume, with defined length, L, and diameter, d, is created (k and l); finally, the upper end of the probe is connected with the permeameter (white box on the left) using a vynil tubing (m). Photos from a to j are taken from the RADON JOK manual (Radon v.o.s).

Measurements carried out using this equipment were compared with those obtained by RADON JOK (Radon v.o.s, www.radon-vos.cz) which is widely employed in the Czech Republic (Neznal et al., 2004) and all over the world (Castelluccio et al., 2012; Friske et al., 2010; Xiao et al., 2012) to determine intrinsic permeability of soil. RADON JOK is also quoted in the frame of the European Geogenic Radon Map developed by the Joint Research Centre of the European Commission, as part of its projected European Atlas of Natural Radiation. Soil effective permeability is there considered among controlling variables to quantify the geogenic radon potential (Gruber et al., 2013).

The new permeameter and RADON JOK were connected to the same probe in a variety of geological settings to detect the value of k of different bedrocks (tuffs, travertine, flysch and sands outcropping in Latium region, central Italy), characterized by a large range of permeability. The flow Q and the pressure difference ΔP (sign-changed, vacuum gauge readings) associated with each determination were inserted in Eq. (1) to obtain the gas permeability of soil, either using the new equipment or RADON JOK.

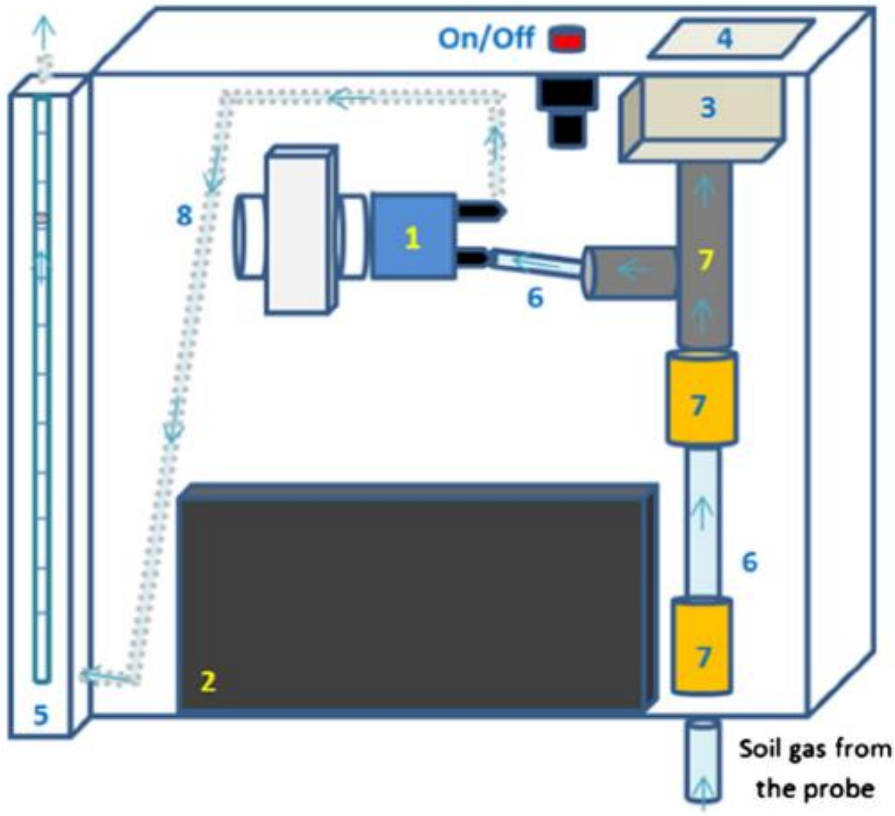

Fig. 2. New permeameter. It consists of a vacuum pump (1), a battery (2), a vacuomete (3), with digital display (4) a fluxmeter (5), vynil tubings (6), metal connectors (7) and electric cables (not shown). Tubings (8) connecting the pump output to the fluxmeter inlet were removed, along with the fluxmeter, at the end of the calibration test (see text for explanation). The arrows indicate air flow within the experimental apparatus.

4. Results and discussion

Table 1 reports the dataset used to create Fig. 3, where air flow data (Q) are plotted against the pressure difference (ΔP), associated with each permeability determination using the new permeameter. Pressure difference data in Table 1 correspond to vacuum gauge readings, because before any measurement the pressure is set to zero and a negative pressure difference compared to the atmospheric value (starting value) is displayed.

Experimental data are aligned along a curve, whose slope 2×10^{-9} m^3 s^{-1} Pa^{-1} is here compared with that provided by Fürgut GmbH for the pump operating in free air

condition. Field data slope is lower than that given by Fürgut (http://www.fuergut.com/pdfs/dc12_fk.pdf), which is 3×10^{-9} m^3 s^{-1} Pa^{-1}.

Moreover, the value of the intercept on the Y axis is about 6.75×10^{-5} m^3 s^{-1} , rather than 7.33×10^{-5} m^3 s^{-1} in free air condition. This demonstrates the reduction of the air flow from the soil through the experimental setup, due to friction/resistance phenomena, reducing the upper limit of air flow and changing the dependence of air flow on pressure difference.

Table 1

Air flow (Q), pressure difference (Dp) and gas permeability data determined using the new permeameter (k1), compared with RADON-JOK permeability (k2). 1,80 10-11 is the upper detection limit of RADON JOK. Dp data correspond to vacuum gauge readings, because before starting the measurement the pressure is set to zero and a negative pressure difference, compared to the atmospheric value (starting value), is displayed.

Identifier	Q (m^3 s^{-1})	DP (Pa)	k1 (m^2)	k2 (m^2)
1	6.23E-05	-2400	3.05E-12	2.80E-12
2	5.00E-05	-8500	6.91E-13	6.40E-13
3	6.50E-05	-400	1.91E-11	1.40E-11
4	6.50E-05	-800	9.54E-12	7.50E-12
5	6.58E-05	-700	1.10E-11	9.10E-12
6	6.17E-05	-2500	2.90E-12	2.70E-12
7	5.83E-05	-4900	1.40E-12	1.20E-12
8	6.00E-05	-3900	1.81E-12	1.80E-12
9	6.58E-05	-800	9.67E-12	8.00E-12
10	6.25E-05	-1500	4.89E-12	3.40E-12
11	6.50E-05	-700	1.09E-11	>1,80E-1
12	6.67E-05	-500	1.57E-11	>1,80E-1
13	6.67E-05	-300	2.61E-11	1.70E-11
14	6.75E-05	-500	1.59E-11	1.30E-11
15	6.58E-05	-700	1.10E-11	1.70E-11
16	6.57E-05	-700	1.10E-11	>1,80E-1
17	5.17E-05	-8400	7.22E-13	6.30E-13
18	4.58E-05	-11600	4.64E-13	4.50E-13
19	6.42E-05	-1300	5.80E-12	4.90E-12
20	5.58E-05	-6200	1.06E-12	9.00E-13
21	4.83E-05	-9100	6.24E-13	5.10E-13
22	4.67E-05	-10000	5.48E-13	6.10E-13
23	4.17E-05	-12000	4.08E-13	4.00E-13

Identifier	Q ($m^3 s^{-1}$)	DP (Pa)	k1 (m^2)	k2 (m^2)
24	6.58E-05	-900	8.59E-12	5.40E-12
25	6.33E-05	-1800	4.13E-12	4.00E-12
26	6.67E-05	-300	2.61E-11	1.80E-11
27	6.25E-05	-2000	3.67E-12	3.50E-12
28	6.58E-05	-800	9.67E-12	7.10E-12
29	5.00E-05	-8700	6.75E-13	9.20E-13
30	6.50E-05	-1500	5.09E-12	4.00E-12
31	6.58E-05	-1900	4.07E-12	3.70E-12
32	6.67E-05	-700	1.12E-11	8.50E-12
33	6.75E-05	-300	2.64E-11	1.50E-11
34	6.67E-05	-900	8.70E-12	6.10E-12
35	6.67E-05	-500	1.57E-11	1.20E-11
36	6.83E-05	-400	2.01E-11	1.60E-11
37	6.50E-05	-1100	6.94E-12	5.50E-12
38	6.51E-05	-1100	6.95E-12	6.10E-12
39	6.67E-05	-200	3.91E-11	1.20E-11
40	6.83E-05	-100	8.03E-11	>1,80E-11
41	6.67E-05	-100	7.83E-11	1.60E-11
42	6.60E-05	-200	3.88E-11	>1,80E-11
43	6.75E-05	-300	2.64E-11	>1,80E-11
44	6.83E-05	-200	4.01E-11	>1,80E-11
45	6.50E-05	-1100	6.94E-12	5.50E-12
46	6.75E-05	-100	7.93E-11	>1,80E-11
47	5.86E-05	-4400	1.56E-12	1.40E-12
48	5.84E-05	-4800	1.43E-12	2.50E-12

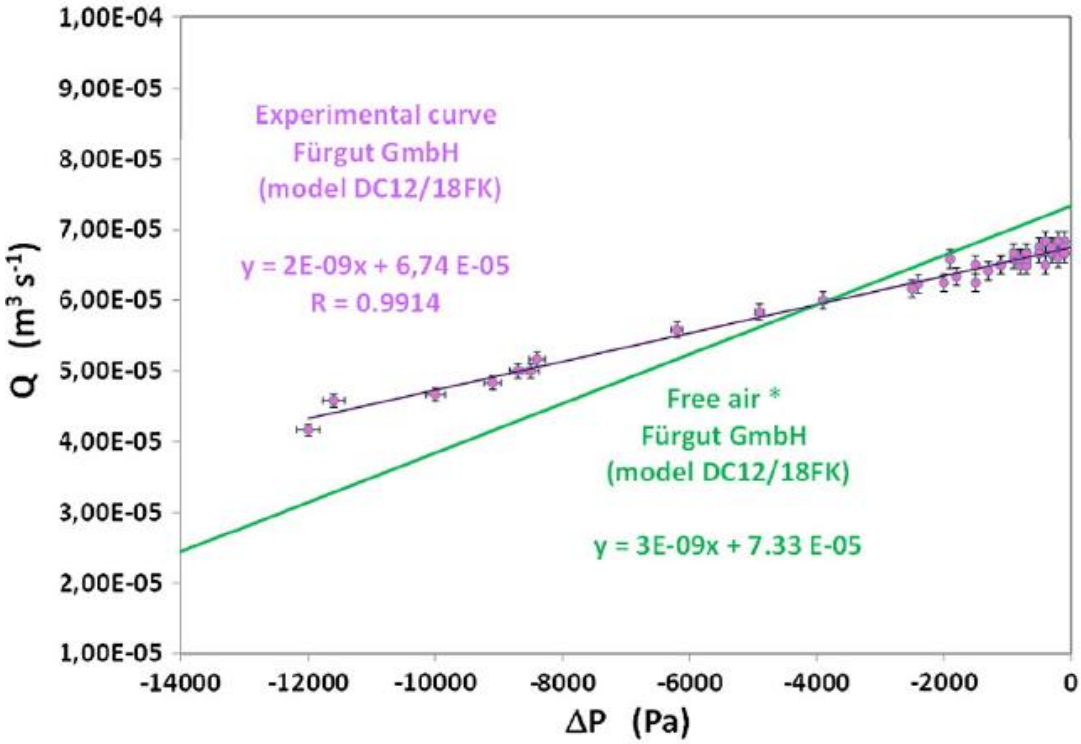

*Fig. 3. Experimental air flows (Q) versus pressure gradients (ΔP) measured using the new permeameter, compared to Q-ΔP data provided by Furgüt GmbH for the vacuum pump operating in free air conditions. * Furgüt supplies this diagram (http://www.fuergut.com/pdfs/dc12_fk.pdf) using different units (mbar and L/min) which have been changed here, according to the International System of Units (SI). Errors are given by instrumental sensitivities (fluxmeter and vacuometer).*

from the soil through the experimental setup, due to friction/resistance phenomena, reducing the upper limit of air flow and changing the dependence of air flow on pressure difference. Table 1 reports the whole dataset used to create the experimental graph (Fig. 4) correlating the value of k obtained with the new permeameter (k1) and that calculated using RADON JOK (k2). It is worth noting that ten data points are not included in the graph because corresponding k2 values are higher than the upper limit of RADON JOK equipment (Neznal et al., 2004), which is 1.80×10^{-11} m^2 . Fig. 4 shows that variables are very well correlated, demonstrating that the new device provides high quality data, comparable with those obtained with conventional and routinely used instruments.

In addition to that, the new permeameter allows to extend the range of detectable values in the area of high permeability (beyond 1.80×10^{-11} m^2). Moreover, when measuring low permeability data, it provides a quicker response, compared to RADON JOK. For example, the time required to detect a value of k equal to 3.0×10^{-13} m^2 is about 3–4 min using RADON JOK and only few seconds using the new apparatus. With reference to that, it is worth reminding that RADON JOK calculates k value using Eq. (1), where the term Q is not measured directly, but is derived from the ratio between the known air volume which is extracted (2 l) and the time required to complete this action (http://www.radon-vos.cz/?lang=en&lmenu=en_measuring&page=en_measuring_jok). Consequently, the lower the permeability, the longer the time required for extracting the air volume. Moreover, the new instrument is very light (1 kg) and can be easily transported everywhere in the field, even on bumpy and rough terrain.

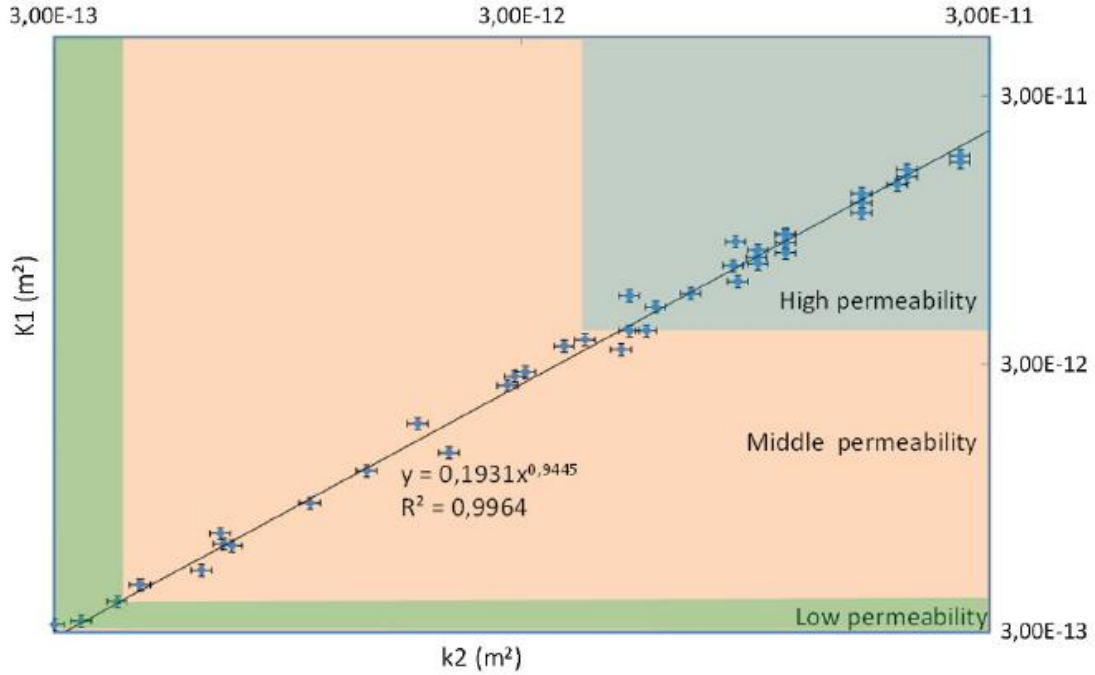

Fig. 4. k1 (gas permeability using the new permeameter) versus k2 (gas permeability using RADON JOK) measured from the same probe driven up to 80 cm depth. Permeability classes defined by the Check protocol (Neznal et al., 2004) for assessing the radon risk of building sites are indicated. Errors are given by instrumental sensitivities (fluxmeter and vacuometer for k1 and chronometer for k2).

In conclusion, a further improvement of the experimental assemblage can be envisaged. Since the relationship between the flux andthe pressure difference using this equipment is constant (see Fig. 3), it is possible to express the value of Q as a function of ΔP. Introducingthis term (m ΔP + c) in Eq. (1), a new calculation may be introduced to determine k only on the basis of ΔP:

$$k = \frac{\mu \cdot (\mathrm{m}\,\Delta\mathrm{P} + \mathrm{c})}{\mathrm{F} \cdot \Delta\mathrm{P}} \tag{3}$$

where m is the slope of the experimental curve (Q vs ΔP) in Fig. 3 and c is the intercept on the Y axis. This allows modifying the experimental device, removing the flux meter (device number 5 in Fig. 2) in orderto obtain a simple assemblage consisting of a single

pump and a vacuometer. This new configuration has also the advantage to reduce further the number of connections, minimizing the possibility of gas leakage.

The new device can be employed in the range of 3×10^{-13} –8.0×10^{-11} m^2 , extending the upper detection limit of RADON JOK (1.8×10^{-11}). This is definitely relevant because a higher permeability enables the increased migration of gas through the soil and into the buildings, enhancing the risk. Moreover, it provides rapid responses and is easy to carry in the field.

The new device for in situ measurement of soil permeability may be employed to investigate gases and volatile compounds transport through unsaturated media and to map radon potentials of a given site. With reference to that, the new European Council Directive 2013/59/Euratom of 5 December 2013, identifies soil permeability as a relevant parameter to estimate the distribution of indoor radon concentration to be considered in preparing the national action plans to address long-term risks from radon exposure.

References

Castelluccio, M.,Giannella, G.,Lucchetti, C.,Moroni, M.,Tuccimei, P., 2012. La classificazione della pericolosità radon nella pianificazione territoriale finalizzata alal gestione del rischio. Classification of radon hazard in urban planning focused to risk management. Ital. J. Eng. Geol. Environ. 2, 5–16.

Damkjaer, A., Korsbech, U.A., 1992. A small-diameter probe for in situ measurements of gas permeability of soil. Radiat. Prot. Dosim. 45, 85–89.

Fischer, D., Uchrin, C.G., 1996. Laboratory simulation of VOC entry into residence basements from soil gas. Environ. Sci. Technol. 30, 2598–2603.

Friske, P.W.B.,Ford, K.L.,Kettles, I.M.,McCurdy, M.W.,McNeil, R.J.,Harvey, B.A., 2010. North American soil geochemical landscapes project: Canadian field protocols for collecting mineral soils and measuring soil gas radon and natural radioactivity. Geological Survey of Canada Open File. 6282, p. 175.

Gan, J., Yates, R.S., Papiernik, S., Crowley, D., 1982. Application of organic amendments to reduce volatile pesticide emissions from Soli. Environ. Sci. Technol. 32, 3094–3098.

Gruber, V., Bossew, P., DeCort, M., Tollefsen, T., 2013. The European map of the geogenic radon potential. J. Radiol. Prot. 33, 51–60.

Moore, C.,Rai, I.S.,Lynch, J., 1982. Computer design of landfill methane migration control. J. Environ. Eng. 108, 89–107.

Mosley, R.B., Snoody, R., Brubaker, S.A., Brown, J., 1996. Experimental evaluation of geometricalshape factor for short cylindrical probes used to measure soil permeability to air. Environ. Int. 22, 509–520.

Neznal, M., Neznal, M., Matolin, M., Barnet, I., Miksova, J., 2004. The new method for assessing the radon risk of building sites. Czech Geological Survey Special Papers. 16. Czech Geological Survey, Prague, (www.radon-vos.cz/pdf/metodika.pdf).

Rathfelder, K.,Lang, J.R.,Abriola, L.M., 1995. Soil vapor extraction and bioventing: applications, limitations and future research directions. U.S. Natl. Rep. Int. Union Geod. Geophys. 1991–1994. Rev. Geophys. 33, 1067–1081.

Thibodeaux, L.J.,Springer, C.,Riley, L.M., 1982. Models and mechanisms for the vapor phase emission of hazardous chemicals from landfills. J. Hazard. Mater. 7, 63–74.

Xiao, L.,Wang, N.P.,Zhou, Z.G.,Hu, X.M.,Zeng, L.H., 2012. Mapping of soil radon concentration in Zhongshan, Guangdong Province. Geoscience 26, 1300–1305.

CHAPTER 10

CONCLUSIONS

This PhD study began with the aim of testing a new methodology for hydrocarbon polluted sites through the use of radon.

The first purpose was to characterise an area polluted by hydrocarbons using indirect analysis of Radon concentrations in soil, in connection with specific reference measurements in nearby sites not affected by the contamination (background areas). This kind of approach is based on surface analysis, not invasive and relatively cheap, if compared with traditional practices.

The use of radon negative anomalies to delineate the spatial extent of NAPL-pollutant zones is demonstrated either by laboratory simulation of a NAPL spill, by laboratory simulation of the exhatation rate or through multi-parameter monitoring and mapping in a contaminated site in Latium Region (Italy).

The use of this technique is fruitful to obtain a sufficiently detailed picture of ground contamination for the preliminary evaluation of NAPL contaminated sites to be joined with conventional investigation methods such as drive point profiling or the direct detection of organic carbons and their derivatives in the soil gas. In addition, it may be employed to assess the effectiveness of NAPL remediation and to provide an indicator that NAPL has been removed.

Once this was achieved, the focus of the study moved ahead, to give not only a qualitative evaluation of pollutant position, but also a quantitative estimate of a NAPL spill in a given site. Many field and laboratory experiments were then made in order to achieve that. Other tests were carried out to refine the measurement techniques, with the

final objective of creating a working protocol to apply to hydrocarbon contaminated sites.

Experimental work showed that the drying system of RAD7 electrostatic-based silicon detectors (drierite) used for the measurement of radon concentrations in soil and water samples, may affect radon concentrations reading measured because of its capacity to absorb hydrocarbons vapors of consequently the Radon dissolved in them. Various laboratory experiments were designed and performed in order to develop corrections for the presence of water in the system so as to eliminate the drying material (Drierite).

In order to use radon as NAPL tracer, we investigated if Drierite interferes with NAPLs in contaminated soil. Proper experiments were carried out in laboratory repeatedly connecting in a closed loop a RAD7 instrument, a Drierite column previously polluted with NAPL vapors and a small radon chamber (2.83 L) with a fixed activity of radon; at the end of each test, after measuring the equilibrium radon concentration, a partial purging of the RAD7 and the Drierite column was performed for a time of 5 min, not long enough to remove completely the absorbed NAPL. Since radon concentration is expected to decrease in successive experiments for decay and dilution, this process has been accounted for; nonetheless we observed firstly a decrease (28%) with respect to the expected value, then successive experiments showed progressive increases of radon concentrations (16 and 23%). As a matter of fact, firstly, NAPL vapor absorbed in the Drierite captures radon (test 2), reducing its concentration in the circuit; successive experiments (test 3 and 4) showed that NAPL still absorbed in the Drierite column is partially released to the closed loop, leading to a consequent rise of radon in the circuit. Accordingly, when soil radon measurements are carried out in presence of recent NAPLs contamination (De Simone et al., 2015a), these substances are extracted during soil gas sampling and then absorbed by desiccant material,

partitioning radon gas between the air and the absorbed liquid phases (the NAPL and the water). This leads to an interference difficult to deal with and thus desiccants should be removed. This is why we developed proper experiments to correct radon concentration detected by RAD7 electrostatic collection-based silicon detectors for the weight of water molecules in the system.

Results obtained performing various experiments showed that the corrective factor depends on i) the amount of water in the detection volume, ii) the history of the measurements done, i.e. increasing water content starting from dry conditions or vice versa.

The following linear interpolation equations have been found:

$Y = 1$ for X (g H_2O) < 0.00075

$Y = (- 68.999 \pm 0.771) X + (1.052 \pm 0.005)$

for $0:00075 < X$ (gH_2O)$< 0:010$; all data

$Y = (- 63.485 \pm 1.344) X + (1.047 \pm 0.008)$

for $0.00075 < X$(gH_2O) < 0.010; humidifying only

$Y = (- 70.715 \pm 1.037) X + (1.053 \pm 0.006)$

for $0.00075 < X$ (gH_2O) < 0.010; drying only

$Y = (- 38.903 \pm 7.474) X + (0.840 \pm 0.087)$

for $0:010 < X$ (gH_2O) < 0.014; humidifying only

$Y = (- 21.323 \pm 4.573) X + (0.558 \pm 0.055)$

for $0:010 < X$ (gH_2O) < 0.014; drying only

In any case, even i) ignoring the history effect and consequently the time required for the recovery of the full efficiency of electrostatic collection and ii) using the linear interpolation of all available data (Fig.5; Cap 6), radon concentration values can be still

inferred also in very critical conditions (water contents up to 0.010g H_2O in the RAD7).

As a consequence the use of Drierite should be avoided, irrespective of manufacturer recommendation, and proper correction for the efficiency of RAD7 electrostatic-based silicon detectors have to be applied to account for the effect of water molecules on the electrostatic collection of ^{218}Po ions. Ad-hoc corrections have been obtained for a specific RAD7 at different water contents. The temperature influence has been ruled out. In this prolific phase of my PhD study we have also created a new way to analyze the concentrations of radon in water samples using RAD7 electrostatic-based silicon detectors. Glass bottles are generally employed for sampling the water, especially when the measurement is not performed rapidly, but a delay may follow, because glass is impervious to radon and is not lost during sample storage. On the other hand, glass is fragile and the transport of glass bottles may induce the rupture, especially when springs or wells to sample are located along bumpy country or mountain roads. The need for shatterproof bottles led us to replace the 2.5 L glass bottles provided by Durridge Company Inc. with 1 L HDPE (High Density PolyEthylene) with other more practical to use, more resistant but with similar containment characteristics of the radon.

Firstly, were tested 1L High Density PolyEthylene (HDPE) bottles

A simplified method based on the measurement at 30 min to calculate dissolved radon concentration has been developed, based on the RAD7 Big Bottle setup replacing glass with HDPE bottles and considering various physical processes: radon loss during storage in HDPE bottles, absorption/desorption caused by diffusion through Drierite and circuit components. In particular, the ‘equivalent’ Drierite volume is somehow independent, within errors, from i) the amount of water already absorbed in Drierite, ii) a recirculation time greater than 30 min minimum time to have a response from the Durridge Big Bottle RAD H_2O instrument) and iii) radon concentrations. The main

advantages of this method employed during geochemical surveys are i) fragile glass bottles have been replaced by HDPE bottles, ii) the time required for each measurement has been shortened and iii) the Drierite consumption has been reduced.

In searching for a better solution, looking bottles readily available commercially, it was noted that Coke and similar bottles, made of polyethylene terephthalate (PET), are engineered to contain CO_2 at high pressures even if heated by the sun; furthermore the availability of a wide range of sizes would be an added benefit. So a special Teflon aerator for soda drinks has been developed and we start to test rhis new solution.

The results suggest that PET, either petrol- or bio-based types, and PLA are much suitable for storing natural water for the assay of radon. Their performances are much better than those of other plastics investigated in the literature (LDPE and HDPE). If radon loss rates after 4 days of storing are compared with available data from literature, PET bottles loose from about 0.1 to 1.4% and PLA 1% against the rates of HDPE, from 15 to 22% (Saito, 1983; Leaney and Herczeg, 2006; De Simone et al., 2015) and LDPE 27% (Leaney and Herczeg, 2006).

Surface/volume ratios and thickness of different PET bottles were examined to verify their role on radon loss rates over a period of 15 days. The main factor affecting radon loss rate of a given material is its surface/volume ratio, because either diffusion or adsorption, indicated as possible involved processes in the literature (Saito, 1983; Arafa, 2002; Fern. andez et al., 2004; Ashry et al., 2011; De Simone et al., 2015), is surface dependent. A higher bottle thickness reduces radon loss rates when considering bottles having similar surface/volume ratios as in the case of 0.5-L Coca-Cola and Acqua di Nepi mineral water PET bottles.

An accurate and precise determination of dissolved ^{226}Ra in water samples is necessary, particularly for measurements after at least a week from sampling.

Performances of Big Bottle RAD H_2O device with the soda bottle aerator kit coupled to RAD7 radon monitor (Durridge Co., Inc.) were evaluated in terms of degassing efficiency, and the effects of temperature and grams of water in the RAD7 inner volume on the radon daughter electrostatic collection were investigated. Proper corrections were developed and applied.

During my PhD studies we have also developed a new tool for measuring the intrinsic permeability of the soils. This study was carried out to obtain a tool easy to use and transport during field activities. The instrument generally used to make these measurements is the RADON JOK (Neznal Company), but this is a heavy instrument (about 18 kilograms), very large and difficult to transport in inaccessible areas. Hence the idea of developing a new, lighter and equally performing tool.

The principle of this equipment consists of air withdrawal by means of negative pressure. Air is pumped out from the soil through a specially designed probe (manufactured by Radon v.o.s.) with a constant surface of contact between the probe head and the soil. The constant active area is created in the head of the probe (driven into the soil to about 80 cm depth) by the extrusion of a lost tip by means of the punch wire inside the probe by an exact distance. The internal volume of the cavity, which is created at the lower end of the sampling probe, is large enough to enable the sample collection. The probes use the approximation L N d, with a shape factor F = 0.149 m (L = 50 mm, d = 12 mm and D = 825 mm).

The experimental setup consists of a miniature vacuum pump produced by Fürgut GmbH, connected to a vacuum gauge, manufactured by SMC, with a

rated pressure range between 0 and -101 kPa. A flux meter from 0 to 5 L min-1 (produced by Key Instruments) was originally included in the experimental arrangement. A battery is used to provide energy to instruments (Fig. 2). The pressure gauge is connected via vynil tubing to the head of the probe on one side and to the pump on the other. Air from the pump was then made to flow through the flux meter and finally escape to the outer environment. The vynil tubings and metal connectors (components 6 and 7 in Fig. 1) have been kept to a minimum to reduce gas leakage. Measurements carried out using this equipment were compared with those obtained by RADON JOK.

Results shows that variables are very well correlated, demonstrating that the new device provides high quality data, comparable with those obtained with conventional and routinely used instruments. In addition to that, the new permeameter allows to extend the range of detectable values in the area of high permeability (beyond 1.80×10^{-11} m^2). Moreover, when measuring low permeability data, it provides a quicker response, compared to RADON JOK.

Moreover, the new instrument is very light (1 kg) and can be easily transported everywhere in the field, even on bumpy and rough terrain.

Then the instrument has been modified since the relationship between the flux and the pressure difference using this equipment is constant (see Fig. 3; Cap12), it is possible to express the value of Q as a function of ΔP. Introducingthis term (m ΔP + c) in Eq. (1), a new calculation has been introducedto determine k only on the basis of ΔP:

$$k = \frac{\mu \cdot (\mathrm{m}\,\Delta\mathrm{P} + \mathrm{c})}{\mathrm{F} \cdot \Delta\mathrm{P}}$$

where m is the slope of the experimental curve (Q vs ΔP) and c is the intercept on the Y axis. This allows modifying the experimental device, removing the flux meter in orderto obtain a simple assemblage consisting of a single pump and a vacuometer. This new configuration has also the advantage to reduce further the number of connections, minimizing the possibility of gas leakage.

The new device can be employed in the range of 3×10^{-13} –8.0×10^{-11} m^2 , extending the upper detection limit of RADON JOK (1.8×10^{-11}). This is definitely relevant because a higher permeability enables the increased migration of gas through the soil and into the buildings, enhancing the risk. Moreover, it provides rapid responses and is easy to carry in the field.

The new device for in situ measurement of soil permeability may be employed to investigate gases and volatile compounds transport through unsaturated media and to map radon potentials of a given site.

All of these studies (the development of new technologies and new methods of analysis of sites polluted by hydrocarbons) have allowed us to complete this cycle of studies (at least in its first phase). Thanks to the last few experiments, carried out in the laboratory and in the field in the study site, it was possible not only to delimit the presence and location of the pollutant, but also to quantify it.

A set of experiments was designed and built to obtain a partition coefficient K NAPL / WATER / AIR.

The pollutant quantification was carried out after a last field survey on the polluted site; the result was to obtain a quantification, well correlated with the pollutant estimation from data provided by Golder company.

Small-scale laboratory experiments were carried out to monitor the dissolution and preferential partition of radon in the vapor plume, occurring in case of recent

NAPL spills. Experiment 1 demonstrated that NAPL vapors may enhance soil radon exhalation and concentration when a large amount of vapors occurs, modifying soil radon distribution patterns. The introduction of a desiccant to dry soil gas emphasizes that radon is preferentially dissolved into NAPL vapors and is transported through the soil, before being absorbed by drierite. This also puts forward the interference that a desiccant may have on soil radon measurements.
Experiment 2 provided radon partition coefficients between kerosene, water and air, considered as the sum of air and kerosene vapors. This is crucial to correctly interpret radon data in a real open-system setting in presence of NAPL vapors, as during the employment of remediation based on soil venting or dual-phase extraction.

Radon-deficit technique was finally applied to the study area (Latium Region) in winter 2016 to assess the contamination due to the NAPL residual component in the vadose zone and to investigate the role of the vapor plume. The presence of significant NAPL vapors is ruled out by the comparison of radon data obtained by two RAD-7s connected in series and separated by a column of drierite. After a rigorous cross-calibration of the two instruments, soil radon data corresponds within the error range and VOCs concentrations are accordingly very low, as expected for an ancient spill. An evaluation of the fraction of residual NAPL in the soil is provided. Its distribution matches very well the radon deficit. In conclusion, we could assess the contamination by residual kerosene, but could not recognize the effect of kerosene vapors on radon transport through the soil and the interference with the drierite. This approach works very well and has the potential to be applied successfully to recent spills where the vapor plume is

supposed to be more extended. A new version of the equation proposed by Schubert (2015) is here developed and applied. An estimate of 58 L (47 Kg) of residual NAPL per cubic meter of terrain is provided.

Very high radon-deficits are found, obviously, when radon concentrations are extremely low: in those cases estimations of fraction of NAPLs in the pore space (NAPLPi) can be affected by very large uncertainties unless errors associated with radon measurements are kept low.

Finally Geophysical investigations have been used to characterize sites affected by hydrocarbons spill based upon the electrical properties of Non-Aqueous Phase Liquids (NAPLs). To evaluate the sensitivity of resistivity and time domain Induced Polarization (IP) techniques to organic contaminant detection, an integrated geophysical and soil radon investigation was conducted in a site affected by an ancient kerosene spill.

Resistivity and time domain IP surveys were carried out using two partially overlaying survey grids.

A resistivity meter was employed according to a pole-dipole configuration array, with a maximum penetration of 3 meters, corresponding to the groundwater table depth. Resistivity data identify a narrow anomalous band trending NNW-SSE, corresponding to the pattern of soil radon deficit. Distribution of positive IP anomalies is well correlated with areas were the soil is leached by groundwater due to induced pumping, whereas areas characterized by low chargeability could identify segments where films of residual NAPL isolate soil grains, inhibiting their chargeability properties. At the current state of knowledge, IP survey seems able to locate areas where NAPL was leached and others where this is still in progress.

Mapping of soil radon concentration at 80 cm depth clearly shows a local radon deficit, due to radon preferential partitioning in the residual NAPL. The comparison of radon patterns in the study area with appropriate backgrounds of nearby sites, where soil radon concentration is much higher, strengthens this. The low radon distribution in the vadose zone is not linked to high intrinsic permeability which would have favored degassing and reduced soil radon concentration.

The combined application of radon deficit technique and geoelectrical surveys opens future scenarios in the study of areas polluted by hydrocarbons.

CHAPTER APPENDIX

In the study area and in the background sites, data were seasonaly collected from 2013 to 2016. A series of maps was created for each measurement campaign. They are reported in the following

Fig. 1 Study area

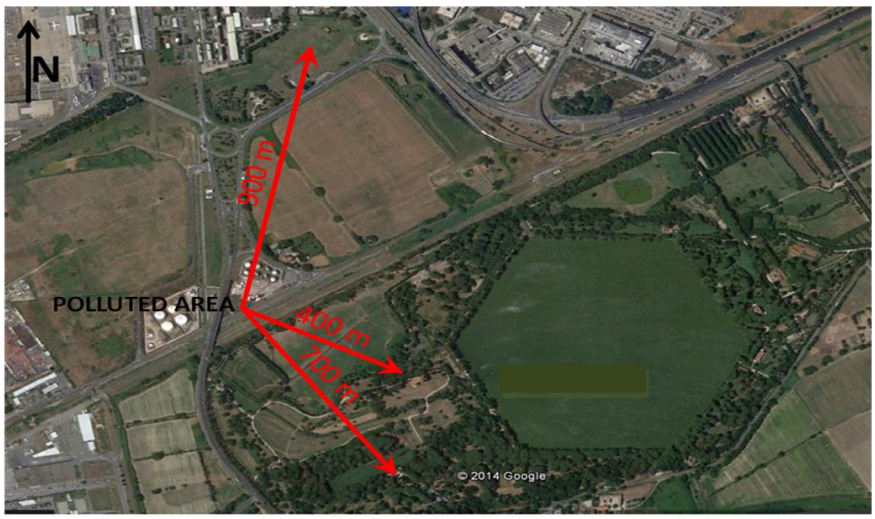

Fig. 2 Background areas

Winter 2013 - Study Area

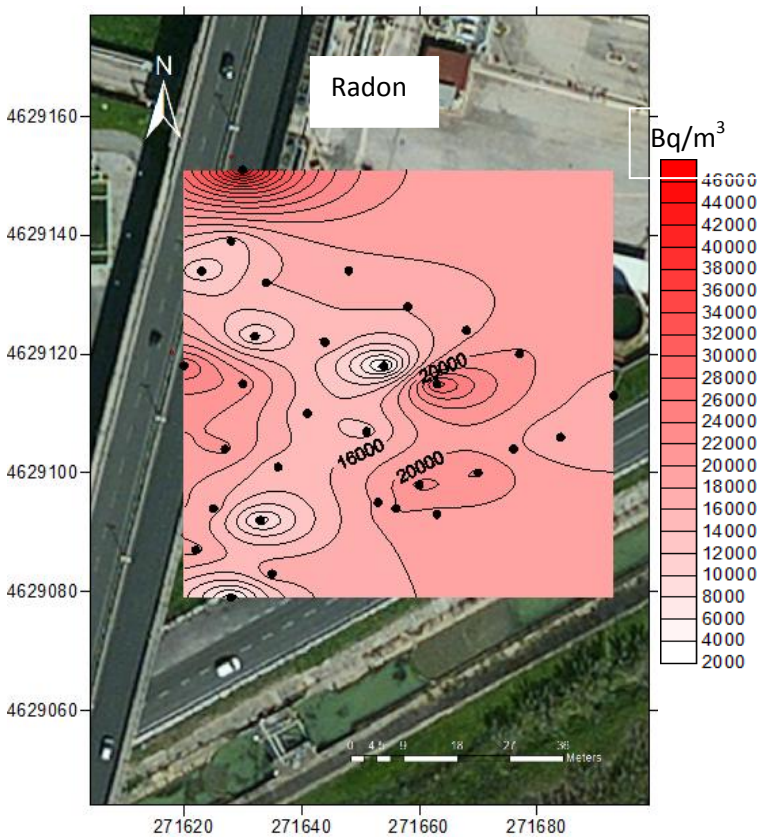

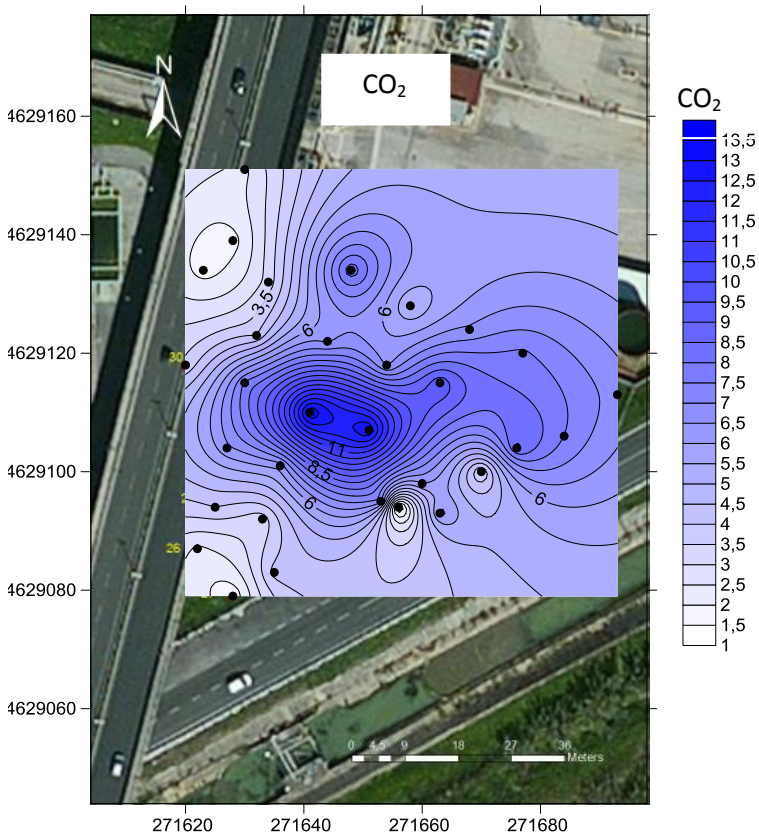

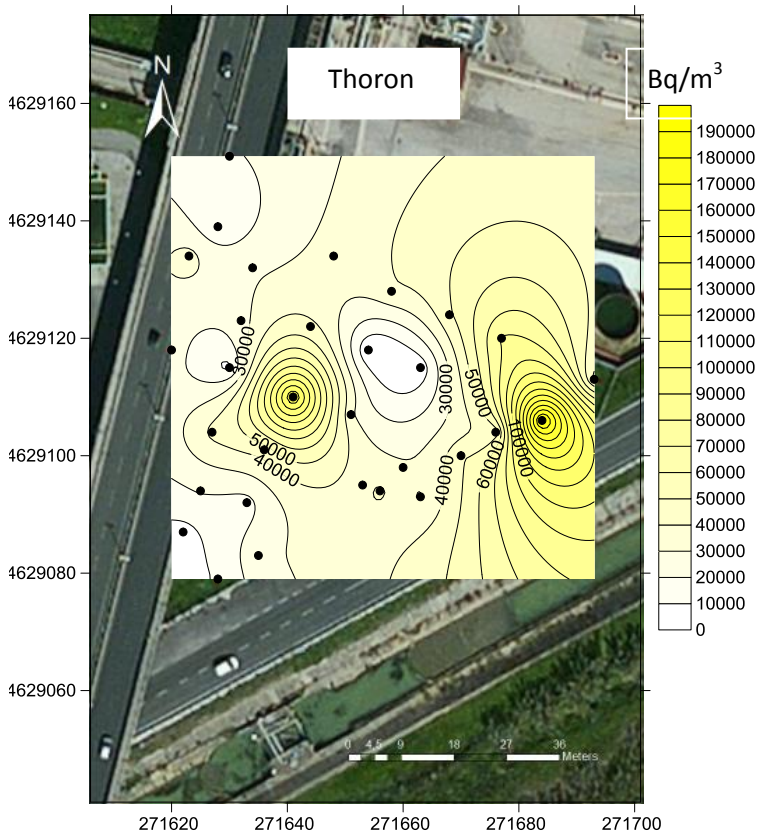

Permeability - Winter 2013 - Study Area

N	X	Y	k (m^2) RADON JOK
1	271634	4629132	5,00E-12
2	271648	4629134	4,80E-13
3	271658	4629128	1,10E-12
4	271668	4629124	4,80E-12
5	271677	4629120	4,80E-12
6	271693	4629113	6,50E-12
7	271684	4629106	5,2E-14
8	271663	4629115	1,60E-11
9	271654	4629118	2,30E-12
10	271644	4629122	5,2E-14
11	271632	4629123	1,50E-12
12	271630	4629115	2,20E-11
13	271641	4629110	5,2E-14
14	271651	4629107	7,30E-12
15	271660	4629098	5,2E-14
16	271670	4629100	1,20E-12
17	271676	4629104	1,90E-12
18	271663	4629093	5,20E-12
19	271656	4629094	5,2E-14
20	271653	4629095	1,40E-12
21	271636	4629101	2,90E-12
22	271627	4629104	3,20E-12
23	271625	4629094	1,60E-11
24	271633	4629092	5,20E-13
25	271635	4629083	8,40E-13
26	271622	4629087	2,70E-11
27	271628	4629079	1,40E-12
28	271628	4629139	2,50E-11
29	271623	4629134	1,70E-11
30	271620	4629118	5,20E-12
31	271630	4629151	1,10E-12
1B	271634	4629132	2,00E-13
SF	271655	4629100	4,90E-12

Winter 2013 – Background area

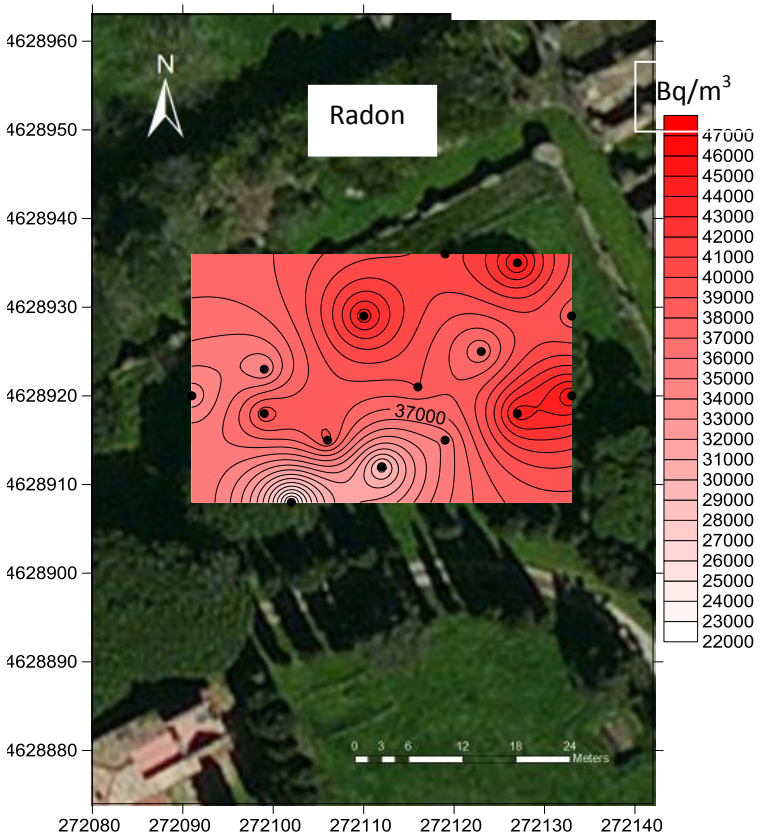

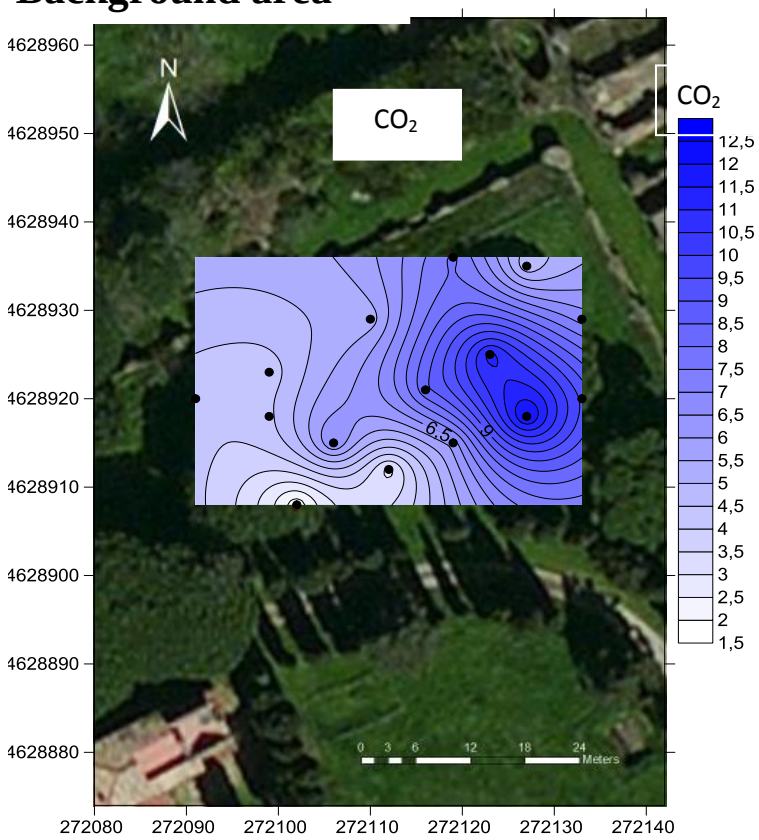

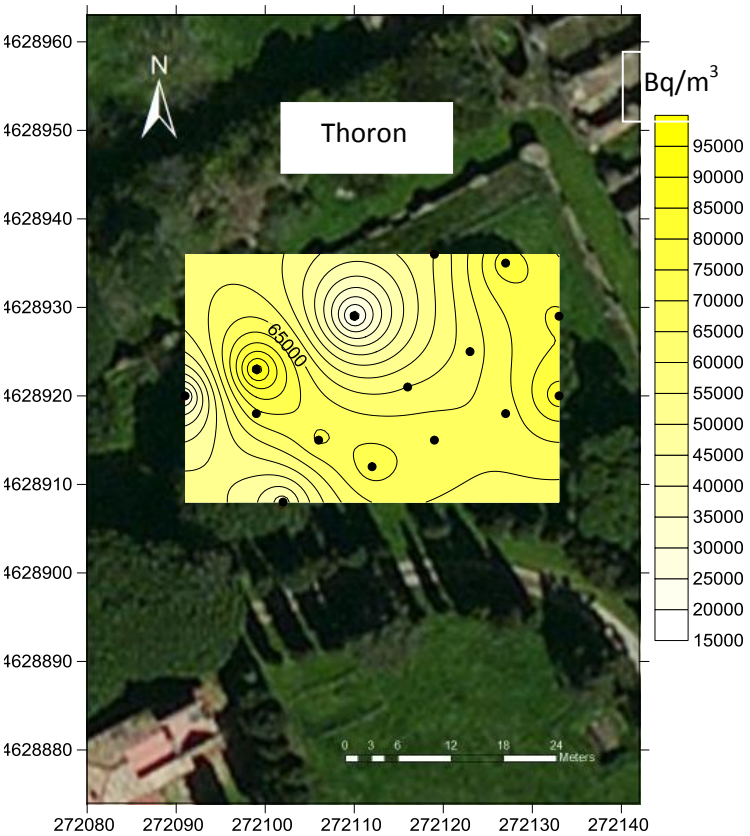

Permeability - Winter 2013 - Background Area

N	X	Y	k (m^2) RADON JOK	k (m^2) PERMEAMETER
1	272106	4628915	4,00E-12	5,10E-12
2	272116	4628921	3,70E-12	4,10E-12
3	272123	4628925	8,50E-12	1,10E-11
4	272133	4628929	1,50E-12	2,60E-11
5	272133	4628920	6,10E-12	8,7E-12
6	272127	4628918	5,6E-12	6,90E-12
7	272119	4628915	9,90E-12	1,30E-11
8	272112	4628912	1,2E-11	1,6E-11
9	272102	4628908	3,10E-11	7,90E-11
10	272099	4628918	1,60E-11	2,00E-11
11	272091	4628920	3,60E-11	7,80E-11
12	272099	4628923	5,50E-12	6,90E-12
13	272110	4628929	2,80E-11	3,90E-11
14	272119	4628936	2,70E-11	n.d.
15	272127	4628935	1,5E-11	2,00E-11

Summer 2013 - Study Area

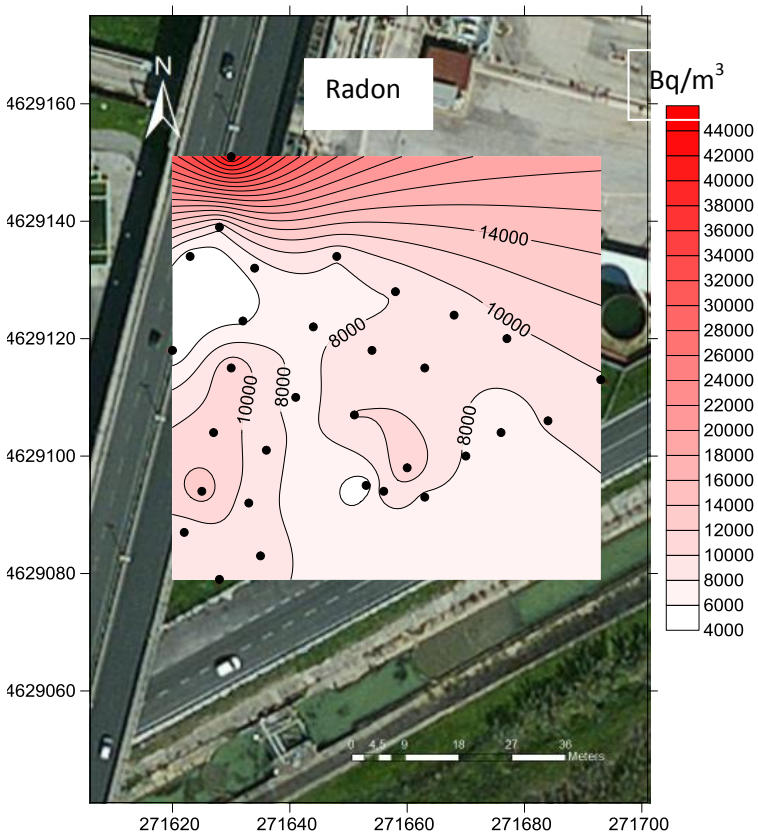

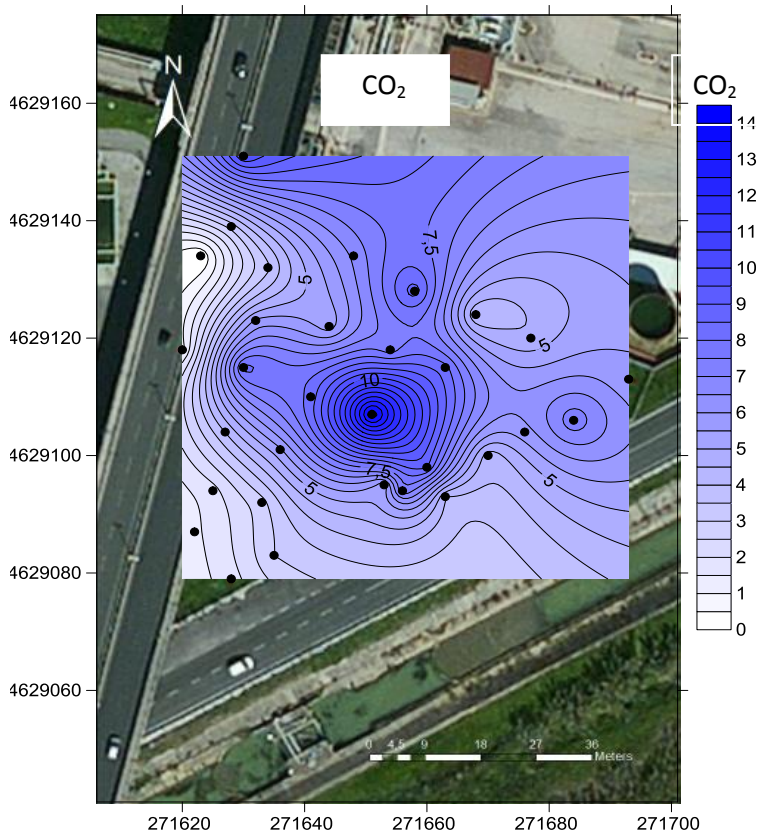

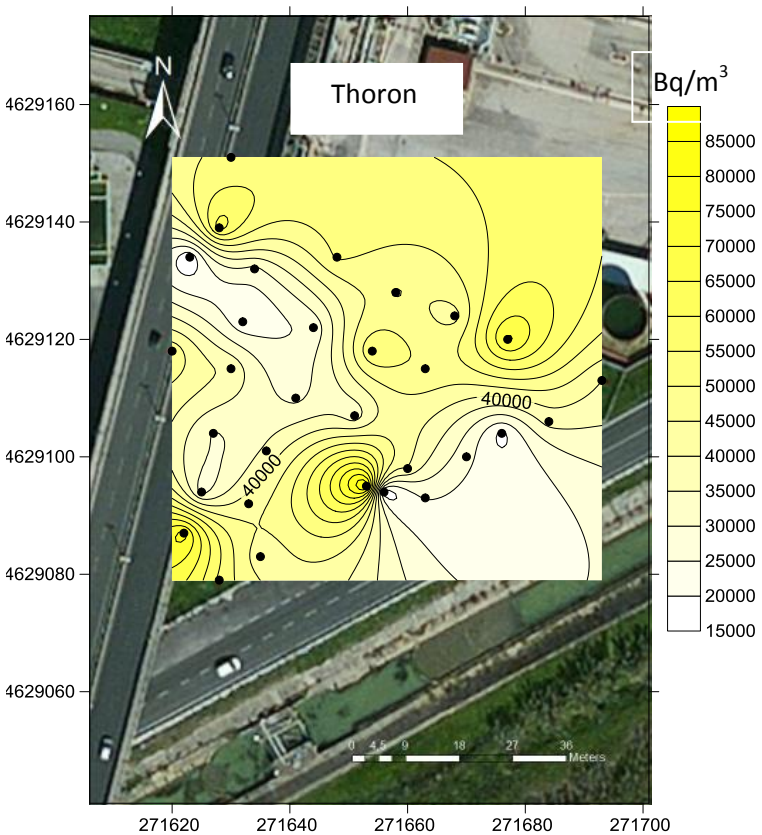

Permeability - Summer 2013 - Study Area

	X	Y	k (m^2) RADON JOK	k (m^2) PERMEAMETER
1	271634	4629132	5,2E-12	8,9E-12
2	271648	4629134	7,8E-12	1E-11
3	271658	4629128	7,2E-12	9,9E-12
4	271668	4629124	1,4E-11	1,6E-11
5	271677	4629120	1,1E-11	1,1E-11
6	271693	4629113	9,3E-12	1,1E-11
7	271684	4629106	3,9E-12	4,5E-12
8	271663	4629115	6,0E-12	6,5E-12
9	271654	4629118	1,6E-12	1,8E-12
10	271644	4629122	2,3E-12	2,6E-12
11	271632	4629123	2,7E-11	8E-11
12	271630	4629115	2,0E-12	2E-12
13	271641	4629110	2,2E-12	2,3E-12
14	271651	4629107	4,4E-13	3,7E-13
15	271660	4629098	9,4E-13	8,5E-13
16	271670	4629100	1,4E-12	1,6E-12
17	271676	4629104	1,9E-12	3,4E-12
18	271663	4629093	1,1E-12	1,3E-12
19	271656	4629094	9,9E-12	1,1E-11
20	271653	4629095	1,8E-13	1E-13
21	271636	4629101	2,2E-11	2,7E-11
22	271627	4629104	1,1E-11	1,3E-11
23	271625	4629094	4,0E-11	4E-11
24	271633	4629092	1,9E-12	2,2E-12
25	271635	4629083	4,2E-12	5,5E-12
26	271622	4629087	5,6E-12	6,6E-12
27	271628	4629079	1,8E-12	1,9E-12
28	271628	4629139	6,7E-13	6,5E-13
29	271623	4629134	3,6E-11	4E-11
30	271620	4629118	1,6E-11	2E-11
31	271630	4629151	2,4E-12	2,9E-12
1B	271634	4629132	7,6E-12	8,6E-12
SF	271655	4629100	7,8E-12	9,9E-12

Summer 2013 Background

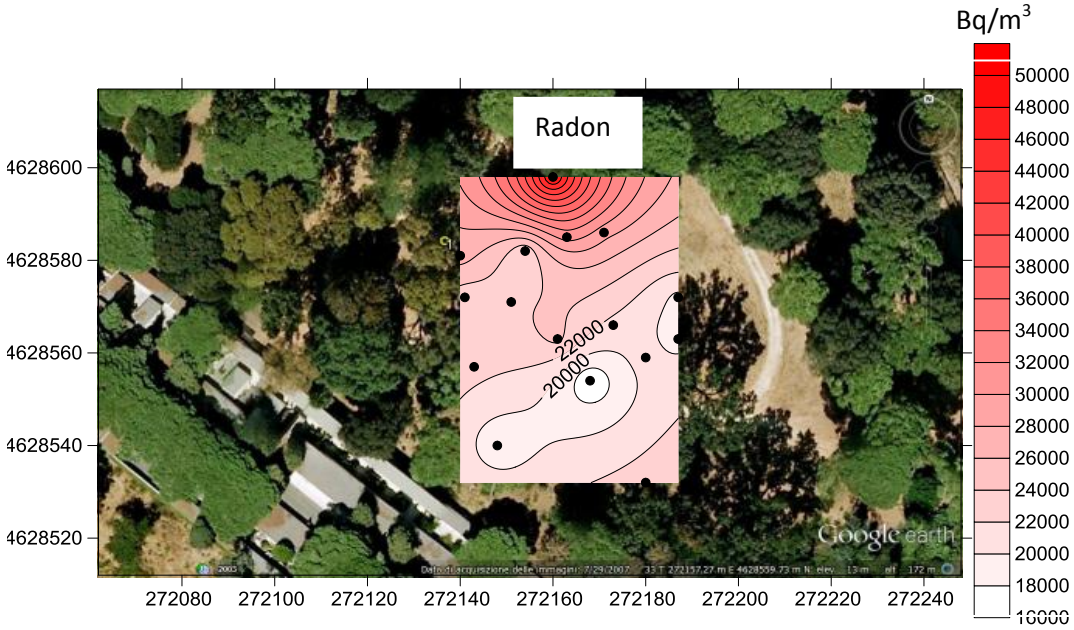

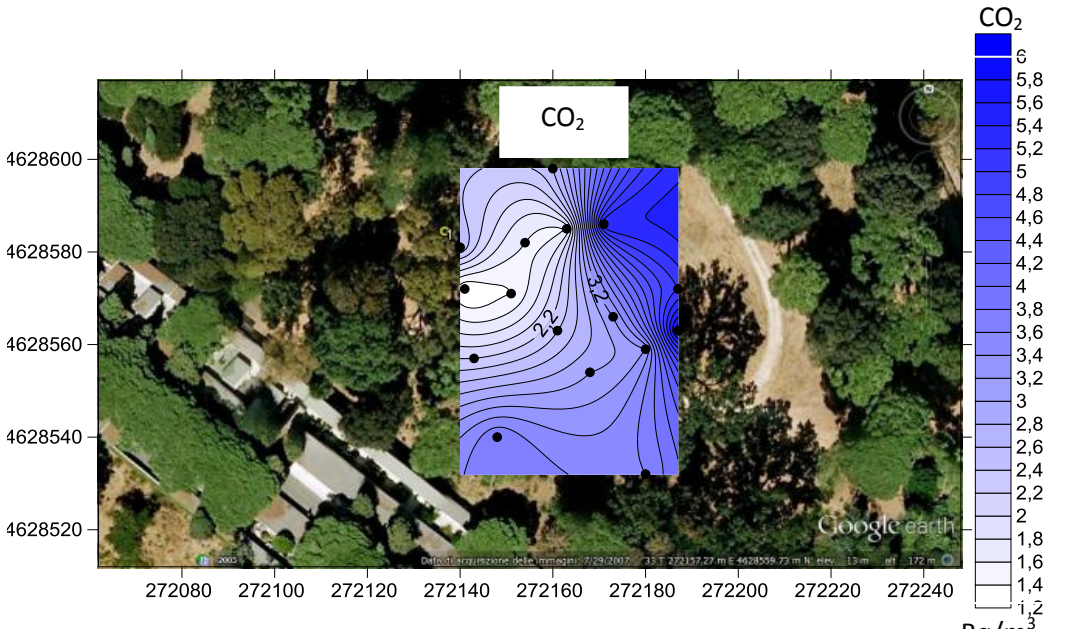

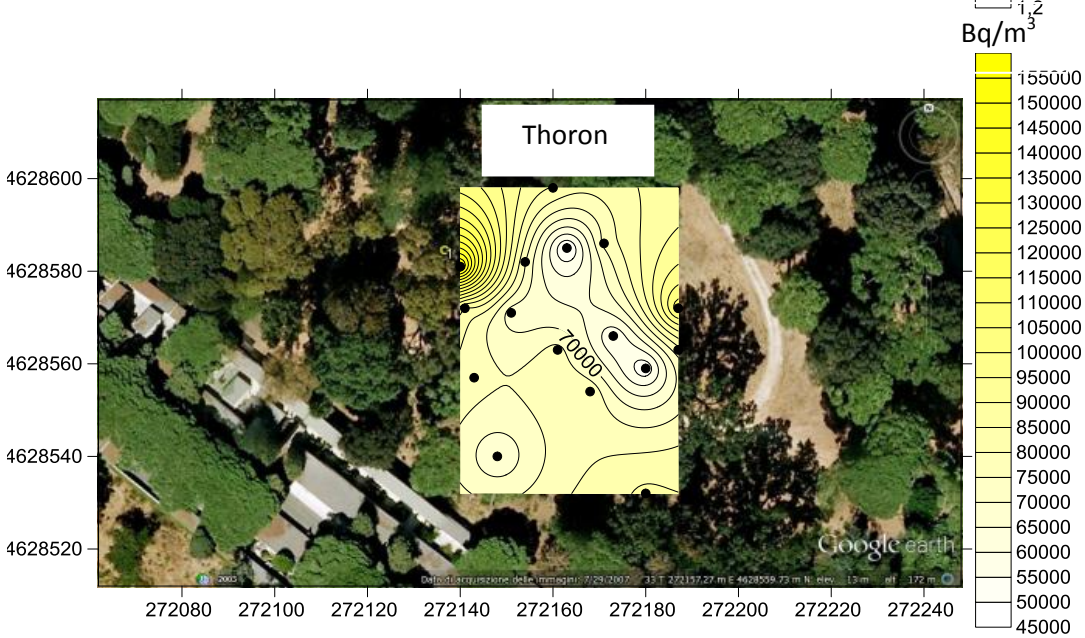

Permeability - Summer 2013 - Background Area

N	X	Y	k (m^2) RADON JOK	k (m^2) PERMEAMETER
1	272140	4628581	1,3E-13	1E-13
2	272141	4628572	4,30E-13	2,30E-13
3	272143	4628557	2,80E-11	4,00E-11
4	272148	4628540	3,60E-11	8,00E-11
5	272168	4628554	5,40E-12	6,00E-12
6	272161	4628563	1,80E-11	3,00E-11
7	272151	4628571	5,70E-12	6,00E-12
8	272154	4628582	2,0E-11	3,0E-11
9	272160	4628598	7,50E-12	1,00E-11
10	272163	4628585	3,60E-11	8,00-11
11	272173	4628566	1,60E-11	3,00E-11
12	272180	4628559	1,60E-11	3,00E-11
13	272187	4628563	1,80E-11	3,00E-11
14	272187	4628572	1,80E-11	3,00E-11
15	272180	4628532	4,50E-12	5,00E-12
16	272171	4628586	3,20E-12	3,00E-12

Winter 2014 - Study area

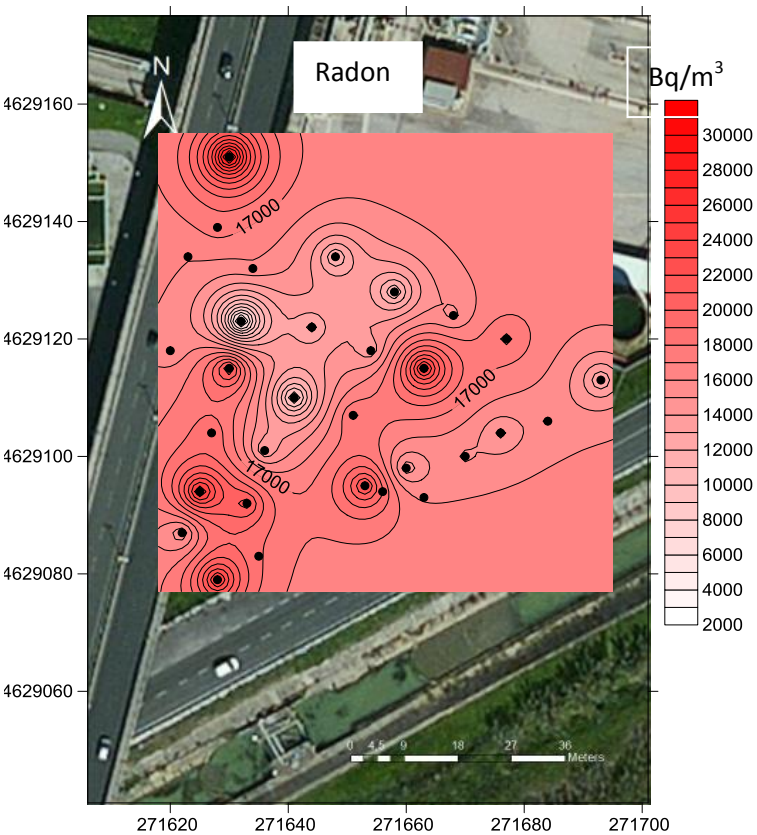

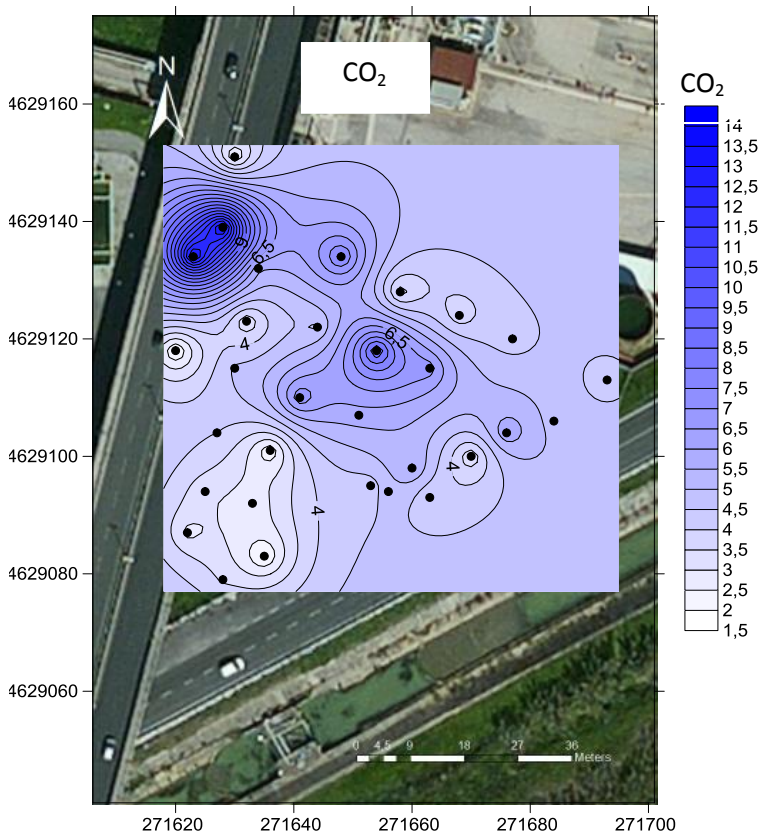

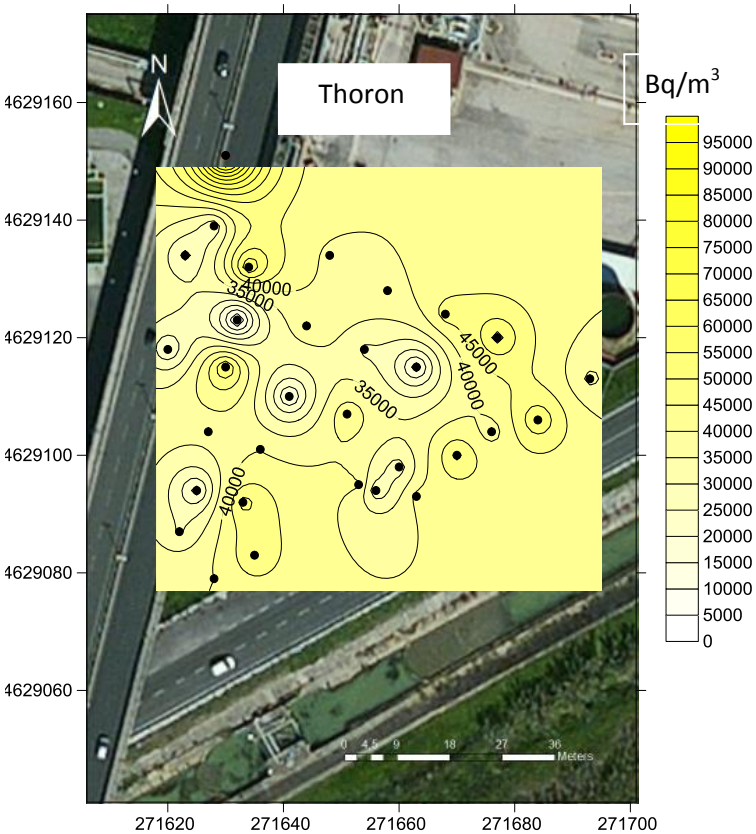

Permeability - Winter 2014 - Study Area

N	X	Y	k (m^2) PERMEAMETER
1	271634	4629132	2.2E-14
2	271648	4629134	1E-12
3	271658	4629128	5.1E-12
4	271668	4629124	1.6E-11
5	271677	4629120	4.8E-12
6	271693	4629113	1.3E-11
7	271684	4629106	4.4E-13
8	271663	4629115	8.2E.11
9	271654	4629118	3E-13
10	271644	4629122	1.3E-13
11	271632	4629123	7.5E-15
12	271630	4629115	4.2E-12
13	271641	4629110	1.2-13
14	271651	4629107	3.1E-12
15	271660	4629098	1.7E-13
16	271670	4629100	1.5E-12
17	271676	4629104	2.4E-12
18	271663	4629093	3.8E-12
19	271656	4629094	6E-12
20	271653	4629095	1.2E-13
21	271636	4629101	4.8-12
22	271627	4629104	1.3E-11
23	271625	4629094	4.1E-11
24	271633	4629092	1.1E-13
25	271635	4629083	3.2E-13
26	271622	4629087	1.3E-11
27	271628	4629079	3.3E-13
28	271628	4629139	1.3E-11
29	271623	4629134	1.1E-11
30	271620	4629118	7.6E-13
31	271630	4629151	5.5E-12
SF	271655	4629100	2.4E-12

Winter 2014 - Background Area

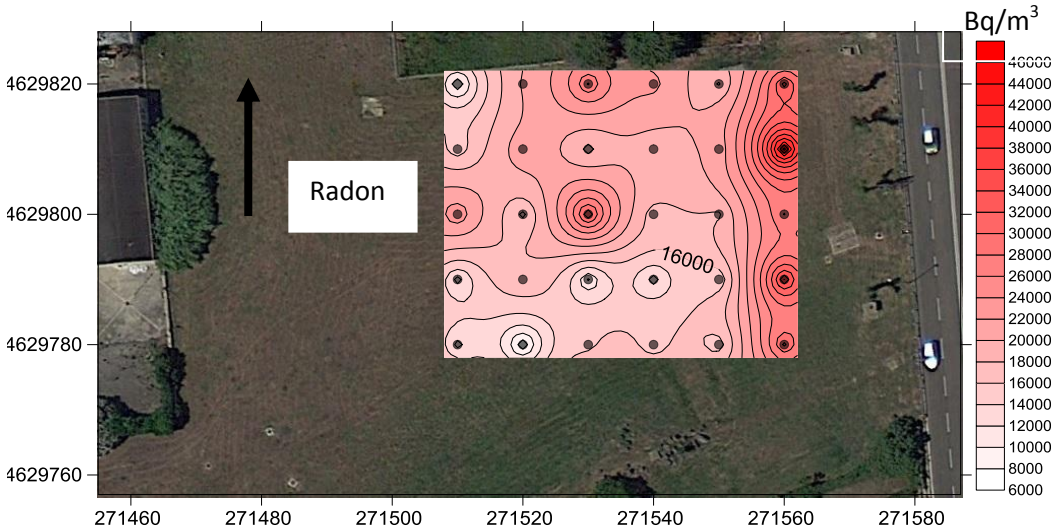

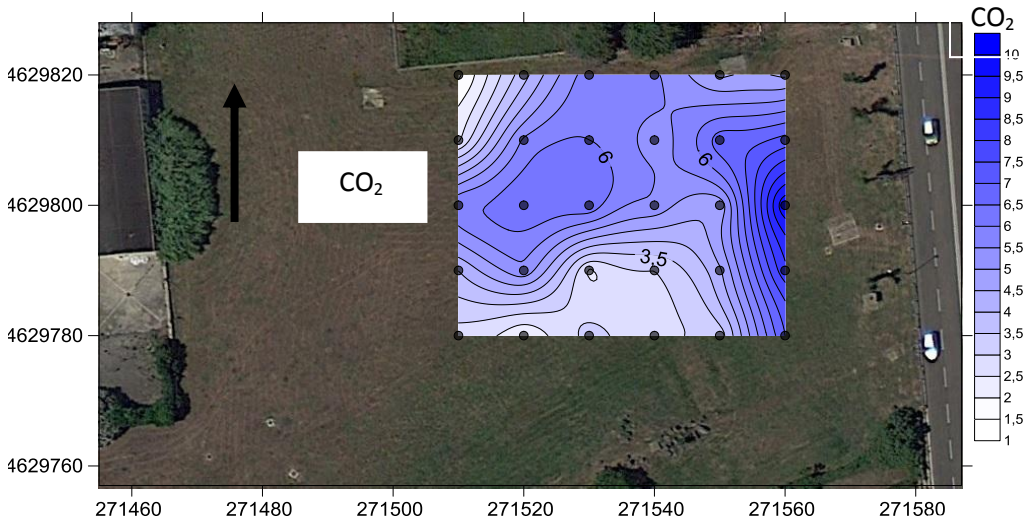

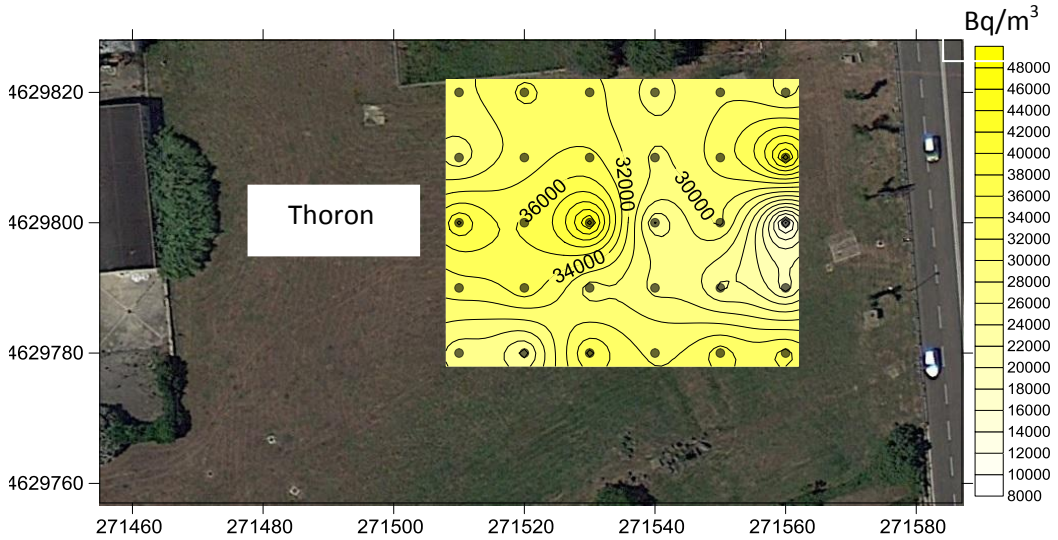

Permeability - Winter 2014 - Background area

N	X	Y	k(m^2) RADON JOK	k(m^2) PERMEAMETER
1	271560	4629810	4E-13	7,9E-13
2	271550	4629810	3,6E-13	2,4E-13
3	271540	4629810	9,6E-12	1,3E-11
4	271530	4629810	1,4E-11	2E-11
5	271520	4629810	7,8E-12	8,8E-12
6	271510	4629810	7,8E-12	8,8E-12
7	271510	4629800	9,9E-12	1,6E-11
8	271520	4629800	2,4E-12	2,6E-12
9	271530	4629800	4E-13	2,6E-13
10	271540	4629800	6,8E-12	8,8E-12
11	271550	4629800	3,2E-12	3,2E-12
12	271560	4629800	2,7E-11	8,2E-11
13	271560	4629790	1,7E-12	1E-12
14	271550	4629790	1,6E-11	2,7-11
15	271540	4629790	1,6E-11	2E-11
16	271530	4629790	1,8E-11	2,7E-11
17	271520	4629790	3,6E-12	4E-12
18	271510	4629790	5,4E-12	6,5E-12
19	271510	4629780	1,7E-11	2,7E-11
20	271520	4629780	1,7E-11	4,1E-11
21	271530	4629780	1,4E-11	2,7E-11
22	271540	4629780	1,3E-11	1,6E-11
23	271550	4629780	5,2E-12	5,5E-12
24	271560	4629780	3,9E-12	3,8E-12
25	271560	4629820	4,2E-12	3,8E-12
26	271550	4629820	7,2E-12	7,9E-12
27	271540	4629820	2,9E-12	2,6E-12
28	271530	4629820	4E-12	4E-12
29	271520	4629820	6E-12	5,1E-12
30	271510	4629820	7,8E-12	9,9E-12
31	271570	4629820	8,2E-13	1,9E-12
32	271570	4629810	1,4E-13	5,6E-14
33	271570	4629810	5,8E-13	3,7E-13
34	271570	4629810	2,2E-13	7,6E-14
35	271570	4629810	2E-12	5,3E-13

Summer 2014 - Study area

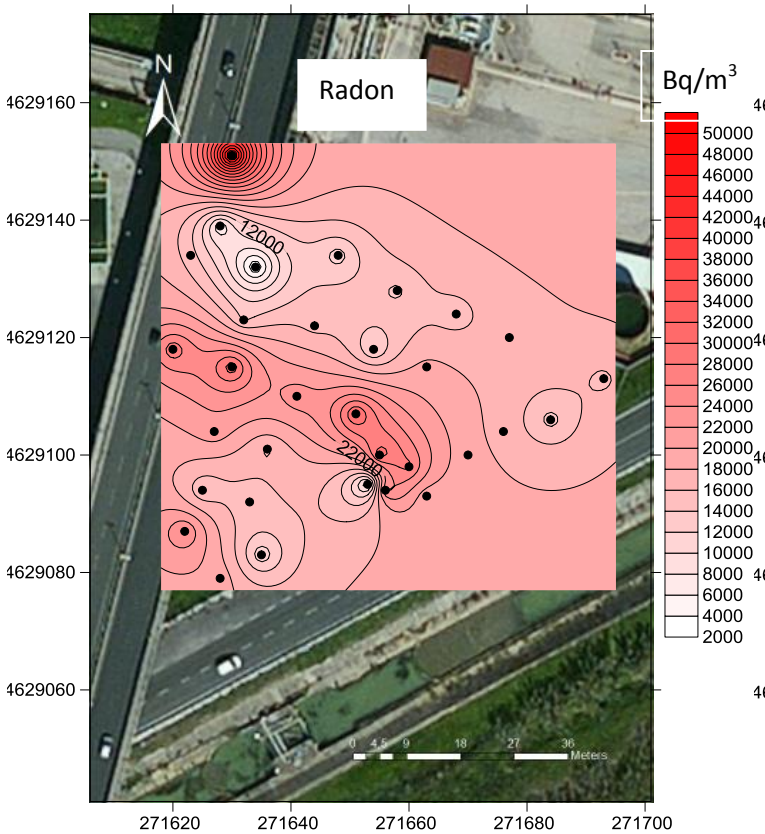

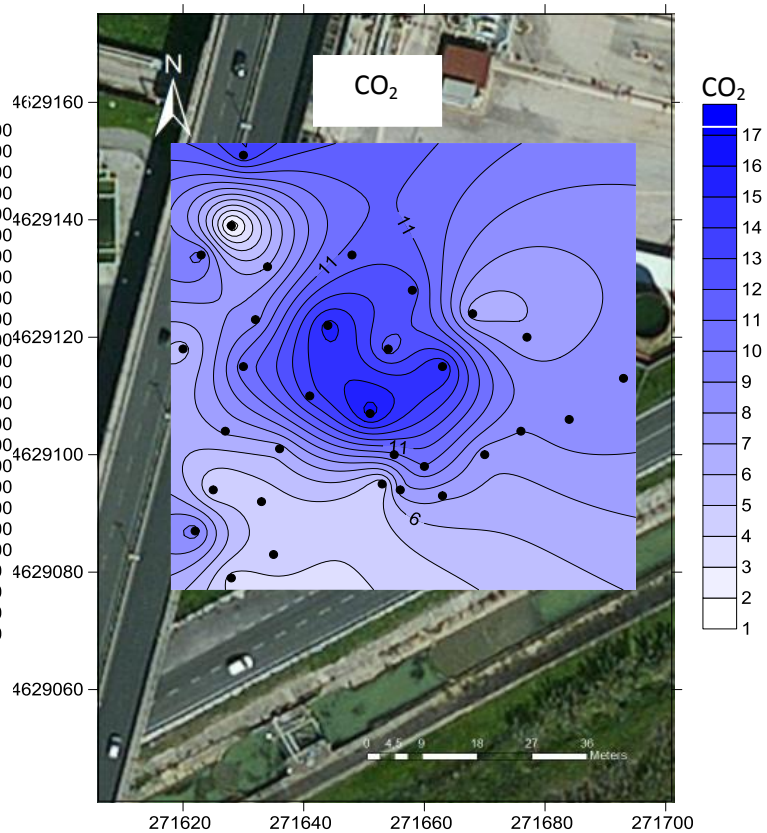

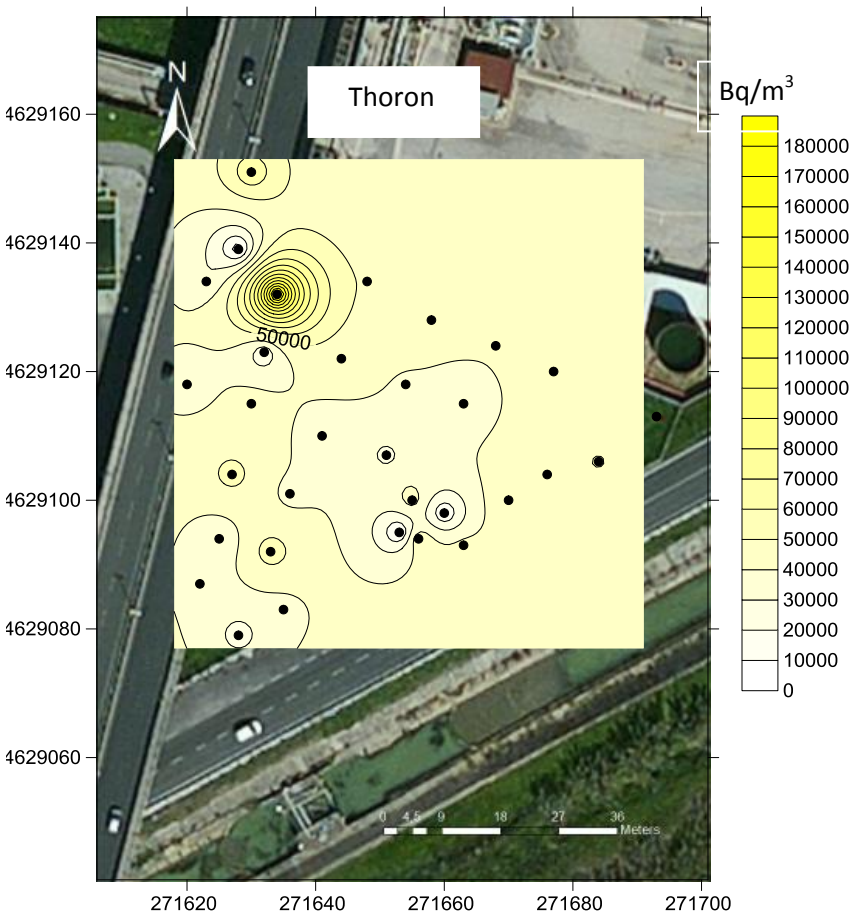

Permeability - Summer 2014 - Study area

N	X	Y	k(m^2) PERMEAMETER
1	271634	4629132	3.5E-14
2	271648	4629134	1.6E-11
3	271658	4629128	8.2E-11
4	271668	4629124	8.2E-11
5	271677	4629120	8.2E-11
6	271693	4629113	4.1E-11
7	271684	4629106	8.2E-11
8	271663	4629115	2E-11
9	271654	4629118	1.4E-11
10	271644	4629122	8.2E-11
11	271632	4629123	1.6E-11
12	271630	4629115	2-11
13	271641	4629110	1.6E-11
14	271651	4629107	3.5E-14
15	271660	4629098	2.5E-12
16	271670	4629100	6.5E-12
17	271676	4629104	7.9E-12
18	271663	4629093	1.1E-11
19	271656	4629094	2.8E-12
20	271653	4629095	4.9E-14
21	271636	4629101	5.5E-12
22	271627	4629104	9.9E-12
23	271625	4629094	8.2E-11
24	271633	4629092	2E-11
25	271635	4629083	1.3E-11
26	271622	4629087	1.2E-13
27	271628	4629079	1.3E-12
28	271628	4629139	2E-11
29	271623	4629134	8.2E-11
30	271620	4629118	1.3E-11
31	271630	4629151	8.2E-11
SF	271655	4629100	5.5E-12

Summer 2014 - Background area

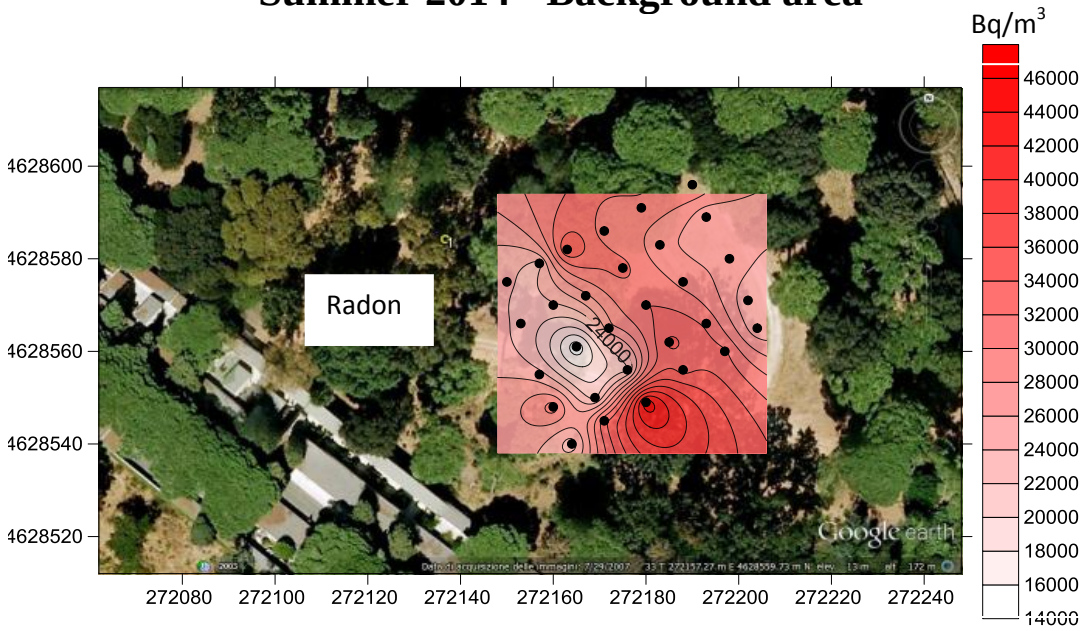

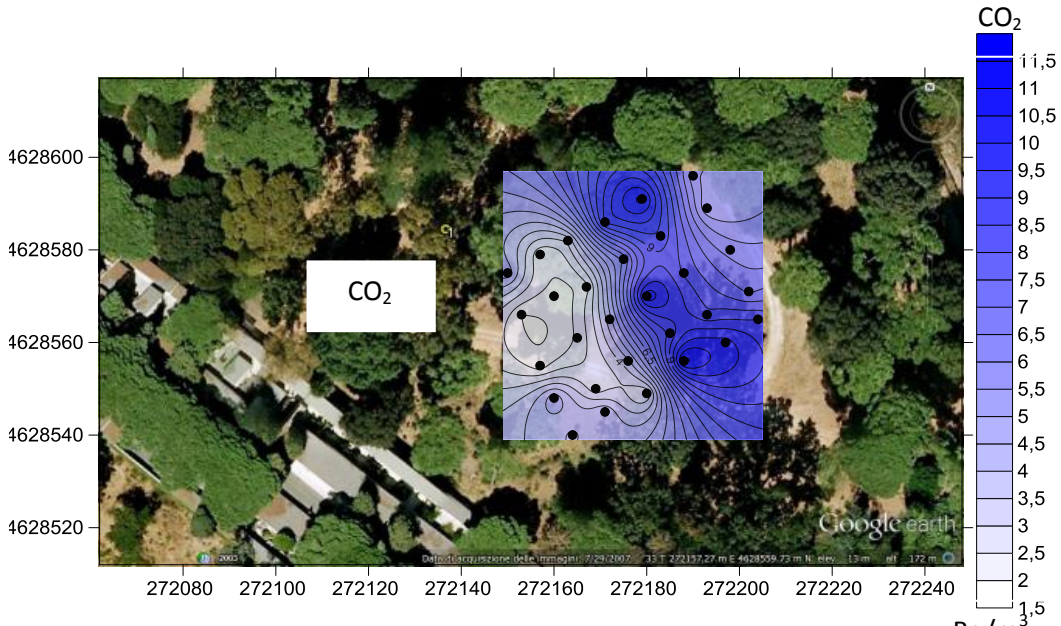

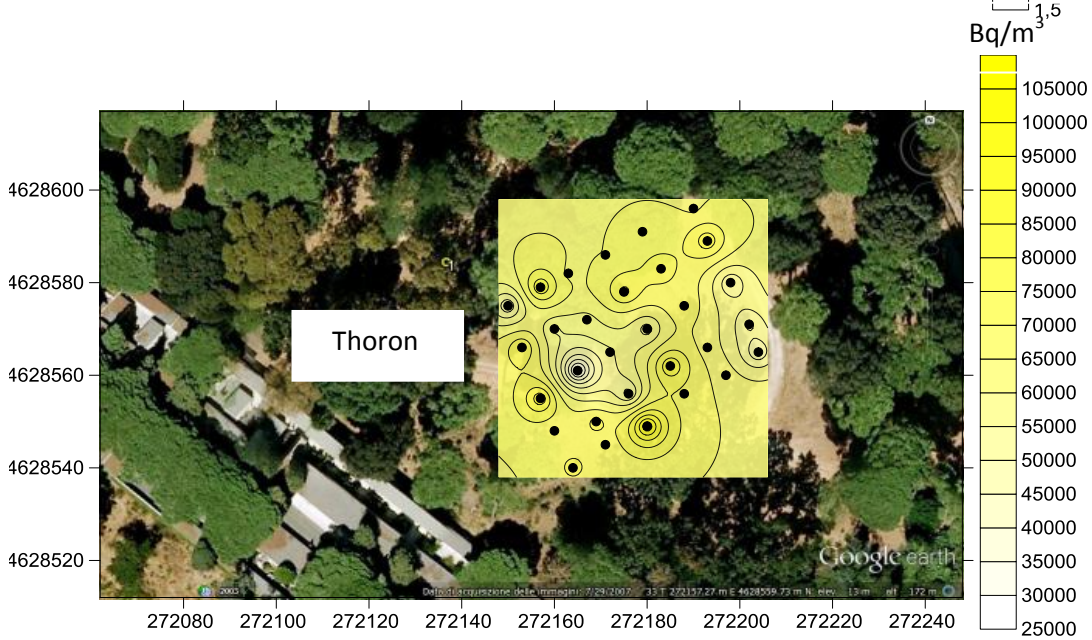

Permeability - Summer 2014 - Background area

N	X	Y	k(m^2) PERMEAMETER
A1	272150	4628575	2E-11
A2	272153	4628566	8.2E-11
A3	272157	4628555	1.1E-11
A4	272159	4628554	1.10E-11
A5	272162	4628545	1.90E-12
B1	272154	4628580	4.5E-12
B2	272161	4628573	8.2E-11
B3	272169	4628554	6E-14
B4	272167	4628554	3.2E-12
B5	272161	4628546	5.5E-12
C1	272157	4628585	2.7E-11
C2	272169	4628581	8.2E-11
C3	272174	4628571	9.9E-12
C4	272178	4628560	9.9E-12
C5	272184	4628554	2.4E-12
D1	272175	4628593	1.6E-12
D2	272180	4628583	3.2E-13
D3	272179	4628574	1.3E-11
D4	272190	4628567	4.1E-11
D5	272188	4628553	7.9E-12
E1	272187	4628591	5.1E-12
E2	272196	4628573	1.9E-12
E3	272197	4628568	2.4E-12
E4	272199	4628559	7.9E-12
E5	272202	4628552	6.5E-12
F1	272203	4628584	1.3E-11
F2	272205	4628575	4E-13
F3	272208	4628577	8.2E-11
F4	272211	4628566	5.5E-12
F5	272213	4628556	7.9E-12

The last field survey in the study was conducted in the winter of 2016 with two radonometers connected in series, the results are discussed in chapter 7.

A short comment to this maps is presented here and discussed more deeply in following chapters.

Soil radon concentrations in the study area are always significantly lower than in close background sites. Radon is not directly correlated with CO_2 as in the background. Permeability is relatively constant and does not influence observed radon oncentration differences.

Winter surveys show much better the radon deficit compared with summer campaigns because of the closed-system conditions of the winter, due to higher water contents and lower temperature in the soil.